Ring Fused Conjugated Polymers for Use in Organic Electronics

Jessica Shaw

Submitted in partial fulfilment of the requirements for the degree of Doctor of Philosophy in Chemistry

Department of Chemistry, Imperial College London

January 2017

Declaration of Originality

The work described in this thesis was carried out in the Department of Chemistry, Imperial College London, between October 2012 and January 2017 under the supervision of Professor Martin Heeney, and is my own work unless otherwise stated.

Jessica Shaw, January 2017

Contributions

I gratefully acknowledge the following people for their valuable contribution to this work:

The work presented in Chapters 3 and 5 was performed in collaboration with Dr Zhuping Fei from Professor Martin Heeney's group in the Department of Chemistry, Imperial College London, UK; who synthesised P7 and P8 (Chapter 3) using monomer 3.5 I provided, and P14-16 (Chapter 5) from the precursor 4,9-dibromo-2,7-bis(4-decylhexadecyl)benzo[*lmn*][3,8]phenanthroline-1,3,6,8(2*H*,7*H*)-tetrone (4.5) I synthesised. The work presented in Chapter 4 was performed in close collaboration with Simeng Wang and Kai Ni Teh also from Professor Martin Heeney's group; who focused on the synthesis of P9 and P11, and P12, respectively, under my supervision as undergraduate research projects.

MALDI-ToF mass spectrometry was carried out by Dr Pierre Boufflet (Chapter 3) from Professor Martin Heeney's group and Dr Lisa Haigh (Chapter 5) in the Department of Chemistry, Imperial College London, UK. Electrospray ionisation and electron ionisation mass spectrometry was also carried out by Dr Lisa Haigh. Elemental analysis was performed by Mr Stephen Boyer at London Metropolitan University. High temperature ^{1}H NMR experiments were run by Mr Peter Haycock and Mr Dick Sheppard at Imperial College London, UK.

Thermogravimetric analysis (Chapters 3 and 5) was carried out by Dr Hannah Leese from Professor Milo Shaffer's group in the Department of Chemistry, Imperial College London, UK. High temperature gel permeation chromatography was performed at Merck Chemicals Ltd., Chilworth Technical Centre, UK. Photoelectron spectroscopy in air measurements were carried out by Dr Scott E. Watkins, Dr Anthony Chesman, Dr Fiona Scholes, and Mr Adam Creamer at CSIRO, Australia. Atomic force microscopy measurements were carried out by Dr Yang Han from Professor Martin Heeney's group in the Department of Chemistry, and Professor Thomas D. Anthopoulos's group in the Department of Physics, Imperial College London, UK. X-ray diffraction measurements were performed by Dr Ester Buchaca-Domingo from Professor Natalie Stingelin's group in the Department of Materials, Imperial College London, UK. Grazing incidence wide angle X-ray scattering measurements were performed at the Australian Synchrotron by Dr Eliot Gann from Dr Chris McNeill's group in the Department of Materials Engineering, Monash University, Australia. Photoluminescence quenching experiments and transient absorption spectroscopy studies were performed by Mr Ching-Hong Tan from Professor James R. Durrant's group in the Department of Chemistry, Imperial College London, UK.

Organic field effect transistors were fabricated and tested by Dr David Sparrowe (Chapter 2) at Merck Chemicals Ltd., Chilworth Technical Centre, UK and Dr Yang Han (Chapters 3-5) from Professor Martin Heeney group in the Department of Chemistry, and Professor Thomas D. Anthopoulos's group in the Department of Physics, Imperial College London, UK.

Organic photovoltaic cells were fabricated and tested by Dr Pabitra Shakya Tuladhar (Chapter 3 P6 and P7) and Dr Raja Shahid Ashraf (Chapter 4) from Professor James R Durrant's group, and Dr Yang Han (Chapter 3 P8) from Professor Martin Heeney group, in the Department of Chemistry, Imperial College London, UK.

Copyright Declaration

Acknowledgements

First, I'd like to thank Martin for taking a chance and rescuing me from the depths of rural Wales all those years ago. In doing so you've changed the course of my life, and for that I am forever grateful. I'd also like to give a big thank you to Will, for always making time to discuss ideas and provide invaluable advice to help push this project forward. Of course, also a huge thanks to Merck Chemicals Ltd., and the EPSRC for generously funding this work.

I'd also like to offer my sincerest thanks to everyone who contributed to this project, and to all the members, past and present, of the Heeney and McCulloch groups. In particular, I'd like to thank Dr Hongliang Zhong, Dr Zhuping Fei, Dr Yang Han, and Dr Bob Schroeder for their guidance throughout this project. Their endless knowledge will always remain a huge source of inspiration.

Last, and perhaps most importantly, I want to thank my parents for their support and encouragement. From an early age you have taught me to believe that anything is possible if you put your mind to it, and this body of work is testament to that. Thank you for everything.

Abstract

The use of conjugated polymers as the active layer in transistor and photovoltaic devices offers many advantages over inorganic materials, such as the potential for low cost, large-scale, solution processed, flexible devices. There has been considerable progress in this area in recent years due to innovative material design, development of new and exciting device architectures, and a deeper understanding of the underlying operating principles, and morphological requirements for optimal performance. Nevertheless, new materials with even higher performance and stable device characteristics are currently needed if commercialisation is to be achieved.

This thesis focuses on the design and synthesis of a range of ring fused conjugated polymers for use in organic electronics. Ring fused polymers are particularly promising for this application since they offer the potential to help planarise the backbone, enhance intermolecular π-π interactions, and thus improve charge transport. In the first chapter a series of five polymers based on a five-membered, dithienogermolodithiophene (DTTG) monomer (an extended version of dithienogermole) is reported. Through careful consideration of the choice of acceptor co-monomer and device optimisation, a peak saturated hole mobility of 0.22 cm^2/Vs was obtained in devices spin-coated from a non-chlorinated solvent mixture, which at the time of writing was the highest reported charge carrier mobility of any germanium based polymer.

The second chapter focuses on the synthesis of a novel bisthieno[2',3':4,5]thieno[3,2-*c*:2',3'-*e*]azepine-4,6(5*H*)-dione (BTTA) monomer in which two thieno[3,2-*b*]thiophene units are bridged by an azepine-2,7-dione ring. The choice of co-monomer on the optoelectronic and surface morphology of the polymers are reported, using a combination of experimental techniques. The photovoltaic and electrical performance of the polymers investigated in inverted BHJ OPV devices and TG-BC field effect transistors was high, with peak values of 6.78% and 0.027 cm^2/Vs observed under optimised conditions.

The third chapter explores the use of side-chain engineering to improve the performance of one of the most promising ring fused electron accepting materials; poly[4,9(benzo[*lmn*][3,8]phenanthroline-1,3,6,8(2*H*,7*H*)-tetrone)-alt-5,5'(2,2'-bithiophene)] (pNDI-BT). In particular, the use of alkyl side-chain branching position as an effective strategy for improving charge carrier mobility was demonstrated, and for the first time, the influence of the branch-point on the performance of all-polymer OPV devices was examined, with a gradual decrease in power conversion efficiency observed as the branch-point was moved further from the polymer backbone. The final chapter builds on this work, and uses a range of fluorinated

and non-fluorinated, thiophene and selenophene containing monomers, to further improve the electrical performance of a series of NDI based polymers.

Table of Contents

List of Schemes and Figures

Chapter 1

Chapter 2

Chapter 3

Chapter 4

Chapter 5

List of Tables

Chapter 2

Chapter 3

Chapter 4

Chapter 5

List of Publications

The following publications have arisen from the work described in this thesis and shall be discussed herein:

Chapter 2

1. Alternating Copolymers Incorporating Dithienogermolodithiophene for Field-Effect Transistor Applications. **J. Shaw**, H. Zhong, C. P. Yau, A. Casey, E. Buchaca-Domingo, N. Stingelin, D. Sparrowe, W. Mitchell and M. Heeney, *Macromolecules*, 2014, **47**, 8602-8610.

Chapter 3

2. Conjugated Polymers. N. Blouin, W. Mitchell, M. Heeney and **J. Shaw**, WO 2016/037678 A1.

Note publications based on the work described in Chapters 3-5 are currently being prepared.

The work for the following publications was carried out during my PhD but will not be discussed further:

3. Fused Ring Cyclopentadithienothiophenes as Novel Building Blocks for High Field Effect Mobility Conjugated Polymers. H. Zhong, Y. Han, **J. Shaw**, T. D. Anthopoulos and M. Heeney, *Macromolecules*, 2015, **48**, 5605-5613.

4. An Eight-Membered Ring-Fused Building Block for High Performing Field-Effect Transistor Polymers. **J. Shaw**, Y. Han, T. D. Anthopoulos, W. Mitchell, and M. Heeney (*in preparation)*.

List of Abbreviations

δ	Chemical shift
°	Degrees
Θ	Angle
Å	Angstrom
λ	Wavelength
Đ	Polydispersity
μ_e	Electron mobility
μ_h	Hole mobility
μ_{lin}	Linear charge carrier mobility
μ_{sat}	Saturated charge carrier mobility
µW	Microwave
A	Acceptor
AFM	Atomic force microscopy
Anal. calcd	Analytically calculated
B3-LYP	Becke three-parameter, Lee-Yang-Parr
BDT	Benzo[1,2-*b*:4,5-*b'*]dithiophene
BG-BC	Bottom-gate, bottom-contact
BG-TC	Bottom-gate, top-contact
BHJ	Bulk heterojunction
BT	2,2'-Bithiophene
BTA	Bisthieno[3,2-*c*:2',3'-*e*]azepine-4,6(5*H*)-dione
BTTA	Bisthieno[2',3':4,5]thieno[3,2-*c*:2',3'-*e*]azepine-4,6(5*H*)-dione
BTz	2,1,3-Benzothiadiazole
C	Celsius
CB	Chlorobenzene
CF	Chloroform
C_i	Capacitance per unit area of the dielectric
CN	1-Chloronaphthalene
D	Donor
D-A	Donor-acceptor
o-DCB	*o*-Dichlorobenzene
DCM	Dichloromethane
DFT	Density Functional Theory
DIAD	Diisopropyl azodicarboxylate
DIO	1,8-Diiodooctane
DMAP	4-(Dimethylamino)pyridine
DMF	Dimethylformamide
DPE	Diphenyl ether

DPP	Diketopyrrolopyrrole
DPPA	Diphenylphosphoryl azide
DSC	Differential scanning calorimetry
DSS	Diseleno[3,2-*b*:2',3'-*d*]selenophene
DTBT	4,7-Bis(thiophen-2-yl)benzo[1,2,5-*c*] thiadiazole
DTG	Dithienogermole
DTT	Dithieno[3,2-*b*:2',3'-*d*]thiophene
DTTG	Dithienogermolodithiophene
E_g	Band gap
EI	Electron ionisation
eq.	Equivalents
EQE	External quantum efficiency
ESI	Electrospray ionisation
ETL	Electron transport layer
eV	Electron Volts
FF	Fill factor
GIWAXS	Grazing incidence wide angle X-ray scattering
GPC	Gel permeation chromatography
HOMO	Highest occupied molecular orbital
HMDS	1,1,1,3,3,3-Hexamethyldisilazane
HRMS	High-resolution mass spectrometry
HT-GPC	High-temperature gel permeation chromatography
HTL	Hole transport layer
Hz	Hertz
ICT	Intramolecular charge transfer
I_D	Drain current
IDT	Indacenodithiophene
IDTT	Indacenodithieno[3,2-*b*]thiophene
$I_{on/off}$	Current on/off ratio
I.P.	Ionisation potential
IPA	Isopropyl alcohol
ITO	Indium tin oxide
J	Coupling constant
J_{max}	Current at maximum power
J_{SC}	Short circuit current density
J-V	Current-voltage
L	Channel length
LUMO	Lowest unoccupied molecular orbital
MALDI	Matrix assisted laser desorption ionisation
min	Minutes

M_n	Number-average molecular weight
mol	Moles
MOSFET	Metal oxide-semiconductor field effect transistor
MS	Mass spectrometry
M_w	Weigh-average molecular weight
m/z	Mass to charge
NBS	*N*-Bromosuccinimide
NDI	Benzo[*lmn*][3,8]phenanthroline-1,3,6,8(2*H*,7*H*)-tetrone synonym: naphthalene-1,4,5,8-tetracarboxylic diimide
NMR	Nuclear magnetic resonance
OFET	Organic field effect transistor
OLED	Organic light emitting diode
OPV	Organic photovoltaic
OTS	Trichloro(octadecyl)silane
PANI	Poly[aniline]
$PC_{61}BM$	[6,6]-Phenyl-C_{61}-butyric acid methyl ester
$PC_{70}BM$	[6,6]-Phenyl-C_{71}-butyric acid methyl ester
PCE	Power conversion efficiency
$Pd_2(dba)_3$	Tris(dibenzylideneacetone)dipalladium(0)
PEDOT	Poly[3,4-ethylenedioxythiophene]
PESA	Photoelectron spectroscopy in air
PFBT	Pentafluorobenzene thiol
P_{in}	Incident light intensity
PL	Photoluminescence
PLQ	Photoluminescence quenching efficiency
PMMA	Poly[methyl methacrylate]
$P(o\text{-}Tol)_3$	Tri(*o*-tolyl)phosphine
ppm	Parts per million
PSS	Poly[styrenesulfonate]
PTB7-Th	Poly[[4,8-bis[5-(2-ethylhexyl)-2-thienyl]benzo[1,2-*b*:4,5-*b'*]dithiophene-2,6-diyl][2-[[(2-ethylhexyl)oxy]carbonyl]-3-fluorothieno[3,4-*b*]thiophenediyl]]
PTFE	Poly[1,1,2,2-tetrafluoroethylene]
RMS	Root-mean-square
rpm	Revolutions per minute
rt.	Room temperature
SAM	Self assembled monolayer
SAXS	Small-angle X-ray scattering
soln.	Solution
TAS	Transient absorption spectroscopy
TCB	Trichlorobenzene

THF	Tetrahydrofuran
TGA	Thermogravimetric analysis
TG-BC	Top-gate, bottom-contact
TG-TC	Top-gate, top-contact
TLC	Thin-layer chromatography
TMS	Trimethylsilyl
ToF	Time-of-flight
TPD	Thienopyrrolodione
UV-vis	Ultraviolet-visible
v	Volume
vacuo	Vacuum
V_D	Drain voltage
V_G	Gate voltage
V_{max}	Voltage at maximum power
V_{OC}	Open circuit voltage
V_S	Source voltage
V_T	Threshold voltage
w	Weight
W	Channel width
WAXS	Wide-angle X-ray scattering
XRD	X-ray diffraction

Chapter 1
Introduction

1.1 Organic Field Effect Transistors

A transistor device is used to amplify and switch electronic signals in integrated circuits.[1] A typical transistor is composed of four main components: three electrodes (source, drain, and gate), an insulating dielectric, an organic semiconductor, and a substrate.[1] Metals (e.g. gold, silver, aluminium, palladium, platinum) or conducting polymers (e.g. PEDOT:PSS, PANI) are commonly used as the source and drain electrodes.[2] Note for p-type transistors the use of a high work function metal is thought to help limit charge injection barriers between the electrodes and the organic semiconductor. If necessary a self-assembled monolayer (e.g. PFBT) can also be applied to the source and drain electrodes to help modify the work function and aid charge injection.[3] The gate electrode is typically a metal or a conducting polymer, although highly doped silicon can also been used.[2] An insulating inorganic such as silicon dioxide, or a polymer such as PMMA, CYTOP, or Lisicon D139 is usually used as the dielectric.[2] Note the dielectric material should ideally have a high capacitance and dielectric constant, and possess good mechanical and electrical strength.[4,5]

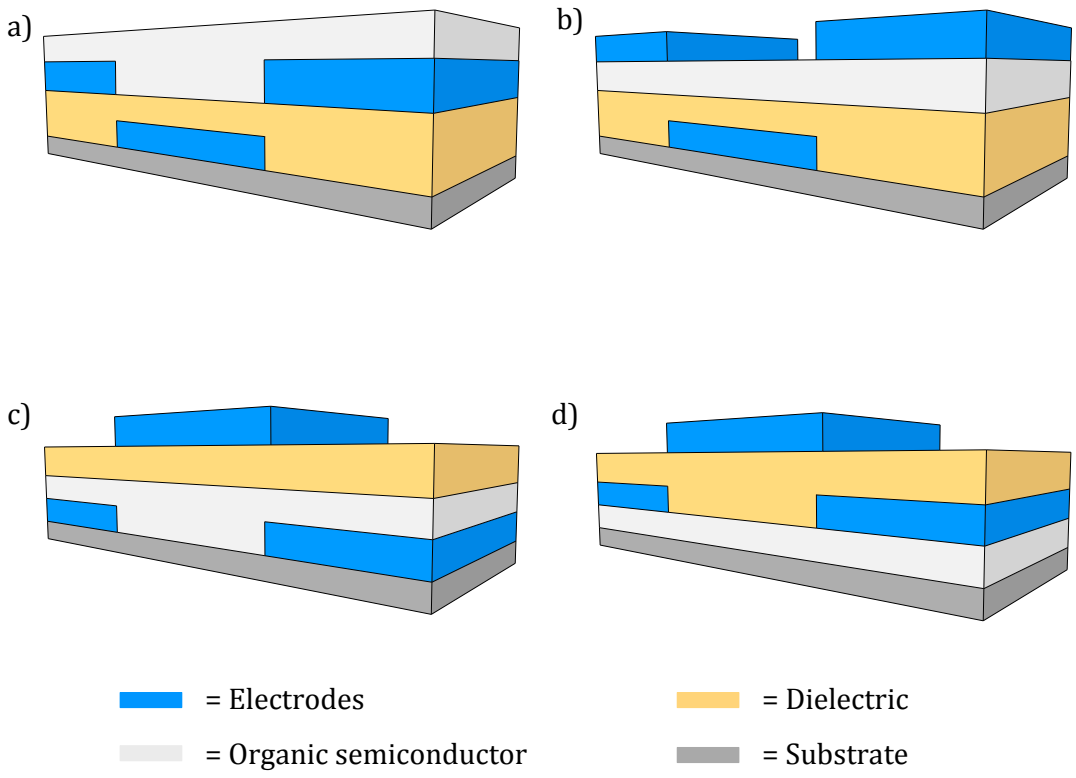

Figure 1.1. Schematic of a) BG-BC, b) BG-TC, c) TG-BC, and d) TG-TC transistor device architectures.

A transistor can be constructed in one of four main architectures (bottom-gate, bottom-contact; bottom-gate, top-contact; top-gate, bottom-contact; or top-gate, top-contact) as depicted in Figure 1.1. There are several advantages and disadvantages associated with each device architecture as a result of differences between the distance charges must travel to reach the conducting channel, the morphology of the interfaces, and depending on the deposition techniques used, the position of the electrodes.[1,2]

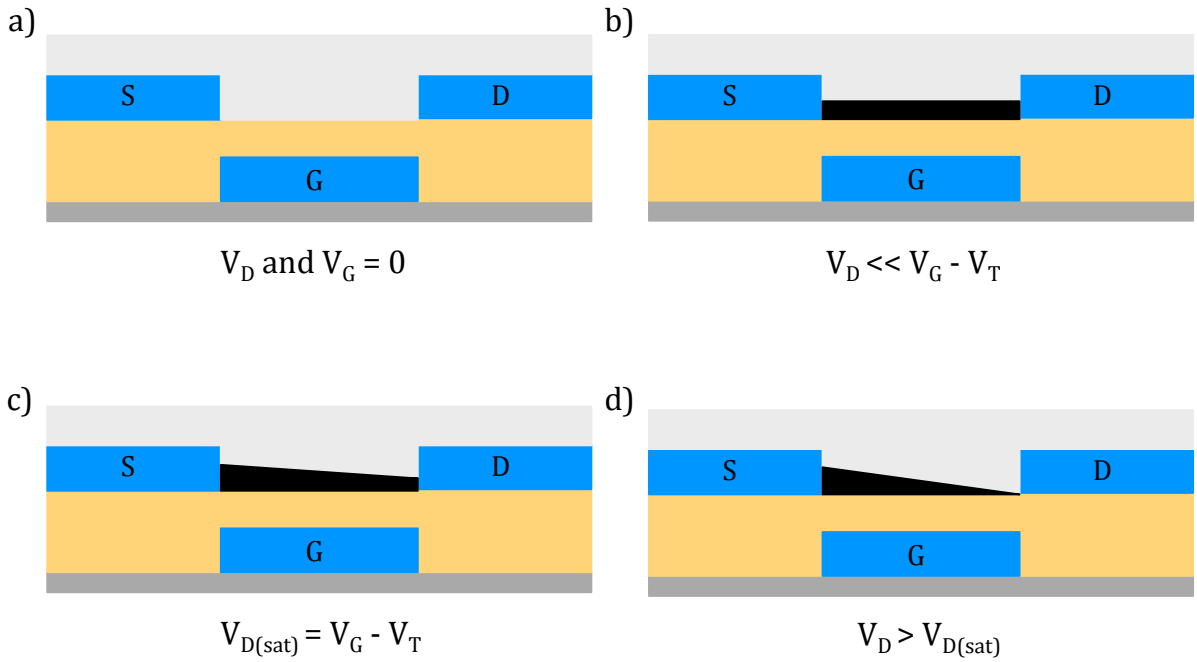

Figure 1.2. Schematic of a BG-BC transistor device in the following stages of operation: a) off-mode, b) linear regime, c) pinch-off, and d) saturation regime. The conducting channel is represented in black.

Figure 1.2 depicts the basic stages of operation of a transistor device which can be summarised as follows:[2]

a) Off-mode. Both the gate and drain voltages are zero. Current is unable to flow between the source and drain electrodes.

b) Linear regime. A gate voltage is applied and charge carriers accumulate at the semiconductor-dielectric interface. A negative gate voltage will induce positive charges (holes), and a positive gate voltage will induce negative charges (electrons), with the charge carrier polarity determining whether the device is p-type, n-type, or ambipolar. Note the organic semiconductor, device architecture, processing conditions, and choice of electrodes can all influence whether a device is p-type, n-type or ambipolar. When a drain voltage is applied, current is able to flow. Provided the drain voltage is less negative than the gate voltage minus the threshold voltage, the device is said to be in the linear regime.

c) Pinch-off. The drain voltage is increased and is now equal to the gate voltage minus the threshold voltage. A depletion region forms next to the drain electrode.
d) Saturation regime. The drain voltage is increased further, and is now greater than the gate voltage minus the threshold voltage. The current saturates and the depletion region increases.

The current-voltage characteristics of a transistor device during the different stages of operation can be calculated from the following expression (Equation 1.1) derived from standard MOSFET equations using the gradual channel approximation:[2]

$$I_D = \frac{W}{L}\mu C_i\left((V_G - V_T)V_D - \frac{V_D^2}{2}\right)$$

Equation 1.1

where I_D is the drain current, W is the channel width, L is the channel length, μ is the charge carrier mobility, C_i is the capacitance per unit area of the dielectric, V_G is the gate voltage, V_T is the threshold voltage, and V_D is the drain voltage.

Hence in the linear regime, where $V_D << V_G - V_T$ this equation can be written as:[2]

$$I_{D(lin)} = \frac{W}{L}\mu_{lin}C_i\left((V_G - V_T)V_D\right)$$

Equation 1.2

And in the saturation regime, where $V_D > V_{D(sat)}$ Equation 1.1 can be simplified to:[2]

$$I_{D(sat)} = \frac{W}{2L}\mu_{sat}C_i(V_G - V_T)^2$$

Equation 1.3

The performance of a transistor device depends on three key parameters: the threshold voltage (V_T), the current on/off ratio (I_{on}/I_{off}), and the charge carrier mobility (μ), which can be derived from the transfer and output characteristics (Figure 1.3).[1] The threshold voltage is defined as the minimum gate voltage needed to obtain a current.[1] The current on/off ratio represents the ratio of the current at the maximum and minimum gate voltage (i.e. at the on and off states).[1] The charge carrier mobility is perhaps the most useful parameter to describe device performance, and is defined as the charge carrier velocity per unit electric field.[1] Using Equations 1.4 and 1.5, values for the mobility in the linear and saturation regimes, respectively, can be calculated.[2]

$$\mu_{lin} = \frac{L}{WC_iV_D}\left(\frac{\partial I_{D(lin)}}{\partial V_G}\right)$$

Equation 1.4

$$\mu_{sat}(V_G) = \frac{L}{W C_i} \frac{1}{(V_G - V_T)} \left(\frac{\partial I_{D(sat)}}{\partial V_G} \right)$$

Equation 1.5

Recently values in excess of 12 cm^2/Vs have been reported for p-type polymer based devices,[6–9] whilst mobilities close to 6 cm^2/Vs have been reported for n-type transistors.[10] Note the performance of n-type materials often lags behind that of p-type materials.[11] This is partly due to problems with device stability, since the negative polaron formed can be chemically reactive.[11] Investigations have shown if the LUMO level is lower than approximately 4.0 eV, then the negative polaron formed is stable in the presence of water (and/or oxygen), and therefore device stability is improved.[11,12] Similarly a high lying LUMO can also lead to injection problems from typical source-drain electrodes.[11]

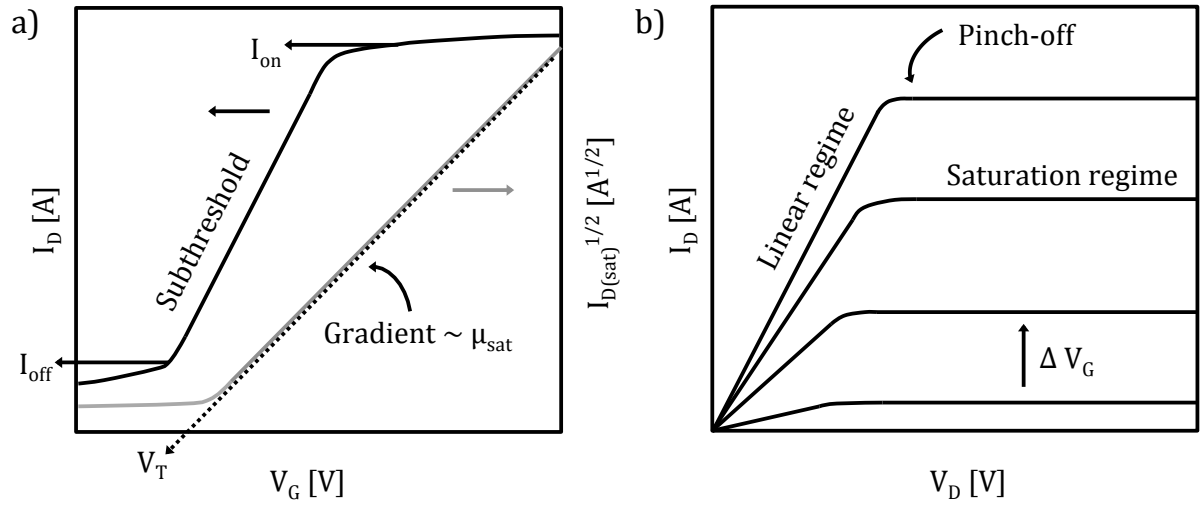

Figure 1.3. Representation of typical a) transfer and b) output characteristics of an OFET device with key terms highlighted.[2]

As shown in Figure 1.4, charge transport in organic semiconductors occurs via intermolecular charge hopping along the π-π and lamellar stacking directions, and intramolecularly along the conjugated backbone.[1,13] Thus a high degree of backbone planarity, strong intermolecular π-π interactions, and appropriate thin film morphology are crucial for efficient charge transport and high charge carrier mobility.[1,13] Note the orientation of the polymer chains relative to the substrate (Figure 1.5) can also have a significant effect on charge transport. Typically since charge migration occurs parallel to the substrate, an edge-on orientation (in which the polymer chains π-π stack parallel to the substrate) usually yields an increase in mobility in a transistor device.[1,13] The use of thermal annealing, side-chain engineering,[14] choice of solvent,[15] and controlled chain alignment (e.g. through the use of a nano-grooved substrate,[9] or off-centre spin-coating[16,17]) are just some examples of ways in which the morphology can be controlled in

order to enhance the mobility. In addition, the molecular weight, polydispersity, and the purity of the polymer can also affect charge transport.[18–22] Typically, a high molecular weight and low polydispersity are needed to enhance connectivity between crystalline regions, and limit grain boundaries.[1] Similarly it is important to control the purity of the material in order to reduce the presence of the charge traps.[13] Note some examples of possible impurities include chemical defects, end groups,[23] and catalytic residues.

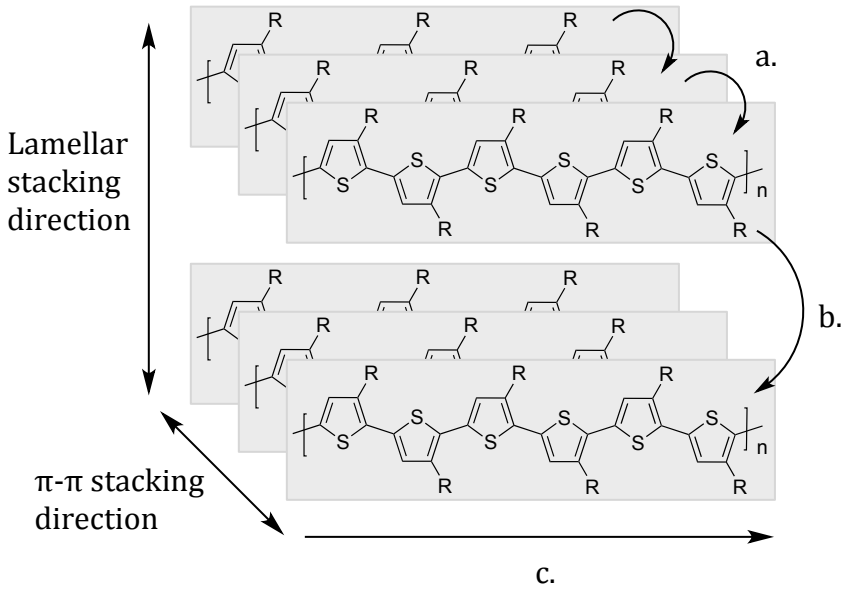

Figure 1.4. Schematic of the modes of charge transport in an OFET device: a) intermolecular along the π-π stacking direction, b) intermolecular along the lamellar stacking direction, and c) intramolecular along the conjugated backbone.[13,24]

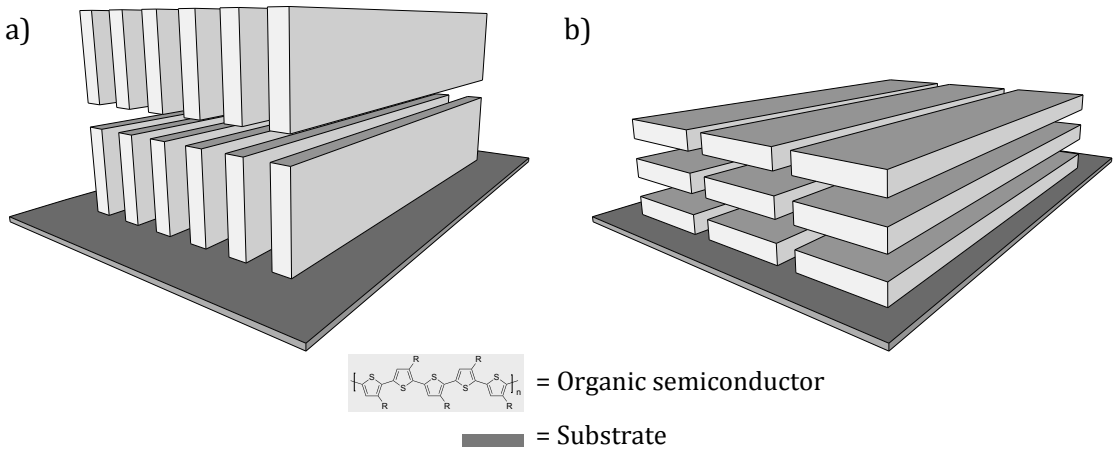

Figure 1.5. Schematic of a) edge-on and b) face-on orientations of the polymer backbone relative to the substrate.

1.2 Organic Photovoltaics

An OPV device is used to convert solar energy to electrical power. It is usually constructed in one of two main architectures (conventional, or inverted) as depicted in Figure 1.6, with the difference between the two being the arrangement of the electrodes.[25] Note other architectures such as bilayer,[26] and tandem[27] also exist but they are beyond the scope of this thesis. In a conventional device the top electrode is the cathode; typically a low work function metal (e.g. calcium, aluminium) that is often prone to atmospheric oxidation.[25] Whilst in an inverted device the structure is reversed, with the cathode now forming the bottom electrode.[25] As such inverted devices are usually more stable and offer improved lifetimes compared to conventional devices.[25] However, due to the position of the cathode, a transparent material (e.g. ITO) must be used.[25] Hole and electron transporting layers are often used to improve charge carrier extraction at the electrodes.[25] Conducting polymers (e.g. PEDOT:PSS) or metal oxides (e.g. V_2O_5, ZnO, MoO_3, TiO_2) are commonly used for these layers.[25] The active layer is typically a binary blend consisting of two components: one donor (e.g. polymer, small molecule) and one acceptor (e.g. fullerene, polymer, small molecule). Note fullerenes (e.g. $PC_{61}BM$, $PC_{70}BM$) are the most widely used acceptor due to their high three-dimensional electron mobility, suitable LUMO energy level, and ability to form favourable phase separated domains in BHJ devices.[28] Despite this, there are several limitations associated with the use of fullerenes (e.g. cost, instability, poor absorption in the visible region), and so recently research into non-fullerene acceptors (e.g. polymers,[29] small molecules[28]) has attracted considerable interest. Non-fullerene acceptors offer several advantages over fullerenes such as high absorption coefficients, and the ability to tune the electronic energy levels to improve photon absorption and charge generation.[28,29]

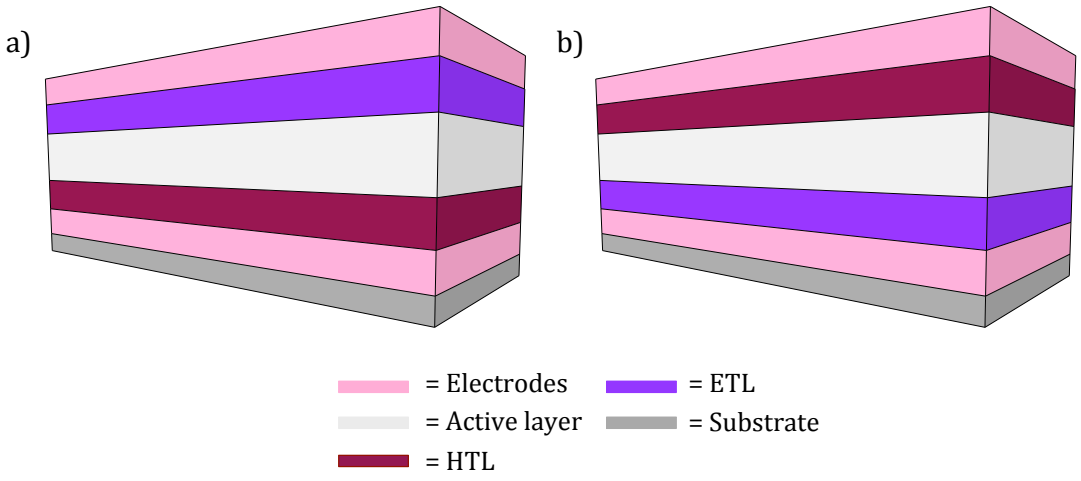

Figure 1.6. Schematic of a) conventional, and b) inverted BHJ OPV device architectures.

In addition, whilst it is beyond the scope of this thesis, it is important to note that there has been a great deal of interest in recent years in the development of ternary blends, in which one additional donor or acceptor with complementary absorption is added to the active layer.[30,31] Depending on the choice of material, the use of a third component has been shown to improve device performance by maximising absorption, enhancing charge transport, and optimising morphology.[30,31] Nevertheless, a great deal of work is still needed to fully understand the fundamental mechanisms, photophysical properties, and morphological features of ternary blends.[30,31]

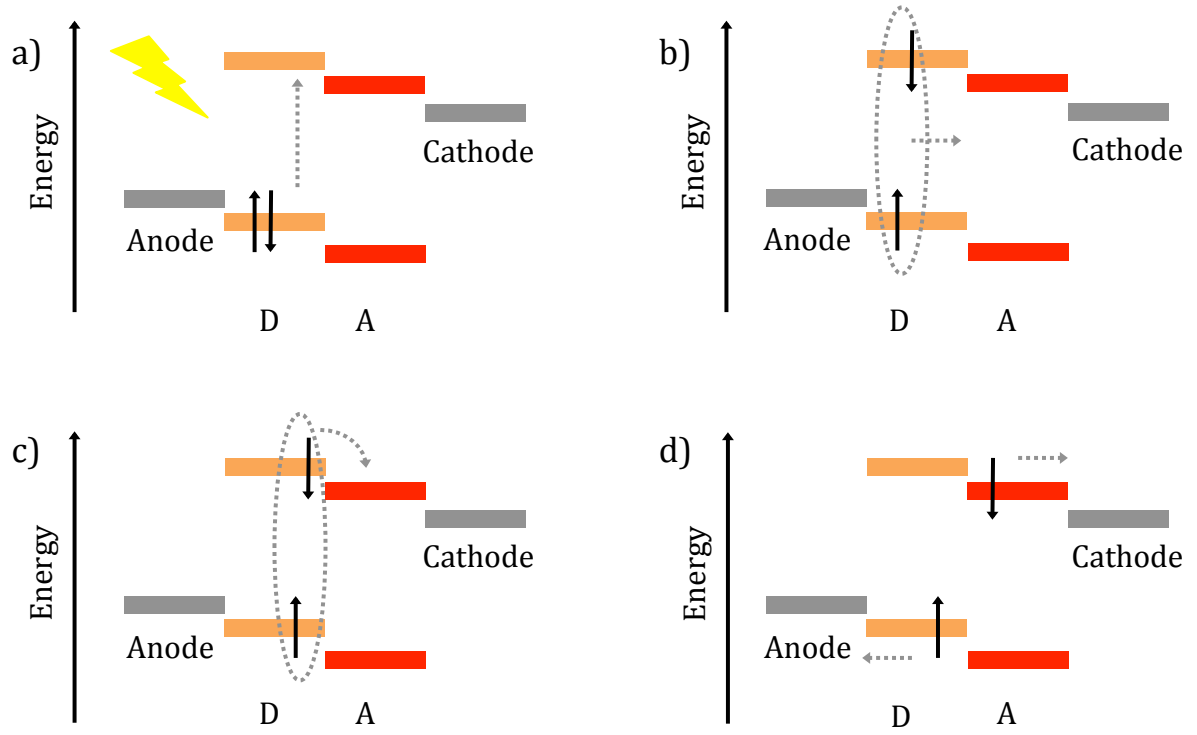

Figure 1.7. Schematic of the following stages of charge generation in a BHJ OPV device: a) absorption of a photon resulting in the excitation of an electron to the LUMO of the donor and the formation of an exciton, b) diffusion of the exciton to the donor-acceptor interface, c) exciton dissociation and charge transfer to the LUMO of the acceptor, and d) charge transport to the electrodes.

The electronic processes involved in charge generation in a BHJ OPV device are depicted in Figure 1.7, and can be summarised as follows:[25,32]

a) Absorption of a photon resulting in the excitation of an electron from the HOMO to the LUMO energy level of the donor. This leads to the formation of an exciton (a Coulombically bound electron-hole pair). Note the wavelength of the incident photon must be greater than or equal to the difference in energy between the HOMO and LUMO levels of the donor in order to be absorbed.

b) Diffusion of the exciton to the donor-acceptor interface. The lifetime of the exciton is short (ranging from 0.1 to 1 ns) which limits the diffusion length to approximately 10 nm.
c) Exciton dissociation and charge transfer to the LUMO of the acceptor. Note the difference in energy between the LUMO levels of the donor and acceptor must be greater than the exciton binding energy (typically between 0.3 and 1 eV) in order for charge separation to occur. At this stage, geminate recombination of the bound charges back to the ground state can occur, limiting charge generation.
d) Charge transport to the electrodes, followed by charge extraction. Note bimolecular recombination of the free charges can compete with charge transport particularly in devices with low intrinsic mobility and poor percolation pathways.

It is important to note that Figure 1.7 shows the process for excitation of the donor but photon absorption in the acceptor is also possible.

The performance of an OPV device depends on four key parameters: the short circuit current density (J_{SC}), the fill factor (FF), the open circuit voltage (V_{OC}), and the power conversion efficiency (PCE), which can be derived from the *J-V* curve and EQE spectra (Figure 1.8).[1] The J_{SC} is defined as the current at zero voltage.[33] It is determined by the number of photons absorbed, the morphology of the active layer, and the intrinsic mobility of the device.[1] As such, control over the optical band gap is particularly important if a high photocurrent is to be achieved. Ideally, a small band gap semiconductor with a broad absorption is necessary.[1] The FF represents the ratio of the actual power output to the theoretical maximum power output, as described by Equation 1.6.[1]

$$FF = \frac{J_{max}V_{max}}{J_{SC}V_{OC}}$$

Equation 1.6

where *FF* is the fill factor, J_{max} is the current at maximum power, V_{max} is the voltage at maximum power, J_{sc} is the short circuit current density, and V_{oc} is the open circuit voltage.

The V_{OC} is defined as the maximum voltage that can be extracted from the device when the current is zero.[33] It is proportional to the difference in energy between the HOMO of the donor and the LUMO of the acceptor, therefore careful consideration of the energetics of co-monomers is important.[1] The power conversion efficiency is perhaps the most important parameter used to describe device performance, and is a measure of the overall conversion of incident photons to electrical power.[1] It can be calculated using the following equation:[34]

$$PCE = \frac{FFJ_{SC}V_{OC}}{P_{in}}$$

Equation 1.7

where *PCE* is the power conversion efficiency and P_{in} is the incident light intensity.

There has been a gradual increase in power conversion efficiency in recent years with values in excess of 9% now reported for polymer:fullerene blends due to improvements in device engineering, material design, morphological control, and a better understanding of the underlying operating principles.[35–39]

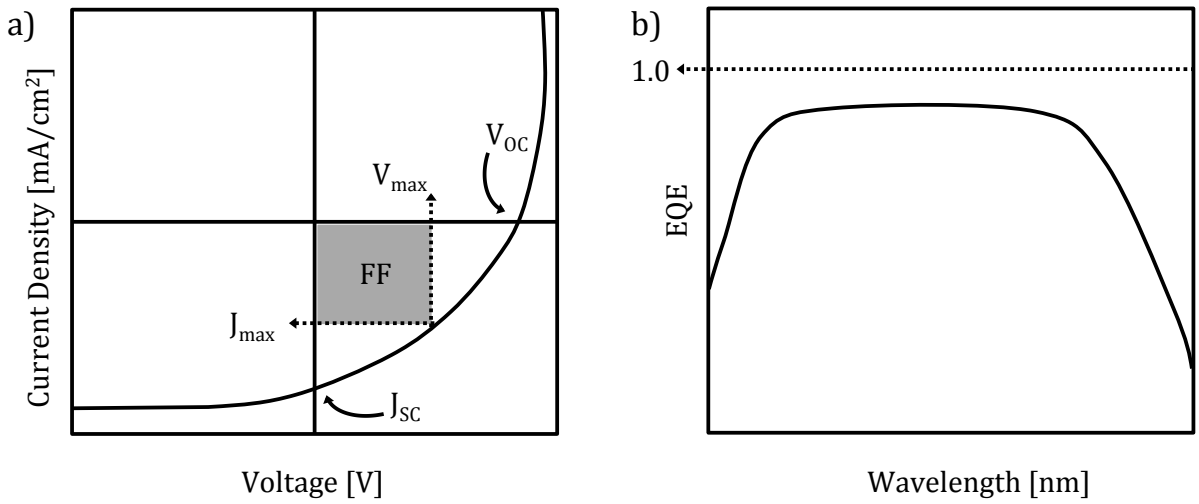

Figure 1.8. Representation of a typical a) *J-V* curve and b) EQE spectra of an OPV device under illumination with key terms highlighted.

The thin film morphology of the active layer blend is crucial for exciton dissociation and efficient charge transport.[40] Early OPV devices were based on a bilayer structure in which thin layers of a donor and acceptor were sandwiched together.[26] Device performance was often low due to the short lifetime of the exciton and the need for very thin active layers, which led to inefficient absorption and charge generation.[25] More recently, the development of BHJ OPV devices has helped significantly improve device performance.[41,42] In a BHJ structure, the active layer is blended together to form an interpenetrating network, which maximises the surface area between the donor and acceptor.[1,25] Often due to the instability of the blend and the crystalline nature of the materials, phase separation occurs resulting in the formation of pure donor and acceptor regions within the amorphous bulk.[43] Whilst to some extent this can be beneficial for device performance, it is important to control the extent of this separation in order to prevent bimolecular recombination and maintain the operational stability of the device.[43] The use of thermal annealing, processing additives (Figure 1.9), and crosslinkers are just some examples of ways in which the blend morphology can be controlled.[43–45]

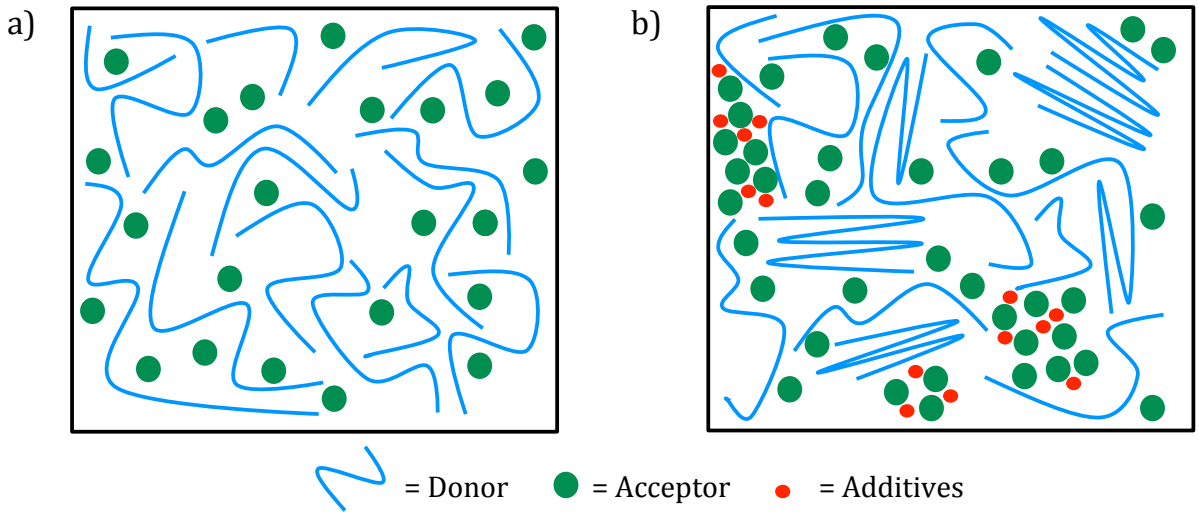

Figure 1.9. Schematic of the typical morphology of a polymer:PCBM blend a) without additives, and b) with additives.[43,46,47]

1.3 Scope and Aims

The aim of this thesis is to design and synthesise novel ring fused conjugated polymers for use in organic electronics. In the first chapter, a series of five polymers based on a novel, five-membered, fused ring dithienogermolodithiophene (DTTG) monomer containing linear tetradecyl side-chains will be reported. The DTTG unit can be considered as an extended version of dithienogermole (DTG). Since co-polymers of DTG have previously demonstrated reasonable transistor performance,[48] it was thought extended analogues could potentially be of interest. Detailed comparisons between the optoelectronic and thin-film morphology of the polymers will be discussed, along with an evaluation of the electrical performance in field-effect transistors.

The second chapter will focus on the synthesis of a novel bisthieno[2',3':4,5]thieno[3,2-*c*:2',3'-*e*]azepine-4,6(5*H*)-dione (BTTA) monomer in which two thieno[3,2-*b*]thiophene units are bridged by an azepine-2,7-dione ring, containing a branched 2-octyldodecyl side-chain. This new unit will be co-polymerised with alkoxy- and alkylthienyl-substituted benzo[1,2-*b*:4,5-*b'*]dithiophene co-monomers to afford a series of three polymers. The choice of co-monomer on the optoelectronic and surface morphology of the polymers will be reported using a combination of experimental techniques. The photovoltaic and electrical performance of the polymers will also be investigated.

The third chapter will explore the use of side-chain engineering to improve the performance of one of the most promising ring fused electron accepting materials;

poly[4,9(benzo[*lmn*][3,8]phenanthroline-1,3,6,8(2*H*,7*H*)-tetrone)-alt-5,5'(2,2'-bithiophene)] (pNDI-BT). In particular, the effect of the alkyl side-chain branching position on the electrical performance will be reported, and for the first time, the influence of the branch-point on the performance of all-polymer OPV devices will be examined. A combination of experimental techniques will be used to investigate the optoelectronic and solid-state organisation of the polymers to help better understand the role of the side-chains. The final chapter will build on this work and use a range of fluorinated and non-fluorinated thiophene and selenophene containing monomers, to further improve the electrical performance of a series of NDI based polymers.

Chapter 2
Dithienogermolodithiophene Polymers for OFET Applications[49]

2.1 Introduction

There has been much recent interest in the development of ring fused monomers as building blocks for high performing conjugated polymers in organic electronics.[50–82] Ring fused monomers are held rigidly co-planar by the use of bridging heteroatoms. This helps reduce the conformational disorder along the backbone and lower the reorganisation energy associated with charge transport, whilst the bridging groups help promote solubility by providing a point of attachment for the side-chains (required for solution processability and high-throughput device fabrication). The nature of the bridging heteroatom is known to have a significant effect on the solid-state packing and optoelectronic properties of the polymer.[55,62,83] Indeed, there have been many reports on how changing the bridging group from for example, C to Si,[84–86] or Ge[48,87–89] can alter the geometry of the monomer due to differences between the C-C, C-Si, and C-Ge bond lengths. In addition, the replacement of C with Si or Ge has also been shown to stabilise the electronic energy levels of the resulting polymer due to the interaction of the σ* orbital of the Si or Ge with the π* orbital of the conjugated backbone.[90] The choice of the side-chains can also have an impact on the solid-state ordering of the polymers,[14,91–94] with branched alkyl-chains often the preferred choice in polymers for solar cell applications where it is important to maintain control over the morphology of the blend, in order to prevent large-scale phase separation. Straight alkyl-chains on the other hand are typically used in polymers for transistor applications where it is important to promote close intermolecular packing.

Recently, we reported the synthesis of a novel, five-membered, ring fused monomer dithienogermolodithiophene (DTTG), in which two thieno[3,2-*b*]thiophene units were bridged by a dialkylgermanium group containing branched 2-ethylhexyl or 2-octyldodecyl side-chains.[95,96] The solar cell performance of donor-acceptor co-polymers of DTTG was promising, with a peak power conversion efficiency of 7.2% reported for a TPD co-polymer in a conventional device, without the use of processing additives.[95] However, the transistor performance was not investigated.

Figure 2.1. Structure of DTG and DTTG monomers.

The DTTG unit can be considered as an extended version of dithienogermole (DTG) (Figure 2.1). Since co-polymers of DTG have previously demonstrated reasonable transistor performance,[48]

it was thought extended analogues could potentially be of interest. Indeed, a recent trend in the development of high performing conjugated polymers has been to increase the number of individual rings in the monomer unit. For example, further extending the length of the five ring indacenodithiophene (IDT) monomer to the seven membered indacenodithieno[3,2-*b*]thiophene (IDTT) unit has been shown to significantly improve the charge carrier mobility and solar cell performance.[70] Hence in this chapter, the transistor performance of a series of DTTG polymers containing straight alkyl-chains was investigated (Figure 2.2).

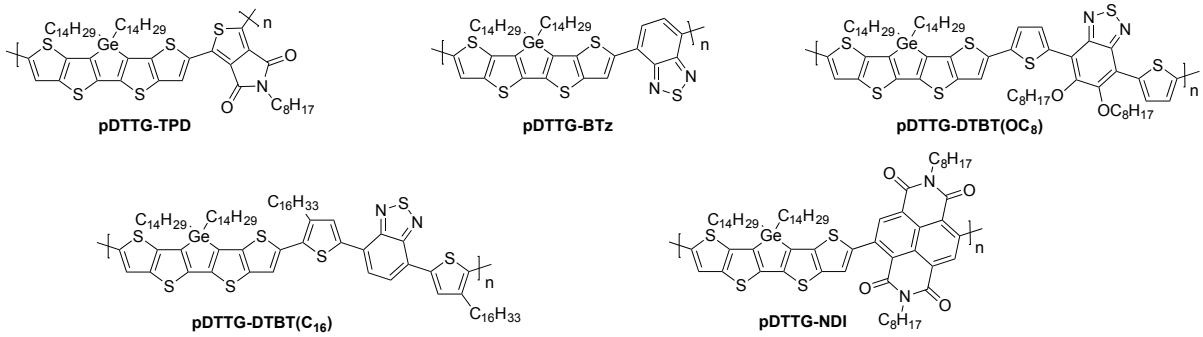

Figure 2.2. Structure of the target polymers.

2.2 Results and Discussion

2.2.1 Monomer Synthesis

The DTTG monomer was synthesised according to our previously reported methodology,[49,95,96] as outlined in Scheme 2.1. First, commercially available thieno[3,2-*b*]thiophene (2.1) was brominated with *N*-bromosuccinimide at room temperature, to afford 2,5-dibromothieno[3,2-b]thiophene (2.2). This was then treated with 1 equivalent of *n*-butyllithium at -78 °C, and reacted with chlorotrimethylsilane to give (5-bromothieno[3,2-*b*]thiophen-2-yl)(trimethyl)silane (2.3) in 86% yield, after purification by column chromatography. 2.3 was then converted to (6-bromothieno[3,2-*b*]thiophen-2-yl)(trimethyl)silane via a halogen dance rearrangement using 1 equivalent of lithium diisopropylamine at -78 °C, and subsequently dimerised in situ via oxidative coupling using copper(II) chloride, to afford (3,3'-dibromo-2,2'-bithieno[3,2-*b*]thiene-5,5'-diyl)bis(trimethylsilane) (2.4). This was then dilithiated with 2 equivalents of *n*-butyllithium at -90 °C, and reacted with dibromobis(tetradecyl)germane (2.5) to form the ring closed [9,9-bis(tetradecyl)-9H-thieno[3,2-*b*]thieno[2",3":4',5']thieno[2',3':4,5]germolo[2,3-*d*]thiene-2,7-diyl]bis(trimethylsilane) (2.6) unit in 54% yield, after purification by column chromatography. Due to the electron rich nature of thieno[3,2-*b*]thiophene, the dianion of 2.4 was found to decompose by ring opening at elevated temperatures. To minimise this the temperature of the reaction was carefully monitored and maintained at -90 °C. Finally, 2.6 was brominated with *N*-bromosuccinimide at

room temperature, and then reacted with 2 equivalents of *tert*-butyllithium at -90 °C, followed by the addition of trimethyltin chloride to afford the requisite distannylated monomer 2,7-bis(trimethylstannyl)-9,9-bis(tetradecyl)-9H-thieno[3,2-*b*]thieno[2",3":4',5']thieno[2',3':4,5]germolo[2,3-*d*]thiophene (2.8). 2.8 was prone to destannylate when purified by column chromatography over normal phase silica, and was instead purified by preparative GPC over cross-linked polystyrene in hexane at 40 °C.

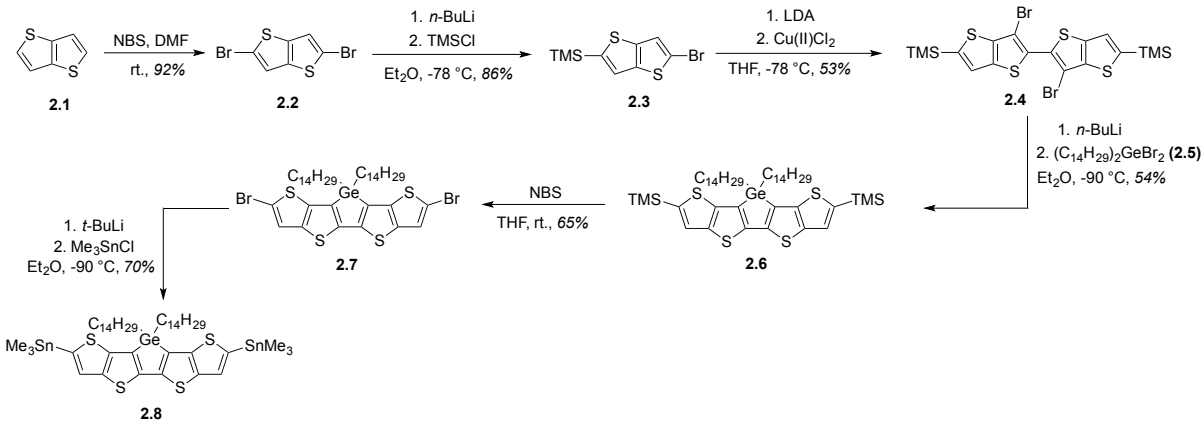

Scheme 2.1. Synthetic pathway to the distannylated DTTG monomer.

2.2.2 Polymer Synthesis

The polymers were synthesised via a combination of microwave assisted Stille (P1 and P3-5),[97–99] and Suzuki-Miyaura (P2) cross-coupling reactions,[100] as outlined in Scheme 2.2. The polymers were purified by sequential Soxhlet extraction to remove low molecular weight oligomers, and polymers of sufficient solubility (P1 and P3-5) were vigorously stirred with aqueous sodium diethyldithiocarbamate trihydrate to remove catalytic impurities,[101,102] and then further purified by preparative GPC (P1 and P4) in chlorobenzene at 80 °C. Due to the absence of any solubilising groups on the 2,1,3-benzothiadiazole-4,7-bis(boronic acid pinacol ester), the solubility of the resulting polymer (P2) was low, and so the polymer was isolated after Soxhlet extraction without further purification. The solubility of P3 was also very poor, even in hot *o*-dichlorobenzene, and therefore purification by preparative GPC was not possible. Instead, the polymer was heated in 1,1,2,2-tetrachloroethane at 140 °C overnight and filtered hot to remove insoluble residues, before a soluble fraction was isolated.[103]

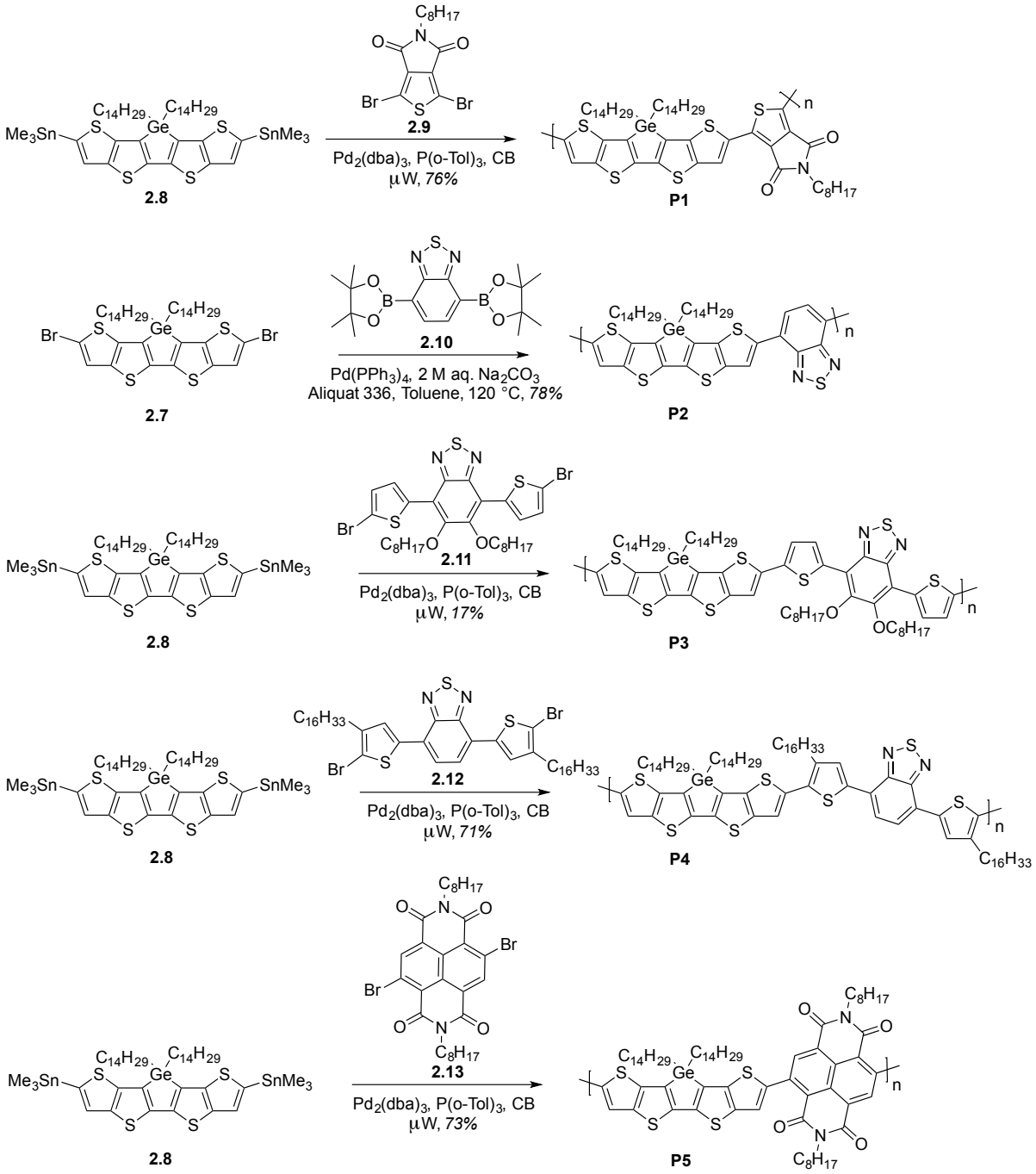

Scheme 2.2. Synthetic pathway to the polymers.

The chemical structure of the polymers was confirmed by elemental analysis, which were in agreement with the theoretical values, and high temperature ^{1}H NMR spectroscopy in 1,1,2,2-tetrachloroethane-d_2 (see Appendix). Consistent with other reports, the ^{1}H spectra of the polymers were rather poorly resolved with broad, featureless peaks. This can be attributed to a combination of the polydisperse nature of the polymers, as well as the aggregation of the polymers in solution.

Polymer molecular weights and dispersities were determined by gel permeation chromatography in either chlorobenzene at 80 °C (P1 and P3-P5), or when polymer solubility was limited, trichlorobenzene at 140 °C (P2). The number-average molecular weights of P1 and P2 were considerably lower than P3, P4, and P5, as shown in Table 2.1. Three separate polymerisations were performed for P1 using different batches and concentrations of the 2,7-bis(trimethylstannyl)-9,9-bis(tetradecyl)-9H-thieno[3,2-*b*]thieno[2",3":4',5']thieno[2',3':4,5]germolo[2,3-*d*]thiophene (2.8) monomer, but in all cases similar molecular weights were obtained. The polymer exhibits reasonable solubility and so it is believed the low weight is associated with poor reactivity of the monomer under the polymerisation conditions, rather than precipitation of the polymer during the reaction. The low weight of P2 on the other hand is believed to be a result of the poor solubility of the polymer, resulting in the early termination of chain growth during polymerisation.

Table 2.1. Molecular Weights and Thermal Properties

	M_n[a] [kg/mol]	M_w[a] [kg/mol]	Đ[a]	T_d[b] [°C]
P1	7	10	1.5	432
P2	7†	10†	1.4†	438
P3	35	88	2.5	350
P4	27	51	1.9	437
P5	42	184	4.4	440

[a] Determined by GPC in CB at 80 °C against polystyrene standards with the exception of † which was determined by HT-GPC in TCB at 140 °C. [b] 5% weight loss temperatures measured by thermal gravimetric analysis under a N_2 atmosphere.

The thermal stability of the polymers was confirmed by thermogravimetric analysis (see Appendix and Table 2.1), in which a 5% weight loss was observed at 350 °C for P3, and after 430 °C for the remaining polymers.

Due to inherent limitations in the solubility of P2 it will not be discussed further.

2.2.3 Optical Properties and Frontier Molecular Orbital Energy Levels

The optical properties of the polymers were investigated by UV-vis absorption spectroscopy. Figure 2.3 and Table 2.2 display the optical data of the polymers in dilute chlorobenzene and as thin-films, spin-coated from chlorobenzene (5 mg/mL). In solution, P1, P3, and P4 exhibit absorption maxima at 590, 595, and 605 nm, respectively. In thin film, these peaks are red-shifted to 598, 612, and 661 nm, respectively. In the case of P1, this is accompanied by the appearance of a pronounced shoulder at 653 nm, and in the case of P4, a less well-defined

shoulder at 726 nm. The significantly larger red-shift of P4 upon film formation is believed to be related to the more torsionally twisted structure of the polymer in solution compared to the other polymers, as discussed further in Section 2.2.4. The red-shifts observed upon film formation and the appearance of the long wavelength shoulders are attributed to enhanced intermolecular ordering and backbone planarisation. The optical spectra of P1 are very similar to those of the previously reported branched chain analogues,[95,96] despite differences in the molecular weights of the polymers. This similarity suggests the effective conjugation length has been reached for P1. In contrast to the other polymers, the optical absorption spectra of P5 are broad and span the visible to near-infrared range. This is due to the inclusion of the strong acceptor NDI in the polymer backbone. In solution, the polymer exhibits an absorption maximum at 752 nm and a pronounced shoulder at 824 nm. In thin film, the intensity of this shoulder increases and it becomes the maximum absorption peak.

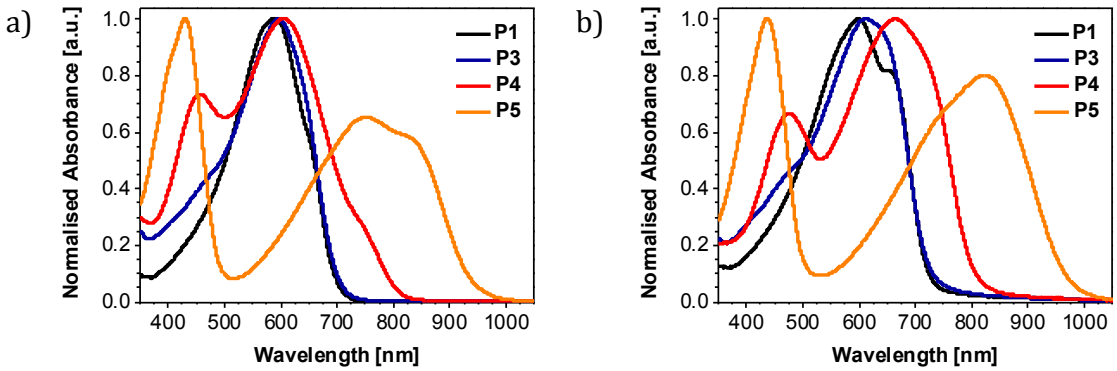

Figure 2.3. Normalised UV-vis absorption spectra of the polymers in a) dilute chlorobenzene solution at 20 °C and b) thin-films spin-coated on glass substrates from chlorobenzene solution (5 mg/mL).

The ionisation potentials of thin films of the polymers, spin-coated from chlorobenzene (5 mg/mL) were measured using photoelectron spectroscopy in air. As shown in Table 2.2, the nature of the co-monomer had a significant impact on the values obtained. The ionisation potential of P1 (5.24 eV) is slightly smaller than that of the previously reported branched 2-ethylhexyl (5.33 eV) and 2-octyldodecyl (5.52 eV) analogues, despite the error of the measurement (± 0.05 eV).[96] This is in contrast to earlier reports that suggest the inclusion of longer alkyl-chains inhibits molecular ordering and results in a lowering of the ionisation potential.[96] Due to the presence of the electron rich thiophene flanking groups in the DTBT co-monomer, the ionisation potentials of P3 (4.80 eV) and P4 (4.84 eV) are substantially smaller than that of P1. It is interesting to note that differences in the substitution pattern of the DTBT unit have little effect on the ionisation potential of the resulting polymer. The inclusion of the

strong electron acceptor NDI in P5, results in a considerably higher ionisation potential of 5.50 eV, compared to the other polymers.

The LUMO energy of the polymers could not be directly measured and were instead estimated by adding the negative of the ionisation potential to the optical band gap (measured from the absorption onset in the solid state). Although such an estimate does not take into account the exciton binding energy,[104] it allows for a convenient comparison between the polymers. Encouragingly, the LUMO energy of P5 (-4.23 eV) is significantly lower than that of the other polymers (-3.09 to -3.53 eV). It is anticipated that at this level, electron injection from common source drain electrodes in OFET devices may be possible.

Table 2.2. Optical Properties and Frontier Molecular Orbital Energy Levels

				PESA		DFT		
	λ_{max} Soln[a] [nm]	λ_{max} Film[b] [nm]	E_g opt[c] [eV]	I.P.[d] [eV]	LUMO[e] [eV]	HOMO[f] [eV]	LUMO[f] [eV]	E_g opt[g] [eV]
P1	590	598 (653)	1.71	5.24	-3.53	-5.10	-3.26	1.84
P3	595	612	1.71	4.80	-3.09	-4.79	-3.17	1.62
P4	605	661 (726)	1.54	4.84	-3.30	-4.85	-3.38	1.47
P5	752 (824)	824	1.27	5.50	-4.23	-5.28	-3.92	1.36

[a] Measured in dilute CB at 20 °C. Shoulder peaks in parentheses. [b] Thin-films spin-coated on glass substrates from 5 mg/mL CB solution. Shoulder peaks in parentheses. [c] Determined from the absorption onset in the solid state. [d] Determined by PESA (error ± 0.05 eV). [e] Estimated by adding the negative of the ionisation potential to the absorption onset in the solid state. [f] Calculated by DFT at the B3-LYP/6-311G(D) level using the minimum energy conformation of the trimers. Alkyl-chains were substituted for methyl groups. [g] Calculated using the following equation: E_g = LUMO - HOMO.

The frontier molecular orbital energy levels of the polymers in vacuum were also evaluated using density functional theory at the B3-LYP[105] hybrid functional level of theory, using a 6-311G(D) basis set. To reduce computational demands each polymer was modelled as a trimer, with alkyl-chains substituted for methyl groups. Although the absolute values are different,[106] the trends predicted in the computationally calculated results are similar to those observed experimentally (Table 2.2). Graphical representations of the computationally calculated HOMO and LUMO energy level, electron density plots are presented in Figure 2.4. In contrast to the other polymers in which the HOMO is delocalised over the whole backbone, the HOMO of P5 is predominantly located on the DTTG unit. The LUMO of the polymers (P3-5) on the other hand, is relatively localised on the acceptor co-monomer except for P1, in which the LUMO is effectively delocalised over the backbone.

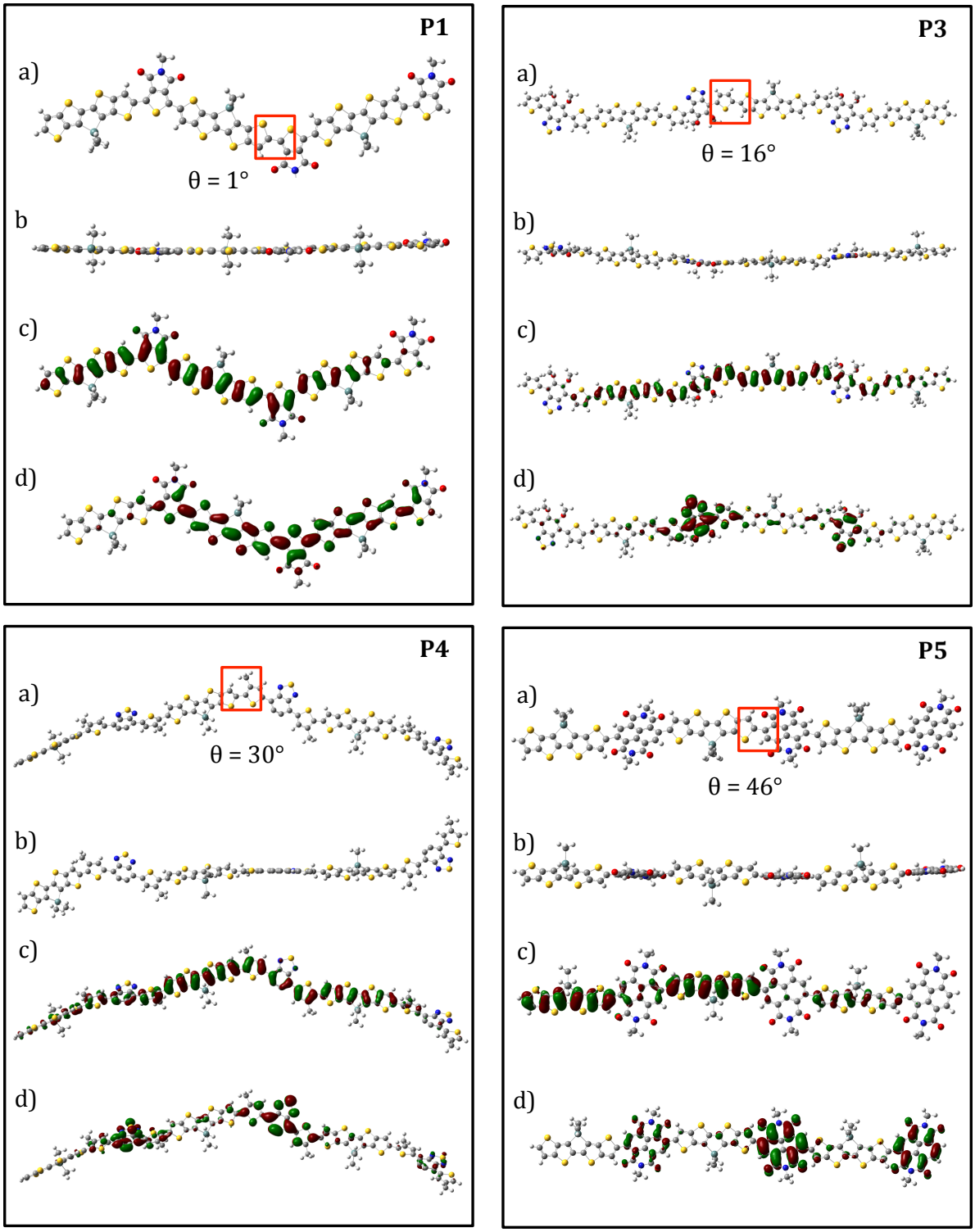

Figure 2.4. a) Face-on, and b) side-on images of the minimum-energy conformation of the polymers modelled as trimers, and visualisation of c) HOMO, and d) LUMO energy level electron density distribution calculated using DFT (B3-LYP/6-311G(D)). The torsional angle (θ) between the central DTTG unit and adjacent co-monomer is highlighted. Alkyl-chains were substituted for methyl groups.

2.2.4 Polymer Conformation and Packing

The optimised geometry of the polymers was investigated using DFT (B3-LYP/6-311G(D)). To avoid the possibility of obtaining local energy minima, the structures were allowed to relax from either an all-cis or an all-trans conformation with respect to the bond between the DTTG unit and adjacent co-monomer. To minimise the number of calculations the relative geometry of the DTBT unit was fixed, so that one thiophene faced the N of the thiadiazole ring and one faced the opposite direction. As shown in Figure 2.4, there are substantial differences in backbone planarity between the polymers. In the case of P1 an essentially coplanar backbone was predicted (θ = 1°), in agreement with the literature,[96] whereas P3, P4, and P5 are predicted to have a relatively twisted backbone. Interestingly, the torsional angle between the DTTG unit and DTBT co-monomer in P3 (θ = 16°) and P4 (θ = 30°) is significantly different, despite the structural similarity. This is due to the regiochemistry of the hexadecyl side-chains in P4 causing a steric interaction with the adjacent DTTG unit, leading to a more contorted backbone.

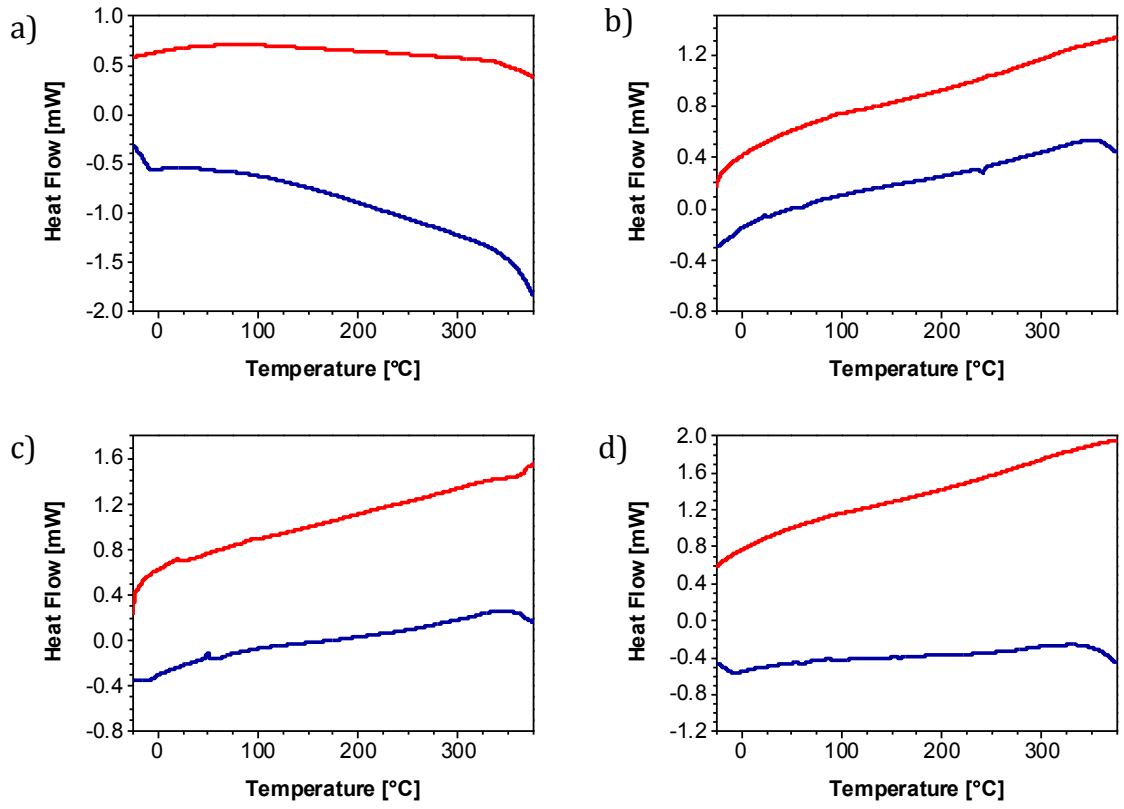

Figure 2.5. Second heating (red) and cooling (blue) scans of a) P1, b) P3, c) P4, and d) P5 measured by DSC, at a rate of 10 °C/min under a N_2 atmosphere.

The thermal properties of the polymers were evaluated using differential scanning calorimetry measurements. Figure 2.5 shows the second heating and cooling scans of the polymers recorded

between -30 and 380 °C under nitrogen. In all cases, no obvious thermal transitions were observed in the temperature range studied.

The solid-state morphology of thin films of the polymers was probed using out-of-plane X-ray diffraction. Figure 2.6 displays the diffraction patterns of the polymers, drop-coated from *o*-dichlorobenzene (7 mg/mL) and annealed at 100, 150, or 175 °C for 2 minutes. Rather surprisingly, no diffraction peaks were observed for P1 at the temperatures studied, despite the essentially coplanar backbone conformation predicted by DFT. However, since previous reports found the 2-octyldodecyl analogue to have a much weaker diffraction pattern than the 2-ethylhexyl derivative,[96] it is believed the incorporation of longer side-chains (tetradecyl) disrupts lamellar ordering. In contrast, P3, P4, and P5 exhibit strong first order diffraction peaks at 3.6°, 3.4°, and 4.8° (2θ), corresponding to a lamellar d-spacing of 24.2, 26.1, and 18.4 Å, respectively, after annealing at 100 °C. A weak second-order diffraction peak at 6.8° (2θ) is also observed for P4 after annealing at 100 °C. However, only after annealing at higher temperatures (150 or 175 °C) are second-order diffraction peaks observed for P3 and P5 (2θ = 6.8° and 10.0°, respectively), and in the case of P3, a third-order diffraction peak is also visible at 11.4° (2θ).

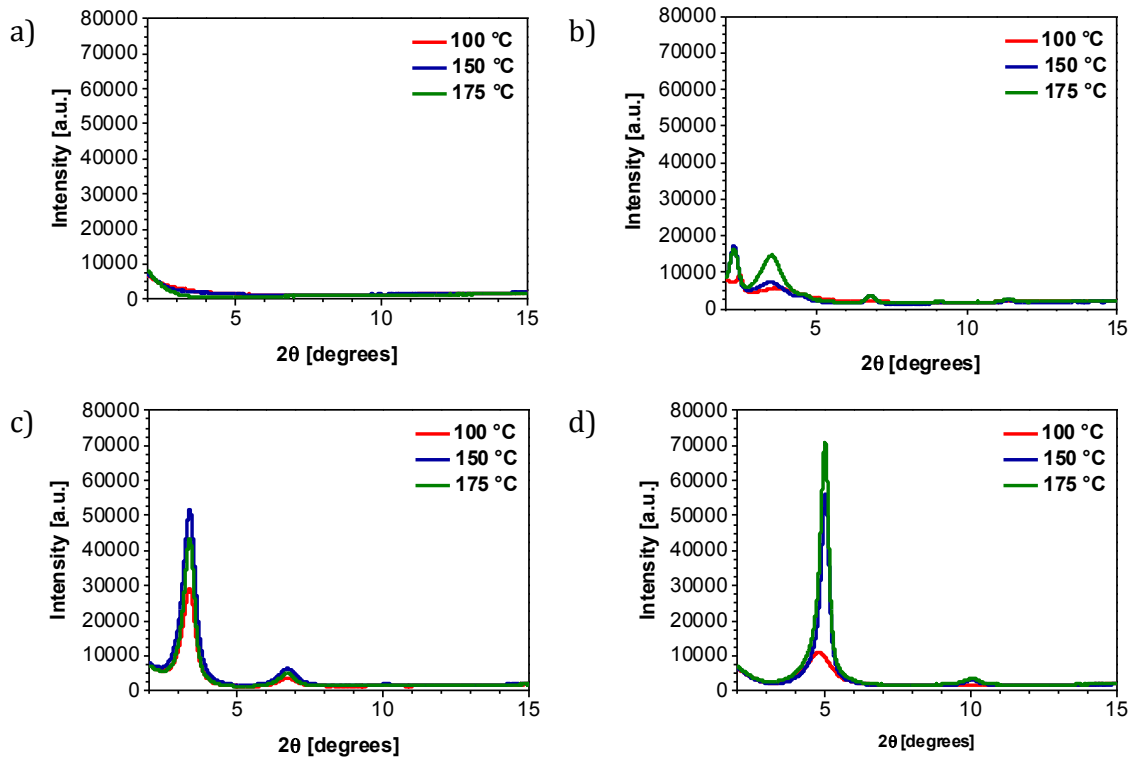

Figure 2.6. X-ray diffraction patterns of a) P1, b) P3, c) P4, and d) P5 drop-coated on glass substrates from *o*-dichlorobenzene solution (7 mg/mL) and thermally annealed at 100 °C (red line), 150 °C (blue line), or 175 °C (green line) for 2 min under an Ar atmosphere.

2.2.5 OFET Device Performance

The electrical performance of the polymers was investigated in TG-BC field effect transistors fabricated on glass, using silver source-drain electrodes, and Lisicon D139 dielectric. For initial testing, polymer films were spin-coated from *o*-dichlorobenzene (7 mg/mL) and annealed at 100 or 150 °C, for 2 min (Table 2.3). P1, P3, and P4 exhibited unipolar, p-type charge transport with average saturated charge carrier mobilities of 0.023, 0.002, and 0.01 cm^2/Vs, respectively, after annealing at 100 °C. The low performance of P3 compared to the other polymers is most likely due to the poor solubility of the polymer and difficulties in forming a homogenous film, as discussed in Section 2.2.2. In contrast to the other polymers, P5 demonstrated ambipolar behaviour with average saturated hole and electron mobilities of 0.0007 and 0.003 cm^2/Vs, respectively. This is in agreement with the low-lying LUMO energy level calculated in Section 2.2.3. Annealing at higher temperatures (150 °C) had little effect on the performance of P1 (0.023 cm^2/Vs), however a modest improvement in mobility was observed for P3 (0.004 cm^2/Vs), while the performance of P4 was significantly enhanced (0.024 cm^2/Vs).

Encouraged by these results, the performance of P4 was evaluated further, in particular focussing on the use of non-chlorinated solvents. A peak saturated charge carrier mobility of 0.22 cm^2/Vs was observed for TG-BC devices of P4, spin-coated from 1,3,5-trimethylbenzene:1-methylnaphthalene solution (1:1) (7 mg/mL) and annealed at 150 °C for 2 min. Note at the time of writing this was the highest reported charge carrier mobility of any germanium based polymer.[107] However since then, mobilities as high as 0.55 cm^2/Vs have been demonstrated for an end-capped DTG based polymer, drop-coated from *o*-dichlorobenzene.[23] One of the major drawbacks limiting the commercialisation of many conjugated polymers is that they are only soluble in high boiling and toxic, chlorinated solvents that are not acceptable for use in industry.[15,108–110] However, the torsionally twisted backbone of P4 and the presence of hexadecyl side-chains on the DTBT unit ensures good solubility of the polymer, even in a non-chlorinated solvent mixture. Moreover, the performance of devices spin-coated from this solvent mixture was remarkably higher than those using *o*-dichlorobenzene. This is most likely due to changes in the morphology of the thin film as a result of the solvent, although further characterisation of the solid-state ordering of films spin-coated from this solvent mixture is needed to validate this.

Table 2.3. OFET Device Characteristics[a]

	Average 100 °C		Average 150 °C		Peak[b]	
	$\mu_{h\ sat}$ [cm²/Vs]	$\mu_{h\ lin}$ [cm²/Vs]	$\mu_{h\ sat}$ [cm²/Vs]	$\mu_{h\ lin}$ [cm²/Vs]	$\mu_{h\ sat}$ [cm²/Vs]	$\mu_{h\ lin}$ [cm²/Vs]
P1	0.023	0.034	0.023	0.029	0.024	0.036
P3	0.002	0.002	0.004	0.004	0.0038†	0.0046†
P4	0.01	0.027	0.024	0.056	0.22‡	0.26‡
P5	0.0007 (0.003)	0.0007 (0.002)	-	-	-	0.0008 (0.01)

[a] TG-BC devices fabricated on glass using Ag source-drain electrodes and Lisicon D139 dielectric. Polymer active layers were spin-coated from *o*-DCB solution (7 mg/mL) and annealed at 100 or 150 °C for 2 min. [b] Peak values reported for devices processed from *o*-DCB solution (7 mg/mL) and annealed at 100 °C for 2 min with the exception of † which was annealed at 150 °C for 2 min, and ‡ which was spin-coated from 1,3,5-trimethylbenzene:1-methylnaphthalene solution (1:1) (7 mg/mL) and annealed at 150 °C for 2 min. Values in parentheses correspond to electron charge transport.

2.3 Conclusion

In this chapter, the synthesis of a novel DTTG monomer containing linear tetradecyl side-chains was described. In order to evaluate the potential of this monomer, a series of five polymers, incorporating monomers of varying electron-accepting strength were prepared, using a combination of microwave assisted Stille, and Suzuki-Miyaura cross-coupling reactions. Initial efforts focused on the synthesis of TPD (P1) and BTz (P2) co-polymers to enable a comparison to our previously reported, high performing, branched chain analogues.[95,96] However, in the straight chain DTTG polymer, the absence of any solubilising groups on the BTz unit resulted in poor polymer solubility, and so BTz co-polymers containing flanking thiophene groups and additional alkyl-chains were synthesised (P3-4). As a final co-monomer, a strong electron acceptor (NDI) was chosen (P5) in order to explore the electron transport properties of the DTTG unit.

The choice of acceptor co-monomer was shown to have a pronounced influence on the optoelectronic properties of the polymers measured using UV-vis and photoelectron spectroscopy in air. As expected, the LUMO energy of P5 (-4.23 eV) was significantly lower than that of the other polymers (-3.09 to -3.53 eV), suggesting electron transport may be possible in transistor devices. The morphology of thin films of the polymers measured using X-ray diffraction, and computational calculations of the polymers modelled as trimers using density functional theory also indicated substantial differences in backbone planarity and polymer packing across the series. In particular, P3-5 were predicted to have a relatively twisted backbone by DFT, and a greater degree of thin film order by XRD, in comparison to P1.

The electrical performance of the polymers investigated in TG-BC field effect transistors was promising, with P1, P3, and P4 exhibiting unipolar, p-type charge transport ranging from 0.004 to 0.024 cm^2/Vs in devices spin-coated from *o*-dichlorobenzene (7 mg/mL) and annealed at 150 °C for 2 min. Upon further optimisation, a peak saturated hole mobility of 0.22 cm^2/Vs was observed for P4 when spin-coated from 1,3,5-trimethylbenzene:1-methylnaphthalene solution (1:1) (7 mg/mL) and annealed at 150 °C for 2 min. It is believed the torsionally twisted backbone calculated by DFT, and the presence of hexadecyl side-chains on the DTBT unit enabled good solubility of the polymer in this non-chlorinated solvent mixture. Note until recently this was the highest reported charge carrier mobility of any germanium based polymer.[23,107] In contrast to the other polymers, P5 demonstrated ambipolar behaviour, as anticipated from the DFT and PESA data.

Chapter 3
Bisthieno[2',3':4,5]thieno[3,2-*c*:2',3'-*e*]azepine-4,6(5*H*)-dione Polymers for OPV and OFET Applications

3.1 Introduction

Recently, a novel ring fused monomer bisthieno[3,2-c:2',3'-e]azepine-4,6(5*H*)-dione (BTA) was reported for use in high performing conjugated polymers in organic electronics (Figure 3.1).[111] Promising charge carrier mobilities were demonstrated in transistor devices for both a BTA-homo-polymer and various donor-acceptor BTA co-polymers, due to a high degree of crystallinity and thin-film order as a result of the planarity of the BTA unit.[112] The solar cell performance of BTA co-polymers was also impressive, with a peak power conversion efficiency of 5.50% reported for a benzo[1,2-*b*:4,5-*b'*]dithiophene (BDT) co-polymer in an inverted device, with the use of an additive.[113] However, despite having a large V_{OC} (0.92 V) the performance of the device was thought to be limited by the large optical band gap (around 1.93 eV),[113] and so further examples of BTA co-polymers were investigated, prompting an increase in OPV performance. For example, a dithienosilole co-polymer demonstrated a power conversion efficiency of 6.41%, as a result of a reduction in the band gap (to around 1.75 eV), which yielded an increase in the J_{SC}.[114] A further increase in performance to 8.66% was also reported for a terthiophene co-polymer with a high V_{OC} of 0.86 V, and FF of 0.78.[115] However, similar to the BDT example the optical band gap was large (1.81 eV),[115] suggesting further efforts to reduce the band gap could potentially be of interest.

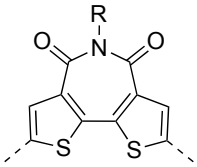

BTA

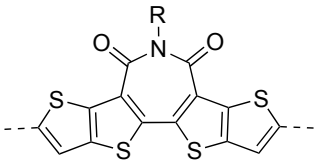

BTTA

Figure 3.1. Structure of BTA and BTTA monomers.

One of the most common ways to reduce the band gap is to increase the effective conjugation length, for example, by increasing the number of individual rings in the monomer unit. Note modification of the optical band gap can also be achieved through careful consideration of the choice of donor and acceptor co-monomer, as well as by minimising backbone twisting, and increasing the molecular weight. Hence in this chapter, the synthesis of an extended version of BTA, known as bisthieno[2',3':4,5]thieno[3,2-*c*:2',3'-*e*]azepine-4,6(5*H*)-dione (BTTA) was reported (Figure 3.1). This novel, five-membered unit was co-polymerised with a range of BDT co-monomers, since previous reports of BDT based polymers demonstrate some of the highest OPV and transistor performances to date, due to the symmetric, rigid, and planar nature of the BDT unit.[68,116–122]

3.2 Results and Discussion

3.2.1 Monomer Synthesis

The BTTA monomer was synthesised following modified literature procedures, as outlined in Scheme 3.1. Initial efforts, based on the related work of Letizia et al.[111] for the analogous thiophene based materials focused upon the formation of [2,2'-bithieno[3,2-*b*]thiophenyl]-3,3'-dicarboxylic acid (3.2) as a key intermediate. Thus (3,3'-dibromo-2,2'-bithieno[3,2-*b*]thiene-5,5'-diyl)bis(trimethylsilane) (2.4) (synthesised as mentioned previously in Chapter 2) was lithiated with 2 equivalents of *n*-butyllithium at -90 °C, and subsequently reacted with gaseous CO_2. However this was unsuccessful, possibly due to the low reactivity of CO_2 at -90 °C, or the difficulty in fully drying the gas, and no desired product was obtained. Instead, 2.4 was first converted to diethyl-5,5'-bis(trimethylsilyl)-[2,2']-bi-[thieno[3,2-*b*]thiophenyl]-3,3'-dicarboxylate (3.1) by reaction of the dilithium salt with ethyl chloroformate at -90 °C. The resulting ester, which was isolated in good yield, was hydrolysed with sodium hydroxide, and treated with concentrated hydrochloric acid, to give [2,2'-bithieno[3,2-*b*]thiophene]-3,3'-dicarboxylic acid (3.2) in 88% yield. Note the trimethylsilyl-protected groups were also removed under these conditions. The diacid was converted to the anhydride by treatment with refluxing acetic anhydride to afford the ring closed bisthieno[2',3':4,5]thieno[3,2-*c*:2',3'-*e*]oxepine-4,6-dione (3.3) unit in 74% yield. Due to the poor solubility of 3.3 in common organic solvents, and the tendency of the anhydride ring to decompose under aqueous conditions, purification was difficult, and so 3.3 was used directly in the following steps without purification. Finally, 3.3 was subjected to a microwave-assisted condensation reaction with a branched amine in the presence of catalytic DMAP to give 5-(2-octyldodecyl)-4H-bisthieno[2',3':4,5]thieno[3,2-*c*:2',3'-*e*]azepine-4,6(5*H*)-dione (3.4) in 18% yield, and subsequently brominated with *N*-bromosuccinimide at room temperature to give the requisite dibrominated monomer, 2,8-dibromo-5-(2-octyldodecyl)-4H-bisthieno[2',3':4,5]thieno[3,2-*c*:2',3'-*e*]azepine-4,6(5*H*)-dione (3.5) in 39% yield, after purification by column chromatography. Note several attempts to optimise the condensation reaction were made (see Appendix), however they all proved unsuccessful. The choice of alkyl-chain (branched vs. linear) on the reaction yield was also explored (see Appendix), since previous reports for the analogous thiophene based materials suggest the use of branched alkyl-chains lowers the yield, but are often necessary to ensure solubility of the resulting polymers.[111,114]

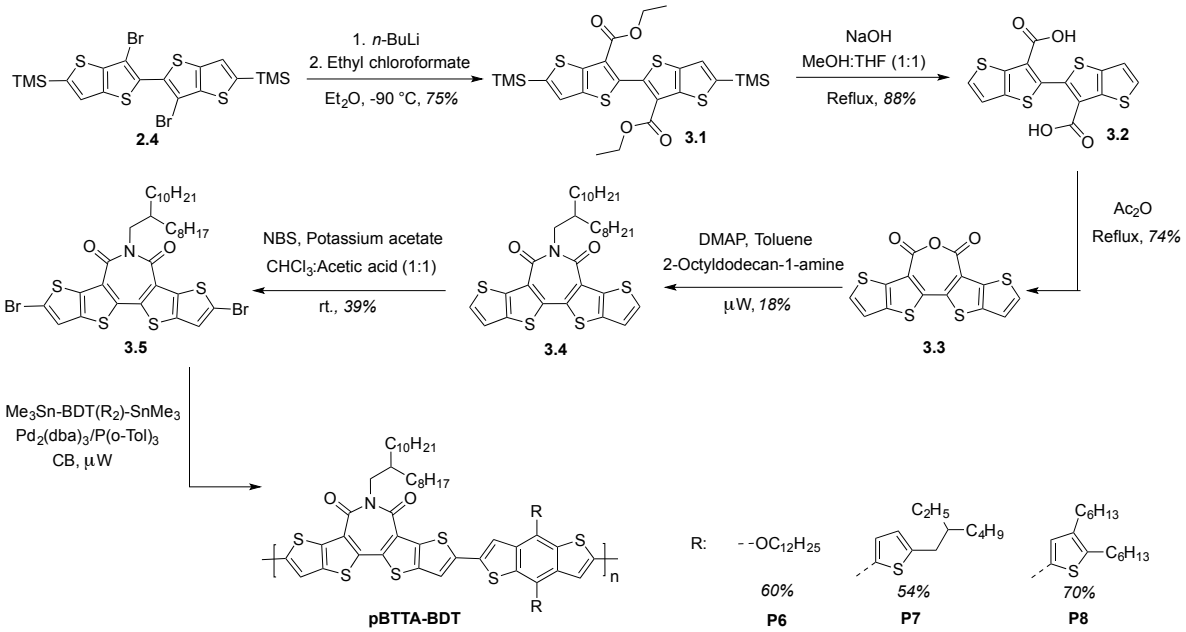

Scheme 3.1. Synthetic pathway to the polymers.

3.2.2 Polymer Synthesis

The polymers were synthesised via microwave assisted Stille cross-coupling reactions[97–99] of the 2,8-dibromo-5-(2-octyldodecyl)-4H-bisthieno[2',3':4,5]thieno[3,2-*c*:2',3'-*e*]azepine-4,6(5*H*)-dione (3.5) unit with the corresponding distannylated co-monomer, as outlined in Scheme 3.1. The polymers were purified by precipitation and subsequent Soxhlet extraction (methanol, acetone, hexane, and chloroform), to remove low molecular weight oligomers. After concentration, the chloroform extracts were further purified by precipitation in methanol, and dried under high vacuum to isolate the polymers. The chemical structure of the polymers was evaluated using elemental analysis, which were in agreement with the theoretical values, and ^{1}H NMR spectroscopy. However, despite the use of a high boiling point, deuterated solvent (1,1,2,2-tetrachloroethane-d_2) at 130 °C, the ^{1}H spectra of the polymers were poorly resolved and difficult to assign (see Appendix), especially for P6 in which no aromatic signals were observed. This is in part believed to be related to the low concentration of the polymer in solution (ca. 4.5 mg/mL), as well as strong intermolecular aggregation.

The solubility of the polymers in chlorobenzene was low, particularly for P6. As such, the molecular weight of P6 was determined by gel permeation chromatography in trichlorobenzene at 140 °C. For P7 and P8, the solubility was sufficient to enable molecular weights to be measured in chlorobenzene at 80 °C. As shown in Table 3.1, the number-average molecular weight of P6 was considerably lower than the other polymers. This is most likely a result of the poor solubility, resulting in precipitation of the polymer during the reaction.

Table 3.1. Molecular Weights and Thermal Properties

	M_n[a] [kg/mol]	M_w[a] [kg/mol]	Đ[a]	T_d[b] [°C]
P6	9†	26†	2.8†	313
P7	50	163	3.3	419
P8	42	172	4.1	419

[a] Determined by gel permeation chromatography in CB at 80 °C against polystyrene standards with the exception of † which was determined by HT-GPC in TCB at 140 °C. [b] 5% weight loss temperatures measured by thermal gravimetric analysis under a N_2 atmosphere.

The thermal stability of the polymers was probed by thermogravimetric analysis (see Appendix and Table 3.1), in which a 5% weight loss was observed at 313 °C for P6, and at 419 °C for P7 and P8. The lower stability of P6 may therefore relate to the alkoxy side-chains on the BDT ring.

3.2.3 Optical Properties and Frontier Molecular Orbital Energy Levels

The optical properties of the polymers in dilute chlorobenzene and as thin-films, spin-coated from chlorobenzene (5 mg/mL), were investigated by UV-vis absorption spectroscopy, as presented in Figure 3.2 and Table 3.2. The solutions of all three polymers in chlorobenzene are broadly similar, with peak onsets around 700 nm, and two major absorption peaks present for all polymers (around 580 and 635 nm). There are subtle differences in the relative intensity of these two peaks for the three polymers, with the higher energy peak (λ_{max} solution = 580 nm) being the most intense in P6 with a shoulder at 632 nm, and the lower energy peak more intense for both P7 and P8 (λ_{max} solution = 638 and 630 nm, respectively) with a shoulder at 589 and 584 nm, respectively. The longer wavelength shoulder is often associated with an extended polymer backbone and aggregation in solution, suggesting that the side-chain on the benzo[1,2-*b*:4,5-*b'*]dithiophene portion of the polymer may influence this. Indeed, an increase in intermolecular π-π interactions with the inclusion of the alkylthienyl side-chains is consistent with previous reports, comparing alkoxy- and alkylthienyl-substituted BDT polymers.[121,123] The solution spectra all closely resemble the thin films, in agreement with the suggestion that the polymers are aggregated or chain extended already in solution.

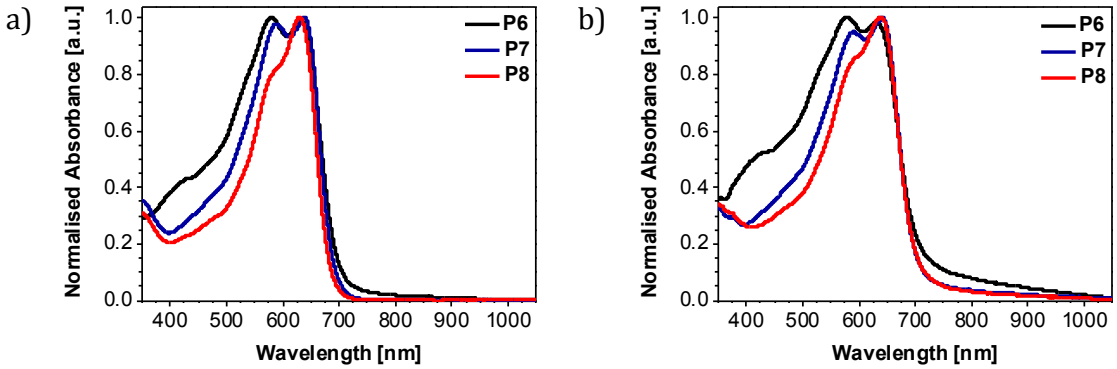

Figure 3.2. Normalised UV-vis absorption spectra of the polymers in a) dilute chlorobenzene solution at 20 °C, and b) thin-films spin-coated on glass substrates from chlorobenzene solution (5 mg/mL).

The ionisation potentials of thin films of P6, P7, and P8 spin-coated from chlorobenzene (5 mg/mL) were measured using photoelectron spectroscopy in air to be 5.30, 5.20, and 5.26 eV, respectively (Table 3.2). Although the values are close considering the error of the technique (± 0.05 eV), it seems that replacement of the alkoxy group with electron rich alkylthienyl side-chains in P7 and P8 results in a small decrease in ionisation potential, suggesting the thienyl groups are overall more electron donating than the alkoxy group. There is a slight difference of 0.06 eV between the ionisation potential of P7 and P8, which may be the result of differences in steric hindrance, with the addition of the dialkylthienyl side-chains in P8 resulting in a more torsionally twisted structure than P7.

Table 3.2. Optical Properties and Frontier Molecular Orbital Energy Levels

	λ_{max} Soln[a] [nm]	λ_{max} Film[b] [nm]	E_g opt[c] [eV]	I.P.[d] [eV]
P6	580 (632)	580 (629)	1.74	5.30
P7	638 (589)	642 (590)	1.75	5.20
P8	630 (584)	638 (593)	1.75	5.26

[a] Measured in dilute CB at 20 °C. Shoulder peaks in parentheses. [b] Thin-films spin-coated on glass substrates from 5 mg/mL CB solution. Shoulder peaks in parentheses. [c] Determined from the absorption onset in the solid state. [d] Determined by PESA (error ± 0.05 eV).

3.2.4 Polymer Conformation and Packing

The thermal properties of the polymers were evaluated using differential scanning calorimetry measurements. As shown in Figure 3.3, no obvious thermal transitions were observed in the second heating and cooling scans of the polymers recorded between -30 and 330 °C under nitrogen.

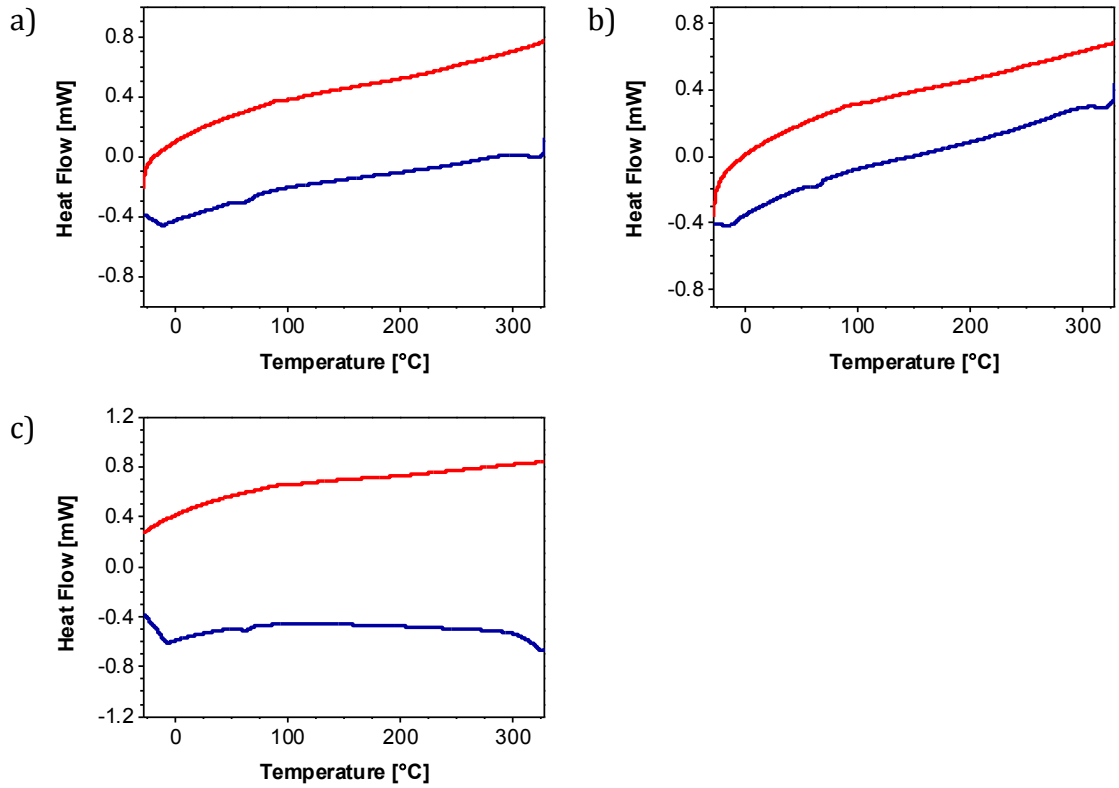

Figure 3.3. Second heating (red) and cooling (blue) scans of a) P6, b) P7, and c) P8 measured by DSC, at a rate of 10 °C/min under a N_2 atmosphere.

The surface morphology of thin films of the polymers, prepared using the same conditions as those used for OFET device fabrication, was probed using atomic force microscopy in tapping mode. As demonstrated in Figure 3.4, the nature of the BDT side-chain had a significant effect on the film structure, with both P7 and P8 exhibiting a more homogenous morphology than P6. In addition, both P7 (RMS = 1.13) and P8 (RMS = 0.79) display smoother, more continuous films compared to P6 (RMS = 4.03 nm), as reflected in the root-mean-square surface roughness of the films. These differences may be related to an increase in intermolecular π-π ordering with the inclusion of the conjugated alkylthienyl side-chains in P7 and P8, relative to the alkoxy equivalent, although further characterisation is needed to validate the packing. Furthermore, the substantial increase in surface roughness observed for P6 is most likely due to a combination of difficulties in filtering the polymer during film preparation, and early precipitation during the film forming process, which both relate to the poor solubility of the polymer under the conditions used.

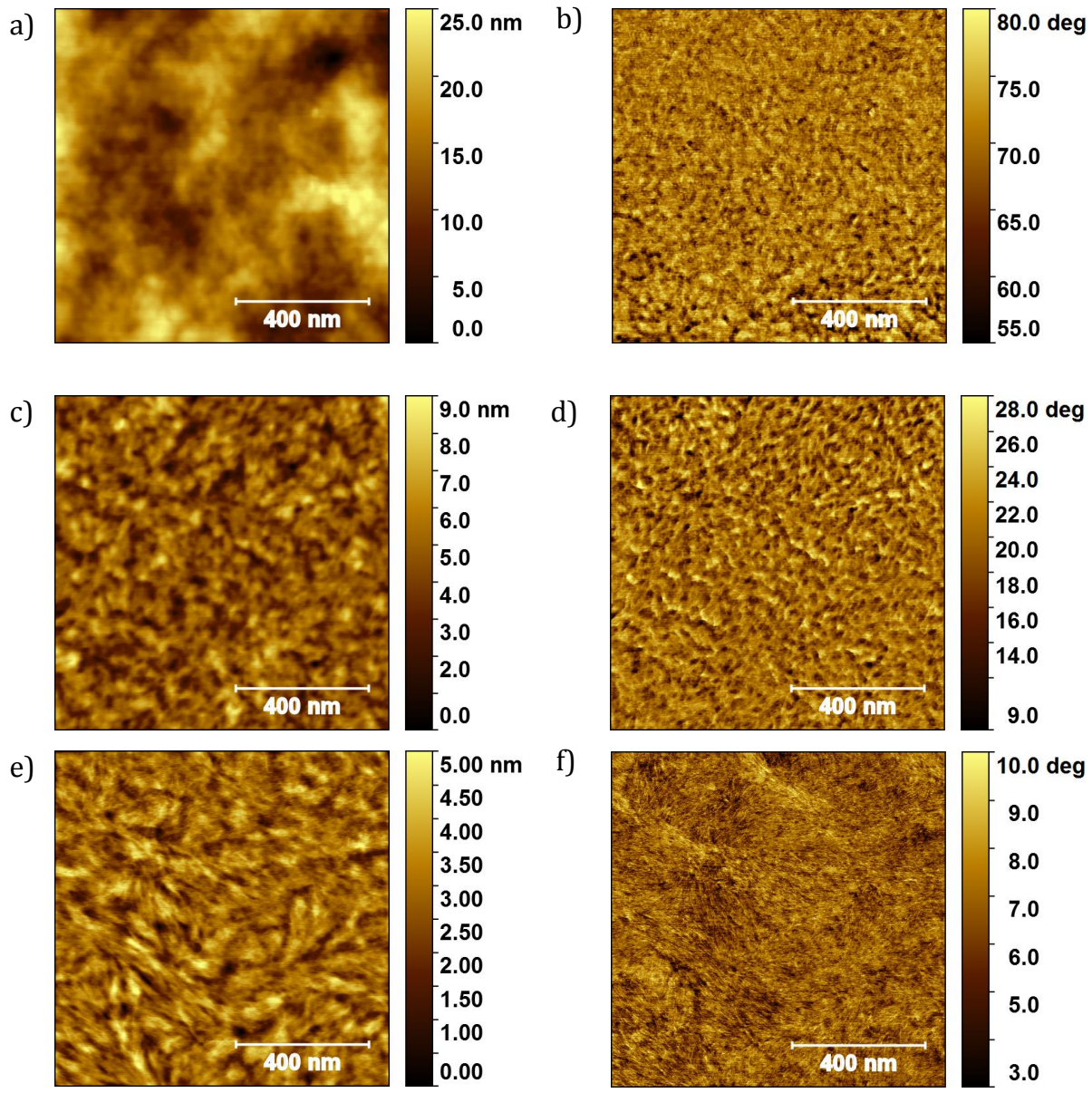

Figure 3.4. AFM topography (left) and phase (right) images of thin films of P6: a) and b), P7: c) and), and P8: e) and f), spin-coated from *o*-dichlorobenzene solution (5 mg/mL), and annealed at 120 °C for 30 min. Scale 1 µm x 1 µm.

3.2.5 OPV Device Performance

The photovoltaic performance of the polymers was investigated in bulk heterojunction OPV devices fabricated in an inverted configuration (ITO/ZnO/P6-8:$PC_{70}BM$/MoO_3/Ag). Figure 3.5 displays the *J-V* characteristics of these devices, and the data is summarised in Table 3.3. Note all available EQE machines were broken at the time of testing, so although the trends observed are expected to be correct, the absolute values may differ slightly. For initial testing the polymer active layers, which consisted of polymer:$PC_{70}BM$ in a blend ratio of 1:2 (w:w), were spin-coated at 3000 rpm from chlorobenzene (24 mg/mL) without the use of any solvent additives. Due to the poor solubility of P6, initial devices were instead prepared from *o*-dichlorobenzene however, even under these conditions there were difficulties in forming a homogeneous film, and all devices shorted. P7 and P8 exhibited promising performance during initial testing, with an average power conversion efficiency of 5.58 and 5.17%, respectively. In an effort to optimise the performance, the addition of an additive (2%) to the polymer active layer was evaluated. Interestingly, for P7 the performance decreased when DIO (2.12%) or CN (5.11%) were added to the blend, whereas for P8 there was a slight improvement in performance (5.80-6.27%), mainly due to an increase in the J_{SC} from 9.50 to 11.30-11.70 mA/cm^2.

Note further attempts to improve the performance of P7 were made using various solvents, spin-coating conditions, and additives. However, in all cases the performance decreased, particularly for devices spin-coated from chloroform (1.32-2.69%), in which a significant decrease in the J_{SC} (from 12.90 to 5.35-8.59 mA/cm^2) and FF (from 0.55 to 0.38-0.42) were observed. The decrease in J_{SC} is most likely due to changes in the thin-film morphology as a result of the choice of solvent. This is in agreement with previous reports that have shown differences between the boiling point, and Hansen solubility parameters[124] of the processing solvent can affect film formation.[110] The observed decrease in the FF on the other hand, is most likely due to changes in the thickness of the active layer as a result of the spin-coating speed, with a slower speed expected to yield a thicker film, and hence a reduction in FF.[125] It is also interesting to note that working devices of P6 were prepared using chloroform, although the power conversion efficiency was considerably lower than the other polymers.

Table 3.3. OPV Device Characteristics[a]

Average

		J_{SC} [mA/cm²]	V_{OC} [V]	FF	PCE [%]
P6	***o*-DCB**	-	-	-	-
	CF	7.88 ± 0.13	0.67 ± 0.13	0.44 ± 0.08	2.37 ± 0.76
	CF + 2% DIO	7.13 ± 0.41	0.73 ± 0.00	0.44 ± 0.01	2.31 ± 0.11
P7	**CB**	12.90 ± 0.50	0.78 ± 0.03	0.55 ± 0.04	5.58 ± 0.64
	CB + 2% DIO	8.63 ± 0.63	0.65 ± 0.19	0.37 ± 0.04	2.12 ± 0.73
	CB + 2% CN	13.23 ± 0.38	0.80 ± 0.00	0.48 ± 0.06	5.11 ± 0.67
	o-DCB†	15.06 ± 1.29	0.64 ± 0.02	0.52 ± 0.06	5.02 ± 0.99
	CF	5.35 ± 0.67	0.85 ± 0.00	0.42 ± 0.01	1.91 ± 0.24
	CF + 2% DIO‡	5.45 ± 0.65	0.64 ± 0.19	0.38 ± 0.06	1.32 ± 0.42
	CF + 2% CN‡	8.59 ± 0.74	0.79 ± 0.08	0.40 ± 0.03	2.69 ± 0.44
P8	**CB**	9.50 ± 0.20	0.85 ± 0.01	0.64 ± 0.03	5.17 ± 0.27
	CB + 2% DIO	11.30 ± 0.48	0.86 ± 0.02	0.59 ± 0.03	5.80 ± 0.58
	CB + 2% CN	11.40 ± 0.50	0.86 ± 0.06	0.64 ± 0.02	6.27 ± 0.38
	CB + 2% DPE	11.70 ± 0.90	0.86 ± 0.08	0.60 ± 0.01	6.11 ± 0.45

Peak

		J_{SC} [mA/cm²]	V_{OC} [V]	FF	PCE [%]
P6	***o*-DCB**	-	-	-	-
	CF	7.99	0.73	0.47	2.75
	CF + 2% DIO	7.67	0.73	0.44	2.44
P7	**CB**	13.58	0.79	0.56	6.09
	CB + 2% DIO	9.15	0.75	0.39	2.64
	CB + 2% CN	13.42	0.81	0.51	5.54
	o-DCB†	16.40	0.65	0.55	5.84
	CF	6.51	0.85	0.42	2.34
	CF + 2% DIO‡	5.79	0.77	0.36	1.59
	CF + 2% CN‡	9.63	0.82	0.41	3.28
P8	**CB**	9.66	0.86	0.66	5.51
	CB + 2% DIO	12.20	0.86	0.64	6.70
	CB + 2% CN	12.10	0.86	0.65	6.78
	CB + 2% DPE	13.20	0.87	0.58	6.70

[a] Inverted devices (ITO/ZnO/P6-8:$PC_{70}BM$/MoO_3/Ag) measured under AM 1.5G illumination at 100 mW/cm². Polymer active layers were spin-coated at 3000 rpm with the exception of † which was spin-coated at 1000 rpm and ‡ 2000 rpm, from the respective solution (24 mg/mL) in a blend ratio of 1:2 (w:w). The pixel size was 0.045 cm².

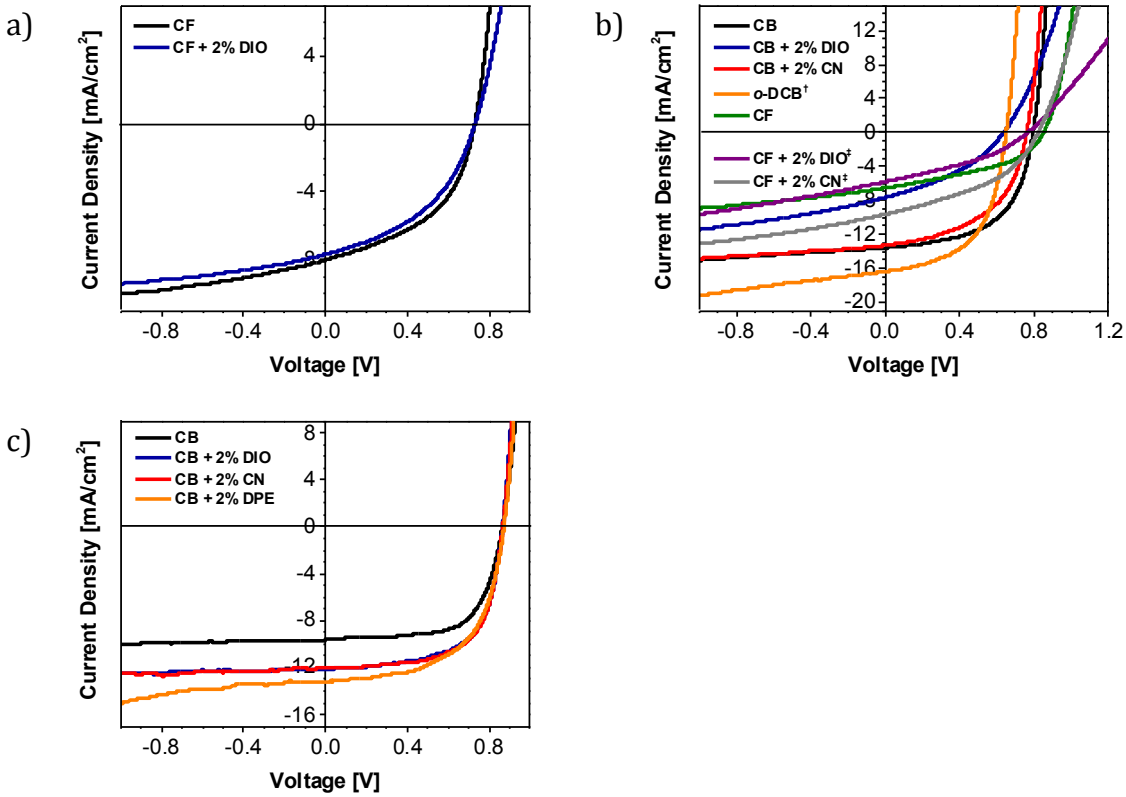

Figure 3.5. *J-V* curves of the best performing devices (ITO/ZnO/Polymer:$PC_{70}BM$/MoO_3/Ag) of a) P6, b) P7, and c) P8, measured under AM 1.5G illumination at 100 mW/cm². Polymer active layers were spin-coated at 3000 rpm with the exception of † which was spin-coated at 1000 rpm and ‡ 2000 rpm, from the respective solution (24 mg/mL) in a blend ratio of 1:2 (w:w). The pixel size was 0.045 cm².

3.2.6 OFET Device Performance

The electrical performance of the polymers was evaluated in TG-BC field effect transistors. Devices were fabricated on glass using gold source-drain electrodes, and a CYTOP dielectric. In an effort to lower the work function of the gold and aid hole injection, the electrodes were treated with pentafluorobenzene thiol prior to polymer deposition. Figure 3.6, shows the transfer and output characteristics of the best performing devices. In all cases, unipolar, p-type charge transport was observed with negligible hysteresis between the forward and reverse gate voltage sweeps. As presented in Table 3.4, P6 exhibited the lowest device performance, with an average saturated charge carrier mobility of 0.00068 cm^2/Vs. This can partially be explained by the difficulties in forming a homogenous film during device fabrication, which resulted in the presence of large aggregates detrimental to charge transport (AFM topography image of P6 Section 3.2.4). Note the low molecular weight of the polymer may also limit the device performance (Table 3.1). In contrast, the performance of P7 and P8 was considerably higher, with average saturated charge carrier mobilities of 0.023 and 0.013 cm^2/Vs, respectively. This is most likely due to both the improved solubility, and film forming ability of these polymers as a result of alkylthienyl side-chains. These side-chains may also result in an increase in intermolecular π-π ordering in P7 and P8, in agreement with the AFM data presented in Section 3.2.4. In addition, the slight difference in mobility (0.01 cm^2/Vs) between P7 and P8 may be due to changes in the solid-state packing and thin-film order as a result of the increase in side-chain density in P8, as suggested by previous reports.[126] However, further characterisation of the morphology is needed to validate this.

Table 3.4. OFET Device Characteristics[a]

	Average	Peak		
	$\mu_{h\ sat}$ [x 10^{-2} cm^2/Vs]	$\mu_{h\ sat}$ [x 10^{-2} cm^2/Vs]	V_T [V]	I_{on}/I_{off}
P6	0.068 ± 0.0088	0.076	-6.4 ± 5.8	1 x 10^2 ~ 1 x 10^3
P7	2.3 ± 0.26	2.7	-12.7 ± 0.8	1 x 10^3 ~ 1 x 10^4
P8	1.3 ± 0.27	1.7	-12.8 ± 0.5	1 x 10^3 ~ 1 x 10^4

[a] TG-BC devices fabricated on glass substrates using Au (40 nm) source-drain electrodes treated with PFBT, and a CYTOP dielectric. Polymer active layers were spin-coated from CB solution (5 mg/mL) and annealed at 120 °C for 30 min.

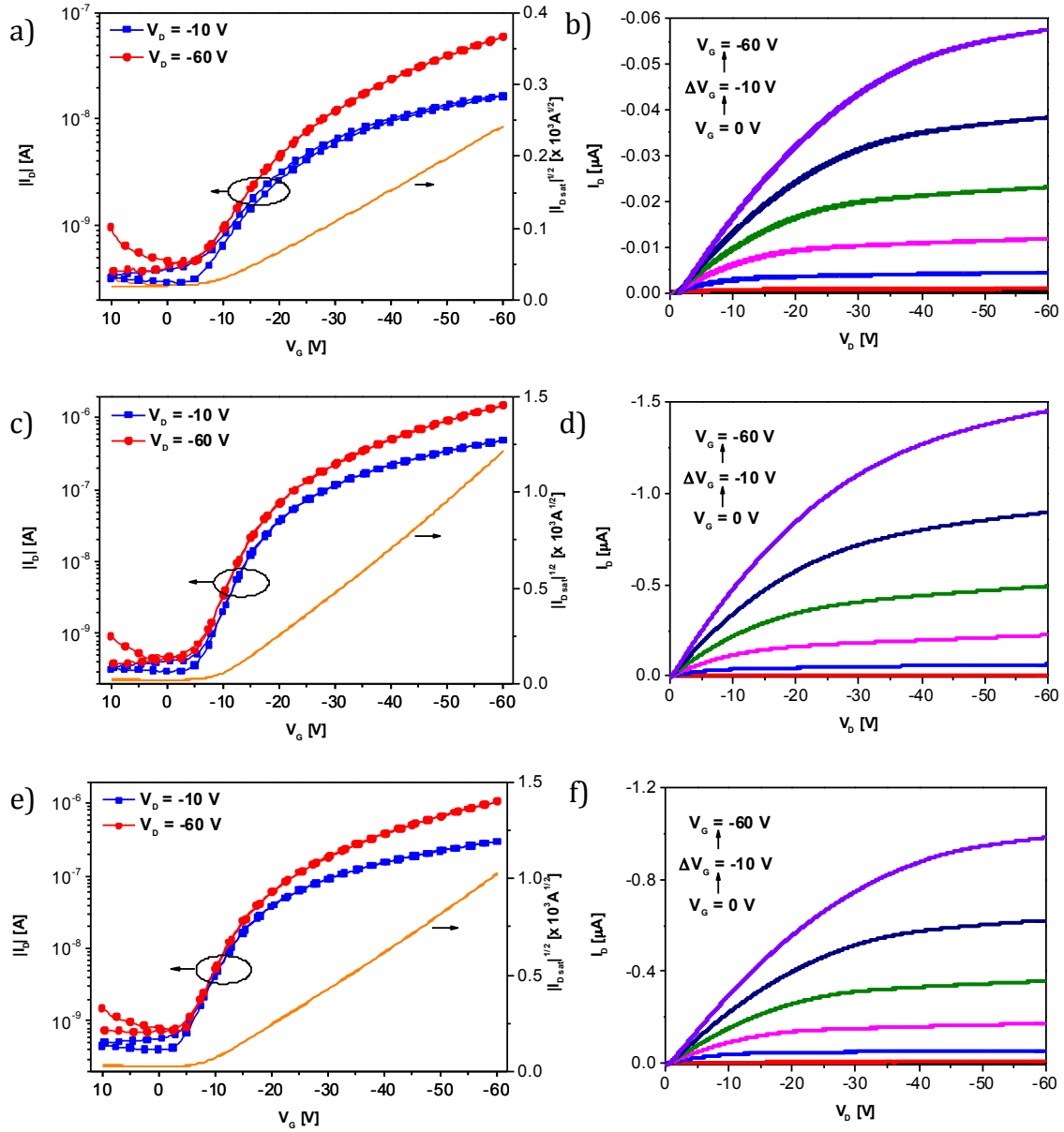

Figure 3.6. Transfer (left) and output (right) characteristics of the best performing TG-BC devices of P6: a) and b), P7: c) and), and P8: e) and f), fabricated on glass substrates using Au (40 nm) source drain electrodes treated with PFBT, and a CYTOP dielectric. Polymer active layers were spin-coated from CB solution (5 mg/mL) and annealed at 120 °C for 30 min. The channel width and length were 1000 μm and 40 μm, respectively.

3.3 Conclusion

In this chapter, the synthesis of a series of novel BTTA polymers was described. Using a combination of experimental techniques (UV-vis, PESA, AFM), the optoelectronic properties and surface morphology of the polymers were investigated. Significant differences between the polymers were highlighted, with perhaps the most noticeable being the solubility and film forming ability, which were found to be strongly influenced by the choice of benzo[1,2-*b*:4,5-*b'*]dithiophene co-monomer. Indeed, the alkoxy-substituted BDT co-polymer (P6) demonstrated poor solubility in comparison to the alkylthienyl-substituted derivatives (P7-8), and as such it was difficult to form homogeneous thin films of P6. In addition, the use of conjugated alkylthienyl side-chains in P7 and P8 resulted in an increase in intermolecular π-π ordering, and polymer aggregation relative to P6.

The photovoltaic and electrical performance of the materials was promising, although varied somewhat across the series as a result of the issues with solubility. Despite this however, a peak power conversion efficiency of 6.78% was achieved for P8 under optimised conditions, whilst a peak saturated hole mobility of 0.027 cm^2/Vs was recorded for P7. These results demonstrate the potential of BTTA as a useful building block for the development of high performing conjugated polymers in organic electronics.

Note at the time of writing, similar work was published detailing the synthesis and photovoltaic performance of a BTTA monomer with 2-octyldodecyl side-chains, co-polymerised with 5,5'-bis(trimethylstannyl)-4,4'-ditetradecyl-2,2'-bithiophene and 2,6-bis-trimethylstannyl-4,8-bis(5-(2-ethylhexyl)thiophen-2-yl)benzo[1,2-*b*:4,5-*b*']dithiophene.[127] The synthetic route to the polymers differed slightly to that presented in Scheme 3.1. However, promising power conversion efficiencies of 4.65 and 5.46%, respectively, were reported for polymer:$PC_{71}BM$ devices fabricated in an inverted configuration from chlorobenzene with 1% DIO additive.[127] The transistor performance was not investigated.

Chapter 4
Branch-point Manipulation in Benzo[*lmn*][3,8]phenanthroline-1,3,6,8(2*H*,7*H*)-tetrone Polymers and its Effect on OFET and All-polymer OPV Performance

4.1 Introduction

Side-chain engineering has received a great deal of interest in recent years in the development of high performing conjugated polymers in organic electronics.[14,94] In particular the choice of alkyl-chain (branched vs. linear), the chain length, symmetry, and the substituting position have all been shown to have a significant impact on the solid-state ordering and device performance of the resulting polymers.[63,116,126,128–134] Recently the effect of the side-chain branching position has also been found to play a crucial role on the material properties. For example, there have been several reports describing how increasing the branch-point can improve the mobility of both p-type and n-type polymers in transistor applications, due to differences between the intermolecular π-π interactions, solid-state packing, and thin film order as a result of changes to the side-chains.[6,8,135–141] There have also been reports on the use of branch-point manipulation in polymers for solar cell applications, where an increase in the power conversion efficiency was demonstrated due to changes in the crystallinity of the polymers.[142] Surprisingly however, the effect of the side-chain branching position on the performance of all-polymer solar cells has yet to be reported.

All-polymer solar cells have attracted considerable interest in recent years due to their potential advantages over typical fullerene based devices (Section 1.2).[29] Whilst promising solar cell performance has been demonstrated, control over the thin film morphology and phase separation of the polymer blend still remains an important issue.[29] The use of thermal annealing,[143] film ageing,[144] processing additives,[145–147] and the choice of solvent[148,149] on the blend morphology have all been explored. In addition, the role of the side-chain length, and the use of a polystyrene group in place of the alkyl-chains has also recently been investigated and shown to have a significant impact on device performance,[150–154] suggesting further studies on the choice of the side-chains could be of interest.

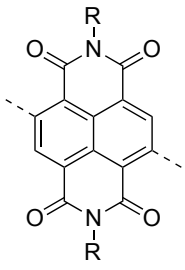

NDI

Figure 4.1. Structure of NDI monomer.

Benzo[*lmn*][3,8]phenanthroline-1,3,6,8(2*H*,7*H*)-tetrone (NDI) based polymers are a promising class of ring fused electron accepting materials that have demonstrated high n-type transistor performance (> 1 cm^2/Vs) and impressive solar cell efficiencies in all-polymer devices (up to 7.7%) (Figure 4.1).[1,144,155–158] Whilst there has been significant effort investigating the role of the co-monomer on polymer performance,[159–164] there have been few reports on the role of the solubilising side-chains.[165] Hence in this chapter, the influence of the alkyl side-chain branching position on the electrical performance of a series of NDI based polymers was evaluated, and for the first time, the influence of the branch-point on the performance of all-polymer OPV devices was examined.

4.2 Results and Discussion

4.2.1 Monomer Synthesis

The NDI monomers were synthesised according to previously reported methods (Scheme 4.1),[166,167] in which commercially available naphtho[1,8-*cd*:4,5-*c'd'*]dipyran-1,3,6,8-tetrone (4.1) was first brominated with dibromoisocyanuric acid at 85 °C, to afford 4,9-dibromonaphtho[1,8-*cd*:4,5-*c'd'*]dipyran-1,3,6,8-tetrone (4.2). Due to the poor solubility of 4.2 in common organic solvents purification was difficult, and so 4.2 was used directly, and converted to the requisite dibrominated monomers (4.3-4.6) via an acid catalysed condensation reaction with the corresponding branched amine. Note the yield for this step was low (4-15%), but could be improved slightly (e.g. 38% for the synthesis of 4.5) when commercially available 4.2 was used.

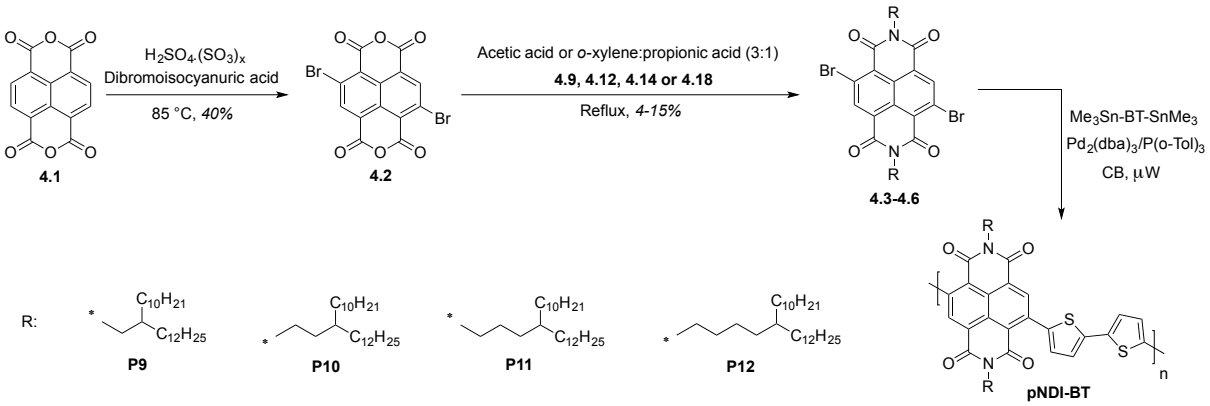

Scheme 4.1. Synthetic pathway to the polymers.

All four branched amines were prepared from commercially available 2-decyltetradecan-1-ol (4.7). Thus for the synthesis of 2-decyltetradecan-1-amine (4.9) (Scheme 4.2), 4.7 was first converted to the corresponding azide (4.8) via a Mitsunobu reaction using diphenyl phosphoryl azide (DPPA), diisopropyl azodicarboxylate (DIAD), and triphenylphosphine at room temperature, and then reduced to 4.9 using lithium aluminium hydride.

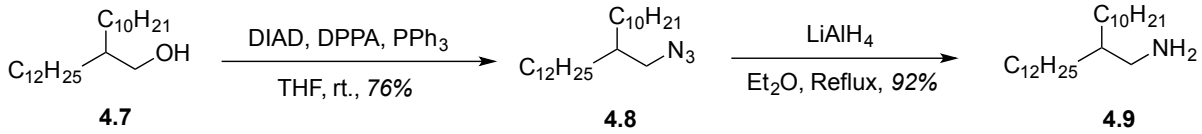

Scheme 4.2. Synthetic pathway to 2-decyltetradecan-1-amine.

For the synthesis of 3-decylpentadecan-1-amine (4.12) (Scheme 4.3), 4.7 was first converted to 11-(bromomethyl)tricosane (4.10) using *N*-bromosuccinimide and triphenylphosphine at room temperature, and then reacted with potassium cyanide and heated to 80 °C for 16 h to form 3-decylpentadecanenitrile (4.11). This was subsequently reduced using lithium aluminium hydride to afford 4.12 in 95% yield.

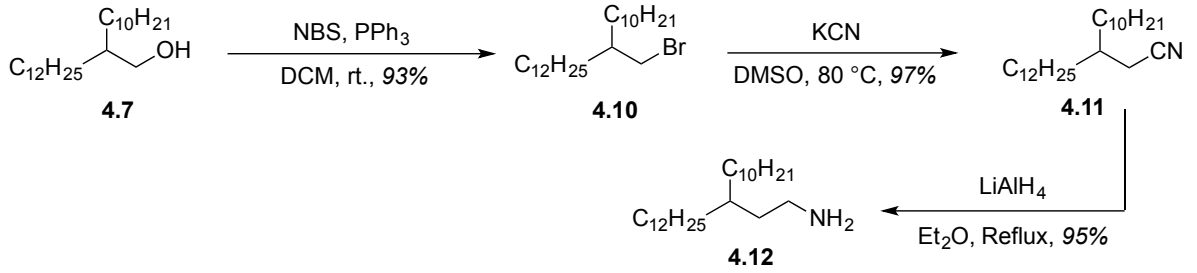

Scheme 4.3. Synthetic pathway to 3-decylpentadecan-1-amine.

In the case of 4-decylhexadecan-1-amine (4.14) (Scheme 4.4), a modified literature procedure[168] based on the lithiation of acetonitrile using *n*-butyllithium at -78 °C, and subsequent reaction with 4.10 was employed. The resulting 4-decylhexadecanenitrile (4.13), which was isolated in reasonable yield, was then reduced to the corresponding amine (4.14), using lithium aluminium hydride.

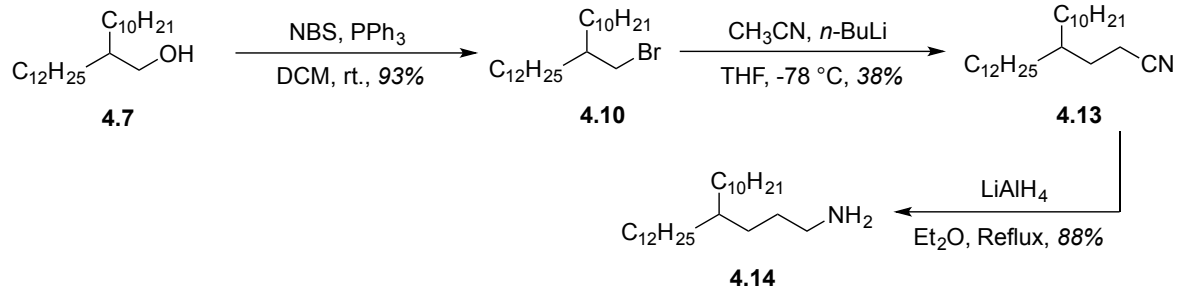

Scheme 4.4. Synthetic pathway to 4-decylhexadecan-1-amine.

Finally for the synthesis of 5-decylheptadecan-1-amine (4.18) (Scheme 4.5), 4.10 was first converted to 11-(but-3-en-1-yl)tricosane (4.15) using a previously reported method[169] in which 4.10 was reacted with allylmagnesium chloride and heated to reflux for 16 h, followed by the

addition of hydrochloric acid. 4.15 was then subjected to a sequential hydroboration-oxidation reaction with borane, and then sodium hydroxide and hydrogen peroxide solution to give 5-decylheptadecan-1-ol (4.16) in good yield, after purification by flash chromatography. This was then converted to the corresponding azide (4.17), via a Mitsunobu reaction, and subsequently reduced to give 4.18 in 92% yield.

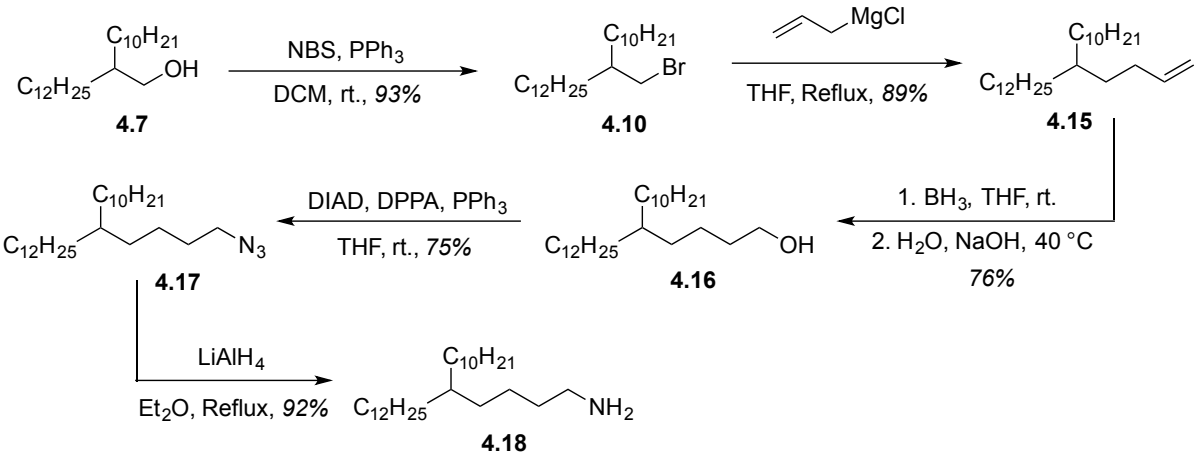

Scheme 4.5. Synthetic pathway to 5-decylheptadecan-1-amine.

4.2.2 Polymer Synthesis

The polymers were synthesised via microwave assisted Stille cross-coupling reactions,[97–99] as described in Scheme 4.1. The polymers were purified by precipitation and subsequent Soxhlet extraction in methanol (24 h), acetone (24 h), hexane (24 h), and chloroform (12 h) to remove low molecular weight oligomers. After concentration, the chloroform extracts were further purified by precipitation in methanol, and dried under high vacuum to isolate the polymers. The chemical structure of the polymers was confirmed by a combination of elemental analysis, which were in agreement with the theoretical values, and high temperature ^{1}H NMR spectroscopy in 1,1,2,2-tetrachloroethane-d_2 (see Appendix).

Polymer molecular weights and dispersities were determined by gel permeation chromatography in chlorobenzene at 80 °C. In all cases, the number-average molecular weights of the polymers were similar (between 30 and 38 kg/mol), as observed in Table 4.1. Since polymer molecular weight is widely reported to have a significant impact on material properties,[19,20,170–176] it is important to note that such effects can be neglected in this study. The thermal stability of the polymers was probed by thermogravimetric analysis (see Appendix and Table 4.1) which demonstrated excellent thermal stability, with a 5% weight loss observed after 400 °C for all polymers.

Table 4.1. Molecular Weights and Thermal Properties

	M_n[a] [kg/mol]	M_w[a] [kg/mol]	Đ[a]	T_d[b] [°C]
P9	38	100	2.6	449
P10	36	200	5.7	402
P11	30	85	2.8	450
P12	31	87	2.8	456

[a] Determined by gel permeation chromatography in CB at 80 °C against polystyrene standards. [b] 5% weight loss temperatures measured by thermal gravimetric analysis under a N_2 atmosphere.

4.2.3 Optical Properties and Frontier Molecular Orbital Energy Levels

The optical properties of the polymers were investigated by UV-vis absorption spectroscopy, as presented in Figure 4.2 and Table 4.2. In order to compare the aggregation properties of the polymers, the solution spectra were recorded in chlorobenzene at the same concentration (2.5 x 10^{-4} M). Compared with P9 and P10 (λ_{max} solution = 661 and 641 nm, respectively), the absorption maxima of P11 and P12 (λ_{max} solution = 707 and 705 nm, respectively) are significantly red-shifted in solution. In addition, upon film formation P11 and P12 exhibit a small shift in absorption maxima, whereas P9 and P10 display a remarkably large red-shift of 40 and 60 nm, respectively. This suggests P11 and P12 have a tendency to aggregate, even in dilute solution. In thin film, pronounced shoulders at 765 and 770 nm are also observed in the absorption spectra of P11 and P12, respectively. The presence of the long wavelength shoulders in the solid state and aggregation in solution are suggestive of enhanced vibronic ordering in these polymers, relative to P9 and P10. This is believed to be related to an increase in intermolecular π-π interactions as the branch-point is increased, as a result of a decrease in steric hindrance between the solubilising alkyl-chains and the conjugated polymer backbone.[142]

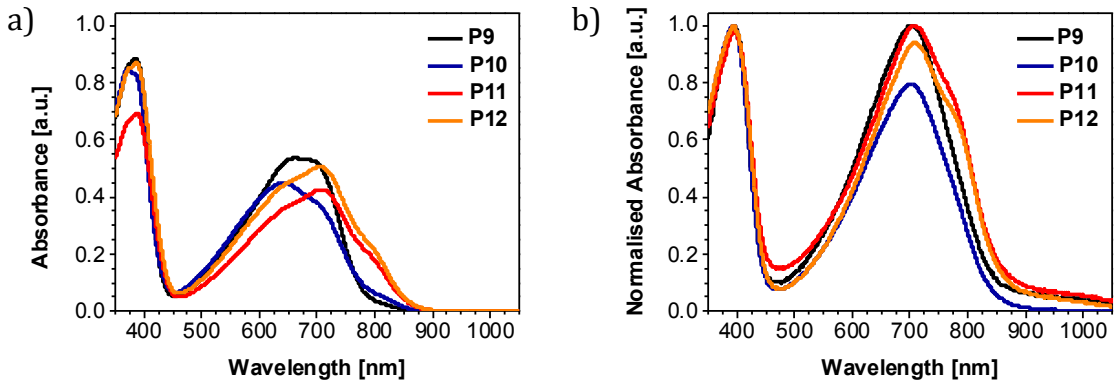

Figure 4.2. a) UV-vis absorption spectra of the polymers in chlorobenzene (2.5 x 10^{-4} M) at 20 °C and b) normalised UV-vis absorption spectra of the polymers in thin-films spin-coated on glass substrates from chlorobenzene solution (5 mg/mL).

The ionisation potentials of thin films of the polymers, spin-coated from chlorobenzene (5 mg/mL) were measured using photoelectron spectroscopy in air, and the LUMO energy levels were estimated by adding the negative of the ionisation potential to the absorption onset in the solid state. Although such an estimate does not take into account the exciton binding energy,[104] it allows for a reasonable comparison between the polymers. As observed in Table 4.2, all four polymers exhibit similar frontier molecular orbital energy levels, which suggest the alkyl-chain branching position has little effect on the polymer energetics.

Table 4.2. Optical Properties and Frontier Molecular Orbital Energy Levels

	λ_{max} Soln[a] [nm]	λ_{max} Film[b] [nm]	E_g opt[c] [eV]	I.P.[d] [eV]	LUMO[e] [eV]
P9	661	701	1.44	5.83	-4.39
P10	641	701	1.43	5.84	-4.41
P11	707	706 (765)	1.41	5.82	-4.41
P12	705	709 (770)	1.41	5.82	-4.41

[a] Measured in CB (2.5×10^{-4} M) at 20 °C. [b] Thin-films spin-coated on glass substrates from 5 mg/mL CB solution. Shoulder peaks in parentheses. [c] Determined from the absorption onset in the solid state. [d] Determined by PESA (error ± 0.05 eV). [e] Estimated by adding the negative of the ionisation potential to the absorption onset in the solid state.

4.2.4 Polymer Conformation and Packing

Differential scanning calorimetry measurements were used to evaluate the thermal properties of the polymers. Figure 4.3 displays the second heating and cooling scans of the polymers recorded between -30 and 330 °C under nitrogen. In contrast to the other polymers, an endothermic transition on heating, at 291 °C, and an exothermic transition upon cooling, at 273 °C, corresponding to backbone melting and crystallisation, respectively, were observed in the DSC trace of P9. The absence of similar transitions in the DSC plots of P10-12 could suggest an increase in intermolecular ordering across the series, leading to a backbone melt beyond the temperature range studied. In addition both P11 and P12 exhibit an endothermic transition at 6 and 1 °C, respectively, followed by an exothermic transition at -6 and -7 °C, respectively. These temperatures are well below the range expected for backbone transitions, and are more likely attributed to alkyl-chain melting and crystallisation, respectively.

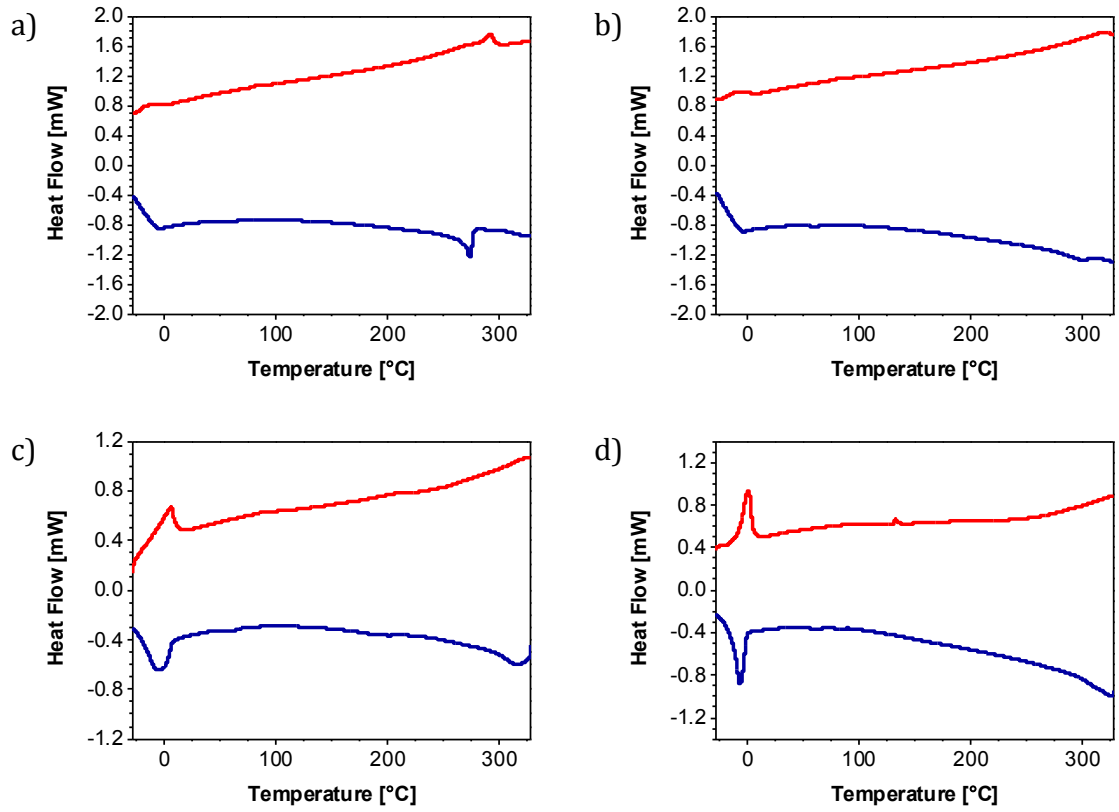

Figure 4.3. Second heating (red) and cooling (blue) scans of a) P9, b) P10, c) P11, and d) P12 measured by DSC, at a rate of 10 °C/min under a N_2 atmosphere.

The surface morphology of thin films of the polymers was probed using atomic force microscopy in tapping mode. Figure 4.4 displays the topography images of the polymers spin-coated from *o*-dichlorobenzene (5 mg/mL), and annealed at 200 °C for 30 min. There are significant differences between the films, with both P11 (RMS = 1.02 nm) and P12 (RMS = 0.30

nm) exhibiting a smoother, more homogenous morphology than P9 (RMS = 2.70 nm) and P10 (RMS = 2.98 nm), as suggested by the root-mean-square surface roughness. Indeed, large aggregates detrimental to charge transport were observed in the AFM images of P9 and P10, while more continuous interconnected fibrillar microstructures were observed in P11 and P12. It is anticipated that the lower surface roughness demonstrated by P11 and P12, may be beneficial for charge transport, and result in a more intimate contact between the polymer active layer and the dielectric in field effect transistors.

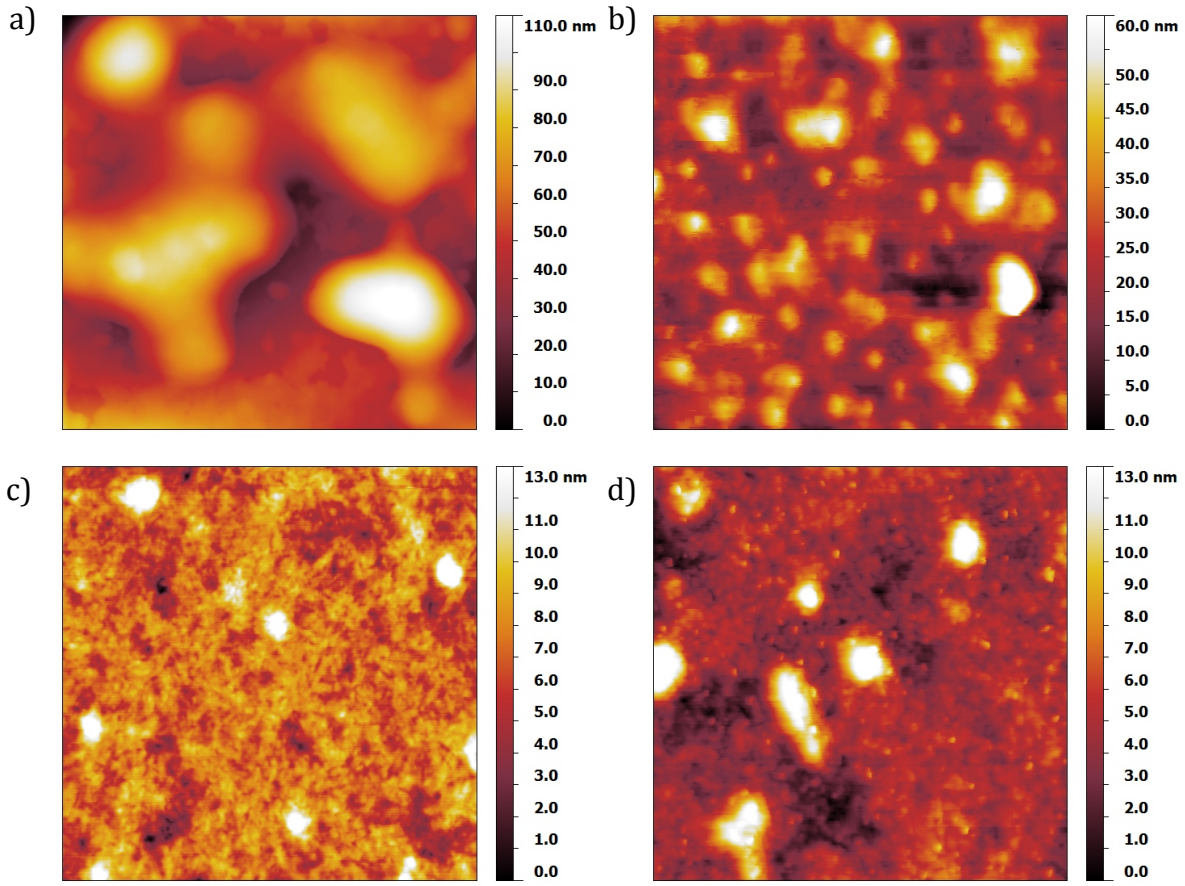

Figure 4.4. AFM topography images of thin films of a) P9, b) P10, c) P11, and d) P12 spin-coated from *o*-dichlorobenzene solution (5 mg/mL), and annealed at 200 °C for 30 min. Scale 2 μm x 2 μm.

The solid-state morphology of thin films of the polymers was studied using grazing incident wide-angle X-ray scattering measurements. The 2D-GIWAXS diffraction patterns of as-cast and annealed (200 °C for 30 min) films of the polymers spin-coated from *o*-dichlorobenzene (10 mg/mL) are presented in Figure 4.5, and the peak fitting data from the 1D-GIWAXS scattering profiles (see Appendix) is summarised in Table 4.3. Note a slightly higher solution concentration was used to prepare the films compared to the transistor devices in order to ensure sufficient thickness to afford a scattering signal. In-plane lamellar diffraction peaks (*h*00)

along the Q_{xy} axis are visible in the as-cast films of the polymers, and out-of-plane π-π stacking peaks along the Q_z axis are also visible, although only in the as-cast films of P11 and P12. These diffraction patterns are consistent with a face-on orientation of the polymers with respect to the substrate. In the annealed films, distinct out-of-plane lamellar diffractions (*h*00) are observed, suggesting a shift in orientation from preferentially face-on to predominately edge-on. This is more prominent across the series, and indicates substantial differences in the solid-state ordering of the polymers as a result of the branch-point and annealing conditions. The changes upon thermal annealing also result in an increase in the scattering intensity, indicating an increase in the relative crystallinity of the polymers. This is most pronounced in the in-plane (100) direction, with the crystalline coherence length significantly increasing in the annealed films (Table 4.3). The increase in the coherence length in the (010) crystallite is more modest upon annealing, but does increase for all polymers except for P9.

In addition as shown in Table 4.3, the lamellar *d*-spacing systematically increases across the series (from between 26.46-26.84 (P9) to 32.04-32.06 Å (P12)) as expected from the lengthening of the alkyl side-chains. The out-of-plane π-π stacking distance on the other hand gradually decreases, although there is little difference between the values for P9 and P10, and P11 and P12 in both the as-cast and annealed films. However, this suggests the polymers do pack more closely as the branch-point is moved further from the conjugated backbone, in agreement with previous reports.[135,136]

Table 4.3. GIWAXS Results[a]

		In-plane (100)		Out-of-plane (010)	
		Lamellar *d*-Spacing [Å]	**Coherence Length [nm]**	**π-π Stacking Distance [Å]**	**Coherence Length [nm]**
As-cast	**P9**	26.46 ± 0.021	13.93 ± 0.151	4.22 ± 0.004	2.22 ± 0.038
	P10	28.83 ± 0.030	12.45 ± 0.184	4.25 ± 0.000	2.85 ± 0.000
	P11	30.37 ± 0.040	10.50 ± 0.128	4.04 ± 0.010	2.63 ± 0.120
	P12	32.04 ± 0.047	11.32 ± 0.158	4.06 ± 0.014	2.84 ± 0.158
Annealed[b]	**P9**	26.84 ± 0.013	24.94 ± 0.267	4.17 ± 0.012	2.21 ± 0.105
	P10	28.93 ± 0.019	22.85 ± 0.293	4.15 ± 0.041	3.33 ± 0.558
	P11	30.72 ± 0.027	18.23 ± 0.242	4.01 ± 0.011	3.85 ± 0.301
	P12	32.06 ± 0.021	20.32 ± 0.208	4.02 ± 0.008	3.54 ± 0.156

[a] Polymer thin films were spin-coated on Si (100) substrates from *o*-DCB (10 mg/mL). [b] 200 °C for 30 min.

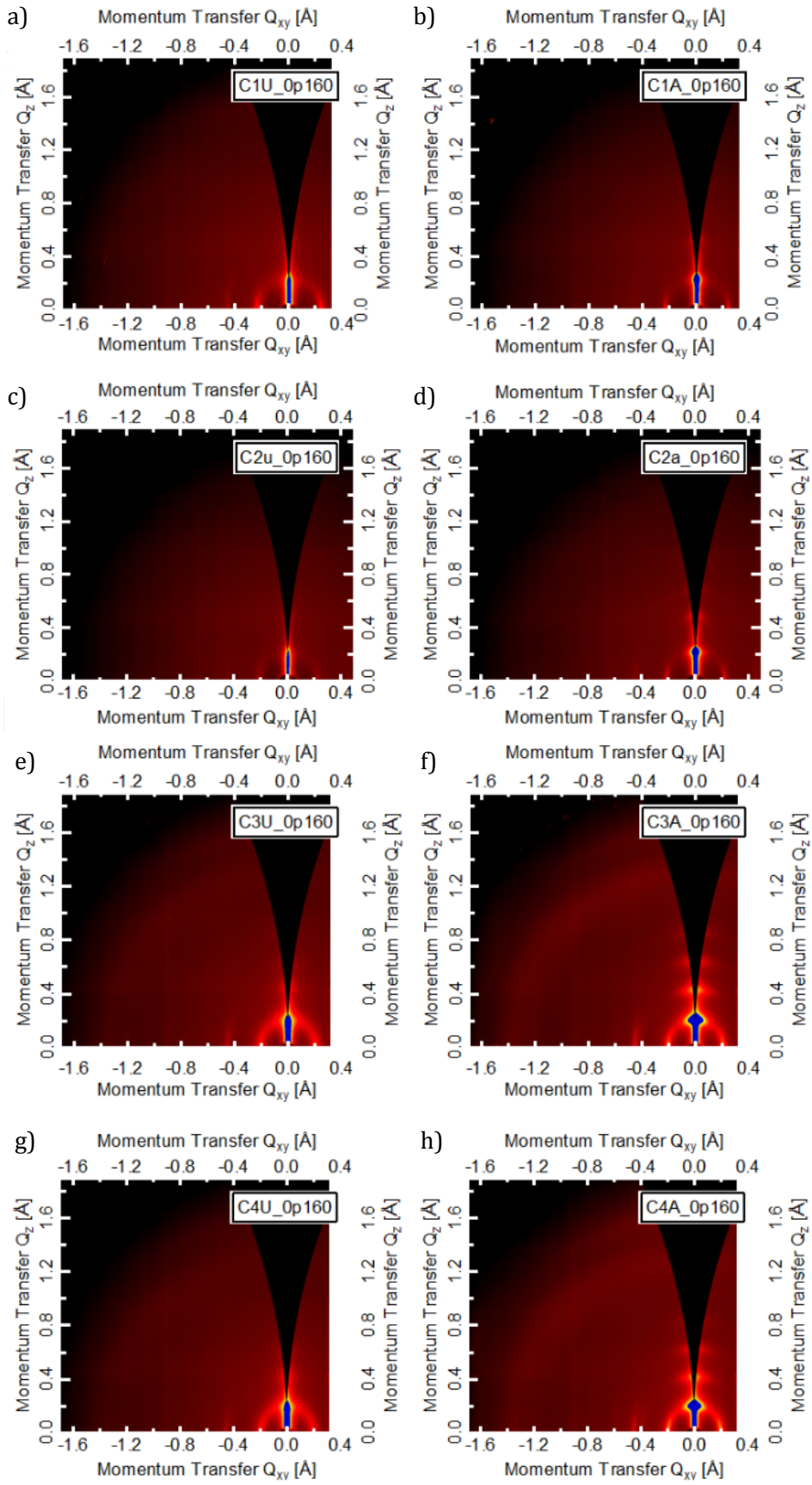

Figure 4.5. 2D-GIWAXS diffraction patterns of as-cast (left) and annealed (200 °C for 30 min, right) films of P9: a) and b), P10: c) and d), P11: e) and f), and P12: g) and h) spin-coated on Si substrates (100) from *o*-dichlorobenzene (10 mg/mL).

4.2.5 OFET Device Performance

The electrical performance of the polymers was investigated in BG-TC field effect transistors. Devices were fabricated on heavily doped n+-Si (100) substrates using silver source-drain electrodes, and a thermally grown SiO_2 dielectric treated with trichloro(octadecyl)silane. Polymer films were spin-coated from *o*-dichlorobenzene (5 mg/mL) and annealed at 200 °C for 30 min. Figure 4.6 shows the transfer and output characteristics of the best performing devices. In all cases unipolar, n-type charge transport was observed, with relatively little hysteresis and moderate I_{on}/I_{off} ratios, under low operating voltages. As shown in Table 4.4, the average charge carrier mobility of P9, P10, and P11, systematically increases from 0.0062 cm^2/Vs (P9) to 0.03 cm^2/Vs (P11) as the branch-point is moved further from the polymer backbone. The mobility peaks for P11 before dropping again for P12 (0.014 cm^2/Vs), which has a similar value to P10 (0.013 cm^2/Vs). Interestingly, the values obtained closely mirror the trend observed in the coherence length of the (010) peak (i.e. the π-π stacking peak) of the annealed films (Section 4.2.4). This appears to be a better indicator of transistor performance than the actual π-π stacking distance, which does not appear to have a significant impact on the mobility. A similar observation was recently reported for a benzodifurandione-based polymer with various branched alkyl-chains, in which there was little correlation between the π-π stacking distance and the charge carrier mobility, despite particularly close backbone packing.[136] Instead, it was suggested that polymer crystallinity, thin film disorder, and solid-state packing conformation were responsible for the trend in device performance.[136]

Table 4.4. OFET Device Characteristics[a]

	Average	Peak		
	μ_e [x 10^{-2} cm^2/Vs]	μ_e [x 10^{-2} cm^2/Vs]	V_T [V]	I_{on}/I_{off} [x 10^3]
P9	0.62 ± 0.09	0.7	6.0	0.6
P10	1.30 ± 0.42	1.8	4.8	4.7
P11	3.00 ± 0.50	3.7	5.4	3.3
P12	1.40 ± 0.39	1.9	4.4	1.7

[a] BG-TC devices fabricated on heavily doped n+-Si (100) substrates with thermally grown SiO_2 (400 nm) dielectric treated with OTS, and Al (40 nm) source drain electrodes. Polymer active layers were spin-coated from *o*-DCB solution (5 mg/mL) and annealed at 200 °C for 30 min.

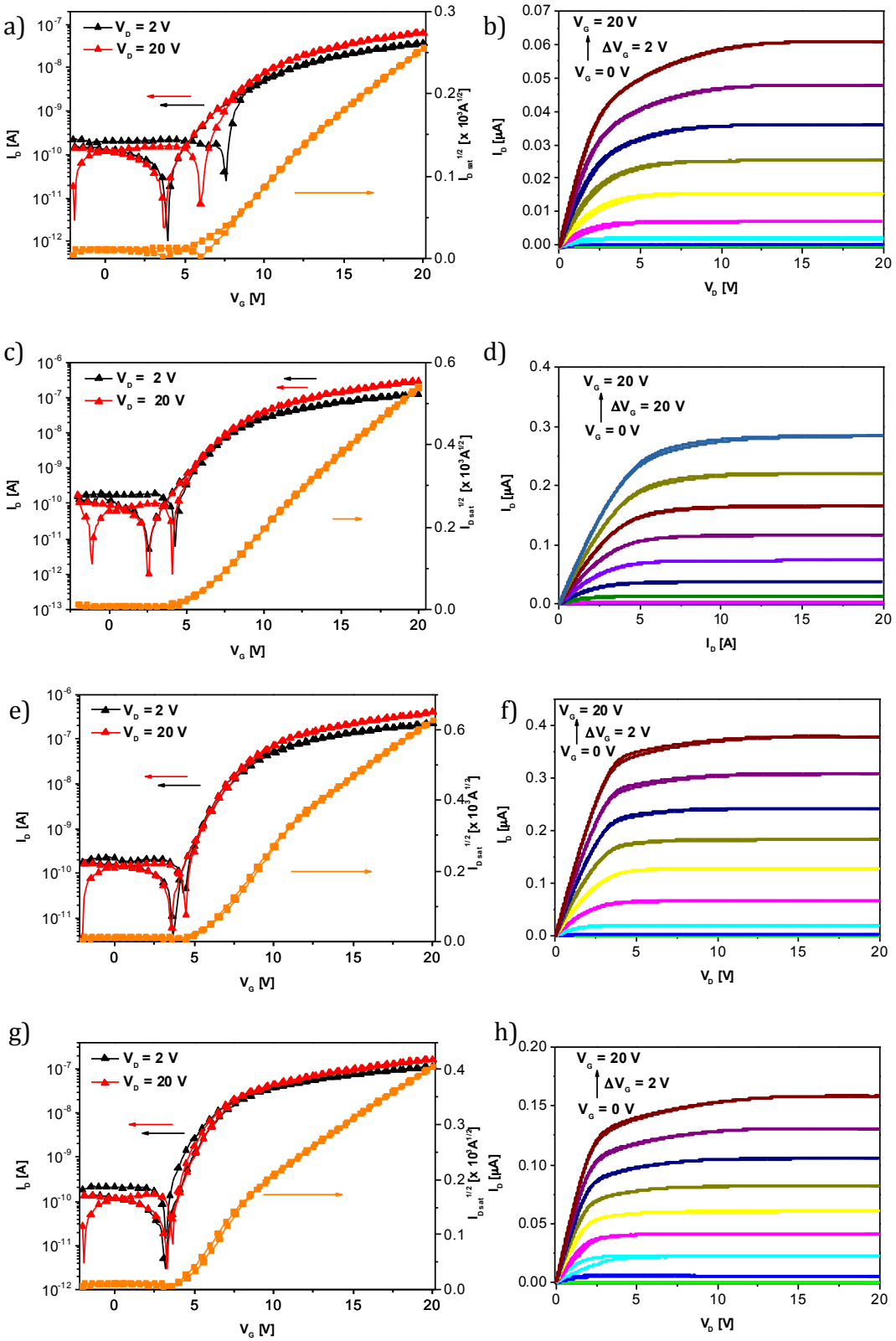

Figure 4.6. Transfer (left) and output (right) characteristics of the best performing BG-TC devices of P9: a) and b), P10: c) and d), P11: e) and f), and P12: g) and h), fabricated on heavily doped n⁺-Si (100) substrates with thermally grown SiO_2 (400 nm) treated with OTS. Polymer active layers were spin-coated from *o*-dichlorobenzene solution (5 mg/mL) and annealed at 200 °C for 30 min. Al (40 nm) source-drain electrodes were deposited under vacuum. The channel width and length were 1000 μm and 40 μm, respectively.

4.2.6 All-polymer OPV Device Performance

The photovoltaic performance of the polymers as an electron acceptor in all-polymer OPV devices was investigated in bulk heterojunction cells with PTB7-Th (Figure 4.7a) as the electron donor. PTB7-Th was chosen as the electron donor due to previous reports of high hole mobility and promising OPV performance in all-polymer blends with NDI based polymers.[152,177] However, it is important to note there is some overlap between the absorption of PTB7-Th and NDI, which is expected to limit the photocurrent and potentially reduce device efficiency.[177] Devices were fabricated in an inverted configuration (ITO/ZnO/PTB7-Th:P9-12/MoO_3/Ag), and measured under simulated AM 1.5G illumination at 100 mW/cm^2. For initial testing polymer active layers which consisted of a donor:acceptor blend ratio of 1:1 (w:w), were spin-coated from chlorobenzene (20 mg/mL) without the use of any solvent additives. Figure 4.7b-c displays the *J-V* characteristics and EQE spectra of these devices. As summarised in Table 4.5, P9 exhibited the highest device performance during initial testing, with a J_{SC} of 9.75 mA/cm^2 and a FF of 0.51, resulting in an average power conversion efficiency of 4.08%. The performance of the other polymers is considerably lower (between 2.62 and 2.08%) and appears to gradually decrease as the branch-point is moved further from the polymer backbone. Indeed, there are significant differences between the J_{SC} and FF across the series, whilst the V_{OC} are similar, in agreement with the LUMO energy levels (between -4.39 and -4.41 eV) calculated in Section 4.2.3. In an effort to optimise the performance, the addition of an additive (3% DIO) to the polymer active layer was evaluated. Interestingly, for all but P11 the performance decreased when DIO was added to the blend, mainly due to a decrease in the J_{SC}, particularly in the case of P9 and P10.

Table 4.5. All-polymer OPV Device Characteristics[a]

	J_{SC} [mA/cm^2]	V_{OC} [V]	FF	PCE [%]
P9	9.75 ± 0.10	0.82 ± 0.01	0.51 ± 0.02	4.08 ± 0.05
P9 + 3% DIO	7.65 ± 0.15	0.82 ± 0.01	0.48 ± 0.02	3.01 ± 0.10
P10	7.10 ± 0.10	0.84 ± 0.01	0.44 ± 0.01	2.62 ± 0.05
P10 + 3% DIO	5.64 ± 0.20	0.84 ± 0.01	0.45 ± 0.01	2.13 ± 0.08
P11	6.00 ± 0.15	0.82 ± 0.01	0.46 ± 0.02	2.26 ± 0.10
P11 + 3% DIO	7.20 ± 0.10	0.82 ± 0.01	0.43 ± 0.02	2.54 ± 0.10
P12	5.77 ± 0.10	0.82 ± 0.01	0.44 ± 0.02	2.08 ± 0.10
P12 + 3% DIO	6.00 ± 0.10	0.82 ± 0.01	0.41 ± 0.01	2.08 ± 0.05

[a] Inverted devices (ITO/ZnO/PTB7-Th:P9-12/MoO_3/Ag) measured under AM 1.5G illumination at 100 mW/cm^2. Polymer active layers were spin-coated from chlorobenzene solution (20 mg/mL) in a blend ratio of 1:1 (w:w). The pixel size was 0.045 cm^2.

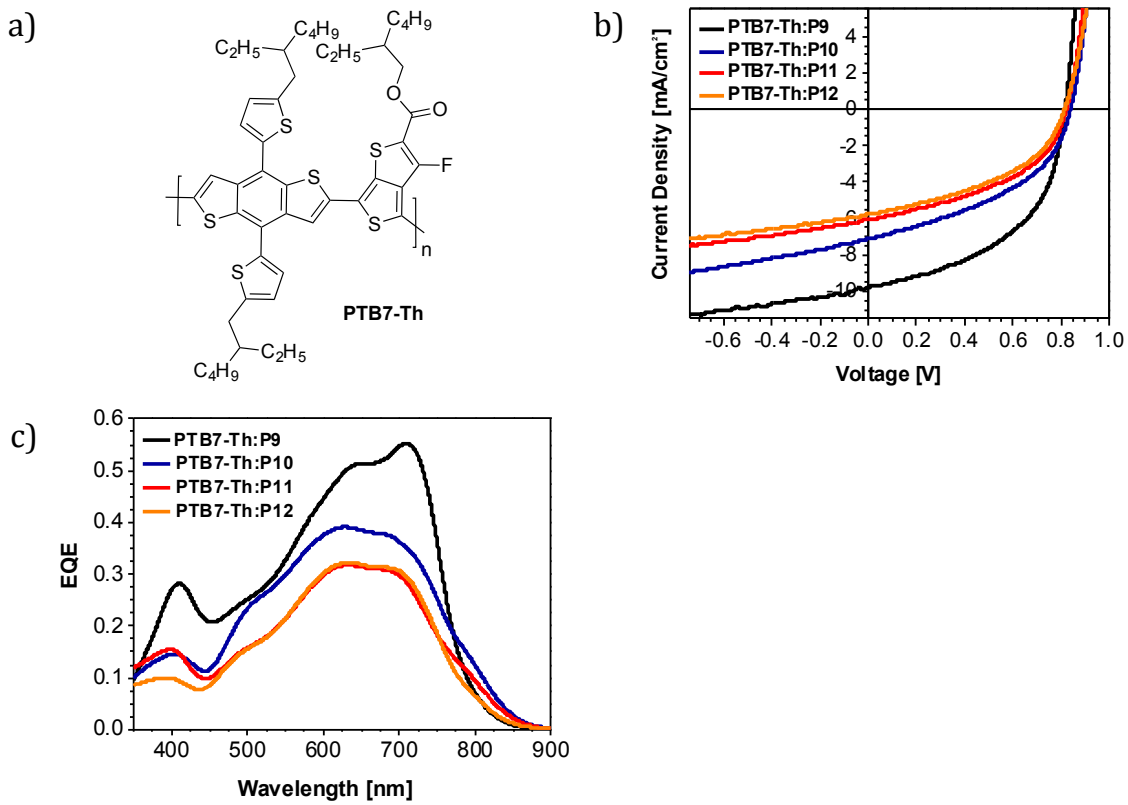

Figure 4.7. a) Structure of PTB7-Th, and b) *J-V* curves and c) EQE spectra of PTB7-Th:P9-12 inverted devices (ITO/ZnO/PTB7-Th:P9-12/MoO_3/Ag) measured under AM 1.5G illumination at 100 mW/cm^2. Polymer active layers were spin-coated from chlorobenzene solution (20 mg/mL) in a blend ratio of 1:1 (w:w) without the use of any solvent additives. The pixel size was 0.045 cm^2.

4.2.7 Blend Morphology and Charge Generation Dynamics

Atomic force microscopy was used to study the surface morphology of thin films of the blends, prepared using the same conditions as those used for OPV device fabrication. As demonstrated in Figure 4.8, there are subtle differences between the films, with a relatively uniform microstructure and no obvious evidence of large-scale phase separation observed in all cases. The RMS surface roughness of the films does however vary somewhat across the series (from 6.03, to 8.13, 9.06, and 5.17 nm, respectively), most likely due to differences between the solid-state ordering and intermolecular π-π interactions of the acceptor polymers (Section 4.2.4), although further characterisation of the blends is needed to validate this. As such, it is difficult to correlate the AFM data with the observed trend in photovoltaic performance.

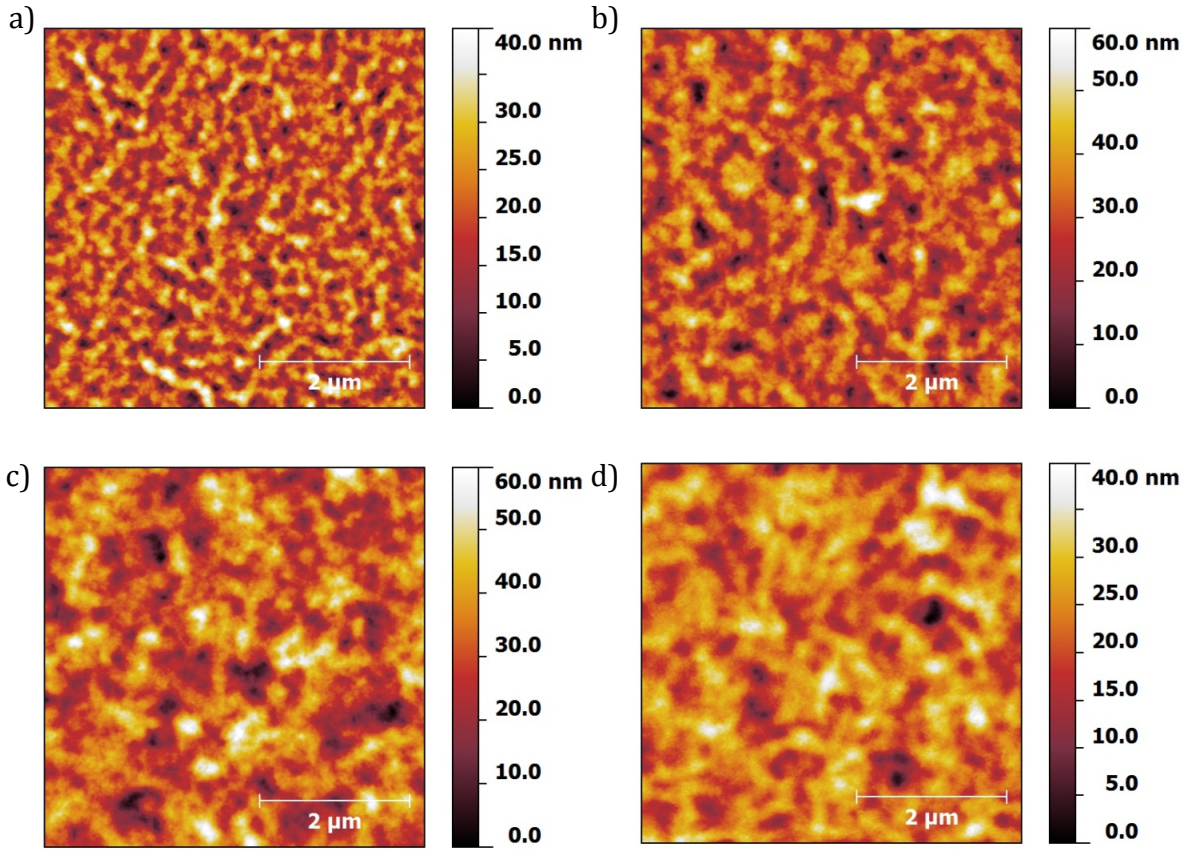

Figure 4.8. AFM topography images of thin films of a) PTB7-Th:P9, b) PTB7-Th:P10, c) PTB7-Th:P11, and d) PTB7-Th:P12 blends, spin-coated from chlorobenzene solution (20 mg/mL) in a blend ratio of 1:1 (w:w). Scale 5 µm x 5 µm.

Photoluminescence quenching experiments and sub-microsecond timescale transient absorption spectroscopy were used to evaluate the charge generation dynamics of neat thin films and PTB7-Th:P9-12 blends (see Appendix). Note however, the preliminary results were inconclusive and further studies are needed before reliable conclusions can be drawn.

4.3 Conclusion

In this chapter, the synthesis of a series of novel NDI based polymers containing various branched alkyl side-chains was described. Through detailed analysis of the optoelectronic properties (UV-vis, PESA) and solid-state organisation (DSC, AFM, GIWAXS) of the polymers, the influence of the alkyl side-chain branching position is revealed. In agreement with previous reports,[135,136] the alkyl-chain branching position was found to have a significant effect on the intermolecular π-π ordering of the polymers, with an increase in branch-point resulting in an increase in polymer aggregation, and a decrease in π-π stacking distance, as a result of a decrease in steric hindrance between the solubilising alkyl-chains and the conjugated polymer backbone.

By investigating the electrical performance of the polymers in BG-TC field effect transistors, the promise of branch-point manipulation as an effective strategy for improving charge carrier mobility is demonstrated, with the average charge carrier mobility of P9-11 systematically increasing as the branch-point is moved further from the polymer backbone from 0.0062 to 0.03 cm^2/Vs, before dropping again to 0.014 cm^2/Vs for P12. Interestingly, the values obtained closely mirror the trend observed in the coherence length of the (010) peak (i.e. the π-π stacking peak) of the annealed films, which appears to be a better indicator of transistor performance than the actual π-π stacking distance.

In addition, for the first time the influence of the alkyl-chain branching position on the performance of all-polymer OPV devices was evaluated. A gradual decrease in power conversion efficiency was observed as the branch-point was moved further from the polymer backbone. A combination of experimental techniques (AFM, PL, TAS) were used to try to understand the observed trend in performance, however further work is needed.

Chapter 5
Expanding the Series: 2,7-Bis(4-decylhexadecyl)benzo[*lmn*][3,8]phenanthroline-1,3,6,8(2*H*,7*H*)-tetrone Polymers for OFET Applications

5.1 Introduction

In Chapter 4 a novel NDI based polymer containing 4-decylhexadecyl side-chains (P11) demonstrated promising electrical performance in transistor applications (0.03 cm^2/Vs), highlighting the potential of branch-point manipulation in the development of high performing conjugated polymers in organic electronics. Encouraged by these results, the scope of this monomer was evaluated further using a range of fluorinated and non-fluorinated, thiophene and selenophene containing co-monomers that have previously been shown to have a beneficial effect on charge transport. Indeed, there have been many reports describing how fluorination can increase the charge carrier mobility of both p-type and n-type polymers due to planarising S···F interactions along the backbone.[178–180] In addition, the strong electron withdrawing ability of the fluorine atom has been shown to result in improved photovoltaic performance due to changes in the electronic energy levels.[181,182] The use of selenophene based monomers have also been found to increase device performance by promoting stronger intermolecular interactions and denser chain packing.[183–185]

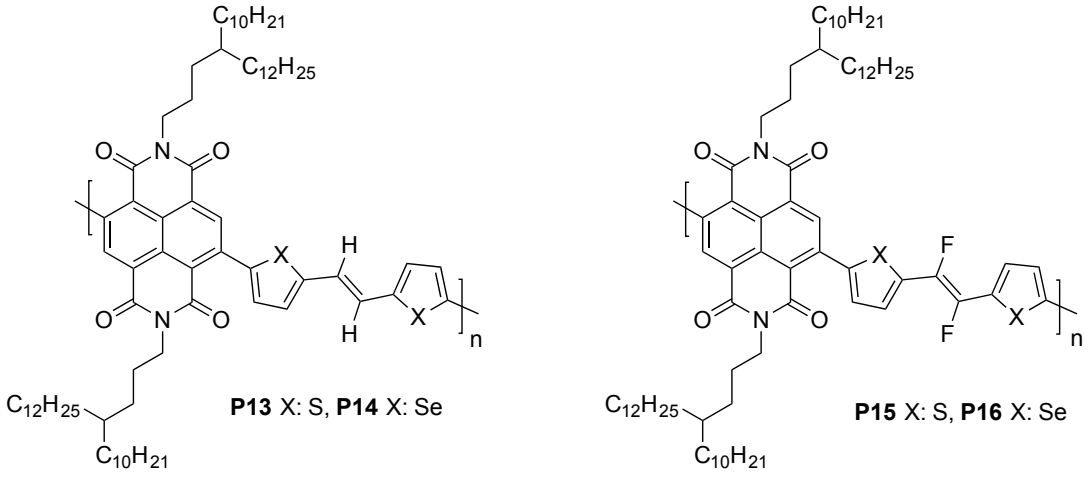

Figure 5.1. Structure of the target polymers.

In the first part of this Chapter, a series of fluorinated and non-fluorinated, (*E*)-1,2-bis(thiophen-2-yl)ethene and (*E*)-1,2-bis(selenophen-2-yl)ethene based polymers are described (Figure 5.1). Recently (*E*)-1,2-bis(thiophen-2-yl)ethene co-polymers have demonstrated impressive transistor performance (up to 2.77 cm^2/Vs) due to enhanced backbone planarity and stronger intermolecular interactions, as a result of the vinylene spacer.[157,186,187] Co-polymers of the selenophene analogue ((*E*)-1,2-bis(selenophen-2-yl)ethene) have also been reported demonstrating a significant improvement in transistor performance (up to 4.97 cm^2/Vs).[187,188] The addition of electron withdrawing (nitrile)[189] and electron donating (alkoxy)[190] substituents to the co-monomer has also been explored yielding further

improvements in device performance. However the addition of strongly electron withdrawing fluorine groups has yet to be reported.

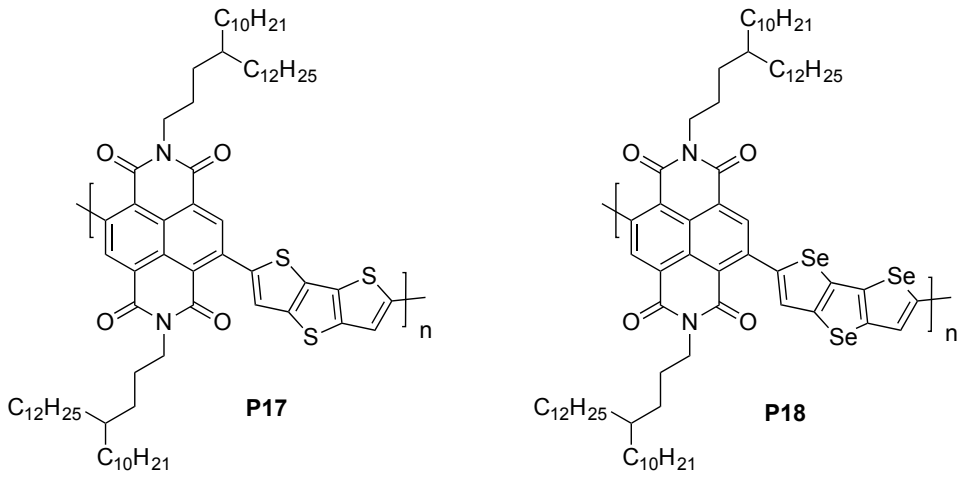

Figure 5.2. Structure of the target polymers.

In the second part of this Chapter, a series of dithieno[3,2-*b*:2',3'-*d*]thiophene (DTT) and diseleno[3,2-*b*:2',3'-*d*]selenophene (DSS) based polymers are described (Figure 5.2). Since NDI based polymers containing fused thiophene co-monomers have previously demonstrated high n-type charge transport (up to 0.012 cm^2/Vs),[162,164] it was thought the selenophene analogue could potentially be of interest.

5.2 Results and Discussion
Fluorinated and non-fluorinated, (*E*)-1,2-bis(thiophen-2-yl)ethene and (*E*)-1,2-bis(selenophen-2-yl)ethene based polymers

5.2.1 Polymer Synthesis

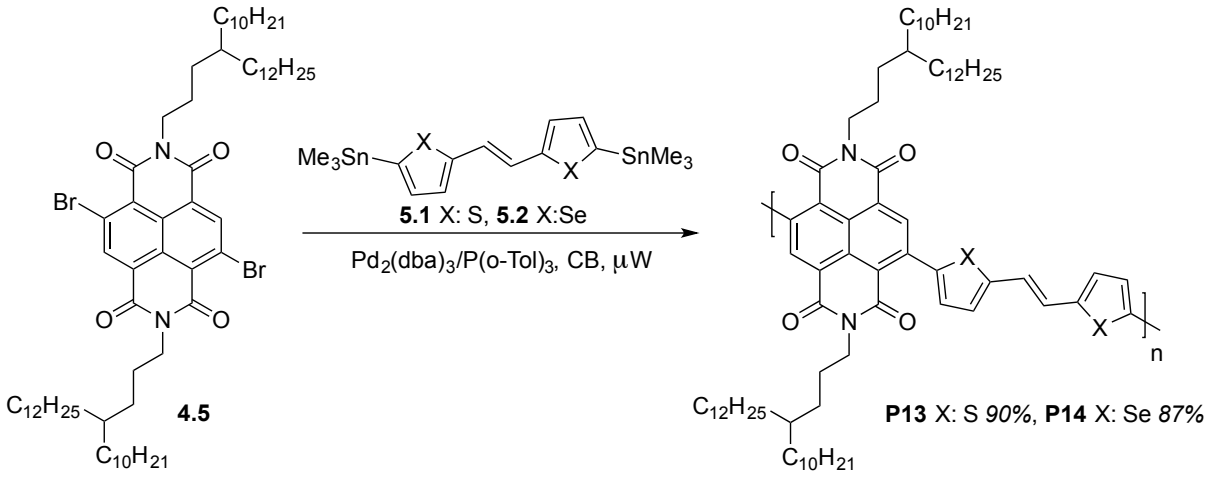

Scheme 5.1. Synthetic pathway to the non-fluorinated polymers.

The non-fluorinated polymers (P13 and P14) were synthesised via microwave assisted, Stille cross-coupling reactions[97–99] of the 4,9-dibromo-2,7-bis(4-decylhexadecyl)benzo[*lmn*][3,8]phenanthroline-1,3,6,8(2*H*,7*H*)-tetrone unit (4.5) (synthesised as described in Chapter 4) with the corresponding distannylated co-monomer (5.1 or 5.2) in anhydrous chlorobenzene, using $Pd_2(dba)_3$ and P(o-Tol)$_3$ as the catalyst system (Scheme 5.1). The fluorinated analogues (P15 and P16) were also synthesised via Stille cross-coupling reactions,[97–99] although under slightly different conditions (Scheme 5.2) due to the small amount of [(*E*)-1,2-difluoroethene-1,2-diyl]bis(tributylstannane) available and a desire to utilise it in the final step of the reaction. The alternative necessitated several moderately yielding synthetic steps from [(*E*)-1,2-difluoroethene-1,2-diyl]bis(tributylstannane) to the stannylated bithiophene or biselenophene co-monomer, and may not have therefore afforded sufficient material for polymerisation. Thus 4.5 was first coupled with either tributyl(thiophen-2-yl)stannane or tributyl(selenophen-2-yl)stannane, and subsequently brominated with *N*-bromosuccinimide to afford the dibrominated monomers 5.5 or 5.6, respectively. 5.5 and 5.6 were then co-polymerised with [(*E*)-1,2-difluoroethene-1,2-diyl]bis(tributylstannane) in a mixture of anhydrous *o*-xylene and DMF, using copper(I) iodide co-catalyst and $Pd(PPh_3)_4$ catalyst. The addition of DMF and copper(I) iodide to the reaction was anticipated to accelerate the reaction time and increase the molecular weight, in accordance with previous reports.[191–196]

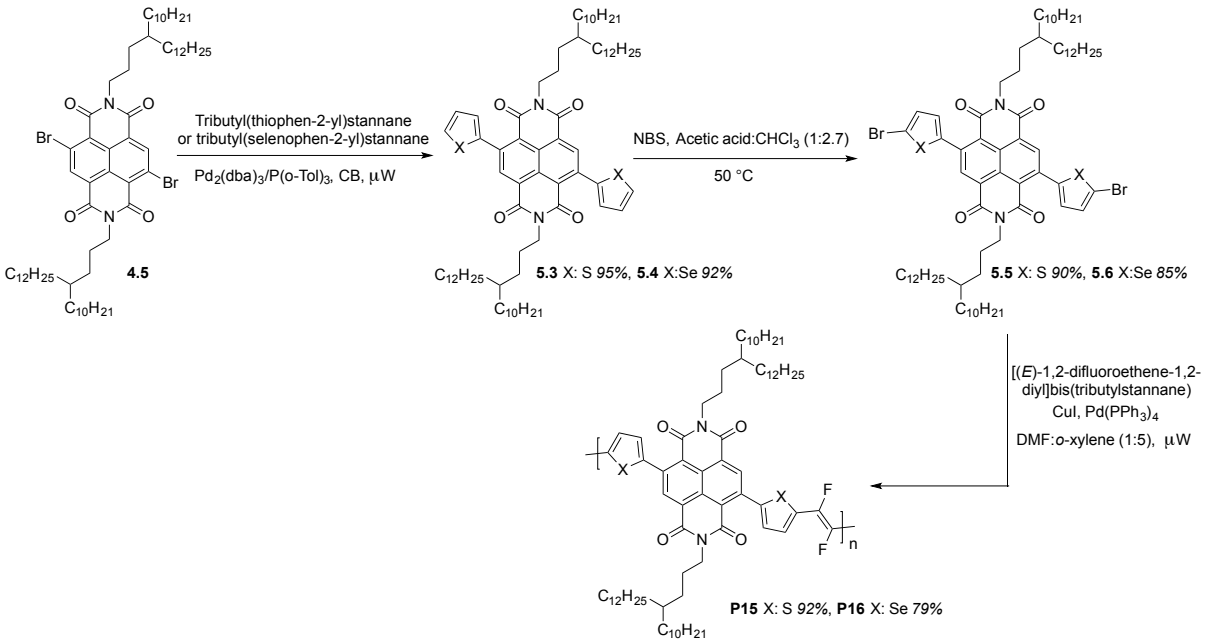

Scheme 5.2. Synthetic pathway to the fluorinated polymers.

The chemical structure of the polymers was confirmed by a combination of elemental analysis, and high temperature ^{1}H NMR spectroscopy in 1,1,2,2-tetrachloroethane-d_2 (see Appendix).

Polymer molecular weights and dispersities were determined by gel permeation chromatography in either trichlorobenzene at 140 °C (P13 and P14), or chlorobenzene at 80 °C (P15 and P16), and are summarised in Table 5.1. The use of trichlorobenzene in the case of P13 and P14 was necessary to prevent polymer aggregation observed when measured in chlorobenzene. The number-average molecular weight of P15 and P16 were slightly lower than P13 and P14. This is most likely associated to the differences between the polymerisation conditions used. The thermal stability of the polymers was probed by thermogravimetric analysis (see Appendix and Table 5.1) in which a 5% weight loss was observed after 410 °C for all polymers.

Table 5.1. Molecular Weights and Thermal Properties

	M_n[a] [kg/mol]	M_w[a] [kg/mol]	Đ[a]	T_d[b] [°C]
P13	51†	116†	2.3†	436
P14	60†	139†	2.3†	421
P15	33	68	2.1	431
P16	44	83	1.9	413

[a] Determined by gel permeation chromatography in CB at 80 °C against polystyrene standards with the exception of † which was determined by HT-GPC in TCB at 140 °C. [b] 5% weight loss temperatures measured by thermal gravimetric analysis under a N_2 atmosphere.

5.2.2 Optical Properties and Frontier Molecular Orbital Energy Levels

The optical properties of the polymers in dilute chlorobenzene, and as thin-films spin-coated from chlorobenzene (5 mg/mL), were investigated by UV-vis absorption spectroscopy, as presented in Figure 5.3 and Table 5.2. Two distinct absorption bands between 350-500 nm and 500-900 nm, are observed in both the solution and thin-film spectra of the four polymers. Consistent with previous reports, these bands can be attributed to π-π* transitions, and ICT between the electron rich and electron deficient units, respectively.[186,188] Interestingly, there are significant differences between the non-fluorinated (P13 and P14) and fluorinated (P15 and P16) polymers. Indeed, a substantial blue-shift in absorption maxima of 144 nm is observed between the solution spectra of P13 (λ_{max} solution = 747 nm) and P15 (λ_{max} solution = 603 nm), whilst a slightly smaller blue-shift of 65 nm is observed upon fluorination of P14 (λ_{max} solution = 770 nm) to P16 (λ_{max} solution = 705 nm). Furthermore, pronounced shoulders at 839 nm (P13) and 860 nm (P14) are observed in the solution spectra of the non-fluorinated polymers. Although a less well-defined shoulder is also present for the fluorinated polymer P15 (705 nm), it appears fluorination may influence the extent of backbone aggregation and intermolecular ordering. Additionally, when comparing the effects of selenophene substitution on the absorption maxima, a distinct red-shift is observed between P13 and P14 (23 nm), and P15 and

P16 (102 nm). This is due to the stronger electron donating properties of the selenophene unit relative to thiophene, as is often reported.[188,197] The thin-film spectra all closely mirror the trends in solution. However, it is interesting to note that the absorption maxima of P13 and P14 are blue-shifted upon film formation, in contrast to P15 and P16 which are red-shifted.

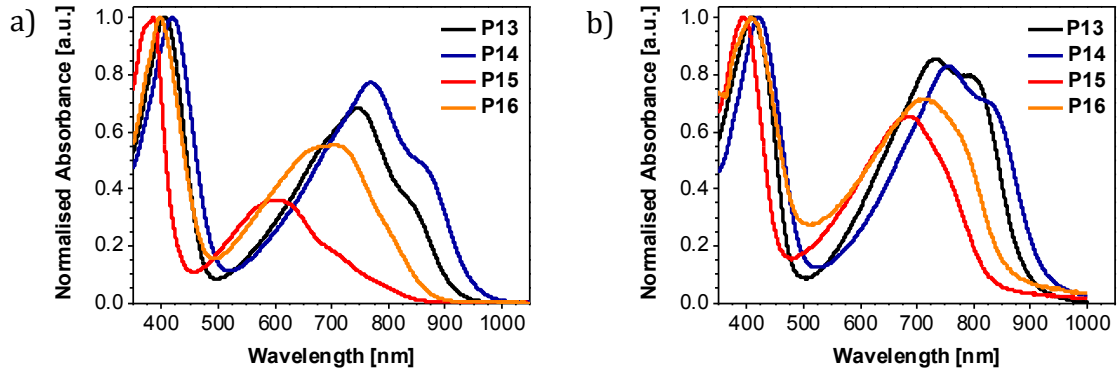

Figure 5.3. Normalised UV-vis absorption spectra of the polymers in a) dilute chlorobenzene solution at 20 °C and b) thin-films spin-coated on glass substrates from chlorobenzene solution (5 mg/mL).

The ionisation potentials of thin films of the polymers, spin-coated from chlorobenzene (5 mg/mL) were measured using photoelectron spectroscopy in air, and the LUMO energy levels were estimated by adding the negative of the ionisation potential to the absorption onset in the solid state (Table 5.2). In line with other reports,[178,198–201] an increase in ionisation potential upon fluorination is observed, due to the strong electron-withdrawing influence of the fluorine atom. Indeed, there is a difference of 0.19 eV between the ionisation potential of P13 (5.63 eV) and P15 (5.82 eV), and a difference of 0.20 eV between P14 (5.58 eV) and P16 (5.78 eV). In addition, although the values are close considering the error of the technique (± 0.05 eV), the replacement of the thiophene units with electron rich selenophene seems to result in a small decrease in ionisation potential, as well as a slight increase in the LUMO energy level, which overall yields a reduction in the optical band gap, in agreement with previous reports.[202]

Table 5.2. Optical Properties and Frontier Molecular Orbital Energy Levels

	λ_{max} Soln[a] [nm]	λ_{max} Film[b] [nm]	E_g opt[c] [eV]	I.P.[d] [eV]	LUMO[e] [eV]
P13	747 (839)	730 (793)	1.38	5.63	-4.25
P14	770 (860)	754 (821)	1.32	5.58	-4.26
P15	603 (705)	682	1.47	5.82	-4.35
P16	705	710	1.41	5.78	-4.37

[a] Measured in dilute CB at 20 °C. Shoulder peaks in parentheses. [b] Thin-films spin-coated on glass substrates from 5 mg/mL CB solution. Shoulder peaks in parentheses. [c] Determined from the absorption onset in the solid state. [d] Determined by PESA (error ± 0.05 eV). [e] Estimated by adding the negative of the ionisation potential to the absorption onset in the solid state.

5.2.3 Polymer Conformation and Packing

The thermal properties of the polymers were evaluated using differential scanning calorimetry measurements. As shown in Figure 5.4, no obvious thermal transitions were observed in the second heating and cooling scans of the polymers recorded between -30 and 330 °C under nitrogen, suggesting that the melting temperature is above 330 °C, since there are clear indications of crystallinity in the GIWAXS measurements (discussed further in Section 5.2.3).

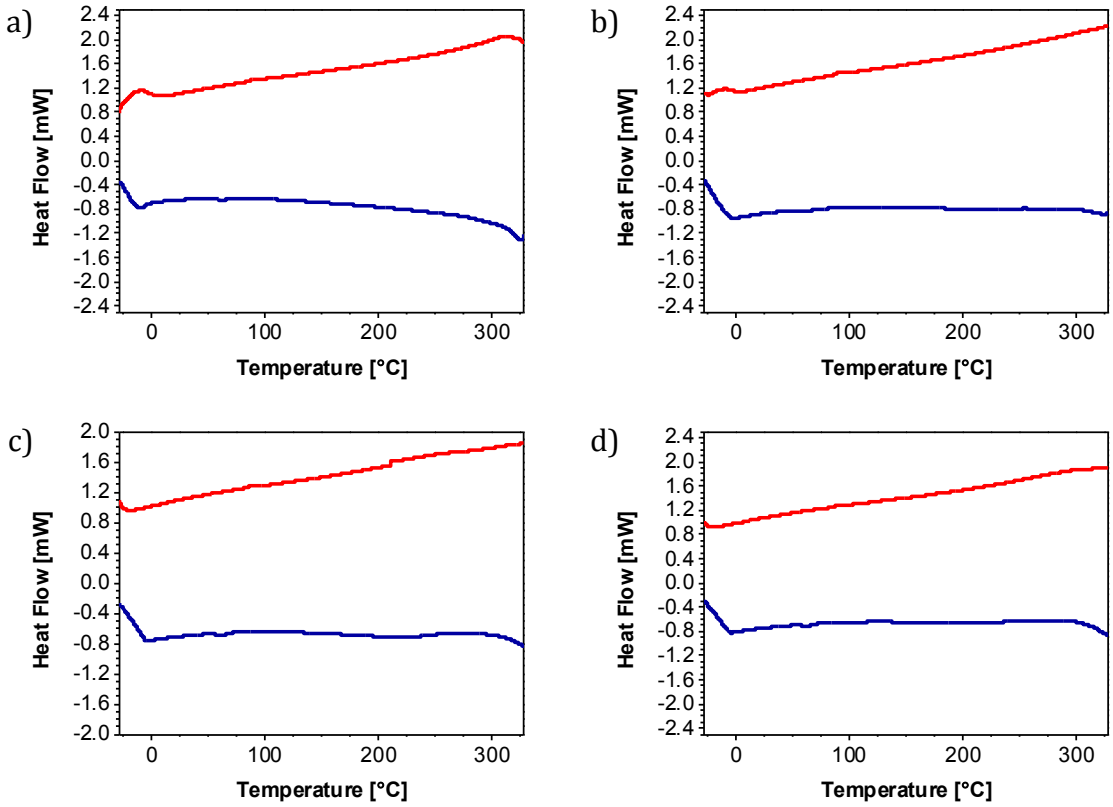

Figure 5.4. Second heating (red) and cooling (blue) scans of a) P13, b) P14, c) P15 and d) P16 measured by DSC, at a rate of 10 °C/min under a N_2 atmosphere.

The solid-state morphology of thin films of the polymers was studied using grazing incident wide-angle X-ray scattering measurements. Figure 5.5 displays the 2D-GIWAXS diffraction patterns of the polymers spin-coated from *o*-dichlorobenzene (5 mg/mL) and annealed at 200 or 300 °C for 30 minutes. Note the diffraction pattern of P14 annealed at 200 °C (Figure 5.5c) is misaligned and therefore will not be discussed further. There are subtle differences in the solid-state ordering of the polymers across the series, with a predominantly edge-on orientation with respect to the substrate observed for all polymers at both annealing temperatures. Indeed, distinct out-of-plane lamellar diffraction peaks (*h*00) and in-plane π-π stacking peaks (010) along the Q_z and Q_{xy} axes, respectively, consistent with edge-on ordering, are visible in Figure 5.5. However, in the films of P13, P15, and P16 annealed at 200 °C, a weak in-plane lamellar diffraction peak (*h*00) along the Q_{xy} axis is also visible. Although the intensity of this peak decreases upon annealing at higher temperatures (300 °C), it indicates some extent of face-on ordering is also present. Interestingly, this peak is not observed in P14.

Table 5.3. GIWAXS Results[a]

	In-plane (010) π-π Stacking Distance [Å]		In-plane (010) Coherence Length [nm]	
	200 °C	**300 °C**	**200 °C**	**300 °C**
P13	3.85 ± 0.000	3.83 ± 0.000	4.11 ± 0.042	4.25 ± 0.036
P14	-	3.88 ± 0.000	-	3.77 ± 0.084
P15	3.85 ± 0.000	3.82 ± 0.010	4.27 ± 0.082	3.65 ± 0.125
P16	3.90 ± 0.010	3.92 ± 0.010	4.84 ± 0.406	3.14 ± 0.080

[a] Polymer thin films were spin-coated on Si (100) substrates from *o*-DCB (5 mg/mL).

Table 5.3 summarises the peak fitting data from the 1D-GIWAXS scattering profiles (see Appendix) of the polymers. Due to misalignment of P14 at 200 °C it is difficult to draw conclusions about the π-π -spacing and coherence length across the series at this annealing temperature. However, at 300 °C it is clear that the in-plane π-π spacing increases when thiophene is replaced with selenophene, from 3.83 and 3.82 Å in P13 and P15, to 3.88 and 3.92 Å in P14 and P16, respectively. This is in contrast to previous reports which typically indicate stronger intermolecular interactions and denser chain packing upon selenophene substitution.[187,203] The effect of fluorination on the π-π stacking distance is less obvious, since there is little difference between the values of P13 and P15, whilst a slight increase of 0.04 Å between the values of P14 and P16. Interestingly, the in-plane π-π coherence length of the polymers appears to decrease upon both fluorination and selenophene substitution.

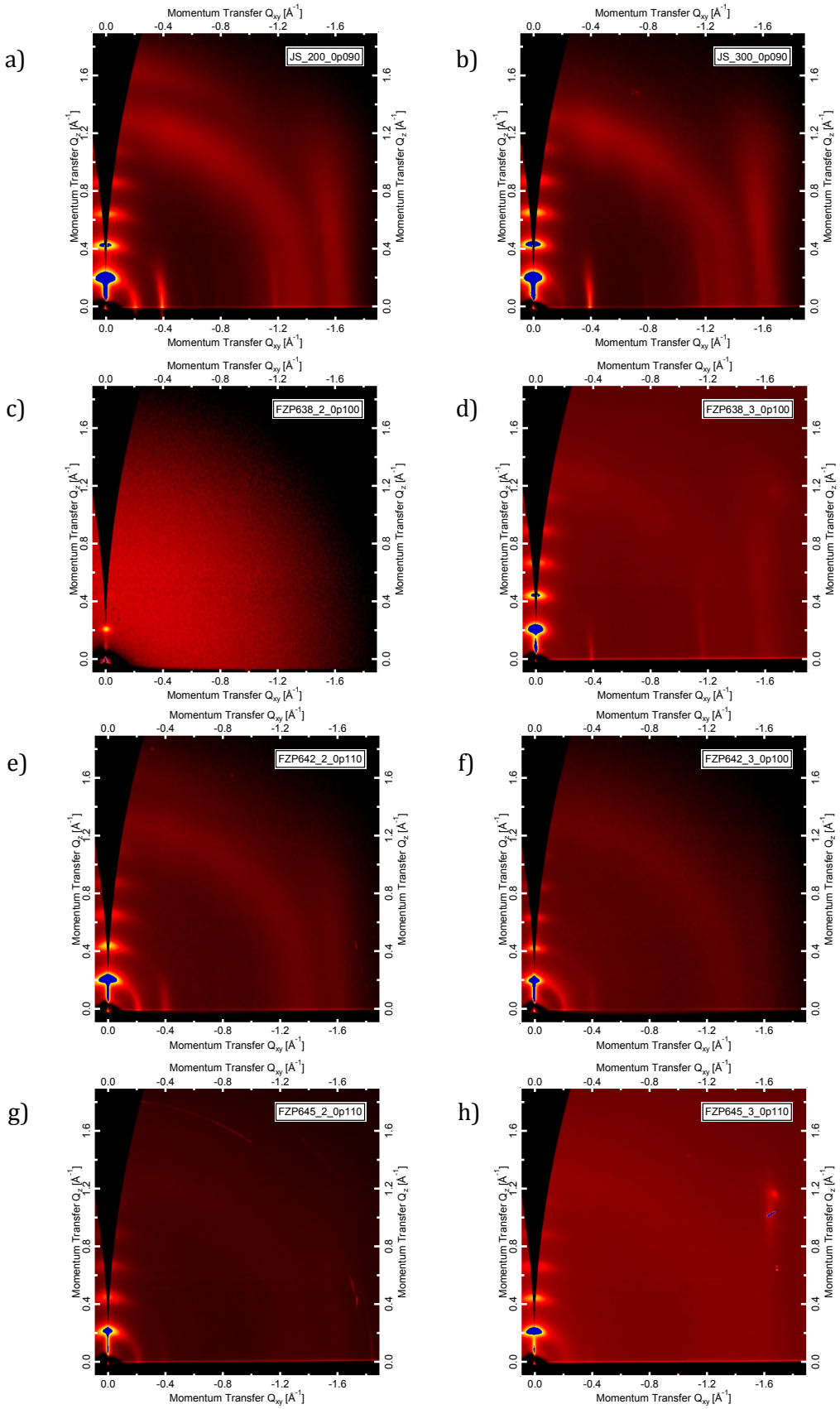

Figure 5.5. 2D-GIWAXS diffraction patterns of films of P13: a) and b), P14: c) and d), P15: e) and f), and P16: g) and h), spin-coated on Si substrates (100) from *o*-dichlorobenzene (5 mg/mL), and annealed at 200 °C (left), and 300 °C (right) for 30 min. N.B. The diffraction pattern of P14 annealed at 200 °C (Figure 5.5c) is misaligned.

5.2.4 OFET Device Performance

The electrical performance of the polymers was investigated in TG-BC field effect transistors. Devices were fabricated on glass, using gold source-drain electrodes and a PMMA dielectric (80 mg/mL in n-butyl acetate, 120 kg/mol). Polymer films were spin-coated from *o*-dichlorobenzene (5 mg/mL) and annealed at 200 °C for 30 min. Note based on the promising data presented in Section 5.2.3 for films annealed at 300 °C, devices annealed at 300 °C were also fabricated (see Appendix). However, at the time of writing only preliminary results were available and so the data will not be discussed further. The transfer and output characteristics of the best performing devices annealed at 200 °C are presented in Figure 5.6. Note high gate leakage is present in the output characteristics of P13 and P14. As shown in Table 5.4, the average charge carrier mobility of the polymers increases upon fluorination from 0.028 (P13) to 0.041 cm^2/Vs for P15, and from 0.015 (P14) to 0.035 cm^2/Vs for P16. Since the solid-state ordering of the polymers by GIWAXS does not include P14 (Section 5.2.3), it is difficult to comment on the likely cause of this apparent increase. However, there are many examples of similar reports in the literature which suggest an increase in backbone planarity upon fluorination is responsible for the improvement in performance, although further characterisation is needed to validate this.[178–180,200] The replacement of thiophene with selenophene on the other hand leads to a slight decrease in performance. This is most likely due to the increase in the in-plane π-π spacing revealed by GIWAXS.

Table 5.4. OFET Device Characteristics[a]

	Average	Peak		
	$\mu_{e\ sat}$ [cm^2/Vs]	$\mu_{e\ sat}$ [cm^2/Vs]	V_T [V]	I_{on}/I_{off}
P13	0.028 ± 0.022	0.053	34.5 ± 3.0	$1 \times 10^4 \sim 1 \times 10^5$
P14	0.015 ± 0.0015	0.016	29.8 ± 0.7	$1 \times 10^2 \sim 1 \times 10^3$
P15	0.041 ± 0.0043	0.047	16.6 ± 3.9	$1 \times 10^4 \sim 1 \times 10^5$
P16	0.035 ± 0.0071	0.045	20.4 ± 0.8	$1 \times 10^3 \sim 1 \times 10^4$

[a] TG-BC devices fabricated on glass substrates using Au (60 nm) source drain electrodes and a PMMA dielectric (80 mg/mL in n-butyl acetate, 120 kg/mol). Polymer active layers were spin-coated from *o*-DCB (5 mg/mL) and annealed at 200 °C for 30 min.

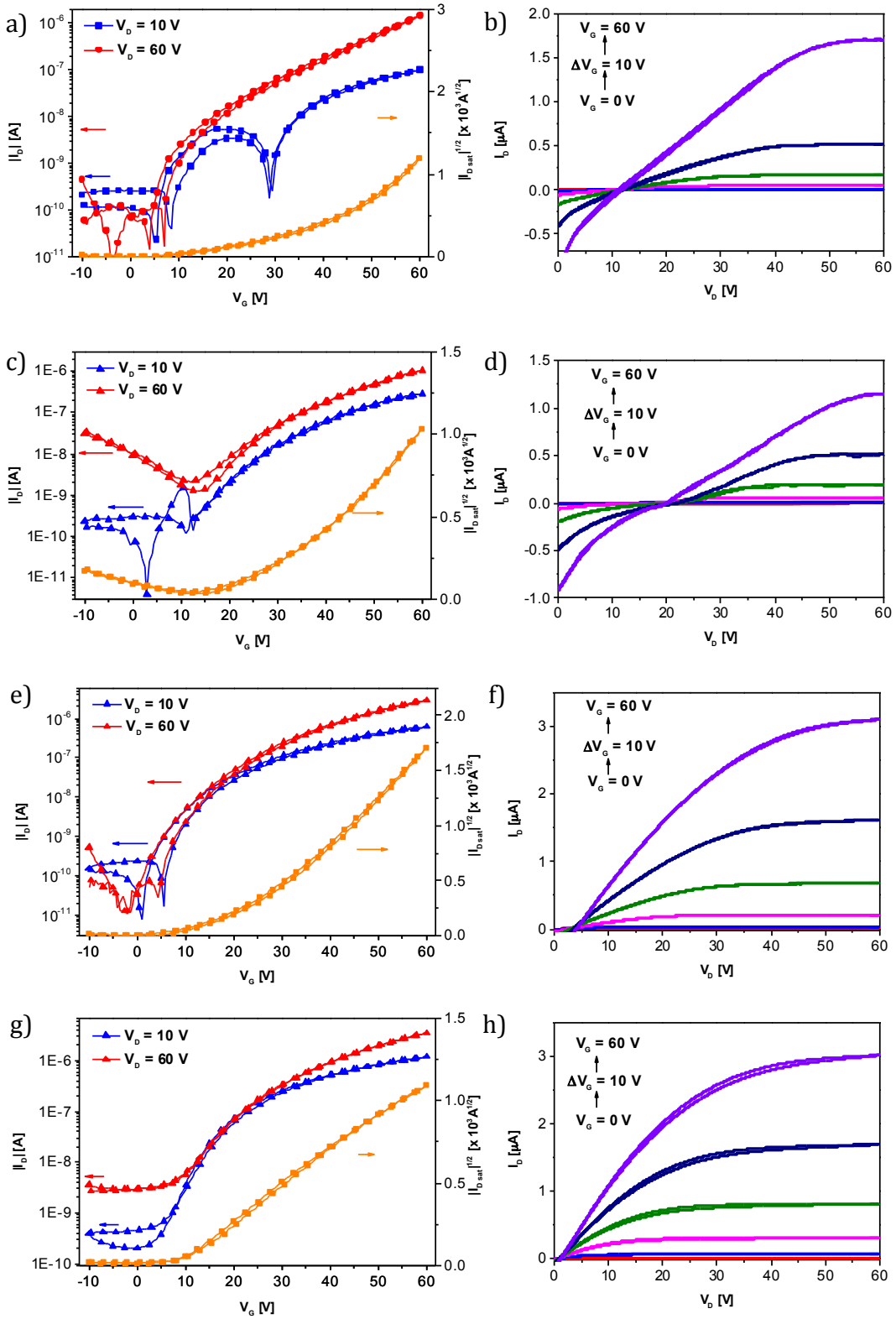

Figure 5.6. Transfer (left) and output (right) characteristics of the best performing TG-BC devices of P13: a) and b), P14: c) and d), P15: e) and f), and P16: g) and h), fabricated on glass substrates using Au (60 nm) source-drain electrodes, and PMMA (80 mg/ml in n-butyl acetate, 120 kg/mol) dielectric. Polymer active layers were spin-coated from *o*-dichlorobenzene solution (5 mg/mL) and annealed at 200 °C for 30 min. The channel width and length were 1000 μm and 40 μm, respectively.

Dithieno[3,2-*b*:2',3'-*d*]thiophene and diseleno[3,2-*b*:2',3'-*d*]selenophene based polymers

5.2.5 Polymer Synthesis

The polymers were synthesised via microwave assisted, palladium-catalysed, Stille cross-coupling reactions[97–99] of the 4,9-dibromo-2,7-bis(4-decylhexadecyl)benzo[*lmn*][3,8]phenanthroline-1,3,6,8(2*H*,7*H*)-tetrone unit (4.5) with the corresponding distannylated co-monomer (5.7 or 5.8) in anhydrous chlorobenzene, as described in Scheme 5.3. The polymers were purified by precipitation, followed by Soxhlet extraction in methanol (24 h), acetone (24 h), hexane (24 h), and chloroform (12 h),to remove low molecular weight oligomers. The polymers were then extracted with chlorobenzene and further purified by precipitation in methanol. Note the solubility of P18 was very poor, even in hot *o*-dichlorobenzene, and so the majority of the yield was insoluble material. As a result full characterisation of the polymer (TGA, PESA, DSC) was not possible. A reduction in the solubility of selenophene polymers is a common observation that is typically associated with enhanced quinoidal character and stronger intermolecular interactions.[204,203,205,206]

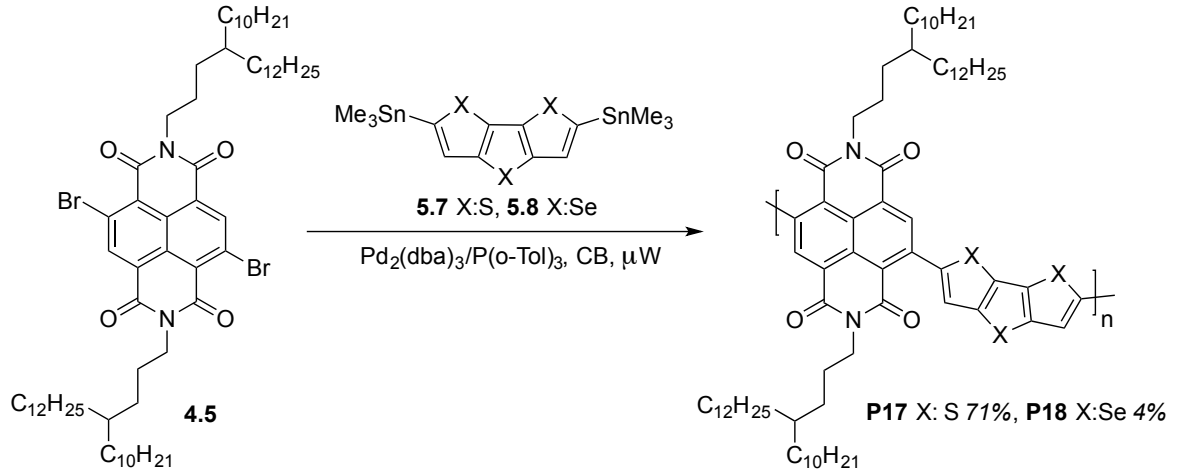

Scheme 5.3. Synthetic pathway to the polymers.

The chemical structure of the polymers was confirmed by elemental analysis, and ^{1}H NMR spectroscopy in 1,1,2,2-tetrachloroethane-d_2 at 130 °C (see Appendix). The number-average molecular weight of P17 and P18 were measured using gel permeation chromatography in chlorobenzene at 80 °C to be 170 and 100 kg/mol, respectively (Table 5.5). Despite the poor solubility of P18, the number-average molecular weight was remarkably high. The thermal stability of P17 was probed by thermogravimetric analysis (see Appendix and Table 5.5) in which a 5% weight loss was observed at 426 °C.

Table 5.5. Molecular Weights and Thermal Properties

	M_n[a] [kg/mol]	M_w[a] [kg/mol]	Đ[a]	T_d[b] [°C]
P17	170	398	2.3	426
P18	100	240	2.4	-

[a] Determined by gel permeation chromatography in CB at 80 °C against polystyrene standards. [b] 5% weight loss temperatures measured by thermal gravimetric analysis under a N_2 atmosphere. N.B. Due to the low reaction yield, the thermal stability of P18 could not be investigated.

5.2.6 Optical Properties and Frontier Molecular Orbital Energy Levels

The optical properties of the polymers were investigated by UV-vis absorption spectroscopy. Figure 5.7 and Table 5.6 display the optical data of the polymers in dilute chlorobenzene, and as thin-films spin-coated from chlorobenzene (5 mg/mL). In solution, a red-shift of 38 nm is observed between the absorption maxima of P17 (λ_{max} solution = 735 nm) and P18 (λ_{max} solution = 773 nm). As previous reports suggest, this shift is attributed to the increase in electron density associated with the selenophene unit.[188] Distinct shoulders at 812 (P17) and 860 (P18) nm are also present, which indicate the polymers may be aggregated or chain extended in solution. This observation is also supported by the similarity between the solution and thin film spectra.

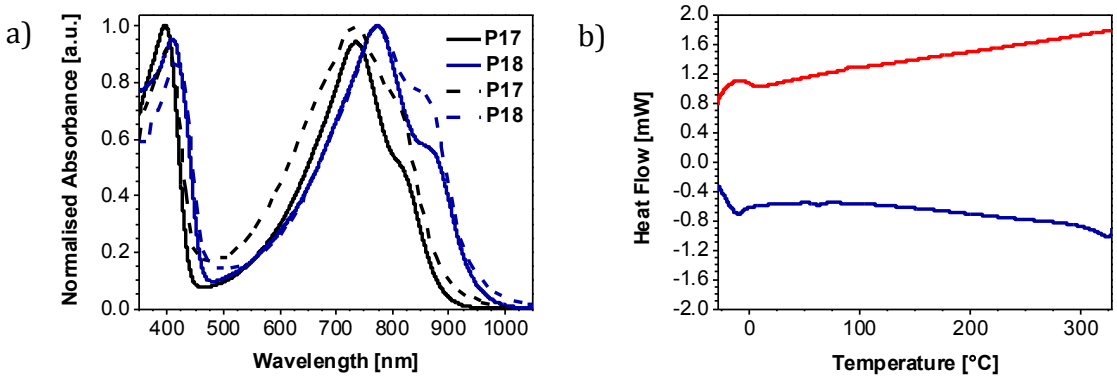

Figure 5.7. a) Normalised UV-vis absorption spectra of P17 and P18 in dilute chlorobenzene solution at 20 °C (solid line), and in thin-films spin-coated on glass substrates from chlorobenzene solution (5 mg/mL) (dashed line), and b) second heating (red) and cooling (blue) scan of P17 measured by DSC, at a rate of 10 °C/min under a N_2 atmosphere.

The ionisation potential of P17 spin-coated from chlorobenzene (5 mg/mL) was measured using photoelectron spectroscopy in air to be 5.79 eV (Table 5.6).

Table 5.6. Optical Properties and Frontier Molecular Orbital Energy Levels

	λ_{max} Soln[a] [nm]	λ_{max} Film[b] [nm]	E_g opt[c] [eV]	I.P.[d] [eV]
P17	735 (812)	736 (811)	1.38	5.79
P18	773 (860)	773 (856)	1.30	-

[a] Measured in dilute CB at 20 °C. Shoulder peaks in parentheses. [b] Thin-films spin-coated on glass substrates from 5 mg/mL CB solution. Shoulder peaks in parentheses. [c] Determined from the absorption onset in the solid state. [d] Determined by PESA (error ± 0.05 eV). N.B. Due to the low reaction yield, the ionisation potential of P18 could not be evaluated.

5.2.7 Polymer Conformation and Packing

The thermal properties of P17 were evaluated using differential scanning calorimetry measurements. As presented in Figure 5.7, no obvious thermal transitions were apparent in the second heating and cooling scan of the polymer recorded between -30 and 330 °C under nitrogen.

5.2.8 OFET Device Performance

The electrical performance of the polymers was investigated in TG-BC field effect transistors fabricated on glass, using gold source-drain electrodes and a PMMA dielectric (80 mg/mL in n-butyl acetate, 120 kg/mol). Polymer films were spin-coated from *o*-dichlorobenzene (10 mg/mL) and annealed at 200 °C for 30 min. Figure 5.8 shows the transfer and output characteristics of the best performing devices, in which n-type charge transport was observed. As presented in Table 5.7, there is a slight difference between the average saturated charge carrier mobility of the polymers, with P17 (0.13 cm^2/Vs) demonstrating a modest improvement in performance relative to P18 (0.11 cm^2/Vs). However, no difference was observed in the peak saturated charge carrier mobility between the polymers (0.13 cm^2/Vs). Note at the time of writing, this was the highest reported charge carrier mobility of any diseleno[3,2-*b*:2',3'-*d*]selenophene based polymer. Although similar trends have been reported,[207–209] this result is largely unexpected since most examples of previous work suggest the replacement of thiophene with selenophene should increase mobility.[183–185,187]

Table 5.7. OFET Device Characteristics[a]

	Average	Peak		
	μ_{sat} [cm^2/Vs]	μ_{sat} [cm^2/Vs]	V_T [V]	I_{on}/I_{off}
P17	0.13 ± 0.011	0.13	24.8 ± 2.9	$1 \times 10^3 \sim 1 \times 10^4$
P18	0.11 ± 0.015	0.13	30.2 ± 2.3	$1 \times 10^4 \sim 1 \times 10^5$

[a] TG-BC devices fabricated on glass substrates using Au (60 nm) source drain electrodes, and a PMMA dielectric (80 mg/mL in n-butyl acetate, 120 kg/mol). Polymer active layers were spin-coated from *o*-DCB (10 mg/mL) and annealed at 200 °C for 30 min.

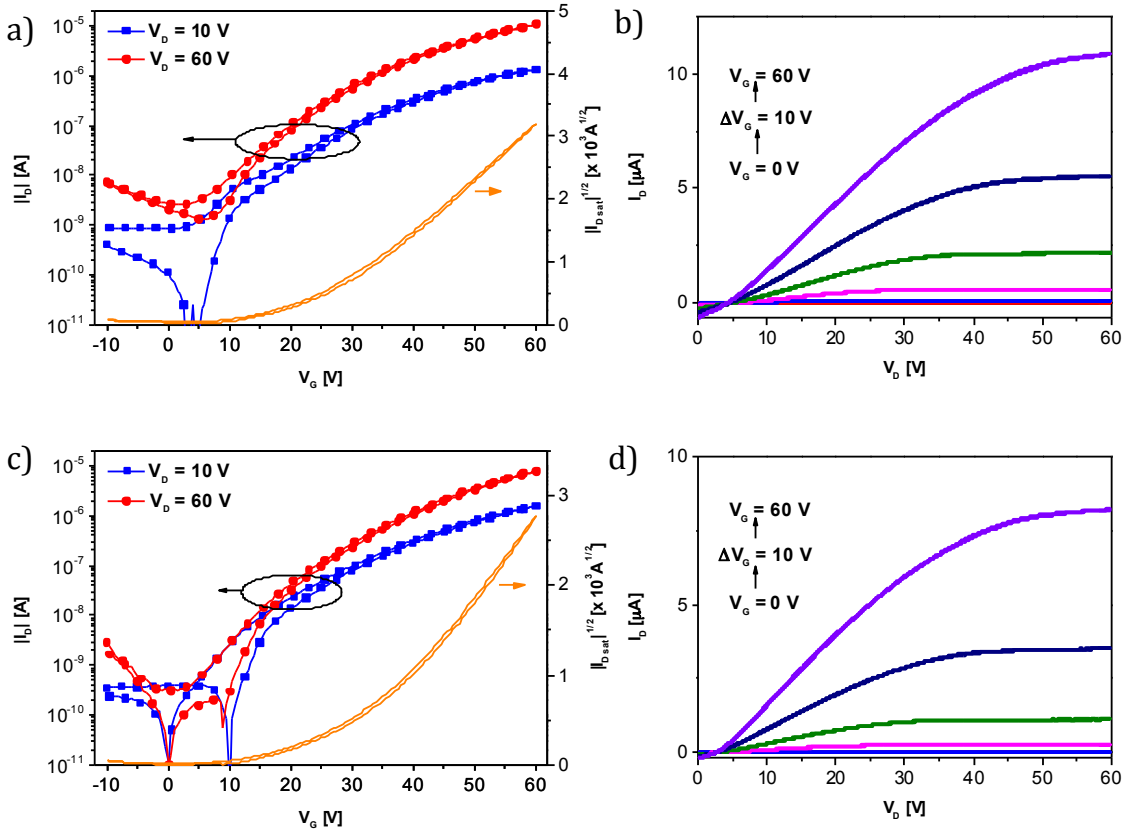

Figure 5.8. Transfer (left) and output (right) characteristics of the best performing TG-BC devices of P17: a) and b), P18: c) and d), fabricated on glass substrates using Au (60 nm) source-drain electrodes, and PMMA (80 mg/ml in n-butyl acetate, 120 kg/mol) dielectric. Polymer active layers were spin-coated from *o*-dichlorobenzene solution (10 mg/mL) and annealed at 200 °C for 30 min. The channel width and length were 1000 μm and 40 μm, respectively.

5.3 Conclusion

In this chapter, building on the promising electrical performance demonstrated by P11 in Chapter 4, a novel series of NDI based polymers containing 4-decylhexadecyl branched side-chains was described. In an effort to explore the scope of this monomer and further improve the performance, it was co-polymerised with a range of fluorinated and non-fluorinated, thiophene and selenophene containing monomers that have previously been shown to have a beneficial effect on charge transport. Using a combination of techniques (UV-vis, PESA, DSC, GIWAXS, OFET) the optoelectronic properties, solid-state ordering, and electrical performance of the polymers were investigated, revealing significant differences across the series as a result of the choice of co-monomer. In particular, fluorination was found to improve transistor performance most likely due to an increase in backbone planarity, although further characterisation is needed to validate this. The replacement of thiophene with selenophene on the other hand resulted in a slight decrease in performance, which was largely unexpected. Interestingly however, all but one of the polymers (P14) demonstrated an increase in charge carrier mobility

(with peak values ranging between 0.045 and 0.13 cm^2/Vs) relative to P11 (0.037 cm^2/Vs) demonstrating the importance of the choice of co-monomer on device performance.

Chapter 6
Experimental Procedures

6.1 General Procedures

All starting materials and reagents were purchased from commercial sources (Derthon Optoelectronic Materials Science Technology Co. Ltd., Sigma Aldrich, TCI, VWR, Wawei Chemicals Ltd.) and used as received, unless otherwise stated. All reactions were conducted under argon using standard Schlenk line techniques and anhydrous solvents, as commercially supplied. Flash column chromatography was performed on silica gel (Merck Kieselgel 60 grade 40-63 μm F254). Thin layer chromatography was performed on Merck Kieselgel 60 F254 aluminum sheets and observed under 254 nm UV light.

The ^{1}H and ^{13}C NMR spectra for chemical intermediates were recorded on a Bruker AV-400 (400 MHz) spectrometer at 20 °C in chloroform-d, DMSO-d_6, 1,1,2,2-tetrachloroethane-d_2, or acetone-d_6. The ^{1}H NMR spectra for polymers were recorded on a Bruker AV-400 (400 MHz) spectrometer at 130 °C in 1,1,2,2-tetrachloroethane-d_2. Chemical shifts are reported in ppm relative to residual protons in the deuterated solvent used and coupling constants are reported in Hz. MestReNova v7.1.2 from MestreLab was used to analyze all spectra. Electron ionisation mass spectrometry was performed with a Micromass AutoSpec Premier Instrument. Electrospray ionisation mass spectrometry was performed with a Micromass LCT Premier Instrument. MALDI-ToF mass spectrometry was performed with a Micromass MALDI micro MX instrument. Elemental analysis was carried out using a Thermo Flash 2000 machine.

All microwave experiments were performed in a Biotage Initiator v2.3. Final stannylated monomers were purified using a Shimadzu preparative GPC in hexane at 40 °C. Polymers were purified using a Shimadzu preparative GPC in chlorobenzene at 80 °C, unless otherwise stated. The system consists of a DGU-20A3 degasser, an LC-20A pump, a CTO-20A column oven, an Agilent PLgel 10 μm MIXED-D column and a SPD-20A UV detector. Number-average and weight-average molecular weights, and polydispersities were determined with either an Agilent Technologies 1200 series Analytical GPC, or an Agilent Technologies 1260 Infinity Analytical GPC, using two PL mixed B columns in series, in chlorobenzene at 80 °C. The machines were calibrated against narrow weight polydispersity polystyrene standards. In cases where polymer solubility was an issue, a Polymer Laboratories PL-GPC-220 machine was used in trichlorobenzene at 140 °C.

Solution and solid-state UV-vis absorption spectra were recorded on a UV-1800 Shimadzu UV-vis spectrometer. Polymer thin films were spin-coated on glass substrates from chlorobenzene (5 mg/mL) using a Laurell WS-400BZ-6NPP/LITE spin coater. Photoelectron spectroscopy in air measurements were recorded with a Riken Keiki AC-2 PESA spectrometer with a power setting

of 5 nW and a power number of 0.5. Differential scanning calorimetry experiments were carried out with a TA Instruments DSC TZero Q20 v24.10 instrument at a scan rate of 10 °C/min and analysed using TA Instruments Universal Analysis 2000 v4.5A software. Thermal gravimetric analysis plots were obtained with either a Perkin Elmer Pyris 1 TGA, or a METTLER TGA/DSC 1 machine, at a scan rate of 10 °C/min, under a nitrogen atmosphere. X-ray diffraction measurements were performed on a Panalytical X'Pert-pro MRD diffractometer equipped with a nickel-filtered Cu K α 1 beam and X'Celerator detector, using a 40 mA current and 40 kV accelerating voltage. Polymer thin films were drop-coated on glass substrates from *o*-dichlorobenzene (7 mg/mL) and annealed for 2 min at 100 °C, 150 °C, or 175 °C, under argon. Grazing incidence wide-angle X-ray scattering measurements were carried out using the SAXS/WAXS beamline at the Australian Synchrotron.[210] As-cast (Chapter 4), and annealed (Chapter 4 and 5) polymer thin films were spin-coated on Si substrates (100) using the same conditions as those used when fabricating the respective transistor device, unless otherwise stated. Atomic force microscopy images were obtained with a Picoscan PicoSPM LE scanning probe in tapping mode, under ambient conditions. Polymer thin films were prepared according to the method used when fabricating the respective transistor (Chapter 3 and 4) or all-polymer OPV (Chapter 4) device. Steady state photoluminescence spectra were measured using a Horiba Jobin Yvon Spex Fluoromax 1 spectrofluorometer. Sub-microsecond timescale transient absorption spectroscopy was performed using a minilite pump Nd:Yag laser and a probe tungsten lamp. Samples were excited at 640 nm and probed at 1020 nm with an energy density of 2uJ/cm^2, under nitrogen. Films for PL and TAS measurements were prepared using the same conditions as those used when fabricating the all-polymer OPV device. Density functional theory calculations were carried out using the Gaussian 03[211] and 09[212] programs, with the Becke three-parameter, Lee-Yang-Parr, hybrid functional level of theory, and a basis set of 6-311G(D).

Names for chemical intermediates and polymers were derived using ACD/I-Lab from the EPSRC funded National Chemical Database Service hosted by the Royal Society of Chemistry.

6.2 Experimental Procedures for Chapter 2

Transistor Device Fabrication and Characterisation

All film preparation was carried out under ambient atmosphere. TG-BC devices were fabricated on glass substrates using photolithiographically defined Ag source-drain and gate electrodes, and Lisicon D139 dielectric. Polymer films were spin-coated from *o*-dichlorobenzene at a concentration of 7 mg/mL and annealed at 100 °C, or 150 °C, for 2 min. In selected cases (P4), films were spin-coated from a mixture of 1,3,5-trimethylbenzene:1-methylnaphthalene (1:1) at a concentration of 7 mg/mL and annealed at 150 °C, for 2 min. Electrical characterisation was carried out under ambient conditions using an Agilent 4155C Semiconductor Parameter Analyser.

2,5-Dibromothieno[3,2-*b*]thiophene[213] (2.2)

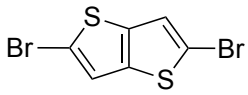

N-Bromosuccinimide (26.5 g, 149.2 mmol) was added in several portions to a stirred solution of thieno[3,2-*b*]thiophene (10.3 g, 73.8 mmol) in *N,N*-dimethylformamide (300 mL) at room temperature, in the absence of light. The reaction was monitored by TLC and upon completion, an aqueous solution of sodium sulfite (150 mL) was added to precipitate the crude product. The crude product was then collected by vacuum filtration and washed with methanol (3 x 50 mL). Purification by recrystallisation (ethyl acetate:ethanol, 2:1, (v:v)) gave the title compound as a white solid (20.2 g, 67.6 mmol, 92%). ^{1}H NMR (400 MHz, $CDCl_3$) δ: 7.17 (2 H, s, ArH); ^{13}C NMR (100 MHz, $CDCl_3$) δ: 138.41, 121.89, 113.75; HRMS (EI) *m/z*: [M^+] calcd for $C_6H_2Br_2S_2$, 295.7965; found, 295.7977.

(5-Bromothieno[3,2-*b*]thiophen-2-yl)(trimethyl)silane[214] (2.3)

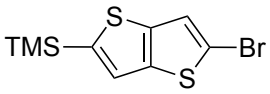

n-Butyllithium (9.4 mL of a 1.6 M solution in hexanes, 15.0 mmol) was added dropwise to a stirred solution of 2,5-dibromothieno[3,2-*b*]thiophene (4.3 g, 14.3 mmol) in anhydrous diethyl ether (200 mL) at -78 °C, under an argon atmosphere. After 30 min, chlorotrimethylsilane (2.2 mL, 17.2 mmol) was added dropwise. Once the addition was complete, the reaction mixture was allowed to warm to room temperature over 16 h. An aqueous saturated solution of sodium hydrogen carbonate (20 mL) was added and the crude product was extracted with diethyl ether (50 mL). The combined organics were washed with water (3 x 50 mL), brine (50 mL), dried ($MgSO_4$) and the volatiles removed *in vacuo*. Purification by column chromatography over silica

(eluent: hexane) gave the title compound as a colourless oil (3.6 g, 12.3 mmol, 86%). HRMS (EI) *m/z*: [M+] calcd for $C_9H_{11}BrS_2Si$, 289.9255; found, 289.9261.

(3,3'-dibromo-2,2'-bithieno[3,2-*b*]thiene-5,5'-diyl)bis(trimethylsilane)[95] (2.4)

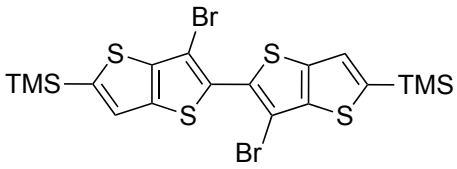

Lithium diisopropylamide (1.2 M solution in THF, 36.8 mmol) was added dropwise to a stirred solution of (5-bromothieno[3,2-*b*]thiophen-2-yl)(trimethyl)silane (10.0 g, 34.3 mmol) in anhydrous tetrahydrofuran (150 mL) at -78 °C, under an argon atmosphere. After 30 min, copper (II) chloride (4.9 g, 36.8 mmol) was added and the reaction mixture was allowed to warm to room temperature over 16 h. Any remaining copper(II) chloride was then removed by vacuum filtration and the resulting solution was extracted with diethyl ether (50 mL). The combined organics were combined, washed with water (3 x 50 mL), brine (50 mL), dried ($MgSO_4$) and the volatiles removed *in vacuo.* Purification of the crude product by column chromatography over silica (eluent: hexane) yielded the title compound as a yellow solid (5.3 g, 9.1 mmol, 53%). ^{1}H NMR (400 MHz, $CDCl_3$) δ: 7.40 (2 H, s, ArH), 0.38 (18 H, s, -CH_3); ^{13}C NMR (100 MHz, $CDCl_3$) δ: 145.70, 140.07, 131.17, 126.14, 105.12, 0.09; HRMS (EI) *m/z*: [M+] calcd for $C_{18}H_{20}Br_2S_4Si_2$, 577.8353; found, 577.8347.

Diphenylbis(tetradecyl) germane[49] (2.5a)

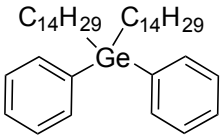

Tetradecylmagnesium chloride solution (15.4 mL of a 1.0 M solution in THF, 15.4 mmol) was added dropwise to a stirred solution of diphenylgermanium dichloride (1.5 g, 5.1 mmol) in anhydrous tetrahydrofuran (25 mL) at 0 °C, under an argon atmosphere. Once the addition was complete, the reaction mixture was warmed to room temperature, stirred for 30 min and then refluxed for 16 h. The reaction mixture was cooled to 0 °C and quenched with methanol (10 mL). The resulting solution was diluted with ethyl acetate (20 mL) and washed with water (3 x 15 mL) and brine (15 mL). After drying ($MgSO_4$), the volatiles were removed *in vacuo*. Purification of the crude product by column chromatography over silica (eluent: hexane) gave the title compound as a colourless oil (2.1 g, 3.3 mmol, 65%). ^{1}H NMR (400 MHz, $CDCl_3$) δ: 7.49 (4 H, m, ArH), 7.37 (6 H, m, ArH), 1.46 (4 H, m, -CH_2-), 1.30 (48 H, m, -CH_2-), 0.91 (6 H, t, *J* 7.0, -CH_3); ^{13}C NMR (100 MHz, $CDCl_3$) δ: 139.09, 134.58, 128.54, 128.09, 33.62, 32.11, 30.06-29.67

(overlapping C), 29.55, 29.35, 25.12, 22.88, 14.30, 13.45; Anal. calcd for $C_{40}H_{68}Ge$: C, 77.29; H, 11.03; found: C, 77.13; H, 11.14.

Dibromobis(tetradecyl) germane[49] (2.5)

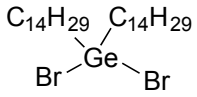

Bromine (0.43 mL, 8.4 mmol) in anhydrous 1,2-dichloroethane (5 mL) was added dropwise to a solution of diphenylbis(tetradecyl) germane (2.5 g, 4.0 mmol) in anhydrous 1,2-dichloroethane (50 mL) in the absence of light. The reaction mixture was heated to reflux for 5 h and then cooled to room temperature. The resulting solution was concentrated under vacuum and then dried under high vacuum, to give the title compound as a pale orange oil (2.4 g, 3.8 mmol, 95%). ^{1}H NMR (400 MHz, $CDCl_3$) δ: 1.73 (4 H, m, -CH_2-), 1.62 (4 H, m, -CH_2-), 1.39 (4 H, m, -CH_2-), 1.26 (40 H, s, -CH_2-), 0.87 (6 H, t, *J* 7.0, -CH_3); ^{13}C NMR (100 MHz, $CDCl_3$) δ: 32.09, 31.77, 29.83-29.76 (overlapping C), 29.57, 29.52, 29.20, 28.23, 24.41, 22.85, 14.28; Anal. calcd for $C_{28}H_{58}Br_2Ge$: C, 53.62; H, 9.32; found: C, 53.50; H, 9.39.

[9,9-Bis(tetradecyl)-9H-thieno[3,2-*b*]thieno[2",3":4',5']thieno[2',3':4,5]germolo [2,3-*d*]thiene-2,7-diyl]bis(trimethylsilane)[49] (2.6)

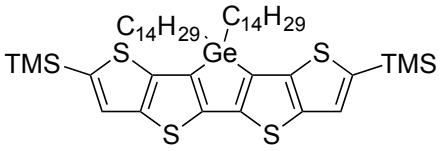

n-Butyllithium (4.3 mL of a 1.6 M solution in hexanes, 6.9 mmol) was added dropwise to a stirred solution of 3,3'-dibromo-2,2'-bithieno[3,2-*b*]thiene-5,5'-diylbis(trimethylsilane) (2.0 g, 3.5 mmol) in anhydrous diethyl ether (200 mL) at -90 °C, under an argon atmosphere. The reaction mixture was stirred for 30 min before a solution of dibromobis(tetradecyl) germane (2.3 g, 3.6 mmol) in anhydrous diethyl ether (5 mL) was added dropwise. Once the addition was complete, the reaction mixture was allowed to warm to room temperature over 16 h, and quenched with wet diethyl ether. The mixture was further diluted with diethyl ether (50 mL), washed with water (3 x 50 mL), brine (50 mL), dried ($MgSO_4$) and the volatiles removed *in vacuo*. Purification by column chromatography over silica (eluent: hexane) yielded the title compound as yellow oil (1.7 g, 1.9 mmol, 54%). ^{1}H NMR (400 MHz, acetone-d_6) δ: 7.52 (2 H, s, ArH), 1.60 (4 H, m, -CH_2-), 1.43 (4 H, m, -CH_2-), 1.34 (4 H, m, -CH_2-), 1.26 (40 H, s, -CH_2-), 0.89 (6 H, t, *J* 6.8, -CH_3), 0.37 (18 H, s, -CH_3); ^{13}C NMR (100 MHz, acetone-d_6) δ: 150.25, 148.71, 143.33, 134.07, 127.24, 33.32, 32.67, 30.49-30.42 (overlapping C), 30.40, 30.23, 30.17, 29.98, 26.40,

23.37, 14.97, 14.41; HRMS (ESI) *m/z*: $[M+H]^+$ calcd for $C_{46}H_{78}GeS_4Si_2$, 889.3815; found, 889.3808.

2,7-Dibromo-9,9-bis(tetradecyl)-9H-thieno[3,2-*b*]thieno[2",3":4',5']thieno [2',3':4,5]germolo[2,3-*d*]thiophene[49] (2.7)

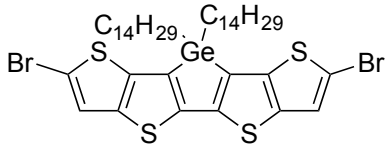

N-Bromosuccinimide (251 mg, 1.4 mmol) was added in several portions to a stirred solution of [9,9-bis(tetradecyl)-9H-thieno[3,2- *b*]thieno[2",3":4',5']thieno[2',3':4,5]germolo[2,3-*d*]thiene-2,7-diyl]bis(trimethylsilane) (620 mg, 0.7 mmol) in anhydrous tetrahydrofuran (60 mL), in the absence of light. Once the addition was complete, the reaction was stirred for 16 h. An aqueous solution of sodium sulfite (20 mL) was then added and the crude product was extracted with diethyl ether (25 mL). The organics were washed with water (3 x 25 mL), brine (25 mL), dried ($MgSO_4$), and the volatiles removed *in vacuo*. Purification of the crude product by column chromatography over silica (eluent: hexane) gave the title compound as a yellow oil (410.0 mg, 0.5 mmol, 65%). ^{1}H NMR (400 MHz, acetone-d_6) δ: 7.58 (2 H, s, ArH), 1.57 (4 H, m, -CH_2-), 1.47 (4 H, m, -CH_2-), 1.23 (44 H, s, -CH_2-), 0.87 (6 H, t, *J* 6.8, -CH_3); ^{13}C NMR (100 MHz, $CDCl_3$) δ: 147.83, 143.34, 138.85, 133.44, 122.69, 111.75, 32.93, 32.10, 29.87-29.84 (overlapping C), 29.75, 29.61, 29.54, 29.26, 25.77, 22.87, 14.49, 14.30; Anal. calcd for $C_{40}H_{60}Br_2GeS_4$: C, 53.29; H, 6.71; found: C, 53.37; H, 6.80.

2,7-Bis(trimethylstannyl)-9,9-bis(tetradecyl)-9H-thieno[3,2-*b*]thieno[2",3":4',5'] thieno[2',3':4,5]germolo[2,3-*d*]thiophene[49] (2.8)

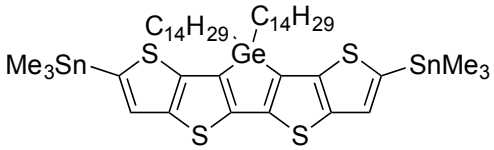

tert-Butyllithium (3.4 mL of a 1.7 M solution in pentane, 5.7 mmol) was added dropwise to a stirred solution of 2,7-dibromo-9,9-bis(tetradecyl)-9H-thieno[3,2-*b*]thieno[2",3":4',5']thieno[2',3':4,5]germolo[2,3-*d*]thiophene (1.1 g, 1.3 mmol) in anhydrous diethyl ether (300 mL) at -90 °C, under an argon atmosphere. The reaction mixture was stirred for 30 min at this temperature before a solution of trimethyltin chloride (6.1 mL of a 1.0 M solution in THF, 6.1 mmol) was added dropwise. Once the addition was complete, the reaction mixture was allowed to warm to room temperature over 16 h. An aqueous solution of sodium hydrogen carbonate (25 mL) was then added and the crude product was extracted with diethyl

ether (50 mL). The organics were washed with water (3 x 50 mL), brine (50 mL), dried (Na_2SO_4), and the volatiles were removed *in vacuo*. Purification of the crude product by recycling GPC (eluent: hexane, 40 °C) gave the title compound as a yellow oil (948.0 mg, 0.9 mmol, 70%). ^{1}H NMR (400 MHz, acetone-d_6) δ: 7.45 (2 H, s, ArH), 1.61 (4 H, m, -CH_2-), 1.42 (4 H, m, -CH_2-), 1.23 (44 H, s, -CH_2-), 0.87 (6 H, t, *J* 6.8, -CH_3), 0.42 (18 H, s, -CH_3); ^{13}C NMR (100 MHz, acetone-d_6) δ: 149.50, 149.33, 143.44, 141.83, 133.67, 128.12, 33.40, 32.77, 30.52-29.37 (overlapping C) 26.50, 23.46, 15.04, 14.50, -8.07.

Poly [2,7(9,9-bis(tetradecyl)-9H-thieno[3,2-*b*]thieno[2",3":4',5']thieno[2'3':4,5] germolo[2,3-*d*]thiophene)-alt-1,3(5-octyl-4H-thieno[3,4-c]pyrrole-4,6(5*H*)-dione)][49] (P1)

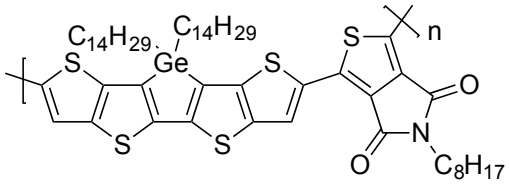

2,7-bis(trimethylstannyl)-9,9-bis(tetradecyl)-9H-thieno[3,2-*b*]thieno[2",3":4',5']thieno[2',3':4,5]germolo[2,3-*d*]thiophene (219.8 mg, 0.2055 mmol), 1,3-dibromo-5-octyl-4H-thieno[3,4-*c*]pyrrole-4,6(5*H*)-dione (87.0 mg, 0.2055 mmol), tris(dibenzylideneacetone)dipalladium(0) (3.8 mg, 0.0041 mmol) and tri(o-tolyl)phosphine (5.0 mg, 0.0164 mmol) were added to an oven dried microwave vial equipped with a stirrer bar. The vial was purged with argon before anhydrous chlorobenzene (0.5 mL) was added. The reaction mixture was purged with argon for a further 30 min and then subjected to the following microwave-heating profile: 100 °C for 2 min, 120 °C for 2 min, 140 °C for 2 min, 160 °C for 2 min, 180 °C for 20 min, and 200 °C for 20 min. Once the reaction mixture had cooled, the crude product was precipitated in methanol, filtered through a Soxhlet thimble, and purified by Soxhlet extraction: methanol (24 h), acetone (24 h), and hexane (24 h). The polymer was extracted into hexane and the resulting solution was concentrated under reduced pressure. The residue was dissolved in chloroform and vigorously stirred with an aqueous sodium diethyldithiocarbamate trihydrate solution (ca. 0.5 g in 100 mL) at 50 °C for 2 h. After cooling, the organics were extracted with chloroform (50 mL), combined and washed with water (3 x 50 mL). The solution was concentrated under vacuum and precipitated in methanol. The resulting precipitate was isolated by filtration and dried under high vacuum, to yield the title compound as a dark purple solid (157.6 mg, 76%). M_n: 7 kg/mol, M_w: 10 kg/mol, Đ: 1.5. ^{1}H NMR (500 MHz, 1,1,2,2-tetrachloroethane-d_2) δ: 8.46 (2 H, br, ArH), 3.73 (2 H, br, -CH_2N-), 1.33 (64 H, br, -CH_2-), 0.94 (9 H, br, -CH_3); Anal. calcd for $(C_{54}H_{77}GeNO_2S_5)_n$: C, 64.53; H, 7.72; N, 1.39; found: C, 64.42; H, 7.81; N, 1.44.

Poly [2,7(9,9-bis(tetradecyl)-9H-thieno[3,2-*b*]thieno[2",3":4',5']thieno[2'3':4,5]germolo[2,3-*d*]thiophene)-alt-4,7(2,1,3-benzothiadiazole)] (P2)

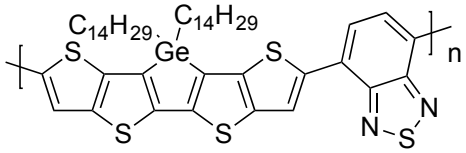

2,7-dibromo-9,9-bis(tetradecyl)-9H-thieno[3,2-*b*]thieno[2",3":4',5']thieno[2',3':4,5]germolo[2,3-*d*]thiophene (132.0 mg, 0.1464 mmol), 2,1,3-benzothiadiazole-4,7-bis(boronic acid pinacol ester) (56.82 mg, 0.1464 mmol) and tetrakis(triphenylphosphine)palladium(0) (3.4 mg, 0.0029 mmol) were added to an oven dried microwave vial equipped with a stirrer bar. The vial was purged with argon before anhydrous toluene (5.5 mL), aqueous sodium carbonate (1 mL of a 2 M solution, 2.0 mmol) and 1 drop of Aliquat 336 were added. The reaction mixture was purged with argon for a further 1 h and then heated to 120 °C for 72 h. Once the reaction mixture had cooled, the crude product was precipitated in methanol, filtered through a Soxhlet thimble, and purified by Soxhlet extraction: methanol (24 h), acetone (24 h) and hexane (24 h). The remaining polymer residue was isolated and dried under high vacuum, to yield the title compound as a dark purple solid (99.4 mg, 78%). M_n: 7 kg/mol, M_w: 10 kg/mol, Đ: 1.4. ^{1}H NMR (500 MHz, 1,1,2,2-tetrachloroethane-d_2) δ: 8.55 (2 H, br, ArH), 7.93 (2 H, br, ArH), 1.42 (52 H, br, -CH_2-), 0.96 (6 H, br, -CH_3); Anal. calcd for $(C_{46}H_{62}GeN_2S_5)_n$: C, 63.08; H, 7.13; N, 3.20; found: C, 59.44; H, 6.46; N, 3.18.

Poly [2,7(9,9-bis(tetradecyl)-9H-thieno[3,2-*b*]thieno[2",3":4',5']thieno[2'3':4,5]germolo[2,3-*d*]thiophene)-alt-5,5'(4,7-bis(thiophen-2-yl)-5,6-bis(octyloxy)-benzo[1,2,5-*c*]thiadiazole)][49] **(P3)**

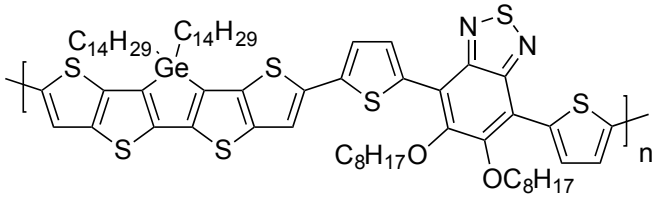

2,7-bis(trimethylstannyl)-9,9-bis(tetradecyl)-9H-thieno[3,2-*b*]thieno[2",3":4',5']thieno[2',3':4,5]-germolo[2,3-*d*]thiophene (263.4 mg, 0.2463 mmol), 4,7-bis(5-bromothiophen-2-yl)-5,6-bis(octyloxy)-benzo[1,2,5-*c*]thiadiazole (176.0 mg, 0.2463 mmol), tris(dibenzylideneacetone)dipalladium(0) (4.5 mg, 0.0049 mmol) and tri(o-tolyl)phosphine (6.0 mg, 0.0197 mmol) were added to an oven dried microwave vial equipped with a stirrer bar. The vial was purged with argon before anhydrous chlorobenzene (0.5 mL) was added. The reaction mixture was purged with argon for a further 30 min and then

subjected to the following microwave-heating profile: 100 °C for 2 min, 120 °C for 2 min, 140 °C for 2 min, 160 °C for 2 min, 180 °C for 20 min, and 200 °C for 20 min. Once the reaction mixture had cooled, the crude product was precipitated in methanol, filtered through a Soxhlet thimble, and purified by Soxhlet extraction: methanol (24 h), acetone (24 h), hexane (24 h) and chloroform (3 h). The remaining polymer residue was dissolved in 1,1,2,2-tetrachloroethane and heated to 140 °C for 16 h. After cooling, the solution was filtered hot, concentrated under vacuum and precipitated in acetone. The resulting precipitate was isolated by filtration and dried under high vacuum to yield the title compound as a dark purple solid (54.9 mg, 17%). M_n: 35 kg/mol, M_w: 88 kg/mol, Đ: 2.5. ^{1}H NMR (500 MHz, 1,1,2,2-tetrachloroethane-d_2) δ: 8.50 (2 H, br, ArH), 7.46 (4 H, br, ArH), 4.32 (4 H, br, -CH_2-), 2.06 (4 H, br, -CH_2-), 1.74 (4 H, br, -CH_2-), 1.61 (4 H, br, -CH_2-), 1.34 (64 H, br, -CH_2-), 0.95 (12 H, br, -CH_3); Anal. calcd for $(C_{70}H_{98}GeN_2O_2S_7)_n$: C, 64.84; H, 7.62; N, 2.16; found: C, 64.92; H, 7.54; N, 2.25.

Poly [2,7(9,9-bis(tetradecyl)-9H-thieno[3,2-*b*]thieno[2",3":4',5']thieno[2'3':4,5]germolo[2,3-*d*]thiophene)-alt-5,5'(4,7-bis(4-hexadecylthiophen-2-yl)-benzo[1,2,5-*c*]thiadiazole)][49] **(P4)**

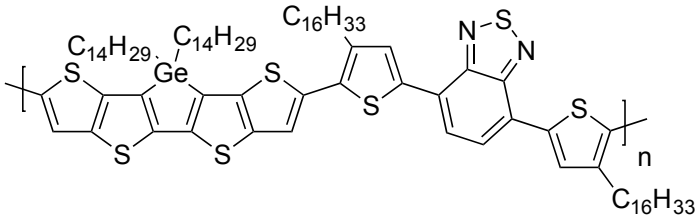

2,7-bis(trimethylstannyl)-9,9-bis(tetradecyl)-9H-thieno[3,2-*b*]thieno[2",3":4',5']thieno[2',3':4,5]-germolo[2,3-*d*]thiophene (206.2 mg, 0.1928 mmol), 4,7-bis(5-bromo-4-hexadecylthiophen-2-yl)-benzo[1,2,5-*c*]thiadiazole (174.9 mg, 0.1928 mmol), tris(dibenzylideneacetone)dipalladium(0) (3.5 mg, 0.0039 mmol) and tri(o-tolyl)phosphine (4.7 mg, 0.0154 mmol) were added to an oven dried microwave vial equipped with a stirrer bar. The vial was purged with argon before anhydrous chlorobenzene (1.0 mL) was added. The reaction mixture was purged with argon for a further 30 min and then subjected to the following microwave-heating profile: 100 °C for 2 min, 120 °C for 2 min, 140 °C for 2 min, 160 °C for 2 min, 180 °C for 20 min, and 200 °C for 20 min. Once the reaction mixture had cooled, the crude product was precipitated in methanol, filtered through a Soxhlet thimble, and purified by Soxhlet extraction: methanol (24 h), acetone (24 h), hexane (24 h) and chloroform (3 h). The chloroform extract was vigorously stirred with an aqueous sodium diethyldithiocarbamate trihydrate solution (ca. 0.5 g in 100 mL) at 50 °C for 2 h. After cooling, the organics were extracted with chloroform (50 mL), combined and washed with water (3 x 50 mL). The solution was concentrated under vacuum and precipitated in methanol. The resulting precipitate was

isolated by filtration, and further purified by preparative GPC (eluent: chlorobenzene, 80 °C) and a final precipitation. Finally, the resulting precipitate was dried under high vacuum to yield the title compound as a dark blue solid (203.7 mg, 71%). M_n: 27 kg/mol, M_w: 51 kg/mol, Đ: 1.9. ^{1}H NMR (500 MHz, 1,1,2,2-tetrachloroethane-d_2) δ: 8.08 (2 H, br, ArH), 7.91 (2 H, br, ArH), 7.48 (2 H, br, ArH), 2.99 (4 H, br, -CH_2-), 1.89 (4 H, br, -CH_2-), 1.74 (4 H, br, -CH_2-), 1.52 (18 H, br, -CH_2-), 1.34 (82 H, br, -CH_2-), 0.94 (12 H, br, -CH_3); Anal. calcd for $(C_{86}H_{130}GeN_2S_7)_n$: C, 69.37; H, 8.80; N, 1.88; found: C, 67.79; H, 10.02; N, 1.76.

Poly [2,7(9,9-bis(tetradecyl)-9H-thieno[3,2-*b*]thieno[2",3":4',5']thieno[2'3':4,5]germolo[2,3-*d*]thiophene)-alt-4,9(2,7-dioctylbenzo[*lmn*][3,8]phenanthroline-1,3,6,8(2*H*,7*H*)-tetrone)][49] **(P5)**

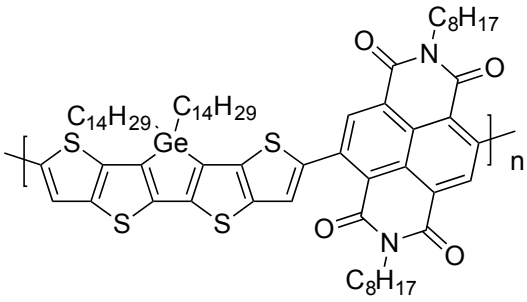

2,7-bis(trimethylstannyl)-9,9-bis(tetradecyl)-9H-thieno[3,2-*b*]thieno[2",3":4',5']thieno[2',3':4,5]-germolo[2,3-*d*]thiophene (258.4 mg, 0.2416 mmol), 4,9-dibromo-2,7-dioctylbenzo[*lmn*][3,8]phenanthroline-1,3,6,8(2*H*,7*H*)-tetrone (156.6 mg, 0.2416 mmol), tris(dibenzylideneacetone)dipalladium(0) (4.4 mg, 0.0048 mmol) and tri(o-tolyl)phosphine (5.9 mg, 0.0193 mmol) were added to an oven dried microwave vial equipped with a stirrer bar. The vial was purged with argon before anhydrous chlorobenzene (0.5 mL) was added. The reaction mixture was purged with argon for a further 30 min and then subjected to the following microwave-heating profile: 100 °C for 2 min, 120 °C for 2 min, 140 °C for 2 min, 160 °C for 2 min, 180 °C for 20 min, and 200 °C for 20 min. Once the reaction mixture had cooled, the crude product was precipitated in methanol, filtered through a Soxhlet thimble, and purified by Soxhlet extraction: methanol (24 h), acetone (24 h), hexane (24 h) and chloroform (3 h). The chloroform extract was vigorously stirred with an aqueous sodium diethyldithiocarbamate trihydrate solution (ca. 0.5 g in 100 mL) at 50 °C for 2 h. After cooling, the organics were extracted with chloroform (50 mL), combined and washed with water (3 x 50 mL). The solution was concentrated under vacuum and precipitated in methanol. The resulting precipitate was isolated by filtration and dried under high vacuum, to yield the title compound as a dark green solid (217.8 mg, 73%). M_n: 42 kg/mol, M_w: 184 kg/mol, Đ: 4.4. ^{1}H NMR (500 MHz, 1,1,2,2-tetrachloroethane-d_2) δ: 8.96 (2 H, br, ArH), 7.74 (2 H, br, ArH), 4.25 (4 H, br, -

CH_2N-), 1.82 (8 H, br, -CH_2-), 1.30 (68 H, br, -CH_2-), 0.95 (12 H, br, -CH_3); Anal. calcd for $(C_{70}H_{96}GeN_2O_4S_4)_n$: C, 68.33; H, 7.86; N, 2.28; found: C, 68.37; H, 7.96; N, 2.31.

6.3 Experimental Procedures for Chapter 3

Transistor Device Fabrication and Characterisation

All film preparation was carried out under inert atmosphere. TG-BC devices were fabricated on glass substrates using Au (40 nm) source-drain electrodes and CYTOP dielectric. Au electrodes were treated with PFBT to form a self-assembled monolayer to increase the work function. Polymers were dissolved in chlorobenzene at a concentration of 5 mg/mL (P7 and P8 were filtered, P6 could not pass through the 0.45 μm PTFE filter), and spin-coated at 2000 rpm for 60 s, from a hot solution. The obtained polymer films were annealed at 120 °C for 30 min before the dielectric was spin-coated. The channel width and length of the transistors was 1000 μm and 40 μm, respectively. Transistor characterisation was carried out under nitrogen using a Keithley 4200 parameter analyser. Mobility was extracted from the slope of $I_D^{1/2}$ vs. V_G.

OPV Device Fabrication and Characterisation

BHJ solar cells were fabricated with inverted (ITO/ZnO/Polymer:$PC_{70}BM$/MoO_3/Ag) configuration and tested under simulated 100 mW/cm^2 AM 1.5G illumination using a Xenon lamp (Oriel Instruments). Prior to deposition, the ITO substrates were cleaned (detergent, acetone and IPA) and subjected to an oxygen plasma treatment at 100 W for 7 min. The ZnO was prepared using the sol-gel method[215,216] from a solution of zinc acetate dehydrate (219.5 mg), 2-methoxyethanol (2 mL) and ethanolamine (0.06 mL), spin-coated onto glass and annealed at 150 °C for 20 min. In all cases polymer active layers were prepared with a donor:acceptor (polymer:$PC_{70}BM$) blend ratio of 1:2 (w:w) (24 mg/mL) and spin-coated at either 1000, 2000, or 3000 rpm from chloroform, chlorobenzene, or *o*-dichlorobenzene. The MoO_3 (10 nm) and Ag (100 nm) layers were then deposited by thermal evaporation through a shadow mask. The pixel size, defined by the spatial overlap of the anode and cathode was 0.045 cm^2.

Diethyl-5,5'-bis(trimethylsilyl)-[2,2']-bi-[thieno[3,2-*b*]thiophenyl]-3,3'-dicarboxylate[217] (3.1)

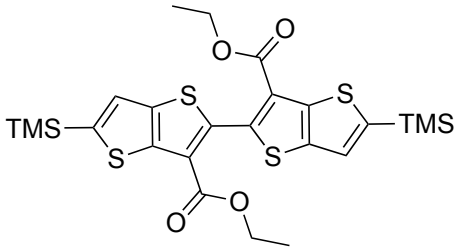

n-Butyllithium (74.8 mL of a 1.6 M solution in hexanes, 119.7 mmol) was added dropwise to a stirred solution of (3,3'-dibromo-2,2'-bithieno[3,2-*b*]thiene-5,5'diyl)bis-(trimethylsilane) (17.4 g, 29.9 mmol) in anhydrous diethyl ether (1.2 L) at -90 °C, under an argon atmosphere. The reaction mixture was stirred for 30 min before a solution of ethyl chloroformate (12.8 mL, 134.2 mmol) in anhydrous diethyl ether (15 mL) was added in one portion. Once the addition was complete, the reaction mixture was allowed to warm to room temperature over 16 h and quenched with water. The crude product was extracted with hexane (500 mL), washed with water (3 x 500 mL), brine (500 mL), dried ($MgSO_4$), and the volatiles removed *in vacuo*. Purification of the crude product by column chromatography over silica (eluent: chloroform) gave the title compound as a brown oil (12.7 g, 22.5 mmol, 75%). ^{1}H NMR (400 MHz, $CDCl_3$) δ: 7.36 (2 H, s, ArH), 4.25 (4 H, q, *J* 7.2, -CH_2-), 1.20 (6 H, t, *J* 7.2, -CH_3), 0.40 (18 H, s, -CH_3); ^{13}C NMR (100 MHz, $CDCl_3$) δ: 161.88, 146.13, 144.93, 142.20, 139.17, 124.70, 124.13, 61.01, 14.07, -0.12; HRMS (ESI) *m/z*: $[M+H]^+$ calcd for $C_{24}H_{30}O_4S_4Si_2$, 567.0644; found, 567.0656.

[2,2'-Bithieno[3,2-*b*]thiophene]-3,3'-dicarboxylic acid[217] (3.2)

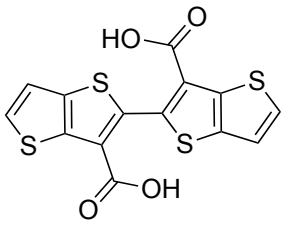

Sodium hydroxide (3.0 g, 75.0 mmol) was added to a stirred solution of diethyl-5,5'-bis(trimethylsilyl)-[2,2']-bi-[thieno[3,2-*b*]thiophenyl]-3,3'-dicarboxylate (4.2 g, 7.5 mmol) in methanol (100 mL) and tetrahydrofuran (100 mL), and heated to reflux for 16 h. The reaction mixture was then cooled to 0 °C before the volatiles were removed *in vacuo*. Concentrated hydrochloric acid (400 mL of a 2 M solution) was added, and the resulting precipitate was collected and dried under high vacuum to yield the title compound as a yellow solid (2.4 g, 6.6 mmol, 88%). ^{1}H NMR (400 MHz, DMSO-d_6) δ: 7.82 (2H, d, *J* 5.2, ArH), 7.51 (2 H, d, *J* 5.2, ArH); ^{13}C NMR (100 MHz, DMSO-d_6) δ: 162.81, 140.38, 139.72, 137.07, 130.49, 125.15, 119.73; HRMS (ESI) *m/z*: $[M+H]^+$ calcd for $C_{14}H_6O_4S_4$, 366.9227; found, 366.9240.

Bisthieno[2',3':4,5]thieno[3,2-*c*:2',3'-*e*]oxepine-4,6-dione[217] (3.3)

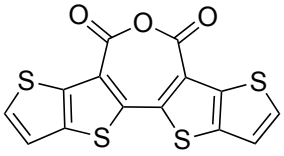

[2,2'-Bithieno[3,2-*b*]thiophene]-3,3'-dicarboxylic acid (282.2 mg, 0.8 mmol) was refluxed in acetic anhydride (15 mL) for 16 h. The reaction mixture was then cooled to 0 °C, filtered and dried under high vacuum, to yield the title compound as a brown solid (212.0 mg, 0.6 mmol, 79%). ^{1}H NMR (400 MHz, DMSO-d_6) δ: 7.96 (2 H, d, *J* 5.2, ArH), 7.59 (2 H, d, *J* 5.2, ArH); ^{13}C NMR (100 MHz, DMSO-d_6) δ: 141.88, 141.43, 135.26, 133.22-132.91 (overlapping C), 120.58-120.21 (overlapping C); MS (MALDI-ToF) *m/z*: $[M+H]^+$ 348.8 (40%); Anal. calcd for $C_{14}H_4O_3S_4$: C, 48.26; H, 1.16; found: C, 46.59; H, 0.99.

5-(2-Octyldodecyl)-4H-bisthieno[2',3':4,5]thieno[3,2-*c*:2',3'-*e*]azepine-4,6(5*H*)-dione (3.4)

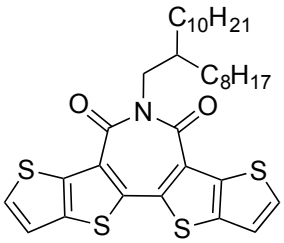

Bisthieno[2',3':4,5]thieno[3,2-*c*:2',3'-*e*]oxepine-4,6-dione (104.8 mg, 0.3 mmol) and 4-(dimethylamino)pyridine (14.0 mg, 0.1 mmol) were added to an oven dried microwave vial equipped with a stirrer bar. The vial was purged with argon before anhydrous toluene (9 mL) was added. A solution of 2-octyldodecyl-1-amine (98.4 mg, 0.3 mmol) in anhydrous toluene (2 mL) was then added dropwise and the reaction mixture was subjected to the following microwave-heating profile: 100 °C for 2 min, 140 °C for 2 min, 180 °C for 2 min and 200 °C for 120 min. Note 9 microwave vials were run sequentially and combined for work-up. After cooling, the crude product was extracted with diethyl ether (150 mL), washed with water (3 x 150 mL), brine (150 mL), dried ($MgSO_4$) and the volatiles removed *in vacuo*, to yield the title compound as a brown solid (618.6 mg, 1.0 mmol, 18% based upon 1.9 g of total starting material). ^{1}H NMR (400 MHz, $CDCl_3$) δ: 7.61 (2 H, d, *J* 5.2, ArH), 7.28 (2 H, d, *J* 5.2, ArH), 4.42 (2 H, d, *J* 7.2, -CH_2N-), 2.05 (1 H, m, -CH-), 1.25 (32 H, m, -CH_2-), 0.86 (6 H, m, -CH_3); ^{13}C NMR (100 MHz, $CDCl_3$) δ: 160.77, 143.33, 140.19, 134.37, 132.39, 125.31, 118.61, 49.43, 36.17, 32.15-31.98 (overlapping C), 31.63, 30.26, 29.90-29.62 (overlapping C), 29.56-29.43 (overlapping C), 26.49, 22.89-22.77 (overlapping C), 14.29; Anal. calcd for $C_{34}H_{45}NO_2S_4$: C, 65.03; H, 7.22; N, 2.23; found: C, 64.73; H, 7.86; N, 2.28.

2,8-Dibromo-5-(2-octyldodecyl)-4H-bisthieno[2',3':4,5]thieno[3,2-*c*:2',3'-*e*]azepine-4,6(5*H*)-dione (3.5)

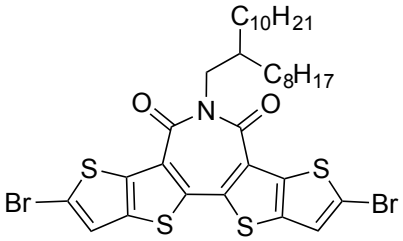

N-Bromosuccinimide (137.4 mg, 0.8 mmol) was added in several portions to a stirred solution of 5-(2-octyldodecyl)-4H-bisthieno[2',3':4,5]thieno[3,2-*c*:2',3'-*e*]azepine-4,6(5*H*)-dione (232.4 mg, 0.4 mmol) and potassium acetate (107.70 mg, 1.1 mmol) in chloroform (25 mL) and acetic acid (25 mL), at room temperature in the absence of light. The reaction was monitored by TLC and upon completion, an aqueous solution of sodium sulfite (50 mL) was added. The crude product was then extracted with chloroform (50 mL) and the combined organics were neutralised with aqueous sodium hydrogen carbonate solution, washed with water (3 x 50 mL), brine (50 mL), dried ($MgSO_4$), and the volatiles removed *in vacuo*. Purification of the crude product by column chromatography over silica (eluent: dichloromethane:hexane, 1:1, (v:v)) gave the title compound as a yellow solid (112.1 mg, 0.1 mmol, 39%). ^{1}H NMR (400 MHz, 1,1,2,2-tetrachloroethane-d_2) δ: 7.22 (2 H, s, ArH), 4.31 (2 H, d, *J* 7.2, -CH_2N-), 1.97 (1 H, m, -CH-), 1.37 (2 H, m, -CH_2-), 1.22 (30 H, s, -CH_2-), 0.87 (6 H, m, -CH_3-); ^{13}C NMR (100 MHz, 1,1,2,2-tetrachloroethane-d_2) δ: 159.84, 142.95, 138.17, 132.80, 124.75, 120.97, 119.60, 49.01, 35.83, 31.90-31.69 (overlapping C), 31.32, 30.02, 29.72-29.44 (overlapping C), 29.27, 26.16, 22.63, 14.17; MS (MALDI-ToF) *m/z*: $[M+H]^+$ 784.2 (95%).

Poly [2,8(5-(2-octyldodecyl)-4H-bisthieno[2',3':4,5]thieno[3,2-*c*:2',3'-*e*]azepine-4,6(5*H*)-dione)-alt-2,6(4,8-(didodecyloxy)benzo[1,2-*b*:4,5-*b'*]dithiophene)] (P6)

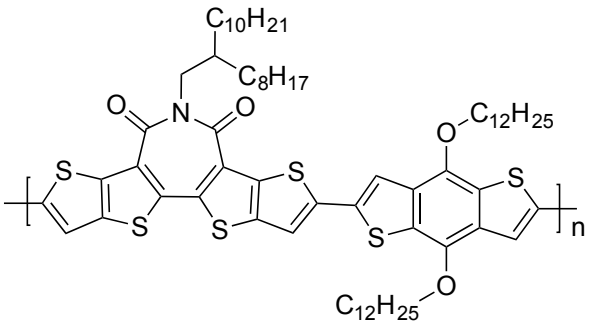

2,8-Dibromo-5-(2-octyldodecyl)-4H-bisthieno[2',3':4,5]thieno[3,2-*c*:2',3'-*e*]azepine-4,6(5*H*)-dione (112.1 mg, 0.1427 mmol), 2,6-bis-trimethylstannyl-4,8-didodecyloxybenzo[1,2-*b*;4,5-*b*']-dithiophene (126.2 mg, 0.1427 mmol), tris(dibenzylideneacetone)dipalladium(0) (2.6 mg, 0.0029 mmol) and tri(o-tolyl)phosphine (3.5 mg, 0.0114 mmol) were added to an oven dried microwave vial equipped with a stirrer bar. The vial was purged with argon before anhydrous chlorobenzene (0.8 mL) was added. The reaction mixture was purged with argon for a further 30 min and then subjected to the following microwave-heating profile: 100 °C for 2 min, 120 °C for 2 min, 140 °C for 2 min, 160 °C for 2 min, 180 °C for 20 min, and 200 °C for 20 min. Once the reaction mixture had cooled, the crude product was precipitated in methanol, filtered through a Soxhlet thimble, and purified by Soxhlet extraction: methanol (24 h), acetone (24 h), hexane (24 h) and chloroform (12 h). The chloroform extract was concentrated under vacuum and precipitated in methanol. The resulting precipitate was isolated by filtration and dried under high vacuum, to yield the title compound as a dark solid (102.0 mg, 60%). M_n: 9 kg/mol, M_w: 26 kg/mol, Đ: 2.8. Anal. calcd for $(C_{68}H_{95}NO_4S_6)_n$: C, 69.05; H, 8.10; N, 1.18; found: C, 68.94; H, 8.21; N, 1.29.

Poly [2,8(5-(2-octyldodecyl)-4H-bisthieno[2',3':4,5]thieno[3,2-*c*:2',3'-*e*]azepine-4,6(5*H*)-dione)-alt-2,6(4,8-bis(5-(2-ethylhexyl)thiophen-2- yl)benzo[1,2-*b*:4,5-*b*']dithiophene)] (P7)

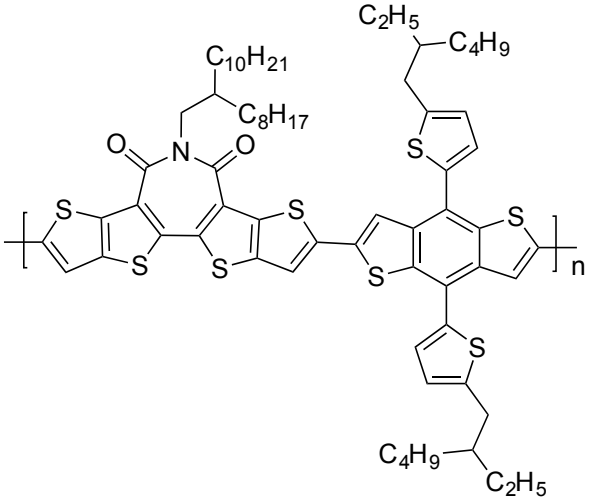

2,8-Dibromo-5-(2-octyldodecyl)-4H-bisthieno[2',3':4,5]thieno[3,2-*c*:2',3'-*e*]azepine-4,6(5*H*)-dione (147.4 mg, 0.1876 mmol), 2,6-bis-trimethylstannyl-4,8-bis(5-(2-ethylhexyl)thiophen-2-yl)benzo[1,2-*b*:4,5-*b*']dithiophene (169.7 mg, 0.1876 mmol), tris(dibenzylideneacetone)dipalladium(0) (3.4 mg, 0.0038 mmol) and tri(o-tolyl)phosphine (4.6 mg, 0.0151 mmol) were added to an oven dried microwave vial equipped with a stirrer bar. The vial was purged with argon before anhydrous chlorobenzene (1.5 mL) was added. The reaction mixture was purged with argon for a further 30 min and then subjected to the following microwave-heating profile: 100 °C for 2 min, 120 °C for 2 min, 140 °C for 2 min, 160 °C for 2 min, 180 °C for 20 min, and 200 °C for 20 min. Once the reaction mixture had cooled, the crude product was precipitated in methanol, filtered through a Soxhlet thimble, and purified by Soxhlet extraction: methanol (24 h), acetone (24 h), hexane (24 h) and chloroform (6 h). The chloroform extract was concentrated under vacuum and precipitated in methanol. The resulting precipitate was isolated by filtration and dried under high vacuum, to yield the title compound as a dark solid (121.0 mg, 54%). M_n: 50 kg/mol, M_w: 163 kg/mol, Đ: 3.3. ^{1}H NMR (500 MHz, 1,1,2,2-tetrachloroethane-d_2) δ: 7.63-7.20 (br, ArH), 7.20-6.71 (br, ArH), 4.58-4.27 (br, -CH_2N-), 3.23-2.88 (br, -CH_2-), 2.26-0.66 (br, -CH_3, -CH_2- and –CH); Anal. calcd for $(C_{68}H_{83}NO_2S_8)_n$: C, 67.90; H, 6.96; N, 1.16; found: C, 67.66; H, 7.09; N, 1.25.

Poly [2,8(5-(2-octyldodecyl)-4H-bisthieno[2',3':4,5]thieno[3,2-*c*:2',3'-*e*]azepine-4,6(5*H*)-dione)-alt-2,6(4,8-bis(4,5-dihexylthiophen-2-yl)benzo[1,2-*b*:4,5-*b*']dithiophene)] (P8)

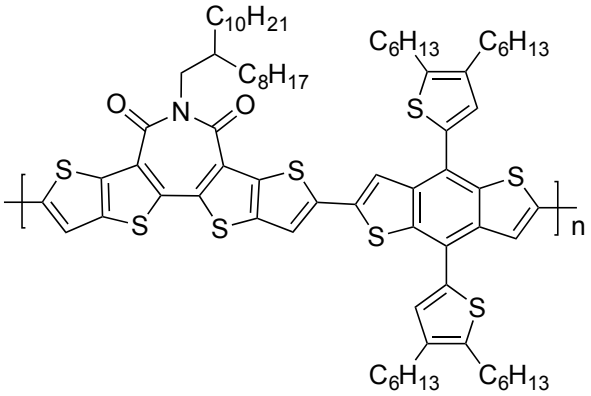

2,8-Dibromo-5-(2-octyldodecyl)-4H-bisthieno[2',3':4,5]thieno[3,2-*c*:2',3'-*e*]azepine-4,6(5*H*)-dione (122.5 mg, 0.1559 mmol), 2,6-bis-trimethylstannyl-4,8-bis(4,5-dihexylthiophen-2-yl)benzo[1,2-*b*:4,5-*b*']dithiophene (158.5 mg, 0.1559 mmol), tris(dibenzylideneacetone)dipalladium(0) (2.9 mg, 0.0032 mmol) and tri(o-tolyl)phosphine (3.8 mg, 0.0125 mmol) were added to an oven dried microwave vial equipped with a stirrer bar. The vial was purged with argon before anhydrous chlorobenzene (1.5 mL) was added. The reaction mixture was purged with argon for a further 30 min and then subjected to the following microwave-heating profile: 100 °C for 2 min, 120 °C for 2 min, 140 °C for 2 min, 160 °C for 2 min, 180 °C for 20 min, and 200 °C for 20 min. Once the reaction mixture had cooled, the crude product was precipitated in methanol, filtered through a Soxhlet thimble, and purified by Soxhlet extraction: methanol (24 h), acetone (24 h), hexane (24 h) and chloroform (6 h). The chloroform extract was concentrated under vacuum and precipitated in methanol. The resulting precipitate was isolated by filtration and dried under high vacuum, to yield the title compound as a dark solid (143.0 mg, 70%). M_n: 42 kg/mol, M_w: 172 kg/mol, Đ: 4.1. ^{1}H NMR (500 MHz, 1,1,2,2-tetrachloroethane-d_2) δ: 7.80-6.86 (br, ArH), 4.61-4.33 (br, -CH_2N-), 3.22-2.67 (m, -CH_2-), 2.20-0.77 (br, -CH_3, -CH_2- and -CH); Anal. calcd for $(C_{76}H_{99}NO_2S_8)_n$: C, 69.41; H, 7.59; N, 1.07; found: C, 69.24; H, 7.57; N, 1.14.

6.4 Experimental Procedures for Chapter 4

Transistor Device Fabrication and Characterisation

All film preparation was carried out under inert atmosphere. BG-TC devices were fabricated on heavily doped n^+-Si (100) substrates with thermally grown SiO_2 dielectric (400 nm). The Si/SiO_2 substrates were then treated with OTS to reduce charge trapping. Polymers were dissolved in *o*-dichlorobenzene at a concentration of 5 mg/mL and spin-coated at 2000 rpm for 60 s, from a

hot solution before being annealed at 200 °C for 30 min. Al (40 nm) source-drain electrodes were deposited onto the polymer film under vacuum through shadow masks. The channel width and length of the transistors are 1000 μm and 40 μm, respectively. Transistor characterisation was carried out under nitrogen using a Keithley 4200 parameter analyser. Mobility was extracted from the slope of $I_D^{1/2}$ vs. V_G.

All-polymer OPV Device Fabrication and Characterisation

BHJ solar cells were fabricated with inverted (ITO/ZnO/PTB7-Th:P9-12/MoO_3/Ag) configuration and tested under simulated 100 mW/cm^2 AM 1.5G illumination using a Xenon lamp (Oriel Instruments). In all cases polymer active layers were prepared with a donor:acceptor (PTB7-Th:P9-12) blend ratio of 1:1 (w:w) (total concentration of 20 mg/mL (10 mg of each)) and solution processed from chlorobenzene. The pixel size, defined by the spatial overlap of the anode and cathode was 0.045 cm^2. The ZnO was prepared by the sol-gel method.[215,216]

2-Decyltetradecan-1-azide (4.8)

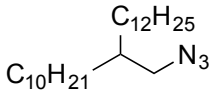

Triphenylphosphine (24.4 g, 92.8 mmol), diisopropyl azodicarboxylate (18.3 mL, 92.8 mmol) and diphenyl phosphoryl azide (20.0 mL, 92.8 mmol) were added to a stirred solution of 2-decyltetradecan-1-ol (23.5 g, 66.3 mmol) in anhydrous tetrahydrofuran (300 mL), under an argon atmosphere. The reaction mixture was stirred at room temperature for 16 h, before the volatiles were removed *in vacuo*. The crude product was extracted with hexane (150 mL), washed with water (3 x 150 mL), brine (150 mL), dried ($MgSO_4$) and the volatiles removed *in vacuo*. Purification by flash chromatography over silica (eluent: hexane) yielded the title compound as a colourless oil (19.1 g, 50.3 mmol, 76%). ^{1}H NMR (400 MHz, $CDCl_3$) δ: 3.23 (2 H, d, *J* 5.9, -CH_2N_3), 1.54 (1 H, m, -CH), 1.26 (40 H, s, -CH_2-), 0.88 (6 H, t, *J* 6.8, -CH_3); ^{13}C NMR (100 MHz, $CDCl_3$) δ: 55.42, 38.36, 32.09, 31.92, 30.07, 29.81, 29.76, 29.52, 26.77, 22.86, 14.27; Anal. calcd for ($C_{24}H_{49}N_3$): C, 75.92; H, 13.01; N, 11.07; found: C, 76.06; H, 13.15; N, 11.18.

2-Decyltetradecan-1-amine (4.9)

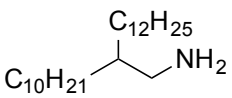

Lithium aluminium hydride (23.5 mL of a 1 M solution in diethyl ether, 23.5 mmol) was added dropwise to a stirred solution of 2-decyltetradecan-1-azide (6.4 g, 16.8 mmol) in anhydrous

diethyl ether (150 mL) at 0 °C, under an argon atmosphere. Once the addition was complete, the reaction mixture was heated to reflux for 2 h. The reaction mixture was then cooled to 0 °C and quenched with an aqueous solution of sodium hydroxide. The crude product was extracted with hexane (100 mL), washed with water (3 x 100 mL), brine (100 mL), dried ($MgSO_4$) and the volatiles removed *in vacuo*, to give the title compound as a colourless oil (5.5 g, 15.5 mmol, 92%). ^{1}H NMR (400 MHz, $CDCl_3$) δ: 2.58 (2 H, d, *J* 4.5, -CH_2NH_2), 1.25 (41 H, s, -CH_2- and -CH-), 1.10 (2 H, s, -NH_2-), 0.87 (6 H, t, *J* 6.8, -CH_3); ^{13}C NMR (100 MHz, $CDCl_3$) δ: 45.40, 41.09, 32.07, 31.69, 30.26, 29.84, 29.51, 26.96, 22.84, 14.27; HRMS (ESI) *m/z*: $[M+H]^+$ calcd for $C_{24}H_{51}N$, 354.4100; found, 354.4093.

11-(Bromomethyl)tricosane[169] (4.10)

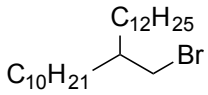

N-Bromosuccinimide (57.3 g, 321.9 mmol) was added in several portions to a stirred solution of 2-decyltetradecan-1-ol (72.2 g, 203.7 mmol) and triphenylphosphine (84.4 g, 321.9 mmol) in dichloromethane (600 mL), in the absence of light. The reaction mixture was stirred at room temperature for 16 h, before the volatiles were removed *in vacuo*. The crude product was extracted with hexane (300 mL) and purified by flash chromatography over silica (eluent: hexane) to yield the title compound as a colourless oil (79.3 g, 189.8 mmol, 93%). ^{1}H NMR (400 MHz, $CDCl_3$) δ: 3.44 (2 H, d, *J* 4.8, -CH_2Br), 1.58 (1 H, m, -CH), 1.26 (40 H, s, -CH_2-), 0.87 (6 H, t, *J* 7.0, -CH_3); ^{13}C NMR (100 MHz, $CDCl_3$) δ: 39.84, 39.66, 32.72, 32.08, 29.95, 29.80, 29.75, 29.52, 26.72, 22.85, 14.27; Anal. calcd for $C_{24}H_{49}Br$: C, 69.04; H, 11.83; found: C, 69.10; H, 11.91.

3-Decylpentadecanenitrile[218] (4.11)

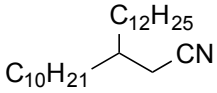

A solution of potassium cyanide (5.9 g, 90.3 mmol) and 11-(bromomethyl)tricosane (25.1 g, 60.2 mmol) in anhydrous DMSO (200 mL) was stirred at 80 °C for 16 h, under an argon atmosphere. The reaction mixture was cooled to room temperature, extracted with diethyl ether (200 mL), and washed thoroughly with water (5 x 500 mL) and brine (200 mL). The organic layer was dried ($MgSO_4$) and the volatiles removed *in vacuo*, to give the title compound as a yellow oil (21.2 g, 58.3 mmol, 97%). ^{1}H NMR (400 MHz, $CDCl_3$) δ: 2.32 (2 H, d, *J* 5.8, -CH_2CN), 1.67 (1 H, m, -CH), 1.38 (4 H, m, -CH_2-), 1.26 (36 H, s, -CH_2-), 0.88 (6 H, t, *J* 6.8, -CH_3); ^{13}C NMR (100 MHz, $CDCl_3$) δ: 150.11, 119.13, 35.25, 33.65, 32.07, 29.80, 29.76, 29.69, 29.50, 26.74, 22.84, 21.86, 14.27; HRMS (EI) *m/z*: $[M^+]$ calcd for $C_{25}H_{49}N$, 363.3865; found, 363.3871.

3-Decylpentadecan-1-amine[218] (4.12)

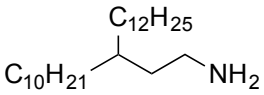

Lithium aluminium hydride (65.5 mL of a 1 M solution in diethyl ether, 65.5 mmol) was added dropwise to a stirred solution of 3-decylpentadecanenitrile (7.9 g, 21.8 mmol) in anhydrous diethyl ether (200 mL) at 0 °C, under an argon atmosphere. Once the addition was complete, the reaction mixture was heated to reflux for 2 h. The reaction mixture was then cooled to 0 °C and quenched with an aqueous solution of sodium hydroxide. The crude product was extracted with hexane (100 mL), washed with water (3 x 100 mL), brine (100 mL), dried ($MgSO_4$) and the volatiles removed *in vacuo*, to give the title compound as a colourless oil (7.6 g, 20.8 mmol, 95%). ^{1}H NMR (400 MHz, $CDCl_3$) δ: 2.67 (2 H, t, *J* 7.2, -CH_2NH_2), 1.37 (3 H, m, -CH_2- and -CH), 1.25 (40 H, s, -CH_2-), 0.87 (6 H, t, *J* 6.7, -CH_3); ^{13}C NMR (100 MHz, $CDCl_3$) δ: 39.82, 37.62, 35.39, 33.78, 32.02, 30.20, 29.80, 29.46, 26.69, 22.77, 14.16; HRMS (ESI) *m/z*: $[M+H]^+$ calcd for $C_{25}H_{53}N$, 368.4256; found, 368.4256.

4-Decylhexadecanenitrile (4.13)

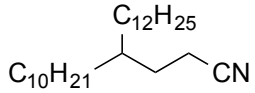

n-Butyllithium (45.0 mL of a 1.6 M solution in hexanes, 72.0 mmol) was added dropwise to a stirred solution of acetonitrile (3.8 mL, 72.0 mmol) in anhydrous tetrahydrofuran (300 mL) at -78 °C, under an argon atmosphere. The temperature was maintained and after 2 h, a solution of 11-(bromomethyl)tricosane (12.0 g, 28.8 mmol) in anhydrous tetrahydrofuran (50 mL) was added. The reaction mixture was then warmed to room temperature over 16 h and quenched with water (50 mL). The crude product was extracted with hexane (200 mL), washed with water (3 x 200 mL), brine (200 mL), dried ($MgSO_4$), and the volatiles removed *in vacuo*. Purification by column chromatography over silica (eluent: hexane:diethyl ether, 95:5, (v:v)) yielded the title compound as a colourless oil (4.1 g, 10.9 mmol, 38%). ^{1}H NMR (400 MHz, $CDCl_3$) δ: 2.30 (2 H, t, *J* 7.6, -CH_2CN), 1.61 (2 H, m, -CH_2), 1.44 (1 H, s, -CH), 1.26 (40 H, s, -CH_2-) 0.88 (6 H, t, *J* 6.8, -CH_3); ^{13}C NMR (100 MHz, $CDCl_3$) δ: 120.17, 36.76, 32.92, 32.04, 30.06, 29.77, 29.75, 29.47, 29.40, 26.47, 22.81, 14.80, 14.22; Anal. calcd for $C_{26}H_{51}N$: C, 82.68; H, 13.61; N, 3.71; found: C, 82.82; H, 13.79; N, 3.59.

4-Decylhexadecan-1-amine (4.14)

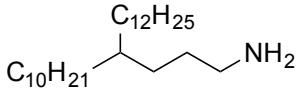

Lithium aluminium hydride (21.4 mL of a 1 M solution in diethyl ether, 21.4 mmol) was added dropwise to a stirred solution of 4-decylhexadecanenitrile (4.0 g, 10.7 mmol) in anhydrous diethyl ether (200 mL) at 0 °C, under an argon atmosphere. Once the addition was complete, the reaction mixture was heated to reflux for 2 h. The reaction mixture was cooled to 0 °C and quenched with an aqueous solution of sodium hydroxide. The crude product was extracted with hexane (100 mL), washed with water (3 x 200 mL), brine (200 mL), dried ($MgSO_4$) and the volatiles removed *in vacuo*, to give the title compound as a colourless oil (3.6 g, 9.4 mmol, 88%). ^{1}H NMR (400 MHz, $CDCl_3$) δ: 2.66 (2 H, t, *J* 7.0, -CH_2NH_2), 1.39 (2 H, m, -CH_2-), 1.26 (43 H, s, -CH_2- and -CH), 0.88 (6 H, t, *J* 6.8, -CH_3); ^{13}C NMR (100 MHz, $CDCl_3$) δ: 42.99, 37.46, 33.80, 32.09, 31.20, 30.98, 30.30, 29.87, 29.52, 26.84, 22.85, 14.28; Anal. calcd for $C_{26}H_{55}N$: C, 81.81; H, 14.52; N, 3.67; found: C, 81.99; H, 14.66; N, 3.46.

11-(But-3-en-1-yl)tricosane[169] (4.15)

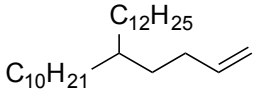

Allylmagnesium chloride (31.8 mL of a 1.7 M solution in THF, 54.1 mmol) was added dropwise to a stirred solution of 11-(bromomethyl)tricosane (5.0 g, 12.1 mmol) in anhydrous tetrahydrofuran (300 mL) at 0 °C, under an argon atmosphere. Once the addition was complete, the reaction mixture was heated to reflux for 16 h. The reaction mixture was cooled to 0 °C and quenched with water. Hydrochloric acid (40 mL of a 10 % aqueous solution) was then added and the crude product was extracted with hexane (150 mL). The organics were washed with water (3 x 200 mL), brine (200 mL), dried ($MgSO_4$) and the volatiles removed *in vacuo*. Purification by flash chromatography over silica (eluent: hexane) gave the title compound as a colourless oil (4.1 g, 10.7 mmol, 89%). ^{1}H NMR (400 MHz, $CDCl_3$) δ: 5.81 (1 H, m, =CH), 4.97 (2 H, m, =CH_2), 2.02 (2 H, m, -CH_2-), 1.26 (43 H, s, -CH_2- and -CH), 0.88 (6 H, t, *J* 6.8, -CH_3); ^{13}C NMR (100 MHz, $CDCl_3$) δ: 139.77, 114.02, 37.08, 33.66, 33.11, 32.10, 31.24, 30.30, 29.88, 29.84, 29.54, 26.77, 22.87, 14.29; HRMS (EI) *m/z*: [M^+] calcd for $C_{27}H_{54}$, 378.4226; found, 378.4210.

5-Decylheptadecan-1-ol (4.16)

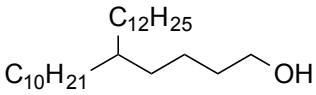

Borane (33 mL of a 1 M solution in THF, 33.0 mmol) was added dropwise to a stirred solution of 11-(but-3-en-1-yl)tricosane (24.5 g, 64.6 mmol) in anhydrous tetrahydrofuran (150 mL) at 0 °C, under an argon atmosphere. Once the addition was complete, the reaction mixture was stirred at room temperature for 3 h. Water (10 mL) and sodium hydroxide (29 mL of a 3 M aqueous solution, 87.0 mmol) were then added dropwise and the reaction mixture was heated to 40 °C for 16 h. The reaction mixture was cooled to 0 °C and quenched with hydrogen peroxide solution (31 mL of a 30 % aqueous solution, 93 mmol). The crude product was extracted with diethyl ether (100 mL), washed with water (3 x 200 mL), brine (200 mL), dried ($MgSO_4$) and the volatiles removed *in vacuo*. Purification by flash chromatography over silica (eluent: hexane) yielded the title compound as a yellow oil (19.5 g, 49.2 mmol, 76%). ^{1}H NMR (400 MHz, $CDCl_3$) δ: 3.64 (2 H, t, *J* 6.6, -CH_2OH), 1.53 (2 H, m, -CH_2-), 1.45 (1 H, s, OH), 1.26 (45 H, s, -CH_2- and -CH), 0.88 (6 H, t, *J* 6.8, -CH_3); ^{13}C NMR (100 MHz, $CDCl_3$) δ: 63.28, 37.57, 33.77, 33.68, 33.45, 32.09, 30.31, 29.87, 29.82, 29.53, 26.86, 23.05, 22.85, 14.27; HRMS (CI) *m/z*: $[M+NH_4]^+$ calcd for $C_{27}H_{56}O$, 414.4675; found, 414.4689.

5-Decylheptadecan-1-azide (4.17)

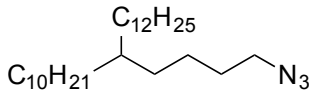

Triphenylphosphine (7.9 g, 30.1 mmol), diisopropyl azodicarboxylate (6.0 mL, 30.5 mmol) and diphenylphosphoryl azide (6.5 mL, 30.2 mmol) were added to a stirred solution of 5-decylheptadecan-1-ol (8.5 g, 21.4 mmol) in anhydrous tetrahydrofuran (250 mL), under an argon atmosphere. The reaction mixture was stirred at room temperature for 16 h, before the volatiles were removed *in vacuo*. The crude product was extracted with hexane (100 mL), washed with water (3 x 200 mL), brine (200 mL), dried ($MgSO_4$), and the volatiles removed *in vacuo*. Purification by flash chromatography over silica (eluent: hexane) yielded the title compound as a colourless oil (6.8 g, 16.0 mmol, 75%). ^{1}H NMR (400 MHz, $CDCl_3$) δ: 3.26 (2 H, t, *J* 7.0, -CH_2N_3), 1.57 (2 H, m, -CH_2-), 1.26 (45 H, s, -CH_2- and -CH), 0.87 (6 H, t, *J* 6.8, -CH_3); ^{13}C NMR (100 MHz, $CDCl_3$) δ: 51.67, 37.47, 33.73, 33.37, 32.09, 30.28, 29.87, 29.83, 29.53, 29.47, 26.83, 24.03, 22.86, 14.28; Anal. calcd for $C_{27}H_{55}N_3$: C, 76.89; H, 13.14; N, 9.96; found: C, 77.03; H, 13.24; N, 9.96.

5-Decylheptadecan-1-amine (4.18)

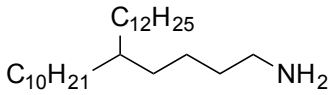

Lithium aluminium hydride (11.5 mL of a 1 M solution in diethyl ether, 11.5 mmol) was added dropwise to a stirred solution of 5-decylheptadecan-1-azide (2.9 g, 6.9 mmol) in anhydrous diethyl ether (200 mL) at 0 °C, under an argon atmosphere. Once the addition was complete, the reaction mixture was heated to reflux for 2 h. The reaction mixture was then cooled to 0 °C and quenched with an aqueous solution of sodium hydroxide. The crude product was extracted with hexane (100 mL), washed with water (3 x 200 mL), brine (200 mL), dried ($MgSO_4$), and the volatiles removed *in vacuo*, to give the title compound as a colourless oil (2.5 g, 6.4 mmol, 92%). ^{1}H NMR (400 MHz, $CDCl_3$) δ: 2.67 (2 H, t, *J* 7.0, -CH_2NH_2), 1.40 (2 H, m, -CH_2-), 1.25 (45 H, s, -CH_2- and -CH), 0.87 (6 H, t, *J* 6.8, -CH_3); ^{13}C NMR (100 MHz, $CDCl_3$) δ: 42.50, 37.54, 34.55, 33.77, 33.71, 32.08, 30.30, 29.87, 29.82, 29.52, 26.84, 24.14, 22.85, 14.27; HRMS (ESI) *m/z*: $[M+H]^+$ calcd for $C_{27}H_{57}N$, 396.4569; found, 396.4571.

4,9-Dibromonaphtho[1,8-*cd*:4,5-*c*'*d*']dipyran-1,3,6,8-tetrone[166] (4.2)

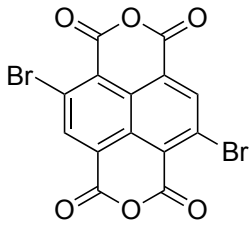

Naphtho[1,8-*cd*:4,5-*c'd'*]dipyran-1,3,6,8-tetrone (7.2 g, 26.7 mmol) in fuming sulfuric acid (200 mL, 20% SO_3) was stirred at 55 °C for 2 h, before a solution of dibromoisocyanuric acid (8.0 g, 28.0 mmol) in fuming sulfuric acid (100 mL, 20% SO_3) was added dropwise. Once the addition was complete, the reaction mixture was stirred at 85 °C for 48 h. The reaction mixture was cooled to room temperature and poured over ice to precipitate the product. The crude product was collected by vacuum filtration, washed with water (3 x 300 mL) and methanol (300 mL), and dried under high vacuum to yield the title compound as a yellow solid (4.5 g, 10.7 mmol, 40%). Anal. calcd for $C_{14}H_2Br_2O_6$: C, 39.48; H, 0.47; found: C, 37.22; H, 0.75.

4,9-Dibromo-2,7-bis(2-decyltetradecyl)benzo[*lmn*][3,8]phenanthroline-1,3,6,8(2*H*,7*H*)-tetrone[219] **(4.3)**

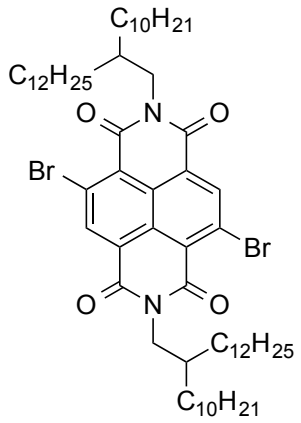

A solution of 4,9-dibromonaphtho[1,8-*cd*:4,5-*c'd'*]dipyran-1,3,6,8-tetrone (1.4 g, 3.2 mmol) and 2-decyltetradecan-1-amine (2.8 g, 7.9 mmol) in acetic acid (150 mL) was refluxed for 16 h, under an argon atmosphere. The reaction mixture was cooled to room temperature, poured over ice and extracted with chloroform (300 mL). The combined organics were washed with water (3 x 400 mL), brine (400 mL), dried ($MgSO_4$) and the volatiles removed *in vacuo*. Purification by column chromatography over silica (eluent: chloroform:hexane, 1:1, (v:v)), followed by recrystallisation (diethyl ether), yielded the title compound as a yellow solid (415.0 mg, 0.4 mmol, 12%). ^{1}H NMR (400 MHz, $CDCl_3$) δ: 8.99 (2 H, s, ArH), 4.14 (4 H, d, *J* 7.3, -CH_2N-), 1.98 (2 H, m, -CH), 1.23 (80 H, s, -CH_2-), 0.87 (12 H, m, -CH_3); ^{13}C NMR (100 MHz, $CDCl_3$) δ: 161.32, 161.16, 139.30, 128.51, 127.89, 125.44, 124.23, 45.61, 36.62, 32.08, 31.71, 30.18, 29.80, 29.75, 29.51, 26.49, 22.85, 14.28; Anal. calcd for $C_{62}H_{100}Br_2N_2O_4$: C, 67.86; H, 9.19; N, 2.55; found: C, 67.94; H, 9.50; N, 2.66.

4,9-Dibromo-2,7-bis(3-decylpentadecyl)benzo[*lmn*][3,8]phenanthroline-1,3,6,8(2*H*,7*H*)-tetrone (4.4)

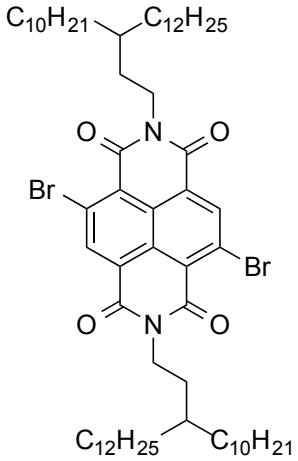

A solution of 4,9-dibromonaphtho[1,8-*cd*:4,5-*c'd'*]dipyran-1,3,6,8-tetrone (4.5 g, 10.7 mmol) and 3-decylpentadecan-1-amine (9.8 g, 26.7 mmol) in *o*-xylene (45 mL) and propionic acid (15 mL) was refluxed for 16 h, under an argon atmosphere. The reaction mixture was cooled to room temperature, poured over ice and extracted with hexane (100 mL). The combined organics were washed with water (3 x 150 mL), brine (150 mL), dried ($MgSO_4$) and the volatiles removed *in vacuo*. Purification by column chromatography over silica (eluent: chloroform:hexane, 1:1, (v:v)), yielded the title compound as a red solid (753.4 mg, 0.7 mmol, 6%). ^{1}H NMR (400 MHz, $CDCl_3$) δ: 8.99 (2 H, s, ArH), 4.19 (4 H, m, -CH_2N-), 1.66 (4 H, m, -CH_2-), 1.47 (2 H, m, -CH), 1.26 (80 H, s, -CH_2-), 0.88 (12 H, m, -CH_3); ^{13}C NMR (100 MHz, $CDCl_3$) δ: 160.82, 139.15, 128.41, 127.86, 125.52, 124.27, 40.15, 36.19, 33.68, 32.09, 31.84, 31.08, 30.21, 29.86, 29.53, 26.75, 22.86, 14.28; Anal. calcd for $C_{64}H_{104}Br_2N_2O_4$: C, 68.31; H, 9.32; N, 2.49; found: C, 68.39; H, 9.39; N, 2.56.

4,9-Dibromo-2,7-bis(4-decylhexadecyl)benzo[*lmn*][3,8]phenanthroline-1,3,6,8(2*H*,7*H*)-tetrone (4.5)

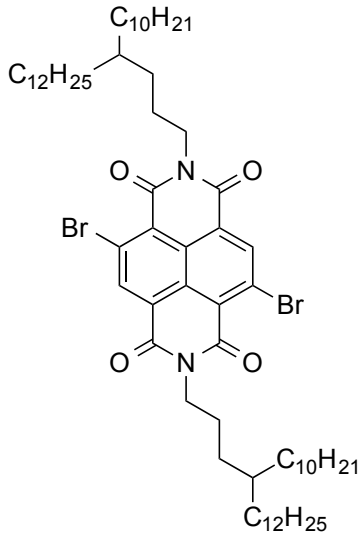

A solution of 4,9-dibromonaphtho[1,8-*cd*:4,5-*c'd'*]dipyran-1,3,6,8-tetrone (0.8 g, 2.0 mmol) and 4-decylhexadecan-1-amine (1.8 g, 4.7 mmol) in acetic acid (120 mL) was refluxed for 16 h, under an argon atmosphere. The reaction mixture was cooled to room temperature, poured over ice and extracted with chloroform (300 mL). The combined organics were washed with water (3 x 400 mL), brine (400 mL), dried ($MgSO_4$) and the volatiles removed *in vacuo*. Purification by column chromatography over silica (eluent: chloroform:hexane, 1:1, (v:v)), followed by recrystallisation (diethyl ether), yielded the title compound as a yellow solid (85.0 mg, 0.1 mmol, 4%). ^{1}H NMR (400 MHz, $CDCl_3$) δ: 9.00 (2 H, s, ArH), 4.16 (4 H, m, -CH_2N-), 1.71 (4 H, m, -CH_2-), 1.36 (6 H, m, -CH_2- and -CH), 1.25 (80 H, s, -CH_2-) 0.86 (12 H, m, -CH_3); ^{13}C NMR (100 MHz, $CDCl_3$) δ: 160.85, 139.20, 128.46, 127.85, 125.50, 124.25, 42.13, 37.39, 33.70, 32.10, 31.76, 31.13, 30.27, 29.84, 29.54, 26.84, 25.34, 22.86, 22.82, 14.28; Anal. calcd for $C_{66}H_{108}Br_2N_2O_4$: C, 68.73; H, 9.44; N, 2.43; found: C, 68.50; H, 9.65; N, 2.63.

4,9-Dibromo-2,7-bis(5-decylheptadecyl)benzo[*lmn*][3,8]phenanthroline-1,3,6,8(2*H*,7*H*)-tetrone (4.6)

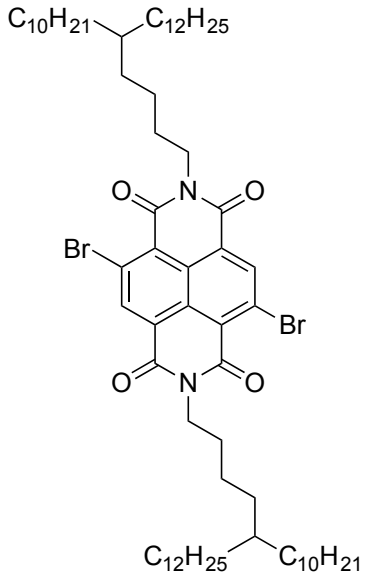

A solution of 4,9-dibromonaphtho[1,8-*cd*:4,5-*c'd'*]dipyran-1,3,6,8-tetrone (1.9 g, 4.5 mmol) and 5-decylheptadecan-1-amine (4.4 g, 11.1 mmol) in acetic acid (100 mL) was refluxed for 16 h, under an argon atmosphere. The reaction mixture was cooled to room temperature, poured over ice and extracted with chloroform (300 mL). The combined organics were washed with water (3 x 400 mL), brine (400 mL), dried ($MgSO_4$) and the volatiles removed *in vacuo*. Purification by column chromatography over silica (eluent: chloroform:hexane, 1:1, (v:v)), followed by recrystallisation (diethyl ether), yielded the title compound as a yellow solid (78.1 mg, 0.1 mmol, 15%). ^{1}H NMR (400 MHz, $CDCl_3$) δ: 8.99 (2 H, s, ArH), 4.18 (4 H, m, -CH_2N-), 1.71 (4 H, m, -CH_2-), 1.40 (6 H, m, -CH_2- and -CH), 1.25 (84 H, s, -CH_2-) 0.87 (12 H, m, -CH_3); ^{13}C NMR (100 MHz, $CDCl_3$) δ: 160.85, 139.19, 128.47, 127.86, 125.50, 124.22, 41.80, 37.54, 33.75, 33.47, 32.09, 30.31, 29.88, 29.83, 29.53, 28.48, 26.85, 24.44, 22.86, 14.29; Anal. calcd for $C_{68}H_{112}Br_2N_2O_4$: C, 69.13; H, 9.56; N, 2.37; found: C, 69.28; H, 9.64; N, 2.43.

Poly [4,9(2,7-bis(2-decyltetradecyl)benzo[*lmn*][3,8]phenanthroline-1,3,6,8(2*H*,7*H*)-tetrone)-alt-5,5'(2,2'-bithiophene)] (P9)

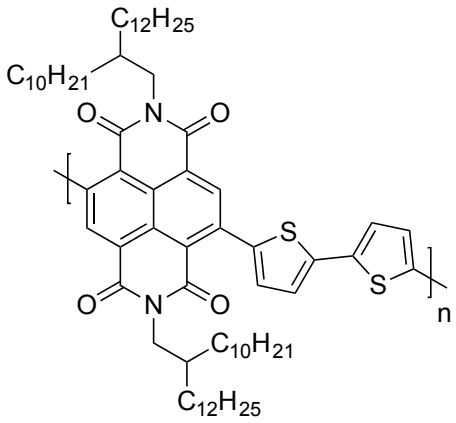

4,9-Dibromo-2,7-bis(2-decyltetradecyl)benzo[*lmn*][3,8]phenanthroline-1,3,6,8(2*H*,7*H*)-tetrone (87.3 mg, 0.0796 mmol), 5,5'-bis(trimethylstannyl)-2,2'-bithiophene (39.1 mg, 0.080 mmol), tris(dibenzylideneacetone)dipalladium(0) (1.5 mg, 0.0016 mmol) and tri(o-tolyl)phosphine (1.9 mg, 0.0063 mmol) were added to an oven dried microwave vial equipped with a stirrer bar. The vial was purged with argon before anhydrous chlorobenzene (0.5 mL) was added. The reaction mixture was purged with argon for a further 30 min and then subjected to the following microwave-heating profile: 100 °C for 2 min, 120 °C for 2 min, 140 °C for 2 min, 160 °C for 2 min, 180 °C for 20 min, and 200 °C for 20 min. Once the reaction mixture had cooled, the crude product was precipitated in methanol, filtered through a Soxhlet thimble, and purified by Soxhlet extraction: methanol (24 h), acetone (24 h), hexane (24 h) and chloroform (12 h). The chloroform extract was concentrated under vacuum and precipitated in methanol. The resulting precipitate was isolated by filtration and dried under high vacuum, to yield the title compound as a dark solid (74.5 mg, 85%). M_n: 38 kg/mol, M_w: 100 kg/mol, Đ: 2.6. ^{1}H NMR (500 MHz, 1,1,2,2-tetrachloroethane-d_2) δ: 8.90 (2 H, s, ArH), 7.41 (4 H, s, ArH), 4.20 (4 H, br, -CH_2N-), 2.11 (2 H, m, -CH), 1.45 (14 H, m, -CH_2-), 1.31 (66 H, s, -CH_2-), 0.92 (12 H, m, -CH_3); Anal. calcd for $(C_{70}H_{104}N_2O_4S_2)_n$: C, 76.31; H, 9.52; N, 2.54; found: C, 76.17; H, 9.62; N, 2.61.

Poly [4,9(2,7- bis(3-decylpentadecyl)benzo[*lmn*][3,8]phenanthroline-1,3,6,8(2*H*,7*H*)-tetrone)-alt-5,5'(2,2'-bithiophene)] (P10)

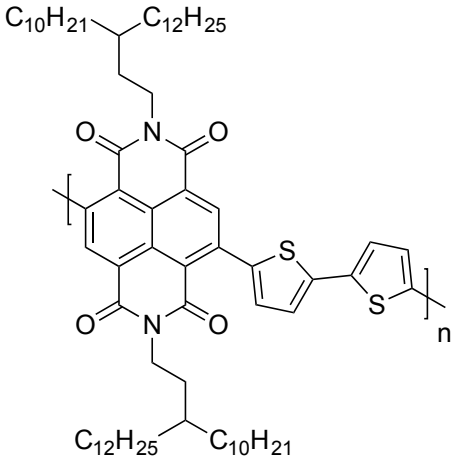

4,9-Dibromo-2,7-bis(3-decylpentadecyl)benzo[*lmn*][3,8]phenanthroline-1,3,6,8(2*H*,7*H*)-tetrone (181.4 mg, 0.1612 mmol), 5,5'-bis(trimethylstannyl)-2,2'-bithiophene (79.3 mg, 0.1612 mmol), tris(dibenzylideneacetone)dipalladium(0) (3.0 mg, 0.0032 mmol) and tri(o-tolyl)phosphine (3.9 mg, 0.0129 mmol) were added to an oven dried microwave vial equipped with a stirrer bar. The vial was purged with argon before anhydrous chlorobenzene (1.0 mL) was added. The reaction mixture was purged with argon for a further 30 min and then subjected to the following microwave-heating profile: 100 °C for 2 min, 120 °C for 2 min, 140 °C for 2 min, 160 °C for 2 min, 180 °C for 20 min, and 200 °C for 20 min. Once the reaction mixture had cooled, the crude product was precipitated in methanol, filtered through a Soxhlet thimble, and purified by Soxhlet extraction: methanol (24 h), acetone (24 h), hexane (24 h) and chloroform (12 h). The chloroform extract was concentrated under vacuum and precipitated in methanol. The resulting precipitate was isolated by filtration and dried under high vacuum, to yield the title compound as a dark solid (101.9 mg, 56%). M_n: 36 kg/mol, M_w: 200 kg/mol, Đ: 5.7. ^{1}H NMR (500 MHz, 1,1,2,2-tetrachloroethane-d_2) δ: 8.90 (2 H, s, ArH), 7.44 (4 H, m, ArH), 4.26 (4 H, br, -CH_2N-), 1.78 (4 H, s, -CH_2-), 1.55 (2 H, s, -CH), 1.33 (80 H, s, -CH_2-), 0.93 (12 H, m, -CH_3); Anal. calcd for $(C_{72}H_{108}N_2O_4S_2)_n$: C, 76.54; H, 9.64; N, 2.48; found: C, 76.41; H, 9.74; N, 2.61.

Poly [4,9(2,7-bis(4-decylhexadecyl)benzo[*lmn*][3,8]phenanthroline-1,3,6,8(2*H*,7*H*)-tetrone)-alt-5,5'(2,2'-bithiophene)] (P11)

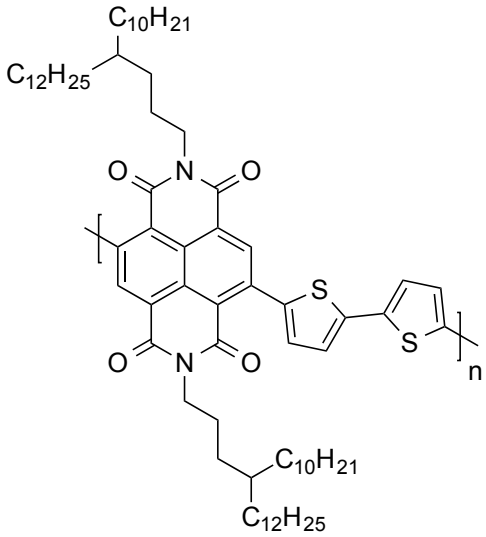

4,9-Dibromo-2,7-bis(4-decylhexadecyl)benzo[*lmn*][3,8]phenanthroline-1,3,6,8(2*H*,7*H*)-tetrone (57.5 mg, 0.0499 mmol), 5,5'-bis(trimethylstannyl)-2,2'-bithiophene (24.5 mg, 0.0499 mmol), tris(dibenzylideneacetone)dipalladium(0) (0.9 mg, 0.0010 mmol) and tri(o-tolyl)phosphine (1.2 mg, 0.0040 mmol) were added to an oven dried microwave vial equipped with a stirrer bar. The vial was purged with argon before anhydrous chlorobenzene (0.5 mL) was added. The reaction mixture was purged with argon for a further 30 min and then subjected to the following microwave-heating profile: 100 °C for 2 min, 120 °C for 2 min, 140 °C for 2 min, 160 °C for 2 min, 180 °C for 20 min, and 200 °C for 20 min. Once the reaction mixture had cooled, the crude product was precipitated in methanol, filtered through a Soxhlet thimble, and purified by Soxhlet extraction: methanol (24 h), acetone (24 h), hexane (24 h) and chloroform (12 h). The chloroform extract was concentrated under vacuum and precipitated in methanol. The resulting precipitate was isolated by filtration and dried under high vacuum, to yield the title compound as a dark solid (42.7 mg, 74%). M_n: 30 kg/mol, M_w: 85 kg/mol, Đ: 2.8. ^{1}H NMR (500 MHz, 1,1,2,2-tetrachloroethane-d_2) δ: 8.91 (2 H, s, ArH), 7.43 (4 H, s, ArH), 4.23 (4 H, br, -CH_2N-), 1.85 (4 H, br, -CH_2-), 1.46 (6 H, m, -CH_2- and -CH), 1.34 (80 H, s, -CH_2-), 0.94 (12 H, m, -CH_3); Anal. calcd for $(C_{74}H_{112}N_2O_4S_2)_n$: C, 76.76; H, 9.75; N, 2.42; found: C, 76.71; H, 9.88; N, 2.47.

Poly [4,9(2,7-bis(5-decylheptadecyl)benzo[*lmn*][3,8]phenanthroline-1,3,6,8(2*H*,7*H*)-tetrone)-alt-5,5'(2,2'-bithiophene)] (P12)

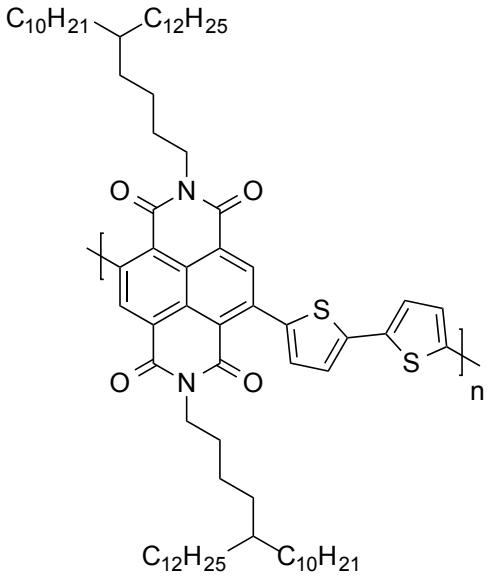

4,9-Dibromo-2,7-bis(5-decylheptadecyl)benzo[*lmn*][3,8]phenanthroline-1,3,6,8(2*H*,7*H*)-tetrone (71.0 mg, 0.0601 mmol), 5,5'-bis(trimethylstannyl)-2,2'-bithiophene (29.6 mg, 0.0601 mmol), tris(dibenzylideneacetone)dipalladium(0) (1.1 mg, 0.0012 mmol) and tri(o-tolyl)phosphine (1.5 mg, 0.0049 mmol) were added to an oven dried microwave vial equipped with a stirrer bar. The vial was purged with argon before anhydrous chlorobenzene (0.5 mL) was added. The reaction mixture was purged with argon for a further 30 min and then subjected to the following microwave-heating profile: 100 °C for 2 min, 120 °C for 2 min, 140 °C for 2 min, 160 °C for 2 min, 180 °C for 20 min, and 200 °C for 20 min. Once the reaction mixture had cooled, the crude product was precipitated in methanol, filtered through a Soxhlet thimble, and purified by Soxhlet extraction: methanol (24 h), acetone (24 h), hexane (24 h) and chloroform (12 h). The chloroform extract was concentrated under vacuum and precipitated in methanol. The resulting precipitate was isolated by filtration and dried under high vacuum, to yield the title compound as a dark solid (47.4 mg, 67%). M_n: 31 kg/mol, M_w: 87 kg/mol, Đ: 2.8. ^{1}H NMR (500 MHz, 1,1,2,2-tetrachloroethane-d_2) δ: 8.91 (2 H, s, ArH), 7.44 (4 H, s, ArH), 4.25 (4 H, br, -CH_2N-), 1.84 (4 H, br, -CH_2-), 1.51 (4 H, m, -CH_2-), 1.34 (86 H, s, -CH_2- and -CH), 0.94 (12 H, m, -CH_3); Anal. calcd for $(C_{76}H_{116}N_2O_4S_2)_n$: C, 76.97; H, 9.86; N, 2.36; found: C, 76.87; H, 9.94; N, 2.38.

6.5 Experimental Procedures for Chapter 5

Transistor Device Fabrication and Characterisation

All film preparation was carried out under inert atmosphere. TG-BC devices were fabricated on glass substrates using Au (60 nm) source-drain electrodes and PMMA (80 mg/ml in *n*-butyl acetate, 120 kg/mol) dielectric. Polymers were dissolved in *o*-dichlorobenzene at a

concentration of 5 mg/mL (P13-16) or 10 mg/mL (P17-18), and spin-coated at 2000 rpm for 60 s. The obtained polymer films were annealed at 200 °C for 30 min (P13-18) or 300 °C for 15 min (P13-16), before the dielectric was spin-coated. The channel width and length of the transistors are 1000 μm and 40 μm, respectively. Transistor characterisation was carried out under nitrogen using a Keithley 4200 parameter analyser. Mobility was extracted from the slope of $I_D^{1/2}$ vs. V_G.

Poly [4,9(2,7-bis(4-decylhexadecyl)benzo[*lmn*][3,8]phenanthroline-1,3,6,8(2*H*,7*H*)-tetrone)-alt-5,5'((*E*)-1,2-bis(thiophen-2-yl)ethene)] (P13)

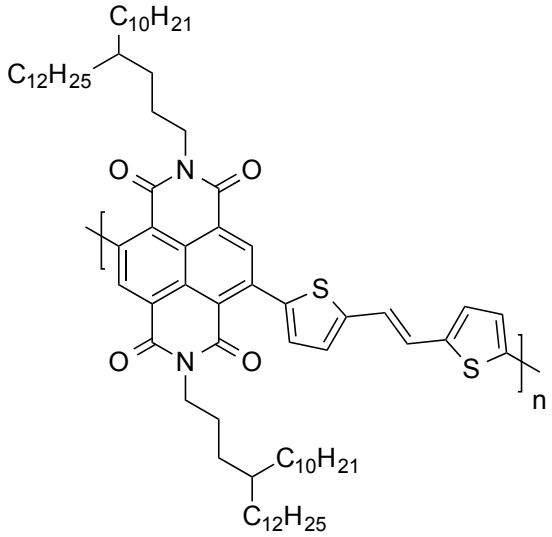

4,9-Dibromo-2,7-bis(4-decylhexadecyl)benzo[*lmn*][3,8]phenanthroline-1,3,6,8(2*H*,7*H*)-tetrone (159.6 mg, 0.1383 mmol), (*E*)-1,2-bis(5-(trimethylstannyl)thiophen-2-yl)ethene (71.6 mg, 0.1383 mmol), tris(dibenzylideneacetone)dipalladium(0) (2.5 mg, 0.0028 mmol) and tri(o-tolyl)phosphine (3.4 mg, 0.0111 mmol) were added to an oven dried microwave vial equipped with a stirrer bar. The vial was purged with argon before anhydrous chlorobenzene (1.0 mL) was added. The reaction mixture was purged with argon for a further 30 min and then subjected to the following microwave-heating profile: 100 °C for 2 min, 120 °C for 2 min, 140 °C for 2 min, 160 °C for 2 min, 180 °C for 20 min, and 200 °C for 20 min. Once the reaction mixture had cooled, the crude product was precipitated in methanol, filtered through a Soxhlet thimble, and purified by Soxhlet extraction: methanol (24 h), acetone (24 h), hexane (24 h) and chloroform (12 h). The chloroform extract was concentrated under vacuum and precipitated in methanol. The resulting precipitate was isolated by filtration and dried under high vacuum, to yield the title compound as a dark solid (146.9 mg, 90%). M_n: 51 kg/mol, M_w: 116 kg/mol, Đ: 2.3. ^{1}H NMR (500 MHz, 1,1,2,2-tetrachloroethane-d_2) δ: 8.87 (2 H, s, ArH), 7.39 (2 H, d, *J* 4.5, -C(H)=C(H)-), 7.26 (4 H, s, ArH), 4.22 (4 H, br, -CH_2N-), 1.82 (4 H, br, -CH_2-), 1.67 (2 H, m, -CH-),

1.33 (84 H, s, -CH_2-), 0.93 (12 H, m, -CH_3); Anal. calcd for $(C_{76}H_{114}N_2O_4S_2)_n$: C, 77.11; H, 9.71; N, 2.37; found: C, 76.98; H, 9.82; N, 2.41.

Poly [4,9(2,7-bis(4-decylhexadecyl)benzo[*lmn*][3,8]phenanthroline-1,3,6,8(2*H*,7*H*)-tetrone)-alt-5,5'((*E*)-1,2-bis(selenophen-2-yl)ethene)] (P14)

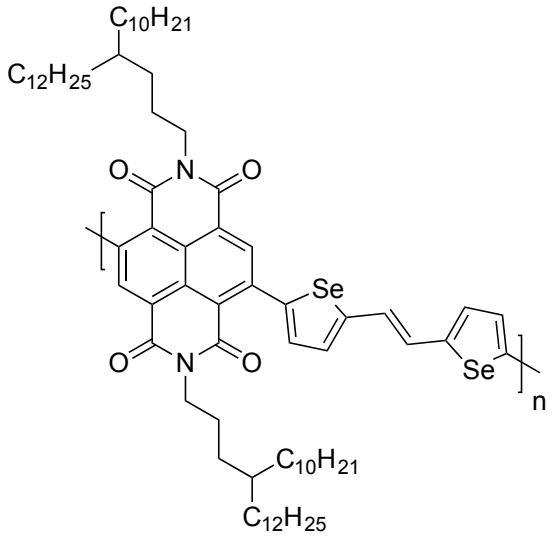

4,9-Dibromo-2,7-bis(4-decylhexadecyl)benzo[*lmn*][3,8]phenanthroline-1,3,6,8(2*H*,7*H*)-tetrone (168.4 mg, 0.1460 mmol), (*E*)-1,2-bis(5-(trimethylstannyl)selenophen-2-yl)ethene (89.3 mg, 0.1460 mmol), tris(dibenzylideneacetone)dipalladium(0) (2.7 mg, 0.0029 mmol) and tri(o-tolyl)phosphine (3.6 mg, 0.0118 mmol) were added to an oven dried microwave vial equipped with a stirrer bar. The vial was purged with argon before anhydrous chlorobenzene (1.5 mL) was added. The reaction mixture was purged with argon for a further 30 min and then subjected to the following microwave-heating profile: 100 °C for 2 min, 120 °C for 2 min, 140 °C for 2 min, 160 °C for 2 min, 180 °C for 20 min, and 200 °C for 20 min. Once the reaction mixture had cooled, the crude product was precipitated in methanol, filtered through a Soxhlet thimble, and purified by Soxhlet extraction: methanol (24 h), acetone (24 h), hexane (24 h) and chloroform (12 h). The chloroform extract was concentrated under vacuum and precipitated in methanol. The resulting precipitate was isolated by filtration and dried under high vacuum, to yield the title compound as a dark solid (162.0 mg, 87%). M_n: 60 kg/mol, M_w: 139 kg/mol, Đ: 2.3. ^{1}H NMR (500 MHz, 1,1,2,2-tetrachloroethane-d_2) δ: 8.88 (2 H, s, ArH), 7.54 (2 H, m, ArH), 7.41 (2 H, m, ArH), 7.22 (2 H, s, -C(H)=C(H)-), 4.23 (4 H, br, -CH_2N-), 1.84 (8 H, br, -CH_2-), 1.40 (82 H, m, -CH_2- and -CH), 0.95 (12 H, m, -CH_3); Anal. calcd for $(C_{76}H_{114}N_2O_4Se_2)_n$: C, 71.44; H, 8.99; N, 2.19; found: C, 71.54; H, 9.15; N, 2.35.

2,7-Bis(4-decylhexadecyl)-4,9-di(thiophen-2-yl)benzo[*lmn*][3,8]phenanthroline-1,3,6,8(2*H*,7*H*)-tetrone (5.3)

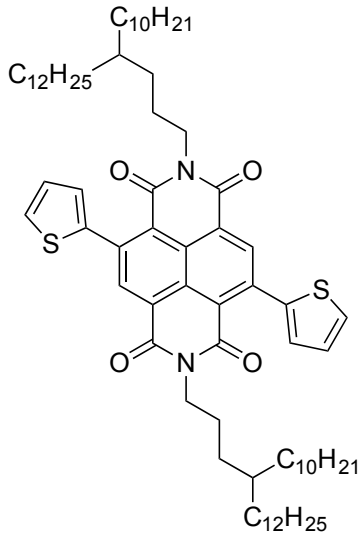

4,9-Dibromo-2,7-bis(4-decylhexadecyl)benzo[*lmn*][3,8]phenanthroline-1,3,6,8(2*H*,7*H*)-tetrone (500.0 mg, 0.4 mmol), tributyl(thiophen-2-yl)stannane (352.2 mg, 0.9 mmol), tris(dibenzylideneacetone)dipalladium(0) (7.8 mg, 0.0085 mmol) and tri(o-tolyl)phosphine (10.4 mg, 0.0342 mmol) were added to an oven dried microwave vial equipped with a stirrer bar. The vial was purged with argon before anhydrous chlorobenzene (12.0 mL) was added. The reaction mixture was purged with argon for a further 30 min and then heated to 150 °C for 60 min. After cooling, the crude product was passed through a flash column over silica:potassium fluoride, (10:1, w:w) (eluent: dichloromethane). The solvent was removed *in vacuo* and the resulting residue was purified further by column chromatography over silica (eluent: dichloromethane:hexane, 1:1, (v:v)), to yield the title compound as a red solid (480.0 mg, 0.4 mmol, 95%). ^{1}H NMR (400 MHz, $CDCl_3$) δ: 8.76 (2 H, s, ArH), 7.58 (2 H, dd, *J* 4.8 and 0.8, ArH), 7.30 (2 H, dd, *J* 3.2 and 0.8, ArH), 7.22-7.20 (2 H, m, ArH), 4.08 (4 H, t, *J* 7.6, -CH_2N-), 1.68-1.61 (4 H, m, -CH_2-), 1.35-1.20 (86 H, m, -CH_2- and -CH), 0.89-0.85 (12 H, m, -CH_3); ^{13}C NMR (100 MHz, $CDCl_3$,) δ: 162.31, 162.13, 140.88, 140.44, 136.79, 128.33, 128.09, 127.56, 125.57, 123.64, 41.65, 37.45, 33.77-33.56 (overlapping C), 32.14-31.93 (overlapping C), 31.14, 30.33-30.11 (overlapping C), 30.04-29.73 (overlapping C), 29.58-29.33 (overlapping C), 26.99-26.66 (overlapping C), 25.48, 23.04-22.68 (overlapping C), 14.40-14.15 (overlapping C); MS (MALDI-ToF) *m/z*: $[M+H]^+$ 1160.8 (11%).

4,9-Bis(5-bromothiophen-2-yl)-2,7-bis(4-decylhexadecyl)benzo[*lmn*][3,8]phenanthroline-1,3,6,8(2*H*,7*H*)-tetrone (5.5)

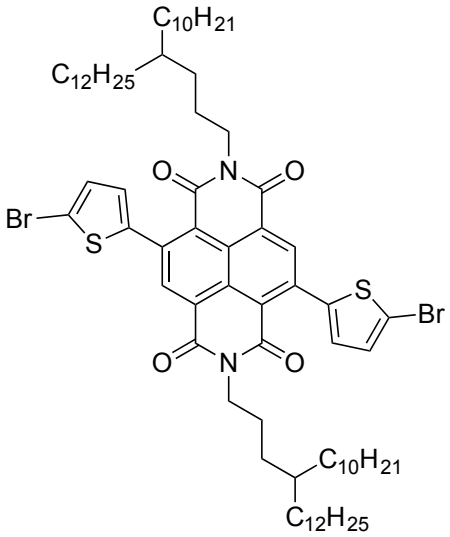

N-bromosuccinimide (162.0 mg, 0.9 mmol) was added in several portions to a stirred solution of 2,7-bis(4-decylhexadecyl)-4,9-di(thiophen-2-yl)benzo[*lmn*][3,8]phenanthroline-1,3,6,8(2*H*,7*H*)-tetrone (480.0 mg, 0.4 mmol) in chloroform (80 mL) and acetic acid (30 mL), in the absence of light. Once the addition was complete, the reaction was stirred at 50 °C for 16 h. An aqueous solution of sodium sulfite (40 mL) was added and the crude product was extracted with chloroform (3 x 30 mL). The organics were washed with water (3 x 100 mL), dried ($MgSO_4$) and the volatiles removed *in vacuo*. Purification of the crude product by column chromatography over silica (eluent: hexane:dichloromethane, 3:2, (v:v)), followed by recrystallisation (ethanol), yielded the title compound as a red solid (490.0 mg, 0.4 mmol, 90%). ^{1}H NMR (400 MHz, $CDCl_3$) δ: 8.72 (2 H, s, ArH), 7.16 (2 H, d, *J* 3.6, ArH), 7.08 (2 H, d, *J* 3.6, ArH), 4.09 (4 H, t, *J* 7.6, -CH_2N-), 1.68-1.61 (4 H, m, -CH_2-), 1.35-1.20 (86 H, m, -CH_2- and -CH), 0.89-0.85 (12 H, m, -CH_3); ^{13}C NMR (100 MHz, $CDCl_3$) δ: 161.93, 142.08, 139.13, 136.46, 130.19, 128.80, 127.53, 125.66, 123.28, 115.45, 41.59, 37.28, 33.60-33.39 (overlapping C), 32.05-31.77 (overlapping C), 31.00, 30.21-30.01 (overlapping C), 29.89-29.52 (overlapping C), 29.52-29.23 (overlapping C), 26.82-26.54 (overlapping C), 25.33, 22.87-22.55 (overlapping C), 14.22-13.98 (overlapping C); MS (MALDI-ToF) *m/z*: $[M+H]^+$ 1318.2 (37%).

Poly [5,5'(4,9-bis(thiophen-2-yl)-2,7-bis(4-decylhexadecyl)benzo[*lmn*][3,8]phenanthroline-1,3,6,8(2*H*,7*H*)-tetrone)-alt-1,2((*E*)-1,2-difluoroethene)] (P15)

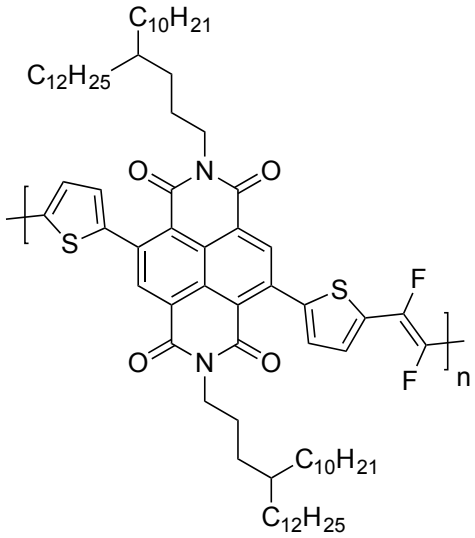

4,9-Bis(5-bromothiophen-2-yl)-2,7-bis(4-decylhexadecyl)benzo[*lmn*][3,8]phenanthroline-1,3,6,8(2*H*,7*H*)-tetrone (79.0 mg, 0.0600 mmol), [(*E*)-1,2-difluoroethene-1,2-diyl]bis(tributylstannane) (38.5 mg, 0.0600 mmol), copper(I) iodide (11.4 mg, 0.0599 mmol) and tetrakis(triphenylphosphine)palladium(0) (3.5 mg, 0.0030 mmol) were added to an oven dried microwave vial equipped with a stirrer bar. The vial was purged with argon before anhydrous *o*-xylene (0.5 mL) and anhydrous DMF (0.1 mL) were added. The reaction mixture was purged with argon for a further 30 min and then subjected to the following microwave-heating profile: 100 °C for 2 min, 120 °C for 2 min, 140 °C for 2 min, 160 °C for 2 min, and 180 °C for 40 min. Once the reaction mixture had cooled, the crude product was precipitated in methanol, filtered through a Soxhlet thimble, and purified by Soxhlet extraction: methanol (24 h), acetone (24 h), hexane (24 h) and chloroform (6 h). The chloroform extract was concentrated under vacuum and precipitated in methanol. The resulting precipitate was isolated by filtration and dried under high vacuum, to yield the title compound as a dark solid (67.0 mg, 92%). M_n: 33 kg/mol, M_w: 68 kg/mol, Đ: 2.1. ^{1}H NMR (500 MHz, 1,1,2,2-tetrachloroethane-d_2) δ: 8.90 (2 H, m, ArH), 7.62 (2 H, m, ArH), 7.45 (2 H, m, ArH), 4.22 (4 H, br, -CH_2N-), 1.83 (4 H, br, -CH_2-), 1.39 (86 H, m, -CH_2- and -CH), 0.94 (12 H, m, -CH_3); Anal. calcd for $(C_{76}H_{112}F_2N_2O_4S_2)_n$: C, 74.83; H, 9.25; N, 2.30; found: C, 74.71; H, 9.17; N, 2.38.

2,7-Bis(4-decylhexadecyl)-4,9-di(selenophen-2-yl)benzo[*lmn*][3,8]phenanthroline-1,3,6,8(2*H*,7*H*)-tetrone (5.4)

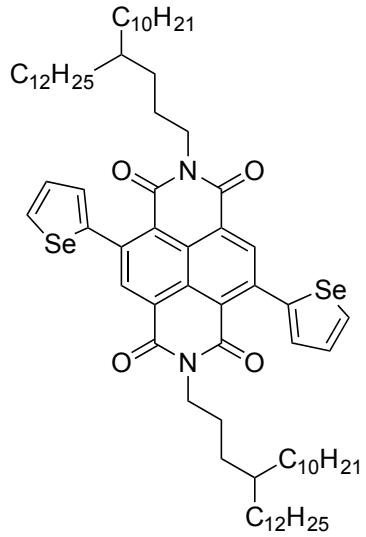

4,9-Dibromo-2,7-bis(4-decylhexadecyl)benzo[*lmn*][3,8]phenanthroline-1,3,6,8(2*H*,7*H*)-tetrone (400.0 mg, 0.3 mmol), tributyl(selenophen-2-yl)stannane (320.5 mg, 0.8 mmol), tris(dibenzylideneacetone)dipalladium(0) (6.3 mg, 0.0069 mmol) and tri(o-tolyl)phosphine (8.4 mg, 0.0276 mmol) were added to an oven dried microwave vial equipped with a stirrer bar. The vial was purged with argon before anhydrous chlorobenzene (15.0 mL) was added. The reaction mixture was purged with argon for a further 30 min and then heated to 150 °C for 60 min. After cooling, the crude product was passed through a flash column over silica:potassium fluoride, (10:1, w:w) (eluent: dichloromethane). The solvent was removed *in vacuo* and the resulting residue was purified further by column chromatography over silica (eluent: dichloromethane:hexane, 1:1, (v:v)), to yield the title compound as a red solid (398.0 mg, 0.3 mmol, 92%). ^{1}H NMR (400 MHz, $CDCl_3$) δ: 8.76 (2 H, s, ArH), 8.28 (2 H, dd, *J* 5.2 and 2.0, ArH), 7.44-7.41 (4 H, m, ArH), 4.09 (4 H, t, *J* 7.6, -CH_2N-), 1.67-1.61 (4 H, m, -CH_2-), 1.33-1.21 (86 H, m, -CH_2- and -CH), 0.89-0.85 (12 H, m, -CH_3); ^{13}C NMR (100 MHz, $CDCl_3$) δ: 162.35, 162.26, 146.89, 142.75, 136.51, 134.03, 130.49, 129.87, 127.52, 125.41, 123.16, 41.62, 37.45, 33.69, 32.20-31.94 (overlapping C), 31.14, 30.42-30.15 (overlapping C), 29.96-29.65 (overlapping C), 29.58-29.39 (overlapping C), 26.82, 25.49, 22.96-22.73 (overlapping C), 14.40-14.14 (overlapping C); MS (MALDI-ToF) *m/z*: $[M+H]^+$ 1254.1 (97%).

4,9-Bis(5-bromoselenophen-2-yl)-2,7-bis(4-decylhexadecyl)benzo[*lmn*][3,8]phenanthroline-1,3,6,8(2*H*,7*H*)-tetrone (5.6)

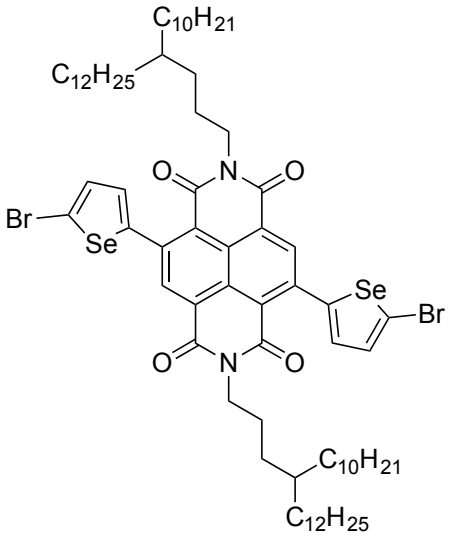

N-bromosuccinimide (121.8 mg, 0.7 mmol) was added in several portions to a stirred solution of 2,7-bis(4-decylhexadecyl)-4,9-di(selenophen-2-yl)benzo[*lmn*][3,8]phenanthroline-1,3,6,8(2*H*,7*H*)-tetrone (390.0 mg, 0.3 mmol) in chloroform (80 mL) and acetic acid (30 mL), in the absence of light. Once the addition was complete, the reaction was stirred at 50 °C for 16 h. An aqueous solution of sodium sulfite (40 mL) was added and the crude product was extracted with chloroform (3 x 30 mL). The organics were washed with water (3 x 100 mL), dried ($MgSO_4$) and the volatiles removed *in vacuo*. Purification of the crude product by column chromatography over silica (eluent: hexane:dichloromethane, 3:2, (v:v)), followed by recrystallisation (ethanol), yielded the title compound as a purple solid (373.0 mg, 0.3 mmol, 85%). ^{1}H NMR (400 MHz, $CDCl_3$) δ: 8.76 (2 H, s, ArH), 7.36 (2 H, d, *J* 4.0, ArH), 7.23 (2 H, d, *J* 4.0, ArH), 4.10 (4 H, t, *J* 7.6, -CH_2N-), 1.68-1.61 (4 H, m, -CH_2-), 1.31-1.22 (86 H, m, -CH_2- and -CH), 0.89-0.85 (12 H, m, -CH_3); ^{13}C NMR (100 MHz, $CDCl_3$) δ: 162.48, 162.13, 147.92, 141.55, 136.24, 133.12, 131.41, 127.49, 125.64, 122.53, 120.58, 53.57, 41.72, 37.40, 33.69, 32.21-31.89 (overlapping C), 31.12, 30.41-30.07 (overlapping C), 29.99-29.71 (overlapping C), 29.55-29.29 (overlapping C), 26.97-26.71 (overlapping C), 25.45, 23.01-22.68 (overlapping C), 14.37-14.11 (overlapping C); MS (MALDI-ToF) *m/z*: $[M+H]^+$ 1412.7 (57%).

Poly [5,5'(4,9-bis(selenophen-2-yl)-2,7-bis(4-decylhexadecyl)benzo[*lmn*][3,8]phenanthroline-1,3,6,8(2*H*,7*H*)-tetrone)-alt-1,2((*E*)-1,2-difluoroethene)] (P16)

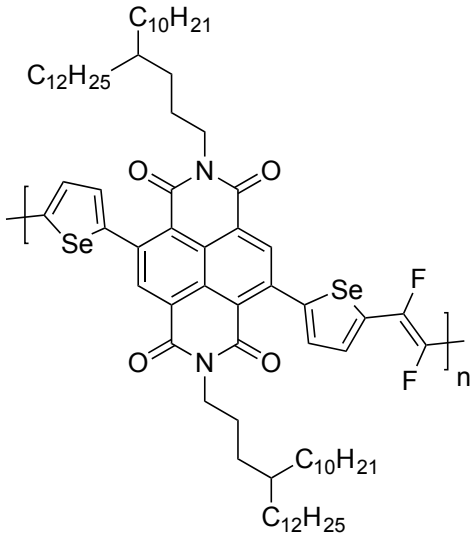

4,9-Bis(5-bromoselenophen-2-yl)-2,7-bis(4-decylhexadecyl)benzo[*lmn*][3,8]phenanthroline-1,3,6,8(2*H*,7*H*)-tetrone (192.5 mg, 0.1364 mmol), [(*E*)-1,2-difluoroethene-1,2-diyl]bis(tributylstannane) (87.6 mg, 0.1364 mmol), copper(I) iodide (25.9 mg, 0.1360 mmol) and tetrakis(triphenylphosphine)palladium(0) (7.8 mg, 0.0067 mmol) were added to an oven dried microwave vial equipped with a stirrer bar. The vial was purged with argon before anhydrous *o*-xylene (1.0 mL) and anhydrous DMF (0.2 mL) were added. The reaction mixture was purged with argon for a further 30 min and then subjected to the following microwave-heating profile: 100 °C for 2 min, 120 °C for 2 min, 140 °C for 2 min, 160 °C for 2 min, and 180 °C for 40 min. Once the reaction mixture had cooled, the crude product was precipitated in methanol, filtered through a Soxhlet thimble, and purified by Soxhlet extraction: methanol (24 h), acetone (24 h), hexane (24 h), THF:Hexane, (47:53, v:v) (24 h) and chloroform (6 h). The chloroform extract was concentrated under vacuum and precipitated in methanol. The resulting precipitate was isolated by filtration and dried under high vacuum, to yield the title compound as a dark solid (142.0 mg, 79%). M_n: 44 kg/mol, M_w: 83 kg/mol, Đ: 1.9. ^{1}H NMR (500 MHz, 1,1,2,2-tetrachloroethane-d_2) δ: 8.90 (2 H, m, ArH), 7.62 (2 H, m, ArH), 7.45 (2 H, m, ArH), 4.22 (4 H, br, -CH_2N-), 1.83 (4 H, br, -CH_2-), 1.39 (86 H, m, -CH_2- and -CH), 0.94 (12 H, m, -CH_3); Anal. calcd for $(C_{76}H_{112}F_2N_2O_4Se_2)_n$: C, 69.49; H, 8.59; N, 2.13; found: C, 69.32; H, 8.40; N, 2.28.

Poly [4,9(2,7- bis(4-decylhexadecyl)benzo[*lmn*][3,8]phenanthroline-1,3,6,8(2*H*,7*H*)-tetrone)-alt-2,6(dithieno[3,2-*b*:2',3'-*d*]thiophene)] (P17)

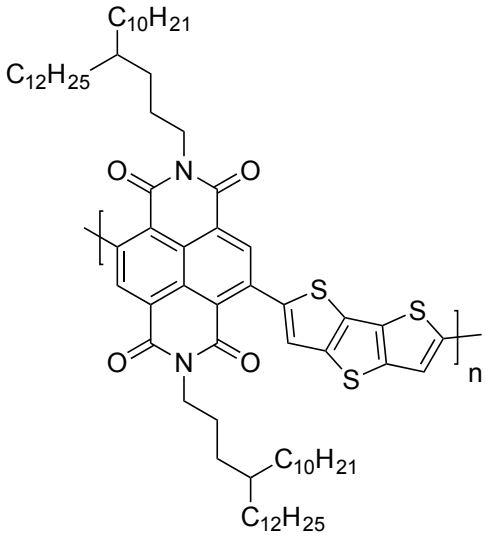

4,9-Dibromo-2,7-bis(4-decylhexadecyl)benzo[*lmn*][3,8]phenanthroline-1,3,6,8(2*H*,7*H*)-tetrone (164.9 mg, 0.1429 mmol), 2,6-bis(trimethylstannyl)dithieno[3,2-*b*:2',3'-*d*]thiophene (74.6 mg, 0.1429 mmol), tris(dibenzylideneacetone)dipalladium(0) (2.6 mg, 0.0029 mmol) and tri(o-tolyl)phosphine (3.5 mg, 0.0114 mmol) were added to an oven dried microwave vial equipped with a stirrer bar. The vial was purged with argon before anhydrous chlorobenzene (1.0 mL) was added. The reaction mixture was purged with argon for a further 30 min and then subjected to the following microwave-heating profile: 100 °C for 2 min, 120 °C for 2 min, 140 °C for 2 min, 160 °C for 2 min, 180 °C for 20 min, and 200 °C for 20 min. Once the reaction mixture had cooled, the crude product was precipitated in methanol, filtered through a Soxhlet thimble, and purified by Soxhlet extraction: methanol (24 h), acetone (24 h), hexane (24 h) and chloroform (12 h). The remaining polymer residue was extracted with chlorobenzene, precipitated in methanol, isolated by filtration and dried under high vacuum, to yield the title compound as a dark solid (120.9 mg, 71%). M_n: 170 kg/mol, M_w: 398 kg/mol, Đ: 2.3. ^{1}H NMR (500 MHz, 1,1,2,2-tetrachloroethane-d_2) δ: 8.97 (2 H, s, ArH), 7.72 (2H, s, ArH), 4.24 (4 H, br, -CH_2N-), 1.84 (4 H, br, -CH_2-), 1.33 (86 H, br, -CH_2- and -CH), 0.92 (12 H, m, -CH_3-); Anal. calcd for $(C_{74}H_{110}N_2O_4S_3)_n$: C, 74.82; H, 9.33; N, 2.36; found: C, 74.74; H, 9.40; N, 2.49.

Poly [4,9(2,7- bis(4-decylhexadecyl)benzo[*lmn*][3,8]phenanthroline-1,3,6,8(2*H*,7*H*)-tetrone)-alt-2,6(diseleno[3,2-*b*:2',3'-*d*]selenophene)] (P18)

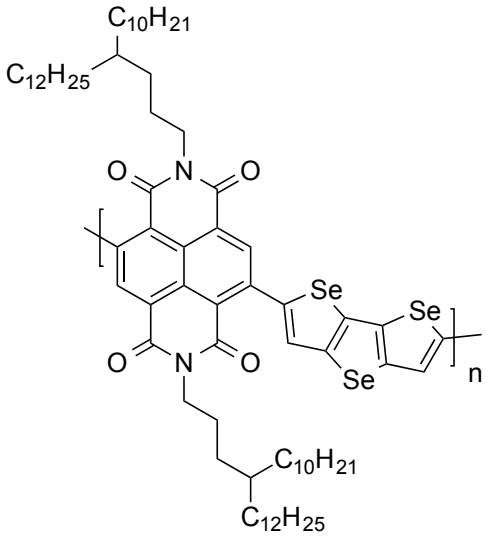

4,9-Dibromo-2,7-bis(4-decylhexadecyl)benzo[*lmn*][3,8]phenanthroline-1,3,6,8(2*H*,7*H*)-tetrone (153.6 mg, 0.1331 mmol), 2,6-bis(trimethylstannyl)diseleno[3,2-*b*:2',3'-*d*]selenophene (88.2 mg, 0.1331 mmol), tris(dibenzylideneacetone)dipalladium(0) (2.4 mg, 0.0027 mmol) and tri(o-tolyl)phosphine (3.2 mg, 0.0106 mmol) were added to an oven dried microwave vial equipped with a stirrer bar. The vial was purged with argon before anhydrous chlorobenzene (1.0 mL) was added. The reaction mixture was purged with argon for a further 30 min and then subjected to the following microwave-heating profile: 100 °C for 2 min, 120 °C for 2 min, 140 °C for 2 min, 160 °C for 2 min, 180 °C for 20 min, and 200 °C for 20 min. Once the reaction mixture had cooled, the crude product was precipitated in methanol, filtered through a Soxhlet thimble, and purified by Soxhlet extraction: methanol (24 h), acetone (24 h), hexane (24 h) and chloroform (12 h). The chloroform extract was concentrated under vacuum and precipitated in methanol. The resulting precipitate was isolated by filtration and dried under high vacuum, to yield the title compound as a dark solid (7.0 mg, 4%). M_n: 100 kg/mol, M_w: 240 kg/mol, Đ: 2.4. ^{1}H NMR (500 MHz, 1,1,2,2-tetrachloroethane-d_2) δ: 9.02 (2 H, s, ArH), 7.95 (2H, s, ArH), 4.26 (4 H, br, -CH_2N-), 1.86 (4 H, br, -CH_2-), 1.39 (86 H, m, -CH_2- and -CH), 0.94 (12 H, m, -CH_3-); Anal. calcd for $(C_{74}H_{110}N_2O_4Se_3)_n$: C, 66.90; H, 8.35; N, 2.11; found: C, 66.80; H, 8.27; N, 2.19.

References

1 X. Guo, A. Facchetti and T. J. Marks, *Chem. Rev.*, 2014, **114**, 8943–9021.
2 J. Zaumseil and H. Sirringhaus, *Chem. Rev.*, 2007, **107**, 1296–1323.
3 K. A. Singh, T. L. Nelson, J. A. Belot, T. M. Young, N. R. Dhumal, T. Kowalewski, R. D. McCullough, P. Nachimuthu, S. Thevuthasan and L. M. Porter, *ACS Appl. Mater. Interfaces*, 2011, **3**, 2973–2978.
4 P. Ortiz, A. Facchetti and T. J. Marks, *Chem. Rev.*, 2010, **110**, 205–239.
5 D. Khim, Y. Xu, K.-J. Baeg, M. Kang, W.-T. Park, S.-H. Lee, I.-B. Kim, J. Kim, D.-Y. Kim, C. Liu and Y.-Y. Noh, *Adv. Mater.*, 2015, **28**, 518–526.
6 J. Y. Back, H. Yu, I. Song, I. Kang, H. Ahn, T. J. Shin, S.-K. Kwon, J. H. Oh and Y.-H. Kim, *Chem. Mater.*, 2015, **27**, 1732–1739.
7 G. Kim, S. J. Kang, G. K. Dutta, Y. K. Han, T. J. Shin, Y. Y. Noh and C. Yang, *J. Am. Chem. Soc.*, 2014, **136**, 9477–9483.
8 I. Kang, H. Yun, D. S. Chung, S. Kwon and Y. Kim, *JACS*, 2013, **135**, 14896–14899.
9 H. R. Tseng, H. Phan, C. Luo, M. Wang, L. A. Perez, S. N. Patel, L. Ying, E. J. Kramer, T. Q. Nguyen, G. C. Bazan and A. J. Heeger, *Adv. Mater.*, 2014, **26**, 2993–2998.
10 B. Sun, W. Hong, Z. Yan, H. Aziz and Y. Li, *Adv. Mater.*, 2014, **26**, 2636–2642.
11 Y. Zhao, Y. Guo and Y. Liu, *Adv. Mater.*, 2013, **25**, 5372–5391.
12 B. A. Jones, A. Facchetti, M. R. Wasielewski and T. J. Marks, *J. Am. Chem. Soc.*, 2007, **129**, 15259–15278.
13 W. Chengliang, D. Huanli, H. Wenping, L. Yunqi and D. Zhu, *Chem. Rev.*, 2012, **112**, 2208–2267.
14 J. Mei and Z. Bao, *Chem. Mater.*, 2014, **26**, 604–615.
15 W. Y. Lee, G. Giri, Y. Diao, C. J. Tassone, J. R. Matthews, M. L. Sorensen, S. C. B. Mannsfeld, W. C. Chen, H. H. Fong, J. B. H. Tok, M. F. Toney, M. He and Z. Bao, *Adv. Funct. Mater.*, 2014, **24**, 3524–3534.
16 N. Kim, S. Jang, G. Pace, M. Caironi, T. Park, D. Khim, J. Kim, D. Kim and Y. Noh, *Chem. Mater.*, 2015, **27**, 8345–8353.
17 Y. Yuan, G. Giri, A. L. Ayzner, A. P. Zoombelt, S. C. B. Mannsfeld, J. Chen, D. Nordlund, M. F. Toney, J. Huang and Z. Bao, *Nat. Commun.*, 2014, **5**, 3005.
18 T. Vangerven, P. Verstappen, J. Drijkoningen, W. Dierck, S. Himmelberger, A. Salleo, D. Vanderzande, W. Maes and J. V. Manca, *Chem. Mater.*, 2015, **27**, 3726–3732.
19 R. J. Kline, M. D. McGehee, E. N. Kadnikova, J. Liu, J. M. J. Fréchet and M. F. Toney, *Macromolecules*, 2005, **38**, 3312–3319.
20 M. Tong, S. Cho, J. T. Rogers, K. Schmidt, B. B. Y. Hsu, D. Moses, R. C. Coffin, E. J. Kramer, G. C. Bazan and A. J. Heeger, *Adv. Funct. Mater.*, 2010, **20**, 3959–3965.
21 J. Kuwabara, T. Yasuda, S. J. Choi, W. Lu, K. Yamazaki, S. Kagaya, L. Han and T. Kanbara, *Adv. Funct. Mater.*, 2014, **24**, 3226–3233.
22 S. Broll, F. Nübling, A. Luzio, D. Lentzas, H. Komber, M. Caironi and M. Sommer, *Macromolecules*, 2015, **48**, 7481–7488.
23 U. Koldemir, S. R. Puniredd, M. Wagner, S. Tongay, T. D. McCarley, G. D. Kamenov, K. Müllen, W. Pisula and J. R. Reynolds, *Macromolecules*, 2015, **48**, 6369–6377.
24 A. Salleo, *Mater. Today*, 2007, **10**, 38–45.
25 L. Dou, J. You, Z. Hong, Z. Xu, G. Li, R. A. Street and Y. Yang, *Adv. Mater.*, 2013, **25**, 6642–6671.
26 C. W. Tang, *Appl. Phys. Lett.*, 1986, **48**, 183–185.
27 T. Ameri, N. Li and C. J. Brabec, *Energy Environ. Sci.*, 2013, **6**, 2390–2413.
28 A. F. Eftaiha, J.-P. Sun, I. G. Hill and G. C. Welch, *J. Mater. Chem. A*, 2014, **2**, 1201–1213.
29 A. Facchetti, *Mater. Today*, 2013, **16**, 123–132.
30 L. Lu, M. A. Kelly, W. You and L. Yu, *Nat. Photonics*, 2015, **9**, 491–500.
31 Q. An, F. Zhang, J. Zhang, W. Tang, Z. Deng and B. Hu, *Energy Environ. Sci.*, 2016, **9**, 281–322.
32 T. M. Clarke and J. R. Durrant, *Chem. Rev.*, 2010, **110**, 6736–6767.
33 A. J. Heeger, *Adv. Mater.*, 2014, **26**, 10–28.
34 A. Facchetti, *Chem. Mater.*, 2011, **23**, 733–758.

35 Y. Liu, J. Zhao, Z. Li, C. Mu, W. Ma, H. Hu, K. Jiang and H. Lin, *Nat. Commun.*, 2014, **5**, 5293.
36 Z. He, B. Xiao, F. Liu, H. Wu, Y. Yang, S. Xiao, C. Wang, T. P. Russell and Y. Cao, *Nat. Photonics*, 2015, **9**, 174–179.
37 H. Choi, S. Ko, T. Kim, P.-O. Morin, B. Walker, B. H. Lee, M. Leclerc, J. Y. Kim and A. J. Heeger, *Adv. Mater.*, 2015, **27**, 3318–3324.
38 C. C. Chen, W. H. Chang, K. Yoshimura, K. Ohya, J. You, J. Gao, Z. Hong and Y. Yang, *Adv. Mater.*, 2014, **26**, 5670–5677.
39 S.-H. Liao, H.-J. Jhuo, P.-N. Yeh, Y.-S. Cheng, Y.-L. Li, Y.-H. Lee, S. Sharma and S.-A. Chen, *Sci. Rep.*, 2014, **4**, 6813.
40 C. J. Brabec, M. Heeney, I. McCulloch and J. Nelson, *Chem. Soc. Rev.*, 2011, **40**, 1185–1199.
41 G. Yu, J. Gao, J. C. Hummelen, F. Wudl and A. J. Heeger, *Science (80-.).*, 1995, **270**, 1789–1791.
42 J. J. M. Halls, C. A. Walsh, N. C. Greenham, E. A. Marseglia, R. H. Friend, S. C. Moratti and A. B. Holmes, *Nature*, 1995, 376, 498–500.
43 J. W. Rumer and I. McCulloch, *Mater. Today*, 2015, **18**, 425–435.
44 H. C. Liao, C. C. Ho, C. Y. Chang, M. H. Jao, S. B. Darling and W. F. Su, *Mater. Today*, 2013, **16**, 326–336.
45 J. Peet, J. Y. Kim, N. E. Coates, W. L. Ma, D. Moses, A. J. Heeger and G. C. Bazan, *Nat. Mater.*, 2007, **6**, 497–500.
46 R. Noriega, J. Rivnay, K. Vandewal, F. P. V Koch, N. Stingelin, P. Smith, M. F. Toney and A. Salleo, *Nat. Mater.*, 2013, **12**, 1038–1044.
47 J. K. Lee, W. L. Ma, C. J. Brabec, J. Yuen, J. S. Moon, J. Y. Kim, K. Lee, G. C. Bazan and A. J. Heeger, *J. Am. Chem. Soc.*, 2008, **130**, 3619–23.
48 Z. Fei, J. S. Kim, J. Smith, E. B. Domingo, T. D. Anthopoulos, N. Stingelin, S. E. Watkins, J.-S. Kim and M. Heeney, *J. Mater. Chem.*, 2011, **21**, 16257–16263.
49 J. Shaw, H. Zhong, C. P. Yau, A. Casey, E. Buchaca-domingo, N. Stingelin, D. Sparrowe, W. Mitchell and M. Heeney, *Macromolecules*, 2014, **47**, 8602–8610.
50 A. Knall, R. S. Ashraf, M. Nikolka, C. B. Nielsen, B. Purushothaman, A. Sadhanala, M. Hurhangee, K. Broch, D. J. Harkin, J. Novák, M. Neophytou, P. Hayoz, H. Sirringhaus and I. McCulloch, *Adv. Funct. Mater.*, 2016, **26**, 6961–6969.
51 W. Zhang, Y. Han, X. Zhu, Z. Fei, Y. Feng, N. D. Treat, H. Faber, N. Stingelin, I. McCulloch, T. D. Anthopoulos and M. Heeney, *Adv. Mater.*, 2016, **28**, 3922–3927.
52 L. Biniek, B. C. Schroeder, J. E. Donaghey, N. Yaacobi-Gross, R. S. Ashraf, Y. W. Soon, C. B. Nielsen, J. R. Durrant, T. D. Anthopoulos and I. McCulloch, *Macromolecules*, 2013, **46**, 727–735.
53 Y. Li, K. Yao, H. L. Yip, F. Z. Ding, Y. X. Xu, X. Li, Y. Chen and A. K.-Y. Jen, *Adv. Funct. Mater.*, 2014, **24**, 3631–3638.
54 J.-S. Wu, Y.-Y. Lai, Y.-J. Cheng, C.-Y. Chang, C.-L. Wang and C.-S. Hsu, *Adv. Energy Mater.*, 2013, **3**, 457–465.
55 J. S. Wu, Y. J. Cheng, T. Y. Lin, C. Y. Chang, P. I. Shih and C. S. Hsu, *Adv. Funct. Mater.*, 2012, **22**, 1711–1722.
56 B. C. Schroeder, R. S. Ashraf, S. Thomas, A. J. P. White, L. Biniek, C. B. Nielsen, W. Zhang, Z. Huang, P. S. Tuladhar, S. E. Watkins, T. D. Anthopoulos, J. R. Durrant and I. McCulloch, *Chem. Commun.*, 2012, **48**, 7699–7701.
57 Y. J. Cheng, C. H. Chen, T. Y. Lin and C. S. Hsu, *Chem. Asian J.*, 2012, **7**, 818–825.
58 Y. L. Chen, C. Y. Chang, Y. J. Cheng and C. S. Hsu, *Chem. Mater.*, 2012, **24**, 3964–3971.
59 Y. J. Cheng, C. H. Chen, Y. S. Lin, C. Y. Chang and C. S. Hsu, *Chem. Mater.*, 2011, **23**, 5068–5075.
60 H. Bronstein, R. S. Ashraf, Y. Kim, A. J. P. White, T. Anthopoulos, K. Song, D. James, W. Zhang and I. McCulloch, *Macromol. Rapid Commun.*, 2011, **32**, 1664–1668.
61 M. He, W. Li, Y. Gao, H. Tian, J. Zhang, H. Tong, D. Yan, Y. Geng and F. Wang, *Macromolecules*, 2016, **49**, 825–832.
62 J.-S. Wu, Y.-J. Cheng, M. Dubosc, C.-H. Hsieh, C.-Y. Chang and C.-S. Hsu, *Chem. Commun.*, 2010, **46**, 3259–3261.

63 B. C. Schroeder, M. Kirkus, C. B. Nielsen, R. S. Ashraf and I. McCulloch, *Macromolecules*, 2015, **48**, 5557–5562.
64 L. Qian, J. Cao and L. Ding, *J. Mater. Chem. A*, 2015, **3**, 24211–24214.
65 T. Wang, H. Wang, G. Li, M. Li, Z. Bo and Y. Chen, *Macromolecules*, 2016, **49**, 4088–4094.
66 H. H. Chang, C. E. Tsai, Y. Y. Lai, D. Y. Chiou, S. L. Hsu, C. S. Hsu and Y. J. Cheng, *Macromolecules*, 2012, **45**, 9282–9291.
67 H. Zhong, Y. Han, J. Shaw, T. D. Anthopoulos and M. Heeney, *Macromolecules*, 2015, **48**, 5605–5613.
68 J.-S. Wu, S.-W. Cheng, Y.-J. Cheng and C.-S. Hsu, *Chem. Soc. Rev.*, 2015, **44**, 1113–1154.
69 Y. Zhang, J. Zou, H. Yip, K.-S. Chen, D. F. Zeigler, Y. Sun and A. K.-Y. Jen, *Chem. Mater.*, 2011, **23**, 2289–2291.
70 Y. X. Xu, C. C. Chueh, H. L. Yip, F. Z. Ding, Y. X. Li, C. Z. Li, X. Li, W. C. Chen and A. K.-Y. Jen, *Adv. Mater.*, 2012, **24**, 6356–6361.
71 J. E. Donaghey, R. S. Ashraf, Y. Kim, Z. G. Huang, C. B. Nielsen, W. Zhang, B. Schroeder, C. R. G. Grenier, C. T. Brown, P. D'Angelo, J. Smith, S. Watkins, K. Song, T. D. Anthopoulos, J. R. Durrant, C. K. Williams and I. McCulloch, *J. Mater. Chem.*, 2011, **21**, 18744–18752.
72 J. J. Intemann, K. Yao, Y. X. Li, H. L. Yip, Y. X. Xu, P. W. Liang, C. C. Chueh, F. Z. Ding, X. Yang, X. Li, Y. Chen and A. K. Y. Jen, *Adv. Funct. Mater.*, 2014, **24**, 1465–1473.
73 X. Zhang, H. Bronstein, A. J. Kronemeijer, J. Smith, Y. Kim, R. J. Kline, L. J. Richter, T. D. Anthopoulos, H. Sirringhaus, K. Song, M. Heeney, W. Zhang, I. McCulloch and D. M. DeLongchamp, *Nat. Commun.*, 2013, **4**, 2238.
74 W. Zhang, J. Smith, S. E. Watkins, R. Gysel, M. McGehee, A. Salleo, J. Kirkpatrick, S. Ashraf, T. Anthopoulos, M. Heeney and I. McCulloch, *J. Am. Chem. Soc.*, 2010, **132**, 11437–11439.
75 X. Xu, P. Cai, Y. Lu, N. S. Choon, J. Chen, B. S. Ong and X. Hu, *Macromol. Rapid Commun.*, 2013, **34**, 681–688.
76 H. Zheng, J. Wang, W. Chen, C. Gu, J. Ren, M. Qiu, R. Yang and M. Sun, *J. Mater. Chem. C*, 2016, **4**, 6280–6286.
77 I. McCulloch, R. S. Ashraf, L. Biniek, H. Bronstein, C. Combe, J. E. Donaghey, D. I. James, C. B. Nielsen, B. C. Schroeder and W. Zhang, *Acc. Chem. Res.*, 2012, **45**, 714–722.
78 W. Gao, T. Liu, M. Hao, K. Wu, C. Zhang, Y. Sun and C. Yang, *Chem. Sci.*, 2016, **7**, 6167–6175.
79 Y.-X. Xu, C.-C. Chueh, H.-L. Yip, C.-Y. Chang, P.-W. Liang, J. J. Intemann, W.-C. Chen and A. K.-Y. Jen, *Polym. Chem.*, 2013, **4**, 5220–5223.
80 J. Y. Wang, S. K. Hau, H. L. Yip, J. A. Davies, K. S. Chen, Y. Zhang, Y. Sun and A. K.-Y. Jen, *Chem. Mater.*, 2011, **23**, 765–767.
81 Q. Zheng, B. J. Jung, J. Sun and H. E. Katz, *J. Am. Chem. Soc.*, 2010, **132**, 5394–5404.
82 J. Lu, F. Liang, N. Drolet, J. Ding, Y. Tao and R. Movileanu, *Chem. Commun.*, 2008, 5315–5317.
83 G. L. Gibson and D. S. Seferos, *Macromol. Chem. Phys.*, 2014, **215**, 811–823.
84 R. S. Ashraf, Z. Chen, D. S. Leem, H. Bronstein, W. Zhang, B. Schroeder, Y. Geerts, J. Smith, S. Watkins, T. D. Anthopoulos, H. Sirringhaus, J. C. De Mello, M. Heeney and I. McCulloch, *Chem. Mater.*, 2011, **23**, 768–770.
85 M. C. Scharber, M. Koppe, J. Gao, F. Cordella, M. A. Loi, P. Denk, M. Morana, H. J. Egelhaaf, K. Forberich, G. Dennler, R. Gaudiana, D. Waller, Z. Zhu, X. Shi and C. J. Brabec, *Adv. Mater.*, 2010, **22**, 367–370.
86 H. Y. Chen, J. Hou, A. E. Hayden, H. Yang, K. N. Houk and Y. Yang, *Adv. Mater.*, 2010, **22**, 371–375.
87 Z. Fei, R. S. Ashraf, Z. Huang, J. Smith, R. J. Kline, P. D'Angelo, T. D. Anthopoulos, J. R. Durrant, I. McCulloch and M. Heeney, *Chem. Commun.*, 2012, **48**, 2955–2957.
88 C. M. Amb, S. Chen, K. R. Graham, J. Subbiah, C. E. Small, F. So and J. R. Reynolds, *J. Am. Chem. Soc*, 2011, **133**, 10062–10065.
89 J. S. Kim, Z. Fei, S. Wood, D. T. James, M. Sim, K. Cho, M. J. Heeney and J.-S. Kim, *Adv. Energy Mater.*, 2014, **4**, 1400527.
90 S. Yamaguchi and K. Tamao, *J. Chem. Soc., Dalt. Trans.*, 1998, 3693–3702.

91 H. H. Chang, C. E. Tsai, Y. Y. Lai, W. W. Liang, S. L. Hsu, C. S. Hsu and Y. J. Cheng, *Macromolecules*, 2013, **46**, 7715–7726.
92 D. Dang, W. Chen, S. Himmelberger, Q. Tao, A. Lundin, R. Yang, W. Zhu, A. Salleo, C. Müller and E. Wang, *Adv. Energy Mater.*, 2014, **4**, 1400680.
93 H. Bronstein, D. S. Leem, R. Hamilton, P. Woebkenberg, S. King, W. Zhang, R. S. Ashraf, M. Heeney, T. D. Anthopoulos, J. De Mello and I. McCulloch, *Macromolecules*, 2011, **44**, 6649–6652.
94 T. Lei, J. Y. Wang and J. Pei, *Chem. Mater.*, 2014, **26**, 594–603.
95 H. Zhong, Z. Li, F. Deledalle, E. C. Fregoso, M. Shahid, Z. Fei, C. B. Nielsen, N. Yaacobi-Gross, S. Rossbauer, T. D. Anthopoulos, J. R. Durrant and M. Heeney, *J. Am. Chem. Soc.*, 2013, **135**, 2040–2043.
96 H. Zhong, Z. Li, E. Buchaca-Domingo, S. Rossbauer, S. E. Watkins, N. Stingelin, T. D. Anthopoulos and M. Heeney, *J. Mater. Chem. A*, 2013, **1**, 14973–14981.
97 S. Tierney, M. Heeney and I. McCulloch, *Synth. Met.*, 2005, **148**, 195–198.
98 B. S. Nehls, U. Asawapirom, S. Füldner, E. Preis, T. Farrell and U. Scherf, *Adv. Funct. Mater.*, 2004, **14**, 352–356.
99 D. Milstein and J. K. Stille, *J. Am. Chem. Soc.*, 1978, **100**, 3636–3638.
100 N. Miyaura, K. Yamada and A. Suzuki, *Tetrahedron Lett.*, 1979, **20**, 3437–3440.
101 F. C. Krebs, R. B. Nyberg and M. Jorgensen, *Chem. Mater.*, 2004, **16**, 1313–1318.
102 K. T. Nielsen, K. Bechgaard and F. C. Krebs, *Macromolecules*, 2005, **38**, 658–659.
103 K. H. Hendriks, G. H. L. Heintges, V. S. Gevaerts, M. M. Wienk and R. A. J. Janssen, *Angew. Chem., Int. Ed.*, 2013, **52**, 8341–8344.
104 J.-L. Bredas, *Mater. Horiz.*, 2014, **1**, 17–19.
105 A. D. Becke, *J. Chem. Phys.*, 1993, **98**, 5648–5652.
106 C. Risko, M. D. McGehee and J.-L. Brédas, *Chem. Sci.*, 2011, **2**, 1200–1218.
107 S. M. Parke, M. P. Boone and E. Rivard, *Chem Comm.*, 2016, **52**, 9485–505.
108 H. Zhang, H. Yao, W. Zhao, L. Ye and J. Hou, *Adv. Energy Mater.*, 2016, **6**, 1502177.
109 R. Po, A. Bernardi, A. Calabrese, C. Carbonera, G. Corso and A. Pellegrino, *Energy Environ. Sci.*, 2014, **7**, 925–943.
110 C.-C. Chueh, K. Yao, H.-L. Yip, C.-Y. Chang, Y.-X. Xu, K.-S. Chen, C.-Z. Li, P. Liu, F. Huang, Y. Chen, W.-C. Chen and A. K.-Y. Jen, *Energy Environ. Sci.*, 2013, **6**, 3241–3248.
111 J. A. Letizia, M. R. Salata, C. M. Tribout, A. Facchetti, M. A. Ratner and T. J. Marks, *J. Am. Chem. Soc.*, 2008, **130**, 9679–9694.
112 X. Guo, R. P. Ortiz, Y. Zheng, Y. Hu, Y. Noh, K. Baeg, A. Facchetti and T. J. Marks, *J. Am. Chem. Soc.*, 2011, **133**, 1405–1418.
113 N. Zhou, X. Guo, R. P. Ortiz, S. Li, S. Zhang, R. P. H. Chang, A. Facchetti and T. J. Marks, *Adv. Mater.*, 2012, **24**, 2242–2248.
114 X. Guo, N. Zhou, S. J. Lou, J. W. Hennek, R. Ponce Ortiz, M. R. Butler, P. L. T. Boudreault, J. Strzalka, P. O. Morin, M. Leclerc, J. T. López Navarrete, M. a. Ratner, L. X. Chen, R. P. H. Chang, A. Facchetti and T. J. Marks, *J. Am. Chem. Soc.*, 2012, **134**, 18427–18439.
115 X. Guo, N. Zhou, S. J. Lou, J. Smith, D. B. Tice, J. W. Hennek, S. Li, J. Strzalka, L. X. Chen, P. Ortiz and J. T. Lo, *Nat. Photonics*, 2013, **7**, 825–833.
116 G. Li, B. Zhao, C. Kang, Z. Lu, C. Li, H. Dong, W. Hu, H. Wu and Z. Bo, *ACS Appl. Mater. Interfaces*, 2015, **7**, 10710–10717.
117 L. Huo, J. Hou, S. Zhang, H. Y. Chen and Y. Yang, *Angew. Chem., Int. Ed.*, 2010, **49**, 1500–1503.
118 M. Zhang, Y. Gu, X. Guo, F. Liu, S. Zhang, L. Huo, T. P. Russell and J. Hou, *Adv. Mater.*, 2013, **25**, 4944–4949.
119 Z. He, C. Zhong, S. Su, M. Xu, H. Wu, Y. Cao, A. K. K. A. Kyaw, D. D. H. Wang, V. Gupta, J. Zhang, S. Chand, G. C. Bazan and A. J. Heeger, *Nat. Photonics*, 2013, **25**, 593–597.
120 H. Pan, Y. Li, Y. Wu, P. Liu, B. S. Ong, S. Zhu and G. Xu, *J. Am. Chem. Soc.*, 2007, **129**, 4112–4113.
121 L. Huo, S. Zhang, X. Guo, F. Xu, Y. Li and J. Hou, *Angew. Chem., Int. Ed.*, 2011, **50**, 9697–9702.

122 M. Wang, X. Hu, P. Liu, W. Li, X. Gong, F. Huang and Y. Cao, *J. Am. Chem. Soc.*, 2011, **133**, 9638–9641.
123 S. H. Liao, H. J. Jhuo, Y. S. Cheng and S. A. Chen, *Adv. Mater.*, 2013, **25**, 4766–4771.
124 C. M. Hansen, *Hansen Solubility Parameters: A User's Handbook*, CRC Press: Boca Raton, FL, 2nd ed., 2007.
125 C. Duan, F. Huang and Y. Cao, *Polym. Chem.*, 2015, **6**, 8081–8098.
126 P. Liu, S. Dong, F. Liu, X. Hu, L. Liu, Y. Jin, S. Liu, X. Gong, T. P. Russell, F. Huang and Y. Cao, *Adv. Funct. Mater.*, 2015, **25**, 6458–6469.
127 D. He, L. Qian and L. Ding, *Polym. Chem.*, 2016, **7**, 2329–2332.
128 J. M. Szarko, J. Guo, Y. Liang, B. Lee, B. S. Rolczynski, J. Strzalka, T. Xu, S. Loser, T. J. Marks, L. Yu and L. X. Chen, *Adv. Mater.*, 2010, **22**, 5468–5472.
129 A. T. Yiu, P. M. Beaujuge, O. P. Lee, C. H. Woo, M. F. Toney, J. M. J. Frechet and A. T. Yiu, *J. Am. Chem. Soc.*, 2011, **134**, 2180–2185.
130 C. Piliego, T. W. Holcombe, J. D. Douglas, C. H. Woo, P. M. Beaujuge and J. M. J. Frechet, *J. Am. Chem. Soc.*, 2010, **132**, 7595–7597.
131 L. Biniek, S. Fall, C. L. Chochos, D. V. Anokhin, D. A. Ivanov, N. Leclerc, P. Leveque and T. Heiser, *Macromolecules*, 2010, **43**, 9779–9786.
132 Y. Liang, D. Feng, Y. Wu, S.-T. T. Tsai, G. Li, C. Ray and L. Yu, *J. Am. Chem. Soc.*, 2009, **131**, 7792–7799.
133 S. Wood, J.-H. Kim, D.-H. Hwang and J.-S. Kim, *Chem. Mater.*, 2015, **27**, 4196–4204.
134 J.-H. Kim, S. Wood, J. B. Park, J. Wade, M. Song, S. C. Yoon, I. H. Jung, J.-S. Kim and D.-H. Hwang, *Adv. Funct. Mater.*, 2016, **26**, 1517–1525.
135 T. Lei, J. H. Dou and J. Pei, *Adv. Mater.*, 2012, **24**, 6457–6461.
136 J. H. Dou, Y. Q. Zheng, T. Lei, S. D. Zhang, Z. Wang, W. Bin Zhang, J. Y. Wang and J. Pei, *Adv. Funct. Mater.*, 2014, **24**, 6270–6278.
137 J. Mei, D. H. Kim, A. L. Ayzner, M. F. Toney and Z. Bao, *J. Am. Chem. Soc.*, 2011, **133**, 20130–20133.
138 G. E. Park, J. Shin, D. H. Lee, M. J. Cho and D. H. Choi, *J. Polym. Sci. Part A Polym. Chem.*, 2015, **53**, 1226–1234.
139 J. Lee, a. R. Han, H. Yu, T. J. Shin, C. Yang and J. H. Oh, *J. Am. Chem. Soc.*, 2013, **135**, 9540–9547.
140 B. Fu, J. Baltazar, A. R. Sankar, P. H. Chu, S. Zhang, D. M. Collard and E. Reichmanis, *Adv. Funct. Mater.*, 2014, **24**, 3734–3744.
141 S. Chen, B. Sun, W. Hong, H. Aziz, Y. Meng and Y. Li, *J. Mater. Chem. C*, 2014, **2**, 2183–2190.
142 I. Meager, R. S. Ashraf, S. Mollinger, B. C. Schroeder, H. Bronstein, D. Beatrup, M. S. Vezie, T. Kirchartz, A. Salleo, J. Nelson and I. McCulloch, *J. Am. Chem. Soc.*, 2013, **135**, 11537–11540.
143 C. R. McNeill, A. Abrusci, I. Hwang, M. A. Ruderer, P. Müller-Buschbaum and N. C. Greenham, *Adv. Funct. Mater.*, 2009, **19**, 3103–3111.
144 Y.-J. Hwang, B. A. E. Courtright, A. S. Ferreira, S. H. Tolbert and S. A. Jenekhe, *Adv. Mater.*, 2015, **27**, 4578–4584.
145 E. Zhou, J. Cong, K. Hashimoto and K. Tajima, *Adv. Mater.*, 2013, **25**, 6991–6996.
146 H. Kang, K. H. Kim, J. Choi, C. Lee and B. J. Kim, *ACS Macro Lett.*, 2014, **3**, 1009–1014.
147 W. Li, W. S. C. Roelofs, M. Turbiez, M. M. Wienk and R. A. J. Janssen, *Adv. Mater.*, 2014, **26**, 3304–3309.
148 T. Earmme, Y. J. Hwang, S. Subramaniyan and S. A. Jenekhe, *Adv. Mater.*, 2014, **26**, 6080–6085.
149 N. Zhou, H. Lin, S. J. Lou, X. Yu, P. Guo, E. F. Manley, S. Loser, P. Hartnett, H. Huang, M. R. Wasielewski, L. X. Chen, R. P. H. Chang, A. Facchetti and T. J. Marks, *Adv. Energy Mater.*, 2014, **4**, 1300785.
150 C. Lee, H. Kang, W. Lee, T. Kim, K.-H. Kim, H. Y. Woo, C. Wang and B. J. Kim, *Adv. Mater.*, 2015, **27**, 2466–2471.
151 J. W. Jung, J. W. Jo, C.-C. Chueh, F. Liu, W. H. Jo, T. P. Russell and A. K.-Y. Jen, *Adv. Mater.*, 2015, **27**, 3310–3317.

152 W. Lee, C. Lee, H. Yu, D.-J. Kim, C. Wang, H. Y. Woo, J. H. Oh and B. J. Kim, *Adv. Funct. Mater.*, 2016, **26**, 1543–1553.
153 Y.-J. Hwang, T. Earmme, S. Subramaniyan and S. A. Jenekhe, *Chem. Commun.*, 2014, **50**, 10801–10804.
154 Y. Zhou, T. Kurosawa, W. Ma, Y. Guo, L. Fang, K. Vandewal, Y. Diao, C. Wang, Q. Yan, J. Reinspach, J. Mei, A. L. Appleton, G. I. Koleilat, Y. Gao, S. C. B. Mannsfeld, A. Salleo, H. Ade, D. Zhao and Z. Bao, *Adv. Mater.*, 2014, **26**, 3767–3772.
155 H. Yan, Z. Chen, Y. Zheng, C. Newman, J. R. Quinn, F. Dötz, M. Kastler and A. Facchetti, *Nature*, 2009, **457**, 679–686.
156 M. Sommer, *J. Mater. Chem. C*, 2014, **2**, 3088–3098.
157 H. Chen, Y. Guo, Z. Mao, G. Yu, J. Huang, Y. Zhao and Y. Liu, *Chem. Mater.*, 2013, **25**, 3589–3596.
158 S. G. Bucella, A. Luzio, E. Gann, L. Thomsen, C. R. McNeill, G. Pace, A. Perinot, Z. Chen, A. Facchetti and M. Caironi, *Nat. Commun.*, 2015, **6**, 8394.
159 A. Luzio, D. Fazzi, D. Natali, E. Giussani, K. J. Baeg, Z. Chen, Y. Y. Noh, A. Facchetti and M. Caironi, *Adv. Funct. Mater.*, 2014, **24**, 1151–1162.
160 Y.-J. Hwang, N. M. Murari and S. A. Jenekhe, *Polym. Chem.*, 2013, **4**, 3187–3195.
161 S. Fukuta, H.-C. Wu, T. Koganezawa, Y. Isshiki, M. Ueda, W.-C. Chen and T. Higashihara, *J. Polym. Sci. Part A Polym. Chem.*, 2015, **54**, 359–367.
162 M. Yuan, M. M. Durban, P. D. Kazarinoff, D. F. Zeigler, A. H. Rice, Y. Segawa and C. K. Luscombe, *J. Polym. Sci. Part A Polym. Chem.*, 2013, **51**, 4061–4069.
163 Z. Fei, Y. Han, J. Martin, F. H. Scholes, M. Al-Hashimi, S. Y. AlQaradawi, N. Stingelin, T. D. Anthopoulos and M. Heeney, *Macromolecules*, 2016, **49**, 6384–6393.
164 X. Guo, F. S. Kim, M. J. Seger, S. A. Jenekhe and M. D. Watson, *Chem. Mater.*, 2012, **24**, 1434–1442.
165 W. Lee, C. Lee, H. Yu, D. J. Kim, C. Wang, H. Y. Woo, J. H. Oh and B. J. Kim, *Adv. Funct. Mater.*, 2016, **26**, 1543–1553.
166 Z. Chen, Y. Zheng, H. Yan and A. Facchetti, *J. Am. Chem. Soc.*, 2009, **131**, 8–9.
167 F. Chaignon, M. Falkenström, S. Karlsson, E. Blart, F. Odobel and L. Hammarström, *Chem Comm.*, 2007, 64–66.
168 D. F. Taber and S. Kong, *J. Org. Chem.*, 1997, **62**, 8575–8576.
169 Y. H. Lee, A. Ohta, Y. Yamamoto, Y. Komatsu, K. Kato, T. Shimizu, H. Shinoda and S. Hayami, *Polyhedron*, 2011, **30**, 3001–3005.
170 C. Müller, E. Wang, L. M. Andersson, K. Tvingstedt, Y. Zhou, M. R. Andersson and O. Inganäs, *Adv. Funct. Mater.*, 2010, **20**, 2124–2131.
171 D. Spoltore, T. Vangerven, P. Verstappen, F. Piersimoni, S. Bertho, K. Vandewal, N. Van den Brande, B. Van Mele, A. De Sio, J. Parisi, L. Lutsen, D. Vanderzande, W. Maes and J. V. Manca, *Org. Electron.*, 2015, **21**, 160–170.
172 H. Kang, M. A. Uddin, C. Lee, K.-H. Kim, T. L. Nguyen, W. Lee, Y. Li, C. Wang, H. Y. Woo and B. J. Kim, *J. Am. Chem. Soc.*, 2015, **137**, 2359–2365.
173 A. Katsouras, N. Gasparini, C. Koulogiannis, M. Spanos, T. Ameri, C. J. Brabec, C. L. Chochos and A. Avgeropoulos, *Macromol. Rapid Commun.*, 2015, **36**, 1778–1797.
174 P. Schilinsky, U. Asawapirom, U. Scherf, M. Biele and C. J. Brabec, *Chem. Mater.*, 2005, **17**, 2175–2180.
175 H. K. H. Lee, Z. Li, I. Constantinou, F. So, S. W. Tsang and S. K. So, *Adv. Energy Mater.*, 2014, **4**, 1400768.
176 Z. Xiao, K. Sun, J. Subbiah, T. Qin, S. Lu, B. Purushothaman, D. J. Jones, A. B. Holmes and W. W. H. Wong, *Polym. Chem.*, 2015, **6**, 2312–2318.
177 D. Mori, H. Benten, I. Okada, H. Ohkita and S. Ito, *Energy Environ. Sci.*, 2014, **7**, 2939–2943.
178 Z. Fei, P. Boufflet, S. Wood, J. Wade, J. Moriarty, E. Gann, E. L. Ratcliff, C. R. McNeill, H. Sirringhaus, J.-S. Kim and M. Heeney, *J. Am. Chem. Soc.*, 2015, **137**, 6866–6879.
179 P. Boufflet, Y. Han, Z. Fei, N. D. Treat, R. Li, D. Smilgies, N. Stingelin, T. D. Anthopoulos and M. Heeney, *Adv. Funct. Mater*, 2015, **25**, 7038–7048.
180 T. Lei, J. H. Dou, Z. J. Ma, C. H. Yao, C. J. Liu, J. Y. Wang and J. Pei, *J. Am. Chem. Soc.*, 2012,

134, 20025–20028.
181 H. Hu, K. Jiang, J.-H. Kim, G. Yang, Z. Li, T. Ma, G. Lu, Y. Qu, H. Ade and H. Yan, *J. Mater. Chem. A*, 2016, **4**, 5039–5043.
182 J. W. Jo, J. W. Jung, H. W. Wang, P. Kim, T. P. Russell and W. H. Jo, *Chem. Mater.*, 2014, **26**, 4214–4220.
183 D. J. Crouch, P. J. Skabara, J. E. Lohr, J. J. W. McDouall, M. Heeney, I. McCulloch, D. Sparrowe, M. Shkunov, S. J. Coles, P. N. Horton and M. B. Hursthouse, *Chem. Mater.*, 2005, **17**, 6567–6578.
184 A. J. Kronemeijer, E. Gili, M. Shahid, J. Rivnay, A. Salleo, M. Heeney and H. Sirringhaus, *Adv. Mater.*, 2012, **24**, 1558–1565.
185 Y. J. Hwang, G. Ren, N. M. Murari and S. A. Jenekhe, *Macromolecules*, 2012, **45**, 9056–9062.
186 R. Kim, P. S. K. Amegadze, I. Kang, H. J. Yun, Y. Y. Noh, S. K. Kwon and Y. H. Kim, *Adv. Funct. Mater.*, 2013, **23**, 5719–5727.
187 I. Kang, T. K. An, J. A. Hong, H. J. Yun, R. Kim, D. S. Chung, C. E. Park, Y. H. Kim and S. K. Kwon, *Adv. Mater.*, 2013, **25**, 524–528.
188 M. J. Sung, A. Luzio, W.-T. Park, R. Kim, E. Gann, F. Maddalena, G. Pace, Y. Xu, D. Natali, C. de Falco, L. Dang, C. R. McNeill, M. Caironi, Y.-Y. Noh and Y.-H. Kim, *Adv. Funct. Mater.*, 2016, **26**, 4984–4997.
189 H.-J. Yun, S.-J. Kang, Y. Xu, S. O. Kim, Y.-H. Kim, Y.-Y. Noh and S.-K. Kwon, *Adv. Mater.*, 2014, **26**, 7300–7307.
190 H. Huang, N. Zhou, R. P. Ortiz, Z. Chen, S. Loser, S. Zhang, X. Guo, J. Casado, J. T. López Navarrete, X. Yu, A. Facchetti and T. J. Marks, *Adv. Funct. Mater.*, 2014, **24**, 2782–2793.
191 A. M. Echavarren and J. K. Stille, *J. Am. Chem. Soc.*, 1987, **109**, 5478–5486.
192 K. H. Hendriks, G. H. L. Heintges, V. S. Gevaerts, M. M. Wienk and R. A. J. Janssen, *Angew. Chem., Int. Ed.*, 2013, **52**, 8341–8344.
193 Z. Bao, W. K. Chan and L. Yu, *J. Am. Chem. Soc.*, 1995, **117**, 12426–12435.
194 L. S. Liebeskind and R. W. Fengl, *J. Org. Chem.*, 1990, **55**, 5359–5364.
195 V. Farina, S. Kapadia, B. Krishnan, C. Wang and L. S. Liebeskind, *J. Org. Chem.*, 1994, **59**, 5905–5911.
196 D. M. Hodgson, J. Witherington, B. A. Moloney, I. C. Richards and J.-L. Brayer, *Synlett*, 1995, **1**, 32–34.
197 M. Shahid, R. S. Ashraf, Z. Huang, A. J. Kronemeijer, T. McCarthy-Ward, I. McCulloch, J. R. Durrant, H. Sirringhaus and M. Heeney, *J. Mater. Chem.*, 2012, **22**, 12817.
198 M. A. Uddin, Y. Kim, R. Younts, W. Lee, B. Gautam, J. Choi, C. Wang, K. Gundogdu, B. J. Kim and H. Y. Woo, *Macromolecules*, 2016, **49**, 6374–6383.
199 M. Zhang, X. Guo, S. Zhang and J. Hou, *Adv. Mater.*, 2014, **26**, 1118–1123.
200 P. Homyak, Y. Liu, F. Liu, T. P. Russel and E. B. Coughlin, *Macromolecules*, 2015, **48**, 6978–6986.
201 L. Cartwright, A. Iraqi, Y. Zhang, T. Wang and D. G. Lidzey, *RSC Adv.*, 2015, **5**, 46386–46394.
202 M. Heeney, W. Zhang, D. J. Crouch, M. L. Chabinyc, S. Gordeyev, R. Hamilton, S. J. Higgins, I. McCulloch, P. J. Skabara, D. Sparrowe and S. Tierney, *Chem Comm.*, 2007, 5061–5063.
203 A. Patra and M. Bendikov, *J. Mater. Chem.*, 2010, **20**, 422–433.
204 I. Kang, T. K. An, J. A. Hong, H. J. Yun, R. Kim, D. S. Chung, C. E. Park, Y. H. Kim and S. K. Kwon, *Adv. Mater.*, 2013, **25**, 524–528.
205 S. S. Zade, N. Zamoshchik and M. Bendikov, *Chem. Eur. J.*, 2009, **15**, 8613–8624.
206 Z. Fei, R. S. Ashraf, Y. Han, S. Wang, C. P. Yau, P. S. Tuladhar, T. D. Anthopoulos, M. L. Chabinyc and M. Heeney, *J. Mater. Chem. A*, 2015, **3**, 1986–1994.
207 K. H. Park, K. H. Cheon, Y.-J. Lee, D. S. Chung, S.-K. Kwon and Y.-H. Kim, *Chem. Commun.*, 2015, **51**, 8120–8122.
208 T. Lei, Y. Cao, X. Zhou, Y. Peng, J. Bian and J. Pei, *Chem. Mater.*, 2012, **24**, 1762–1770.
209 A. A. B. Alghamdi, D. C. Watters, H. Yi, S. Al-Faifi, M. S. Almeataq, D. Coles, J. Kingsley, D. G. Lidzey and A. Iraqi, *J. Mater. Chem. A*, 2013, **1**, 5165–5171.
210 N. M. Kirby, S. T. Mudie, A. M. Hawley, D. J. Cookson, H. D. T. Mertens, N. Cowieson and V.

Samardzic-Boban, *J. Appl. Cryst.*, 2013, **46**, 1670–1680.
211 M. J. Frisch, G. W. Trucks, H. B. Schlegel, G. E. Scuseria, M. A. Robb, J. R. Cheeseman, J. A. Montgomery, Jr., T. Vreven, K. N. Kudin, J. C. Burant, J. M. Millam, S. S. Iyengar, J. Tomasi, V. Barone, B. Mennucci, M. Cossi, G. Scalmani, N. Rega, G. A. Petersson, H. Nakatsuji, M. Hada, M. Ehara, K. Toyota, R. Fukuda, J. Hasegawa, M. Ishida, T. Nakajima, Y. Honda, O. Kitao, H. Nakai, M. Klene, X. Li, J. E. Knox, H. P. Hratchian, J. B. Cross, V. Bakken, C. Adamo, J. Jaramillo, R. Gomperts, R. E. Stratmann, O. Yazyev, A. J. Austin, R. Cammi, C. Pomelli, J. W. Ochterski, P. Y. Ayala, K. Morokuma, G. A. Voth, P. Salvador, J. J. Dannenberg, V. G. Zakrzewski, S. Dapprich, A. D. Daniels, M. C. Strain, O. Farkas, D. K. Malick, A. D. Rabuck, K. Raghavachari, J. B. Foresman, J. V. Ortiz, Q. Cui, A. G. Baboul, S. Clifford, J. Cioslowski, B. B. Stefanov, G. Liu, A. Liashenko, P. Piskorz, I. Komaromi, R. L. Martin, D. J. Fox, T. Keith, M. A. Al-Laham, C. Y. Peng, A. Nanayakkara, M. Challacombe, P. M. W. Gill, B. Johnson, W. Chen, M. W. Wong, C. Gonzalez and J. A. Pople, Gaussian 03, Revision E.01, 2004.
212 M. J. Frisch, G. W. Trucks, H. B. Schlegel, G. E. Scuseria, M. A. Robb, J. R. Cheeseman, G. Scalmani, V. Barone, B. Mennucci, G. A. Petersson, H. Nakatsuji, M. Caricato, X. Li, H. P. Hratchian, A. F. Izmaylov, J. Bloino, G. Zheng, J. L. Sonnenberg, M. Hada, M. Ehara, K. Toyota, R. Fukuda, J. Hasegawa, M. Ishida, T. Nakajima, Y. Honda, O. Kitao, H. Nakai, T. Vreven, J. Montgomery, J. A., J. E. Peralta, F. Ogliaro, M. Bearpark, J. J. Heyd, E. Brothers, K. N. Kudin, V. N. Staroverov, R. Kobayashi, J. Normand, K. Raghavachari, A. Rendell, J. C. Burant, S. S. Iyengar, J. Tomasi, M. Cossi, N. Rega, J. M. Millam, M. Klene, J. E. Knox, J. B. Cross, V. Bakken, C. Adamo, J. Jaramillo, R. Gomperts, R. E. Stratmann, O. Yazyev, A. J. Austin, R. Cammi, C. Pomelli, J. W. Ochterski, R. L. Martin, K. Morokuma, V. G. Zakrzewski, G. A. Voth, P. Salvador, J. J. Dannenberg, S. Dapprich, A. D. Daniels, Ö. Farkas, J. B. Foresman, J. V. Ortiz, J. Cioslowski and D. J. Fox, Gaussian 09, Revision C.01, 2009.
213 P. Li, B. Ahrens, N. Feeder, P. R. Raithby, S. J. Teat and M. S. Khan, *Dalt. Trans.*, 2005, 874–883.
214 L. San Miguel and A. J. Matzger, *J. Org. Chem.*, 2008, **73**, 7882–7888.
215 A. E. Danks, S. R. Hall and Z. Schnepp, *Mater. Horiz.*, 2016, **3**, 91–112.
216 L. Znaidi, *Mater. Sci. Eng. B*, 2010, **174**, 18–30.
217 N. Blouin, W. Mitchell, M. Heeney and J. Shaw, *WO 2016/037678 A1*.
218 B. Zhao, C.-Z. Li, S.-Q. Liu, J. J. Richards, C.-C. Chueh, F. Ding, L. D. Pozzo, X. Li and A. K.-Y. Jen, *J. Mater. Chem. A*, 2015, **3**, 6929–6934.
219 X. Guo and M. D. Watson, *Org. Lett.*, 2008, **10**, 5333–5336.
220 T. Basel, U. Huynh, T. Zheng, T. Xu, L. Yu and Z. V. Vardeny, *Adv. Funct. Mater*, 2015, **25**, 1895–1902.
221 V. D'Innocenzo, A. Luzio, A. Petrozza, D. Fazzi and M. Caironi, *Adv. Funct. Mater.*, 2014, **24**, 5584–5593.
222 J. R. Moore, S. Albert-Seifried, A. Rao, S. Massip, B. Watts, D. J. Morgan, R. H. Friend, C. R. McNeill and H. Sirringhaus, *Adv. Energy Mater.*, 2011, **1**, 230–240.

Appendix

Appendix for Chapter 2

Sunday, 22 January 2017 02:21:40 Greenwich Mean Time

Subject: Request to Reproduce Published Paper
Date: Sunday, 22 January 2017 02:18:40 Greenwich Mean Time
From: Shaw, Jessica
To: macro@macromol.acs.org

Dear Editor-in-Chief of ACS Macromolecules: Professor Timothy P. Lodge,

I am completing my PhD thesis at Imperial College London entitled 'Ring Fused Conjugated Polymers for Use in Organic Electronics'.

I seek your permission to reprint, in my thesis, the published version of a paper I published in: *Macromolecules*, **2014**, *47*(24), pp 8602-8610, **DOI:** 10.1021/ma5021038.

I would like to include the paper in my thesis which will be added to Spiral, Imperial's institutional repository http://spiral.imperial.ac.uk/ and made available to the public under a Creative Commons Attribution-NonCommercial-NoDerivs licence.

If you are happy to grant me all the permissions requested, please return a signed copy of the letter attached. If you wish to grant only some of the permissions requested, please list these and then sign.

Yours sincerely,

Miss Jessica Shaw

Page 1 of 1

Figure A2.1. Copy of an email sent to the Editor-in-Chief of ACS Macromolecules requesting permission to reproduce own published paper. N.B. At the time of writing no reply has been received.

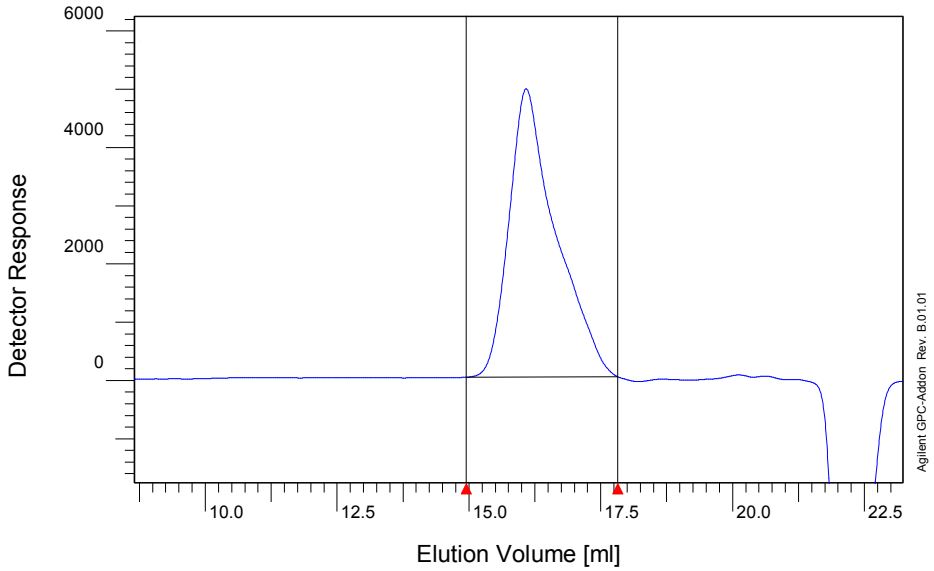

Figure A2.2. GPC trace of P1 measured in CB at 80 °C against polystyrene standards.

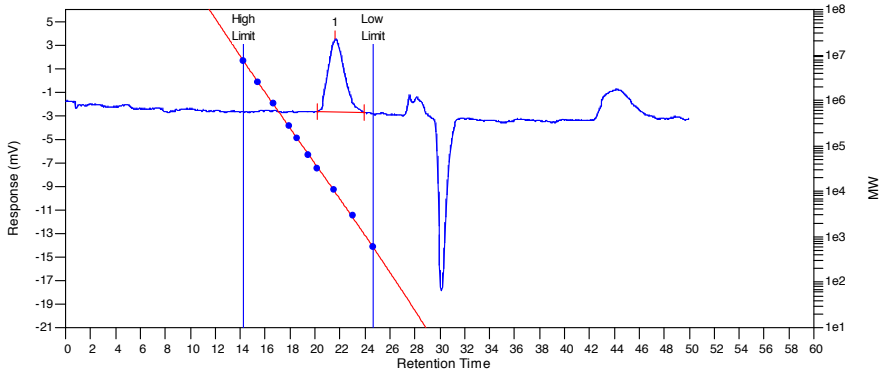

Figure A2.3. GPC trace of P2 measured in TCB at 140 °C against polystyrene standards.

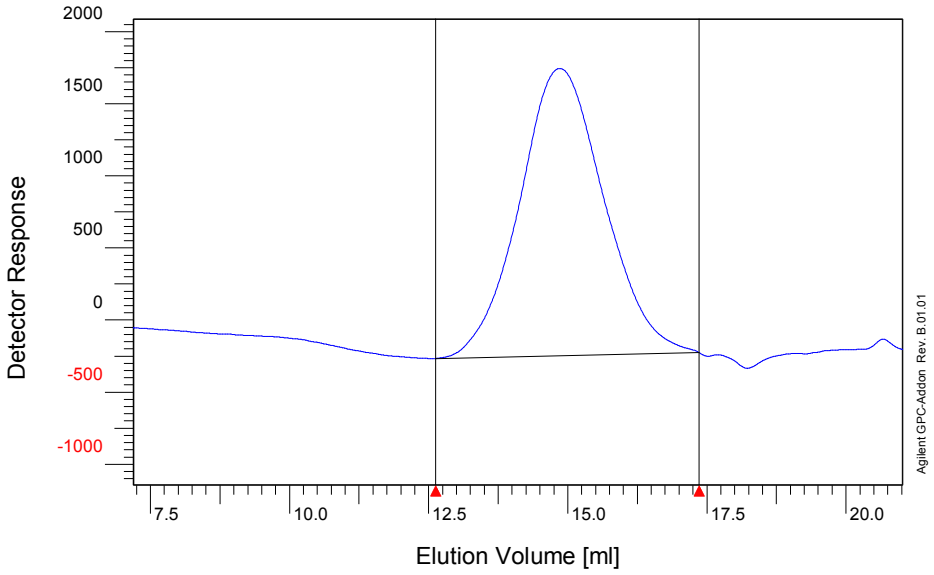

Figure A2.4. GPC trace of P3 measured in CB at 80 °C against polystyrene standards.

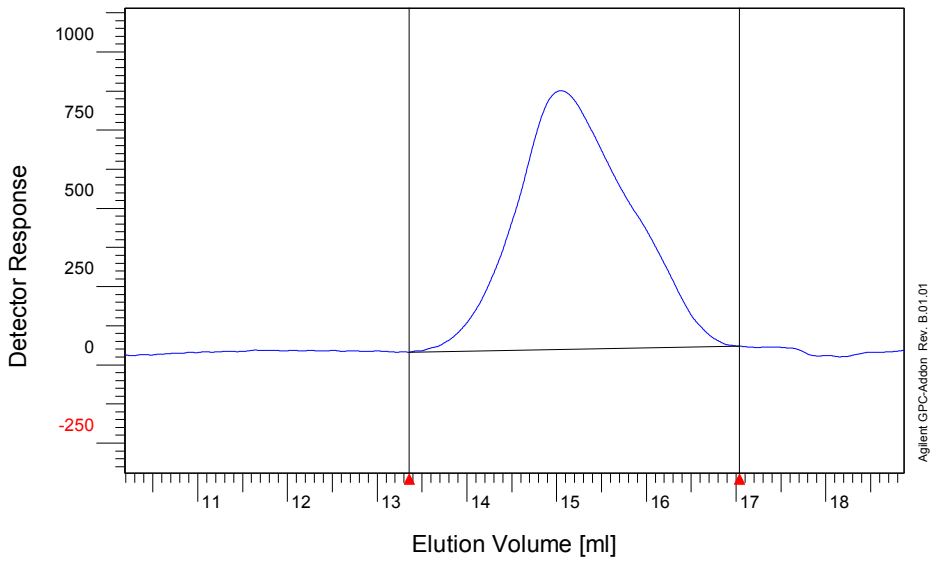

Figure A2.5. GPC trace of P4 measured in CB at 80 °C against polystyrene standards.

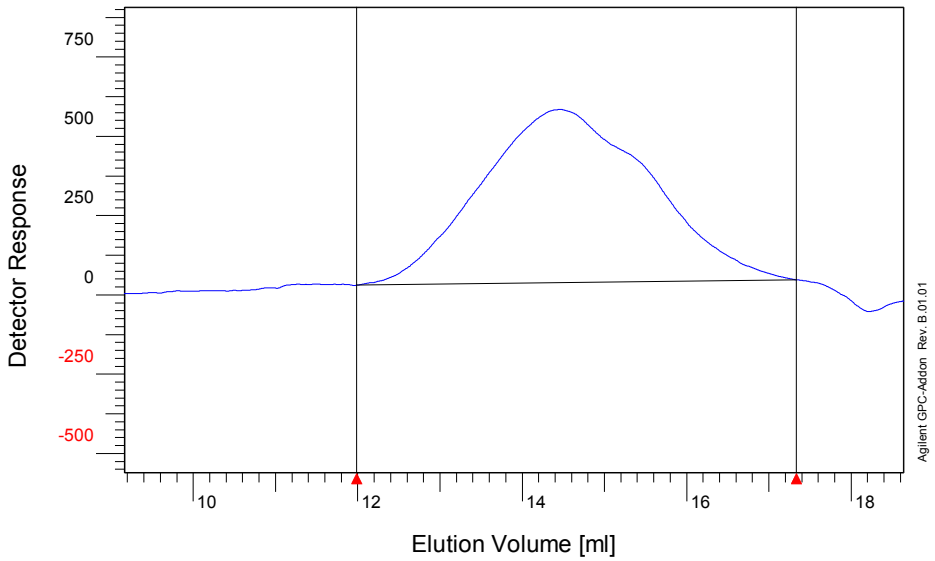

Figure A2.6. GPC trace of P5 measured in CB at 80 °C against polystyrene standards.

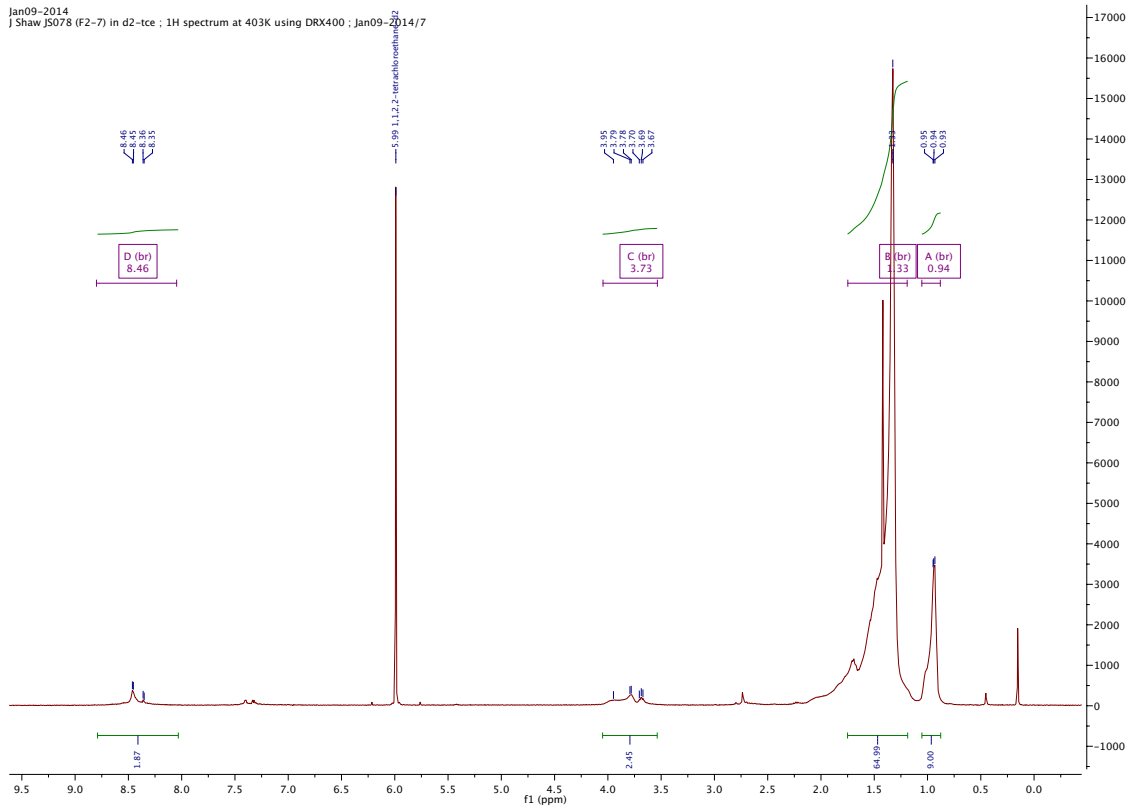

Figure A2.7. ^{1}H NMR of P1 at 130 °C in 1,1,2,2-tetrachloroethane-d_2.

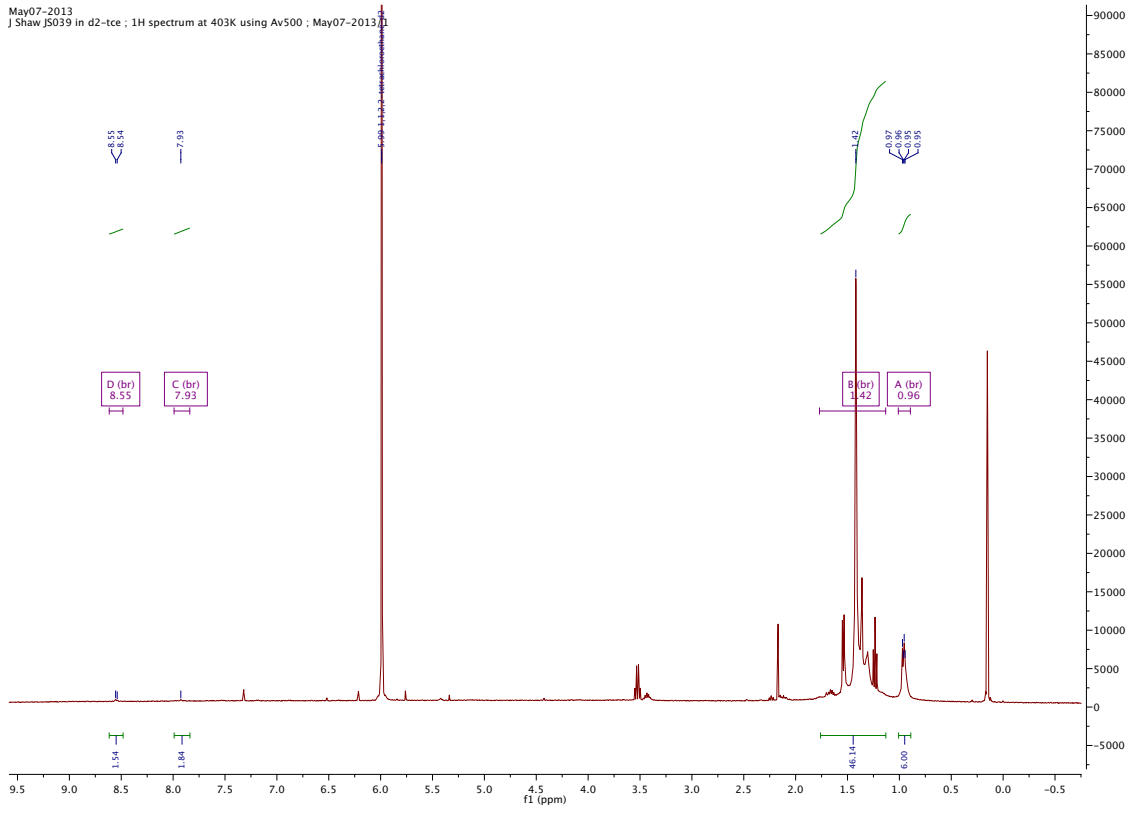

Figure A2.8. ^{1}H NMR of P2 at 130 °C in 1,1,2,2-tetrachloroethane-d_2.

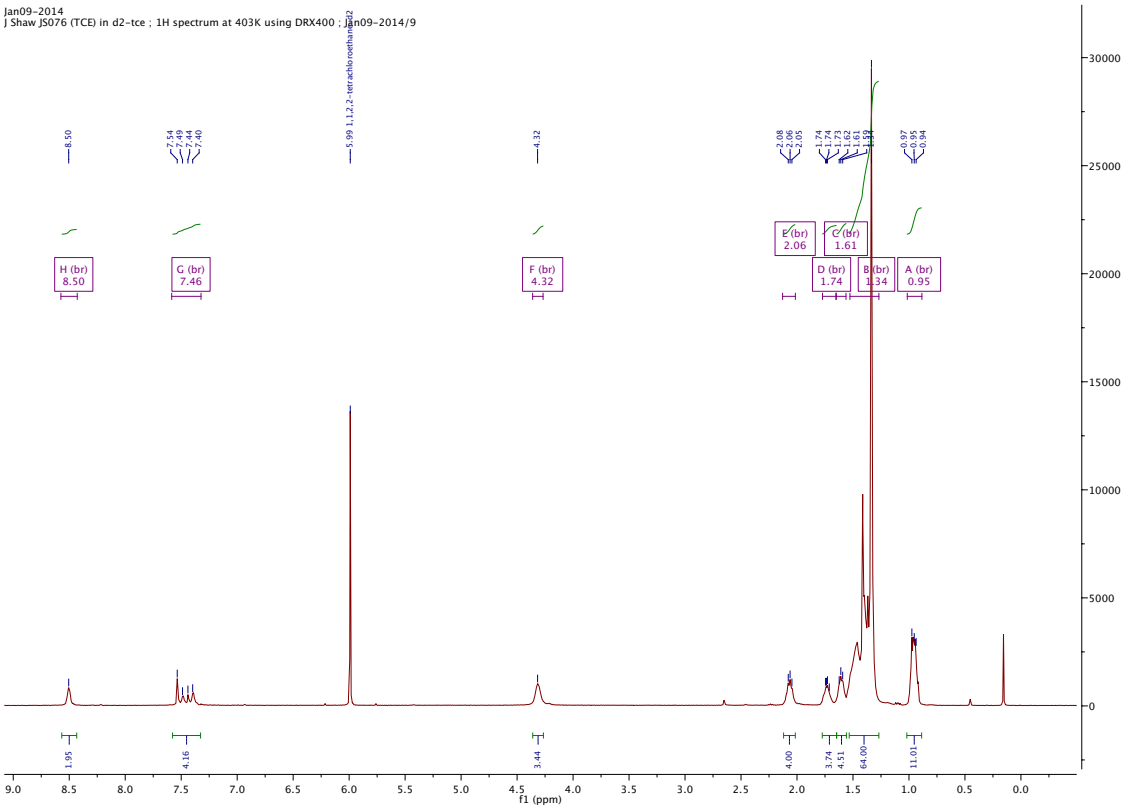

Figure A2.9. ^{1}H NMR of P3 at 130 °C in 1,1,2,2-tetrachloroethane-d_2.

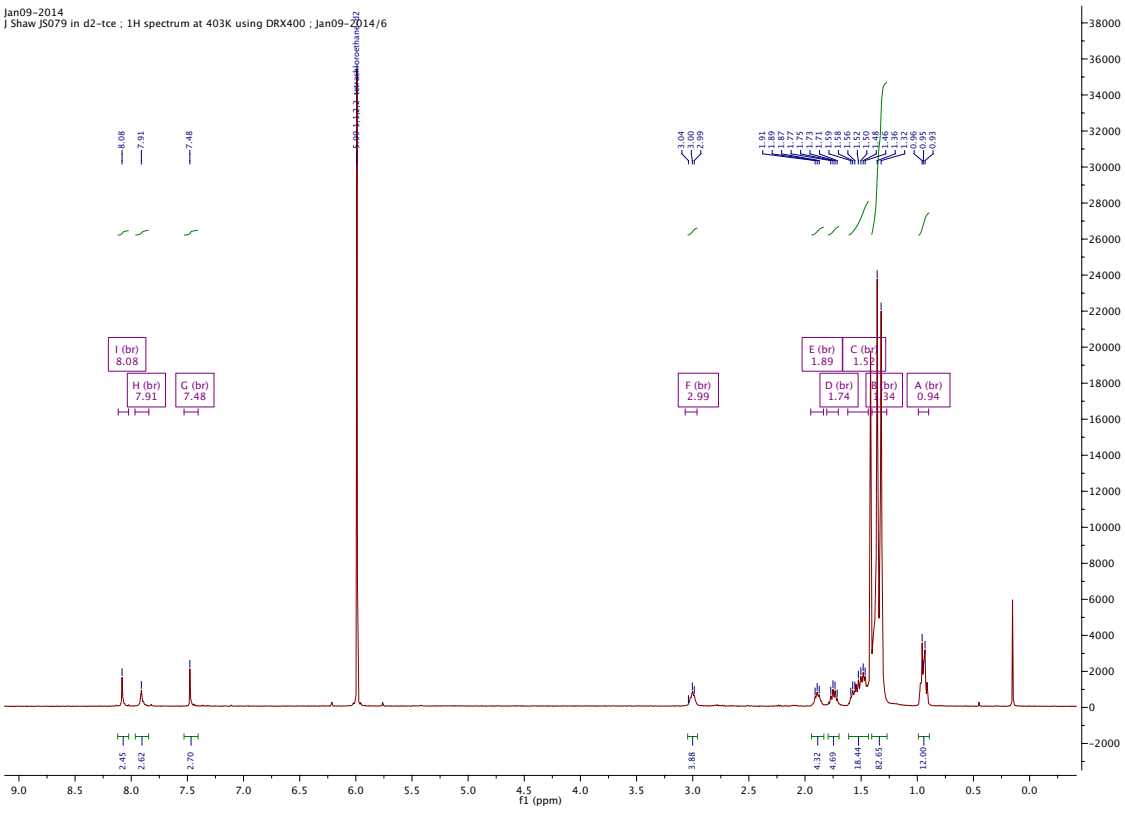

Figure A2.10. ^{1}H NMR of P4 at 130 °C in 1,1,2,2-tetrachloroethane-d_2.

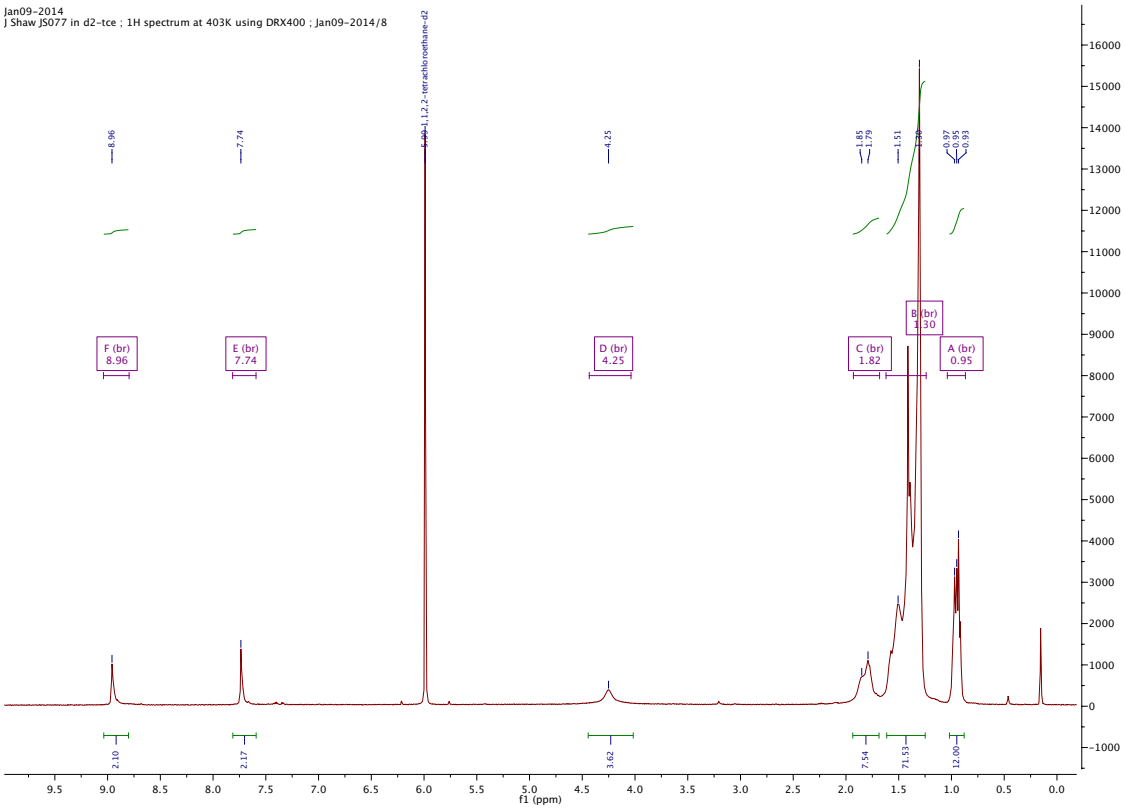

Figure A2.11. ^{1}H NMR of P5 at 130 °C in 1,1,2,2-tetrachloroethane-d_2.

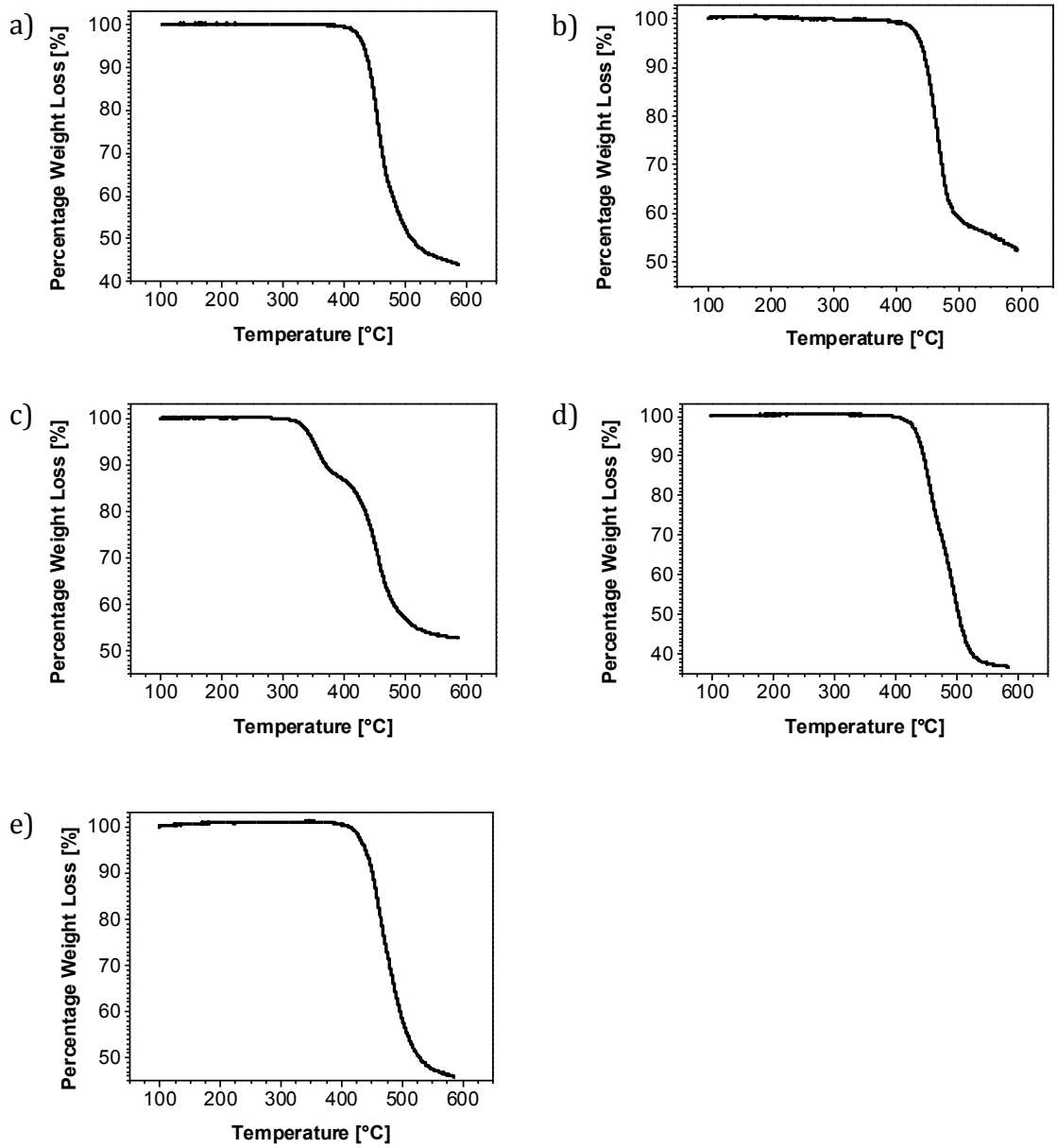

Figure A2.12. TGA thermograms of a) P1, b) P2, c) P3, d) P4, and e) P5, heating at a scan rate of 10 °C/min under a N_2 atmosphere.

Appendix for Chapter 3

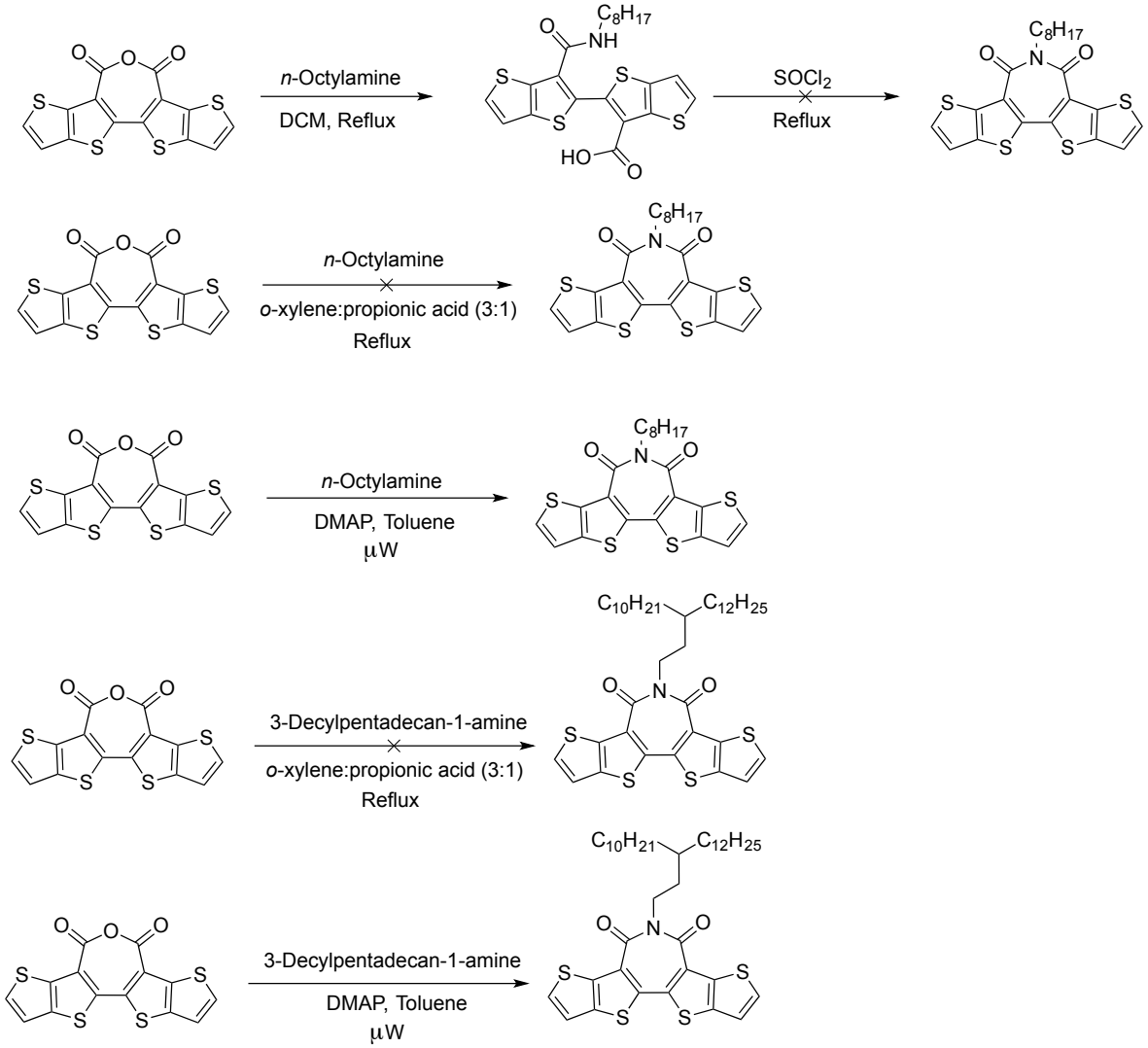

Scheme A3.1. Attempts to optimise the condensation reaction and evaluate the choice of alkyl-chain on the reaction yield.

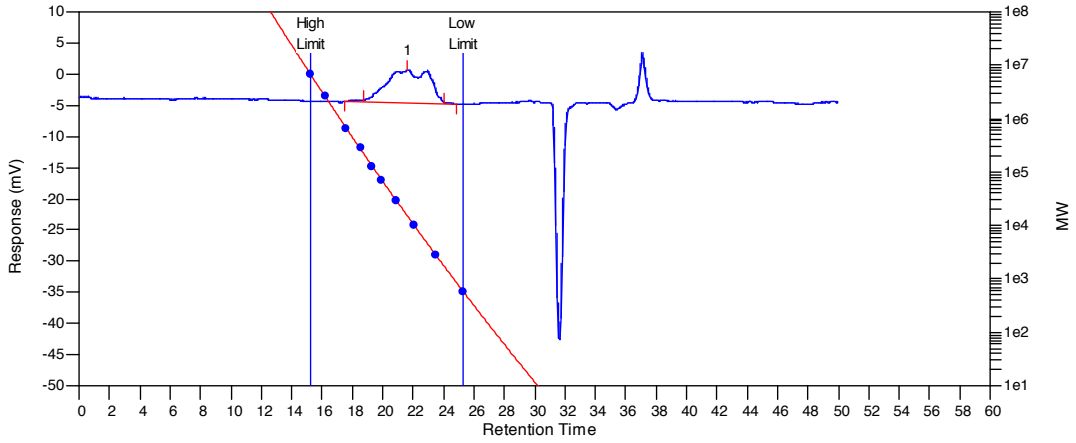

Figure A3.1. GPC trace of P6 measured in TCB at 140 °C against polystyrene standards.

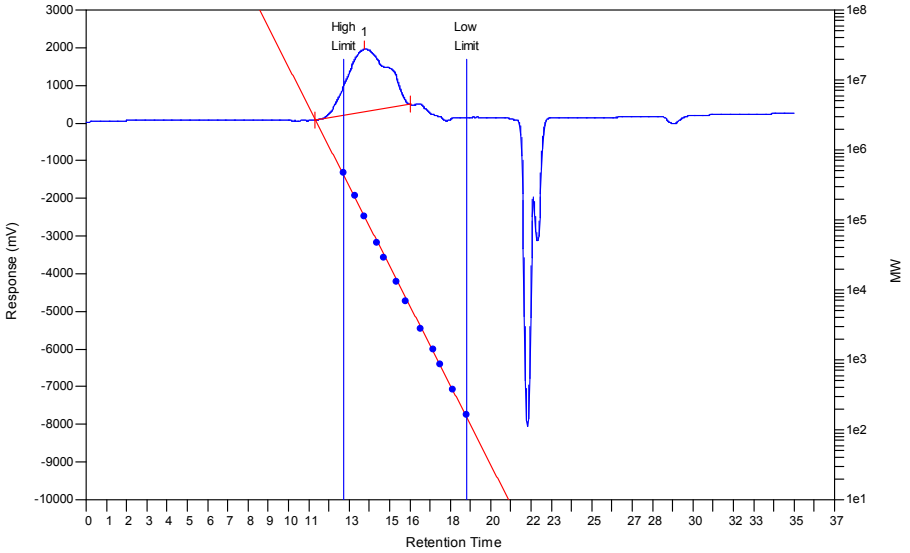

Figure A3.2. GPC trace of P7 measured in CB at 80 °C against polystyrene standards.

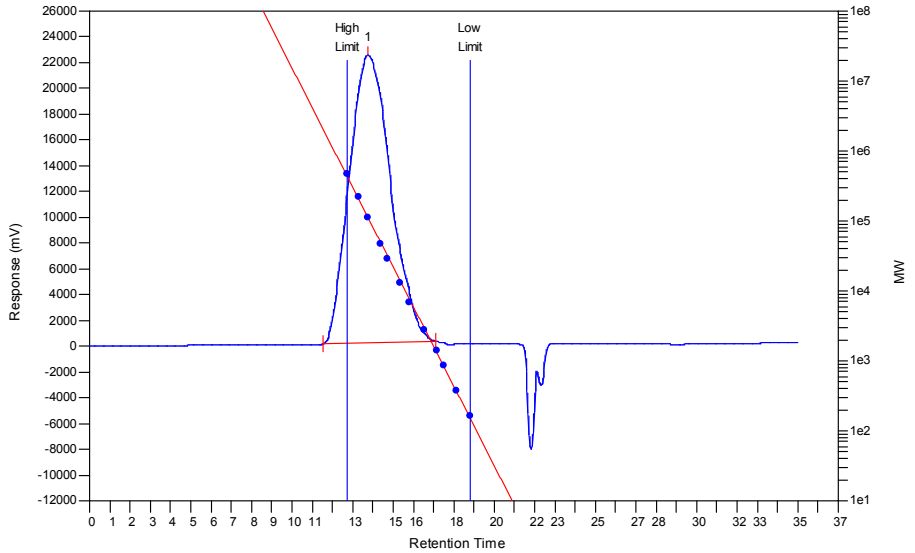

Figure A3.3. GPC trace of P8 measured in CB at 80 °C against polystyrene standards.

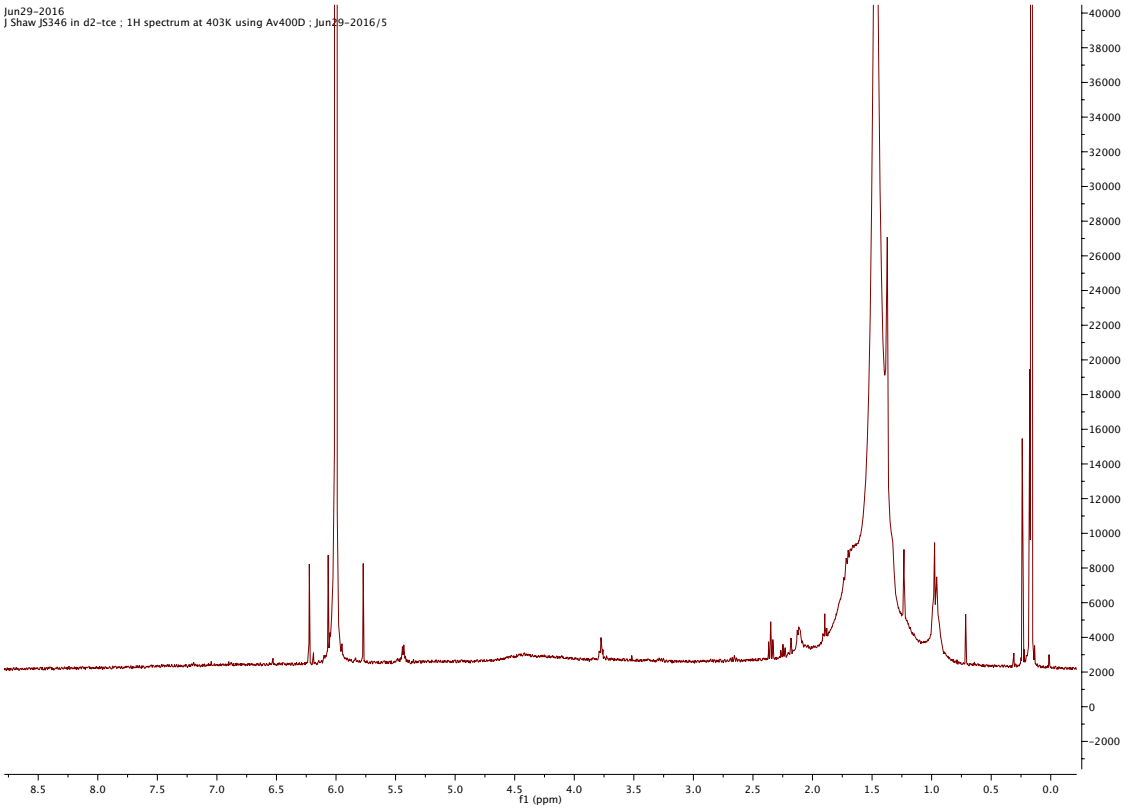

Figure A3.4. ^{1}H NMR of P6 at 130 °C in 1,1,2,2-tetrachloroethane-d_2.

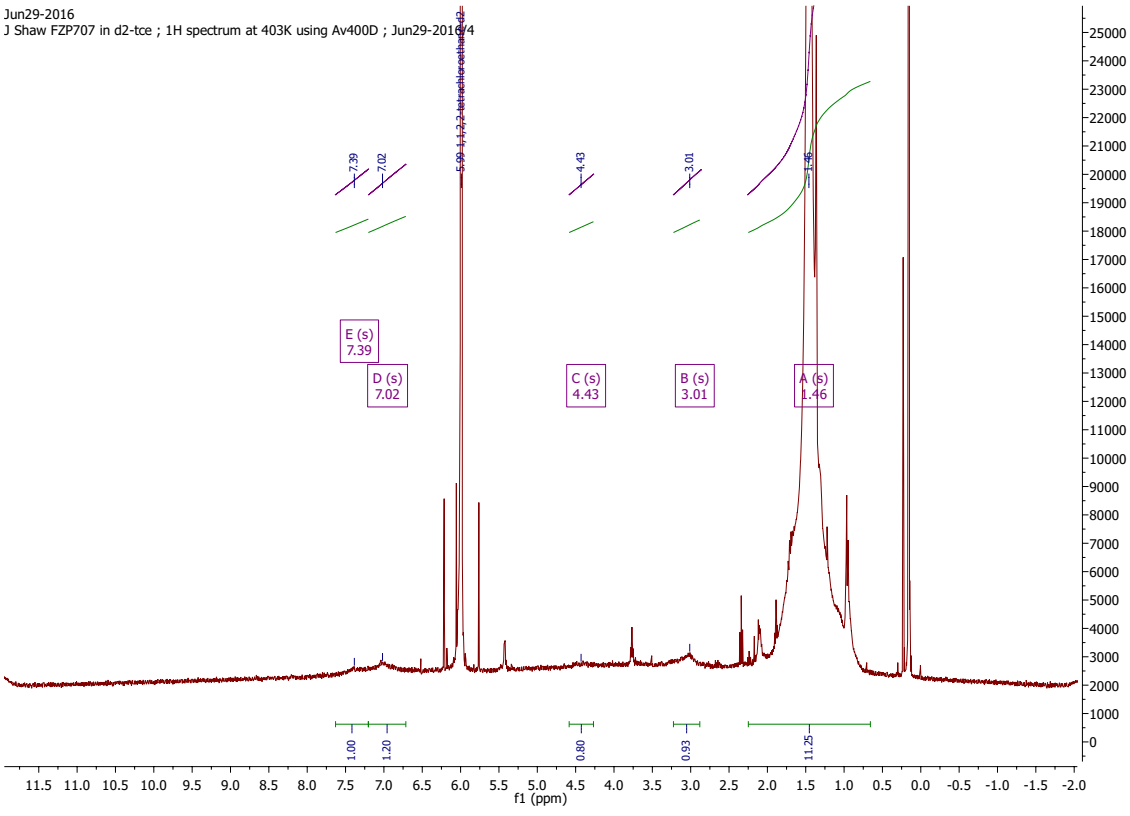

Figure A3.5. ^{1}H NMR of P7 at 130 °C in 1,1,2,2-tetrachloroethane-d_2.

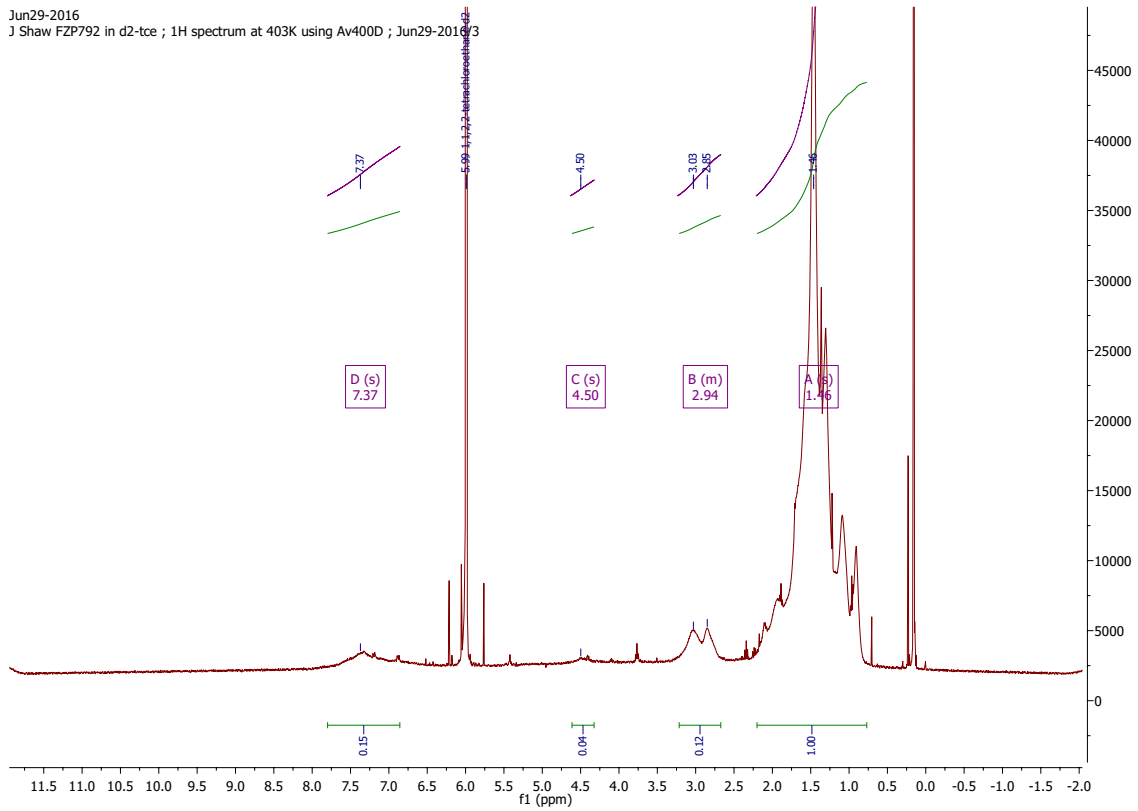

Figure A3.6. ^{1}H NMR of P8 at 130 °C in 1,1,2,2-tetrachloroethane-d_2.

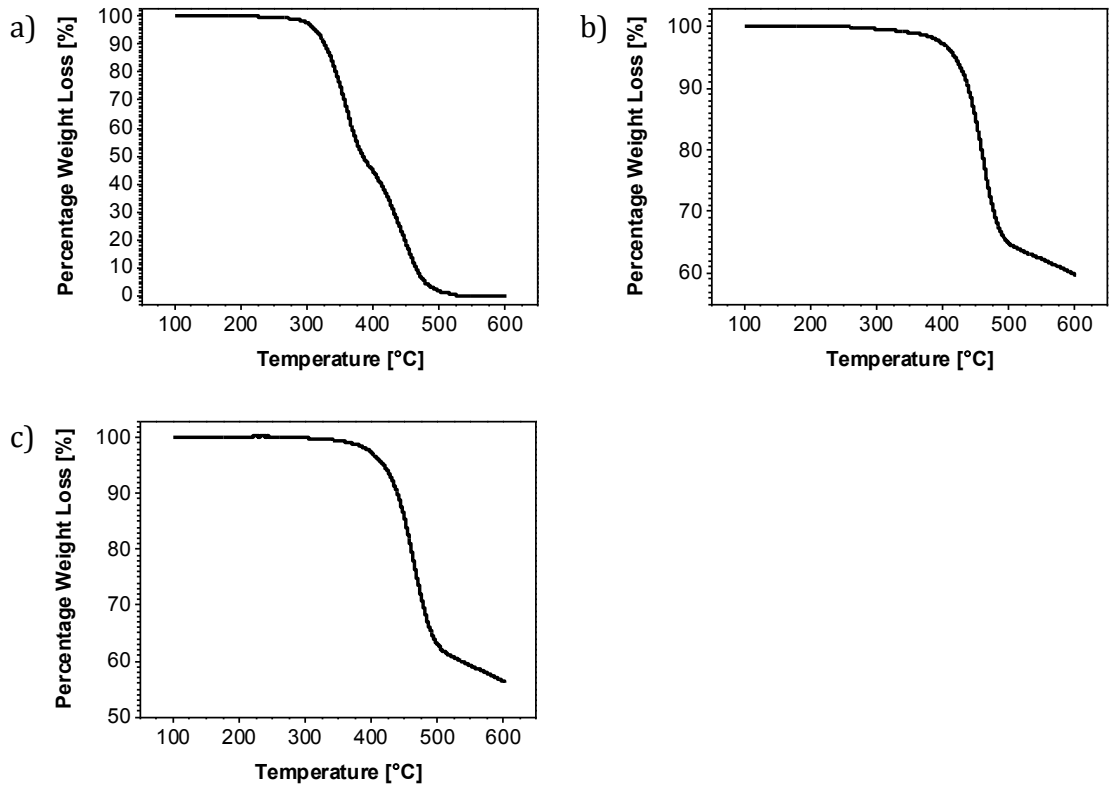

Figure A3.7. TGA thermograms of a) P6, b) P7, and c) P8, heating at a scan rate of 10 °C/min under a N_2 atmosphere.

Appendix for Chapter 4

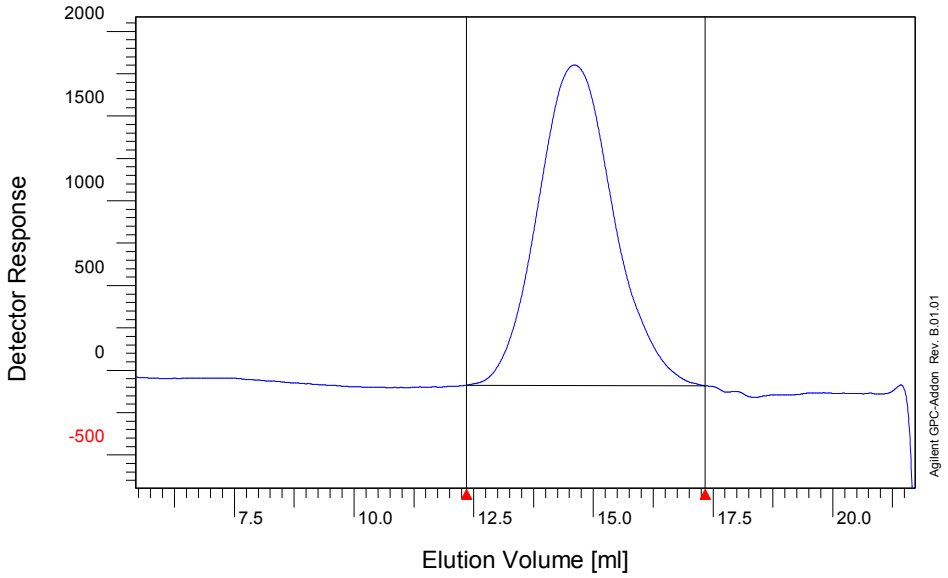

Figure A4.1. GPC trace of P9 measured in CB at 80 °C against polystyrene standards.

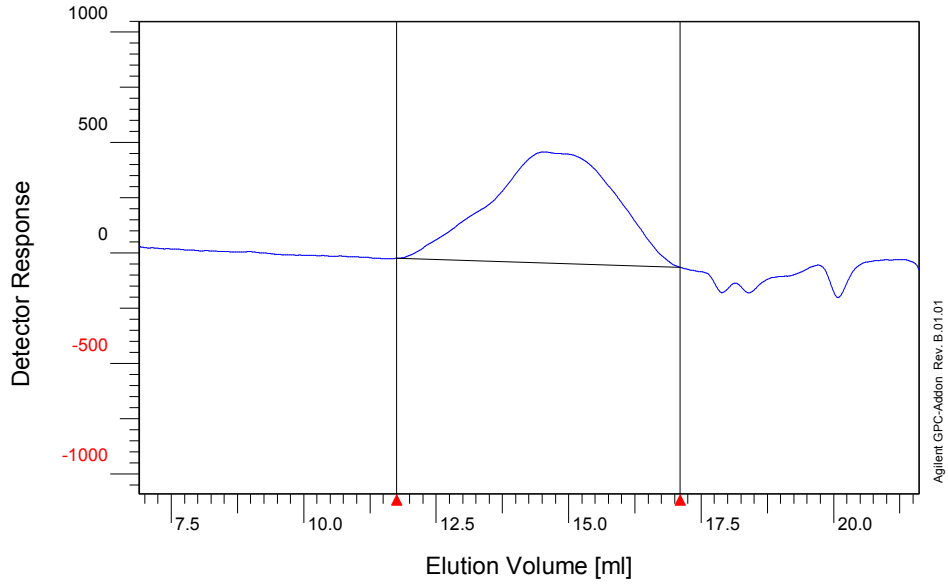

Figure A4.2. GPC trace of P10 measured in CB at 80 °C against polystyrene standards.

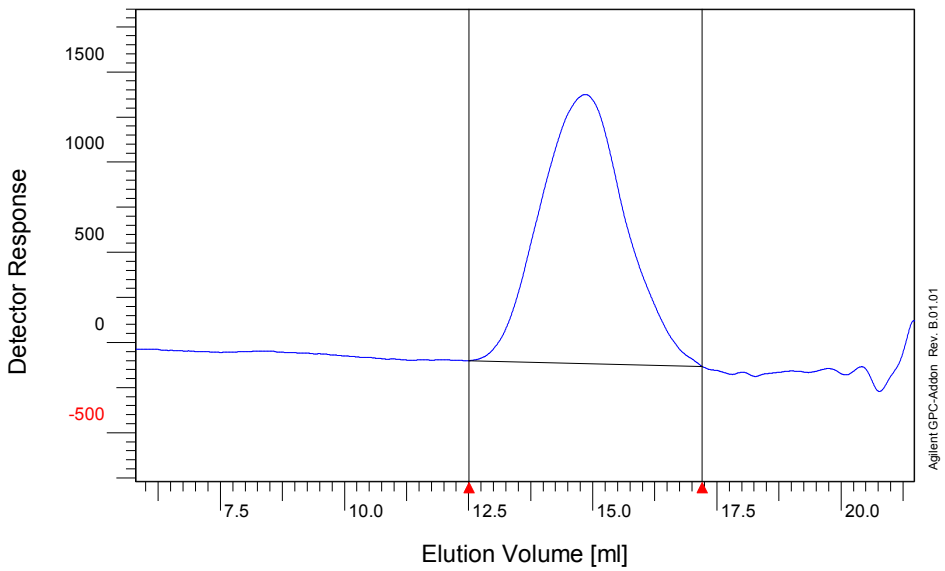

Figure A4.3. GPC trace of P11 measured in CB at 80 °C against polystyrene standards.

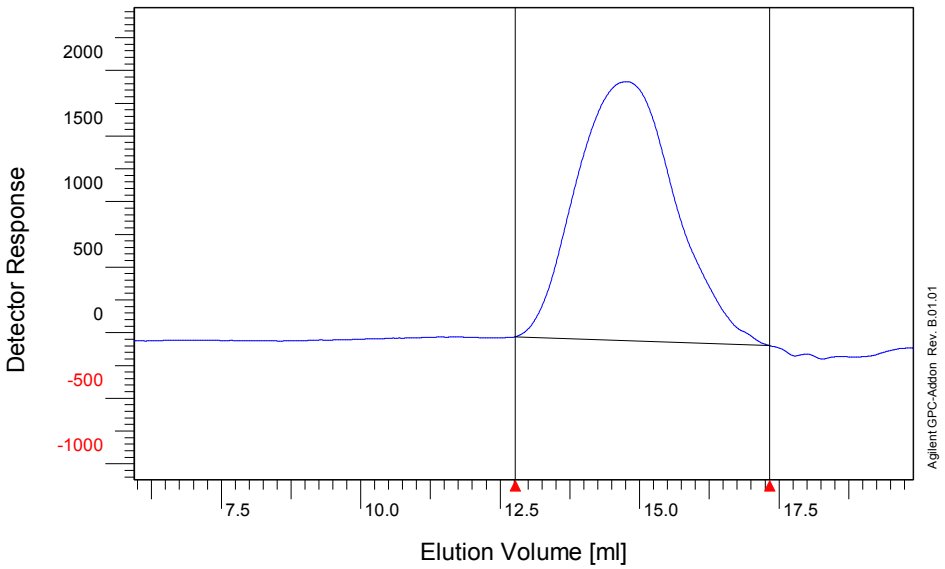

Figure A4.4. GPC trace of P12 measured in CB at 80 °C against polystyrene standards.

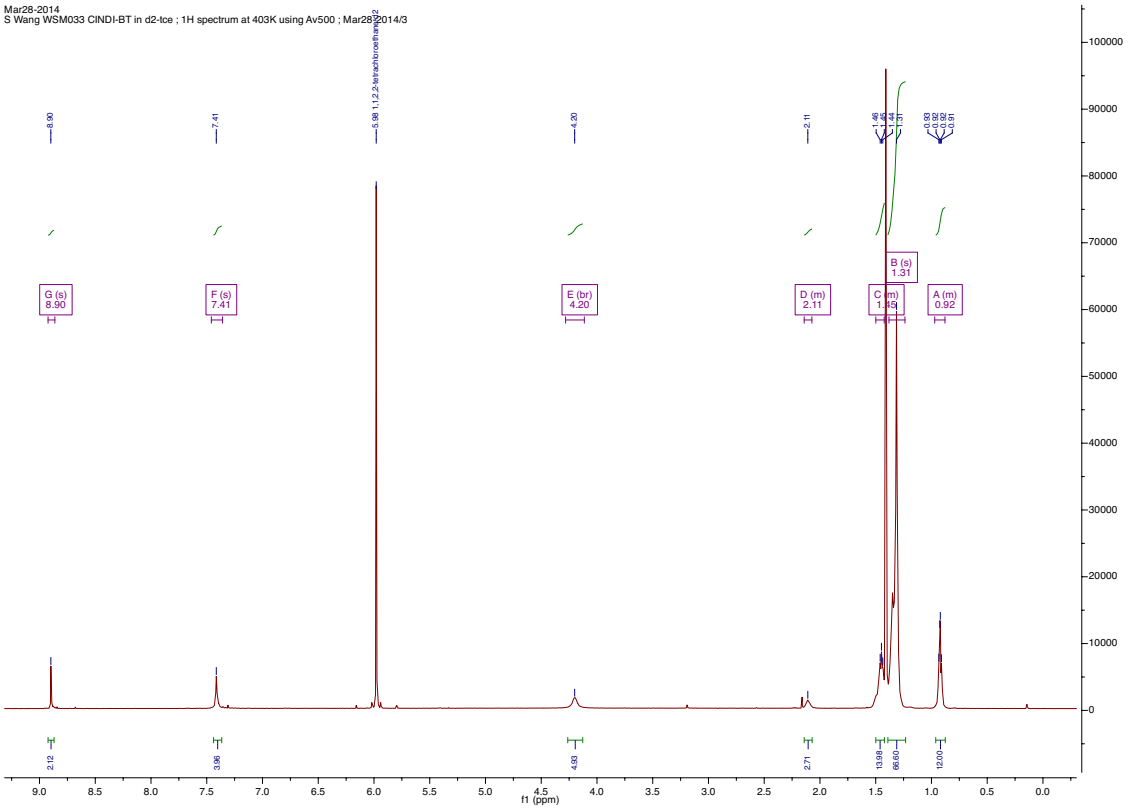

Figure A4.5. ^{1}H NMR of P9 at 130 °C in 1,1,2,2-tetrachloroethane-d_2.

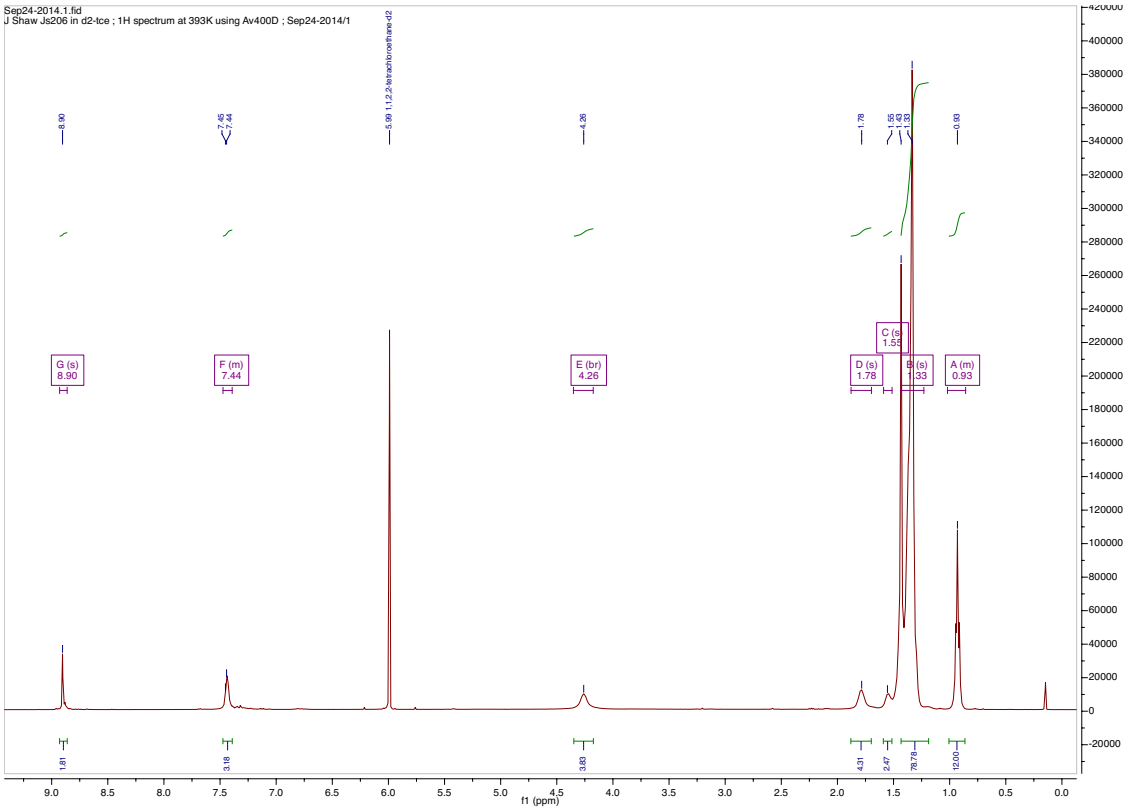

Figure A4.6. ^{1}H NMR of P10 at 130 °C in 1,1,2,2-tetrachloroethane-d_2.

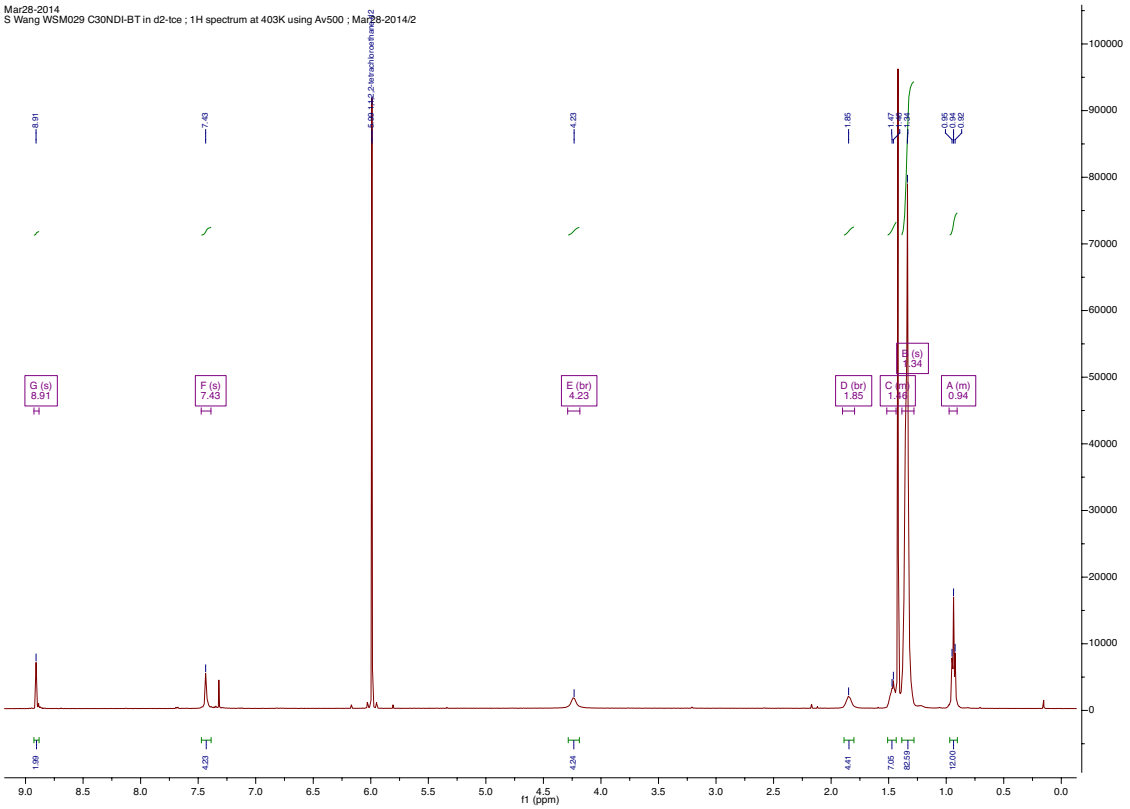

Figure A4.7. ^{1}H NMR of P11 at 130 °C in 1,1,2,2-tetrachloroethane-d_2.

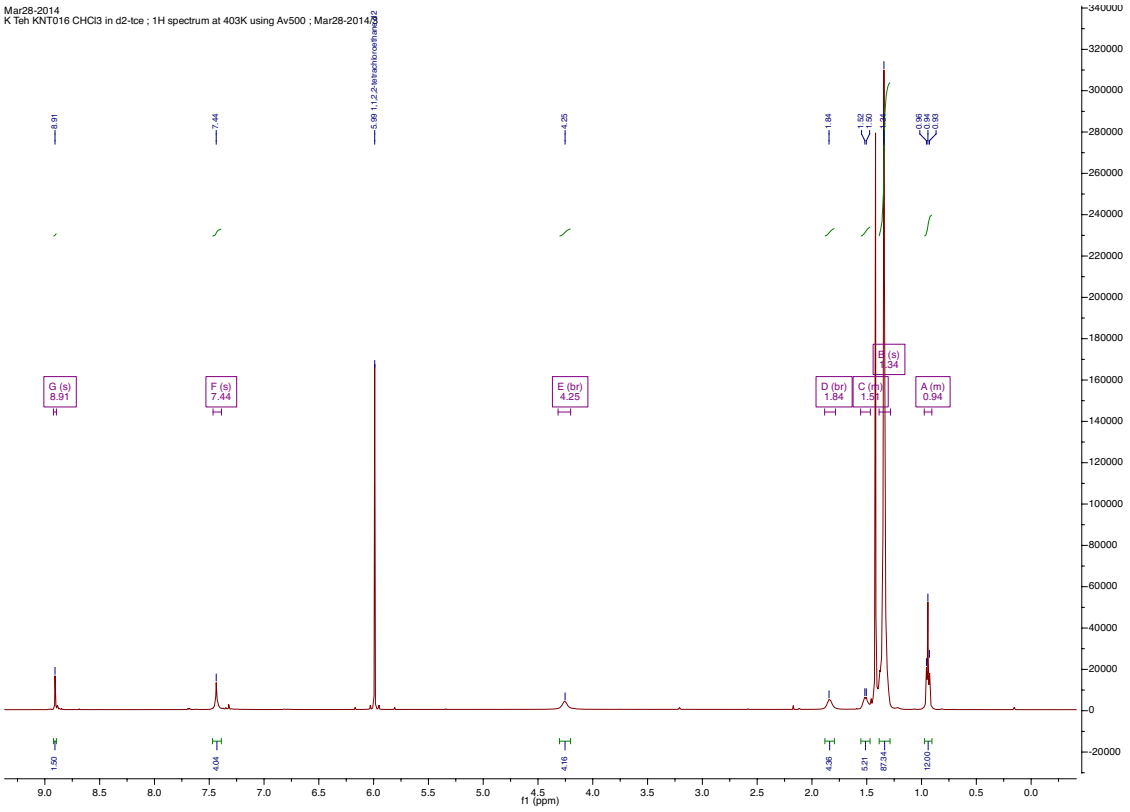

Figure A4.8. ^{1}H NMR of P12 at 130 °C in 1,1,2,2-tetrachloroethane-d_2.

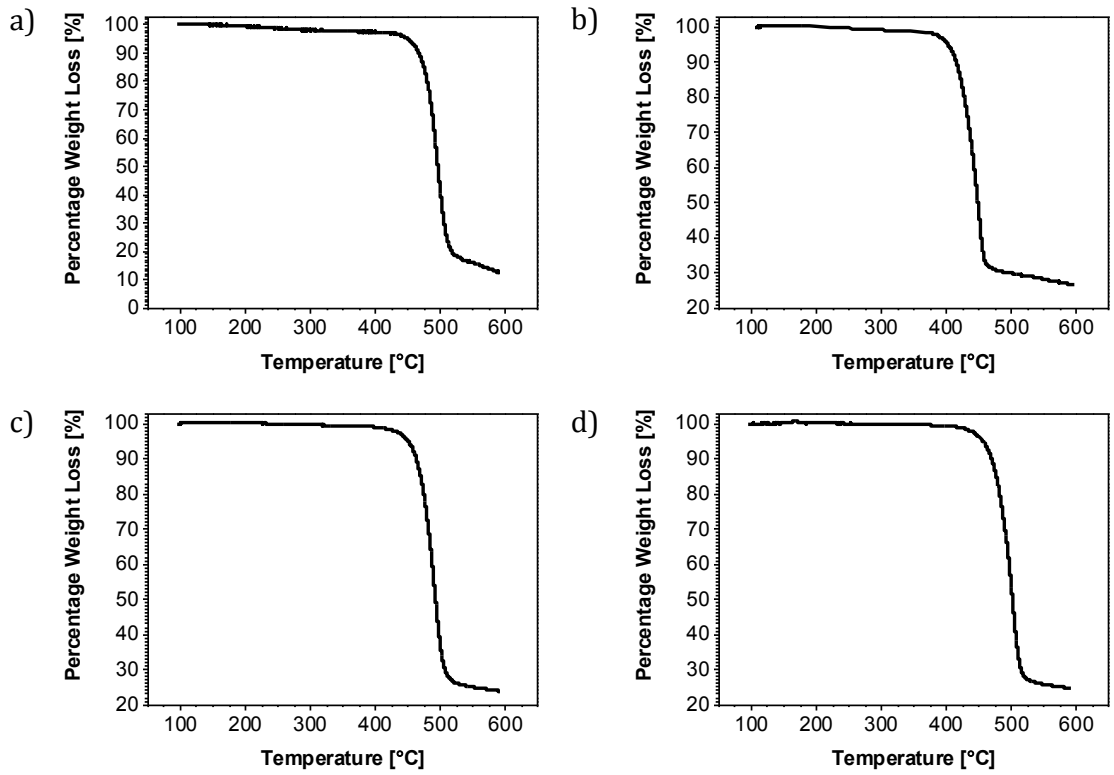

Figure A4.9. TGA thermograms of a) P9, b) P10, c) P11, and d) P12, heating at a scan rate of 10 °C/min under a N_2 atmosphere.

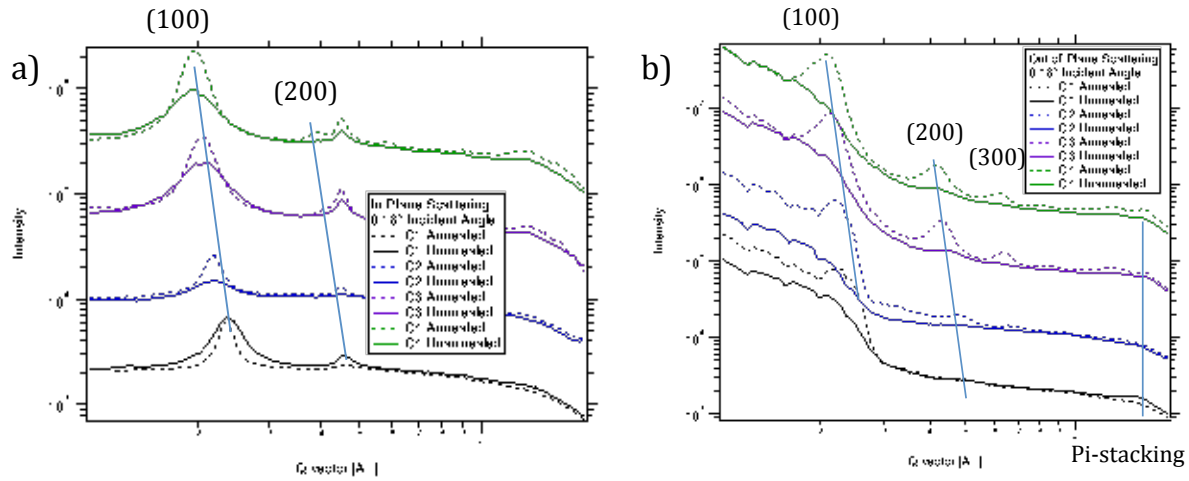

Figure A4.10. 1D-GIWAXS scattering profiles a) in-plane, and b) out-of-plane of as-cast (solid line), and annealed (200 °C for 30 min) (dashed line) films of P9 (black), P10 (blue), P11 (purple), and P12 (green), spin-coated on Si substrates (100) from *o*-dichlorobenzene (10 mg/mL).

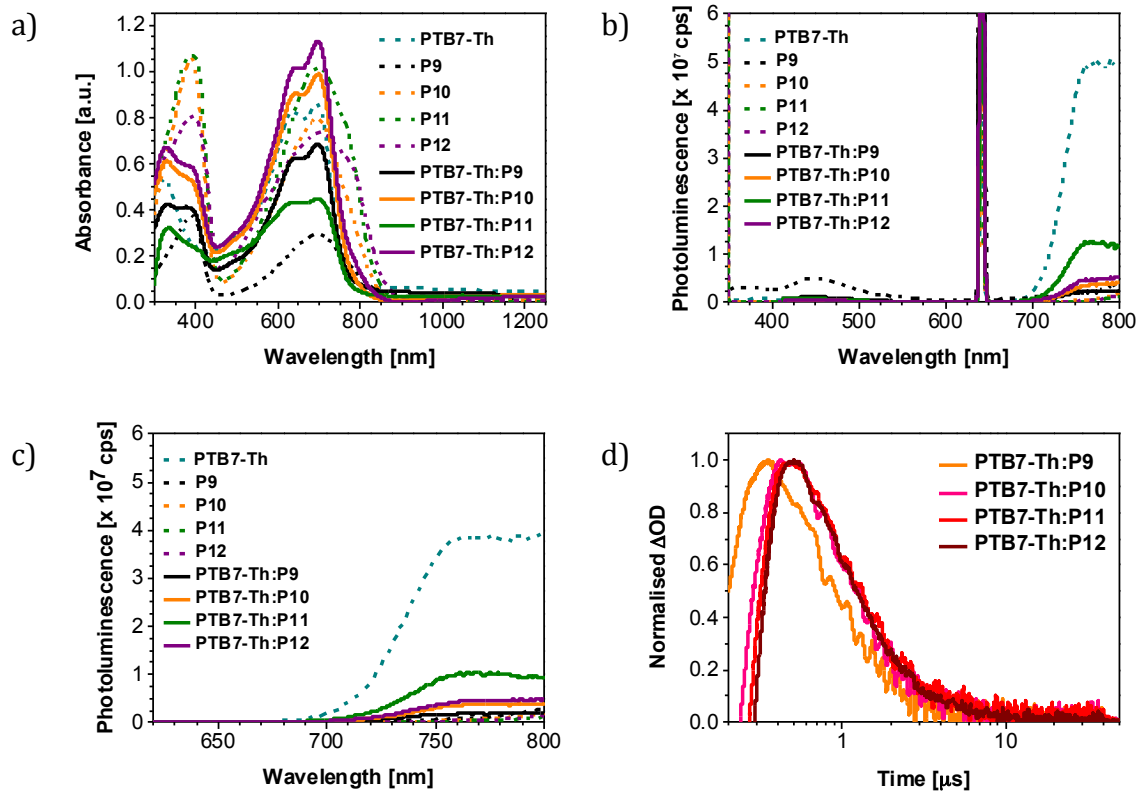

Figure A4.11. a) UV-vis absorption spectra of neat PTB7-Th and P9-12 films (dashed line), and PTB7-Th:P9-12 blends (solid line), b) photoluminescence spectra excited at 320 nm and c) 600 nm, and d) normalised sub-microsecond timescale transient absorption decays of PTB7-Th:P9-12 blends excited at 640 nm with an excitation density of 2 μJ/cm^2, and probed at 1020 nm under a N_2 atmosphere.

Photoluminescence quenching experiments on the PTB7-Th:P9-12 blends and neat thin films were used to evaluate exciton dissociation and charge transfer. The films were excited at 320 (Figure A4.11b) and 600 nm (Figure A4.11c) in order to selectively excite the PTB7-Th (donor) and P9-12 (acceptor), respectively. Photoluminescence quenching efficiencies were then determined by comparing the relative emission between the blends and neat thin films. Unfortunately there was some overlap between the absorption of the donor and acceptor at 600 nm (Figure A4.11a), and so reliable PLQ data could not be obtained for the acceptor. However, for the donor the PLQ efficiencies were 96, 93, 75, and 91% for the P9 to P12 blends, respectively. The higher value for the P9 blend suggests a more optimal morphology for efficient charge transfer, in agreement with the all-polymer OPV device data (Chapter 4, Section 4.2.6). Whilst the decrease in PLQ observed for blends of P10-12 suggests the increase in branch-point increases phase-separation and leads to the formation of larger crystalline acceptor domains.

The charge generation dynamics of thin films of the PTB7-Th:P9-12 blends was probed using sub-microsecond timescale transient absorption spectroscopy. Figure A4.11d displays the transient absorption decays of the blend films, prepared using the same conditions as those used for OPV device fabrication. The films were selectively excited at the lowest energy absorption maximum of the polymers (640 nm) using a low excitation density (2 μJ/cm^2), and a probe wavelength of 1020 nm, which is assigned to the polaron signal. Note however, it is difficult to distinguish between the PTB7-Th[220] and P9-12[221,222] polarons. As shown in Figure A4.11d, slower polaron formation and exciton decay is observed across the series from the P9-12 blends, although there is little difference in the timescale for the P10-12 blends. This suggests an increase in phase separation as the branch-point is increased, with the P9 blend demonstrating a more intimately mixed morphology than the other blends, in agreement with the PL data and GIWAXS studies of the neat thin films (Chapter 4, Section 4.2.4).

Appendix for Chapter 5

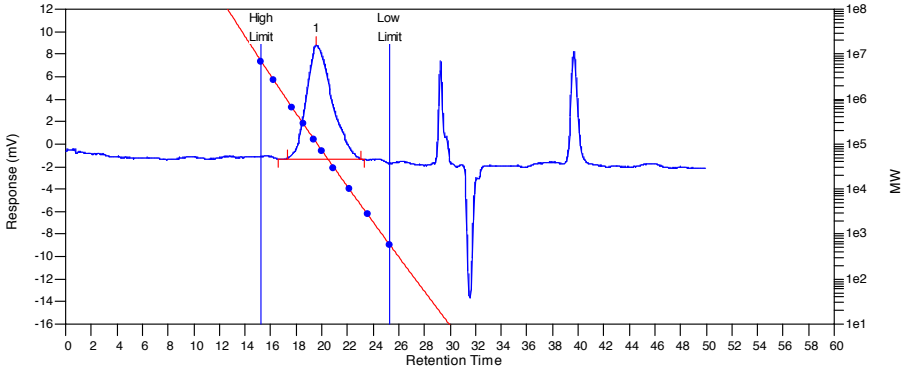

Figure A5.1. GPC trace of P13 measured in TCB at 140 °C against polystyrene standards.

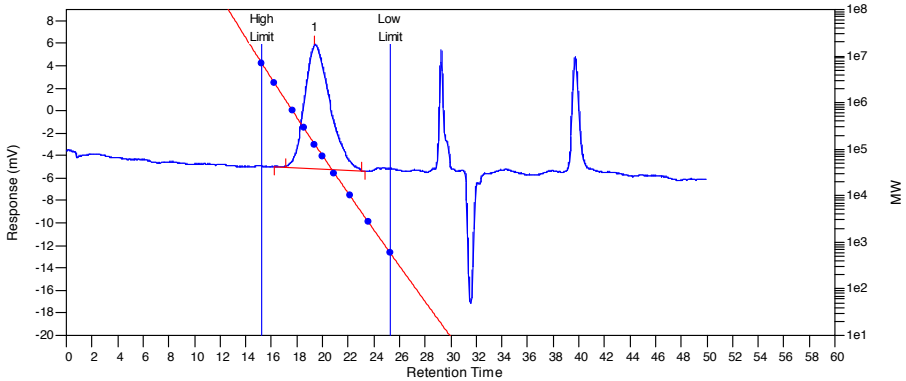

Figure A5.2. GPC trace of P14 measured in TCB at 140 °C against polystyrene standards.

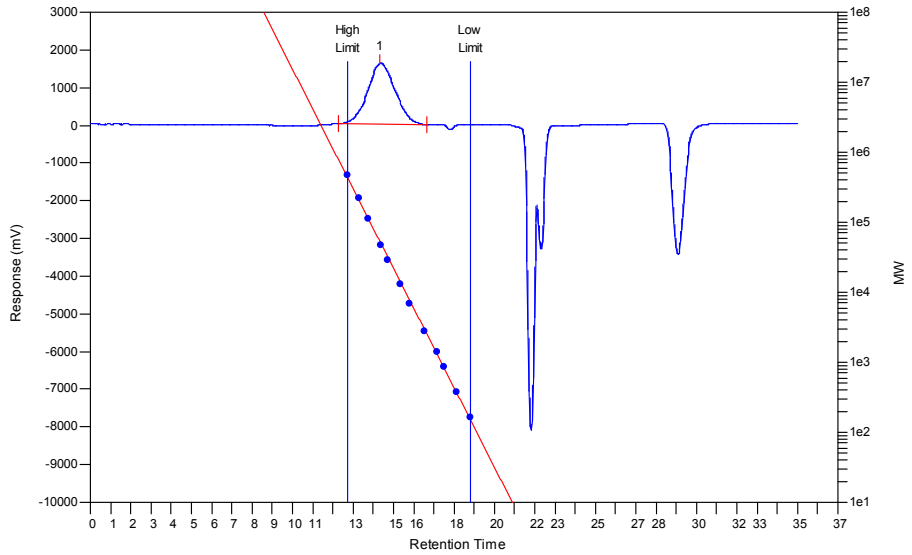

Figure A5.3. GPC trace of P15 measured in CB at 80 °C against polystyrene standards.

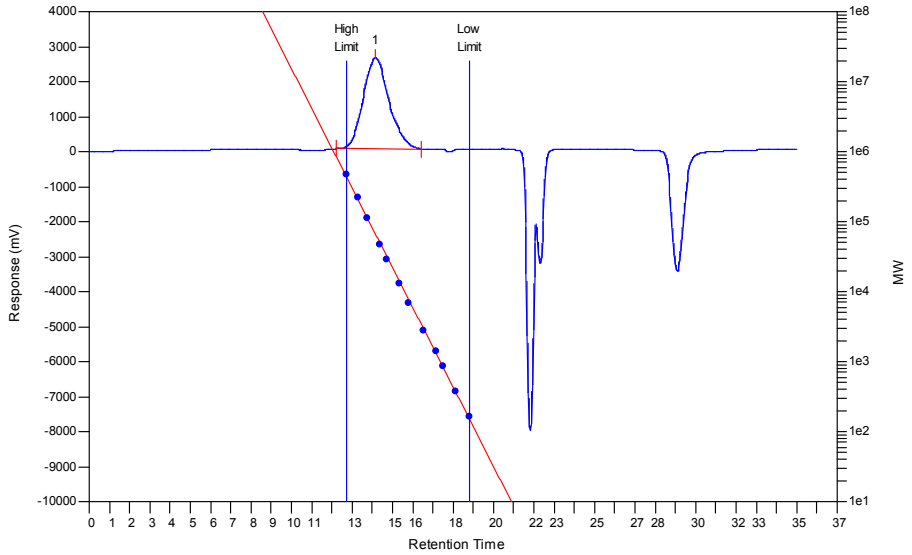

Figure A5.4. GPC trace of P16 measured in CB at 80 °C against polystyrene standards.

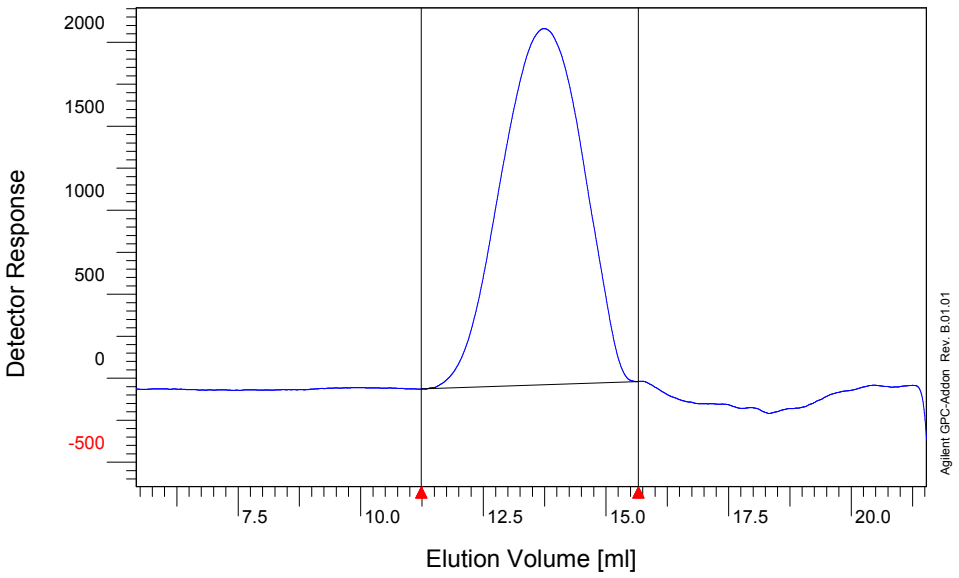

Figure A5.5. GPC trace of P17 measured in CB at 80 °C against polystyrene standards.

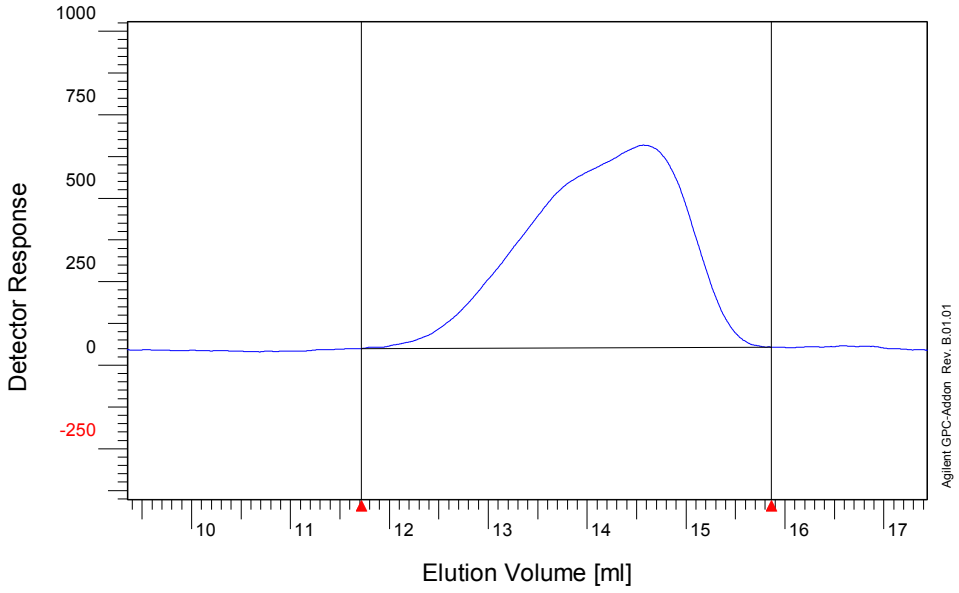

Figure A5.6. GPC trace of P18 measured in CB at 80 °C against polystyrene standards.

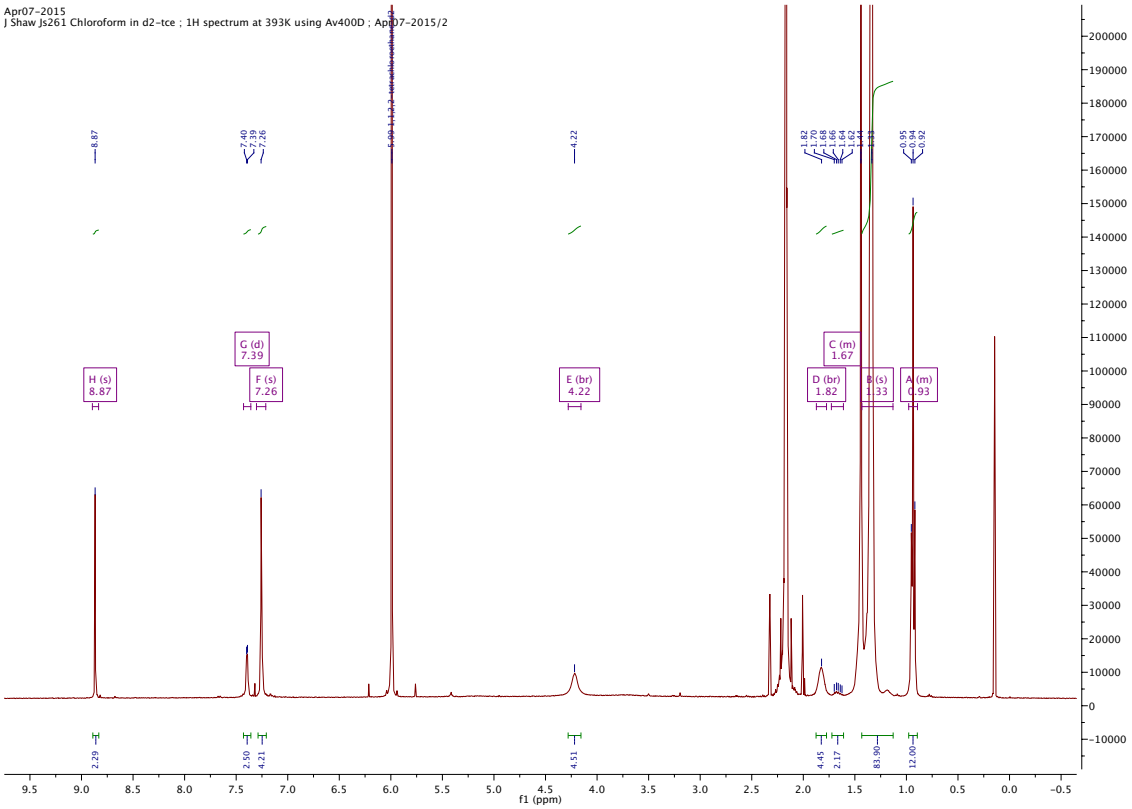

Figure A5.7. ^{1}H NMR of P13 at 130 °C in 1,1,2,2-tetrachloroethane-d_2.

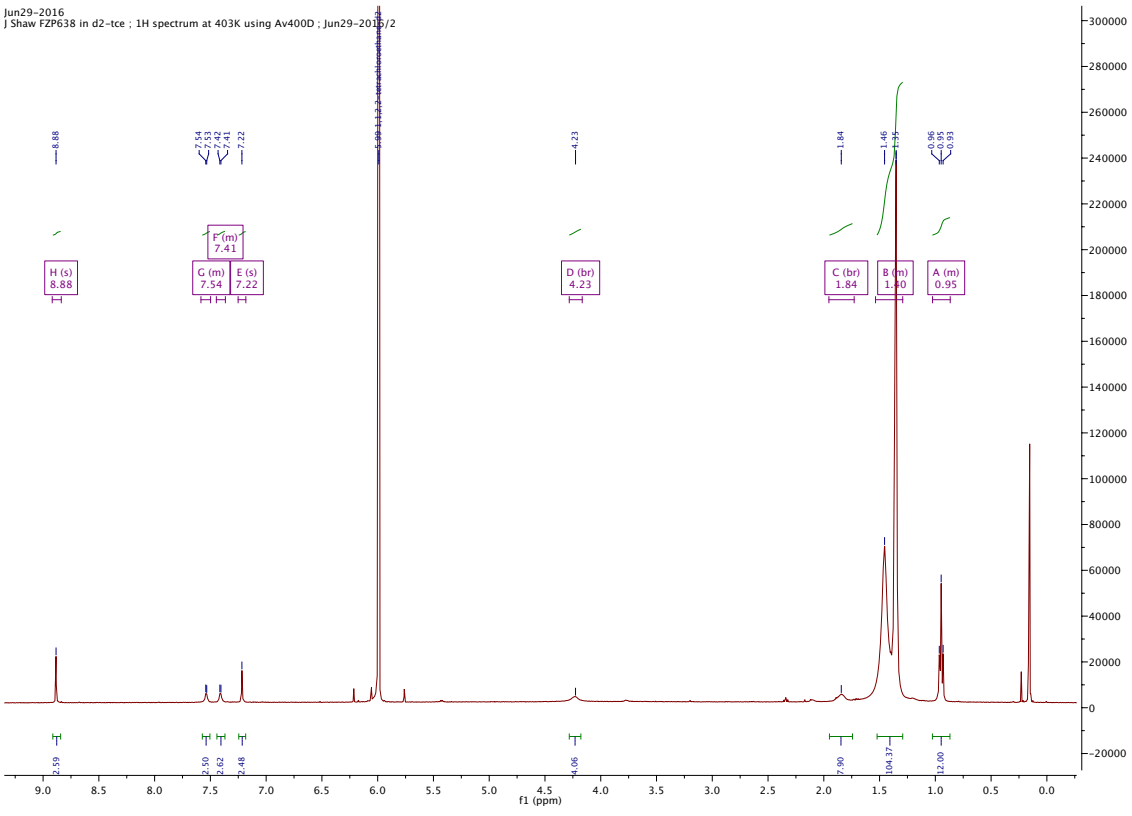

Figure A5.8. ^{1}H NMR of P14 at 130 °C in 1,1,2,2-tetrachloroethane-d_2.

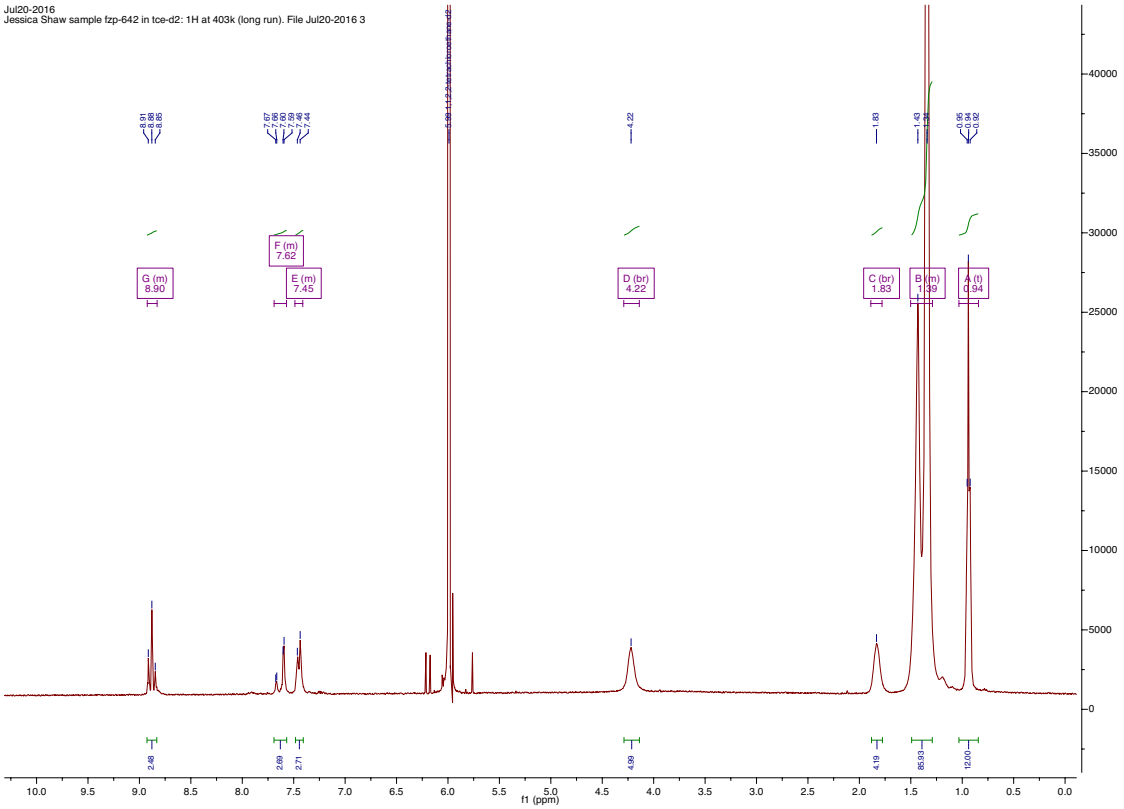

Figure A5.9. ^{1}H NMR of P15 at 130 °C in 1,1,2,2-tetrachloroethane-d_2.

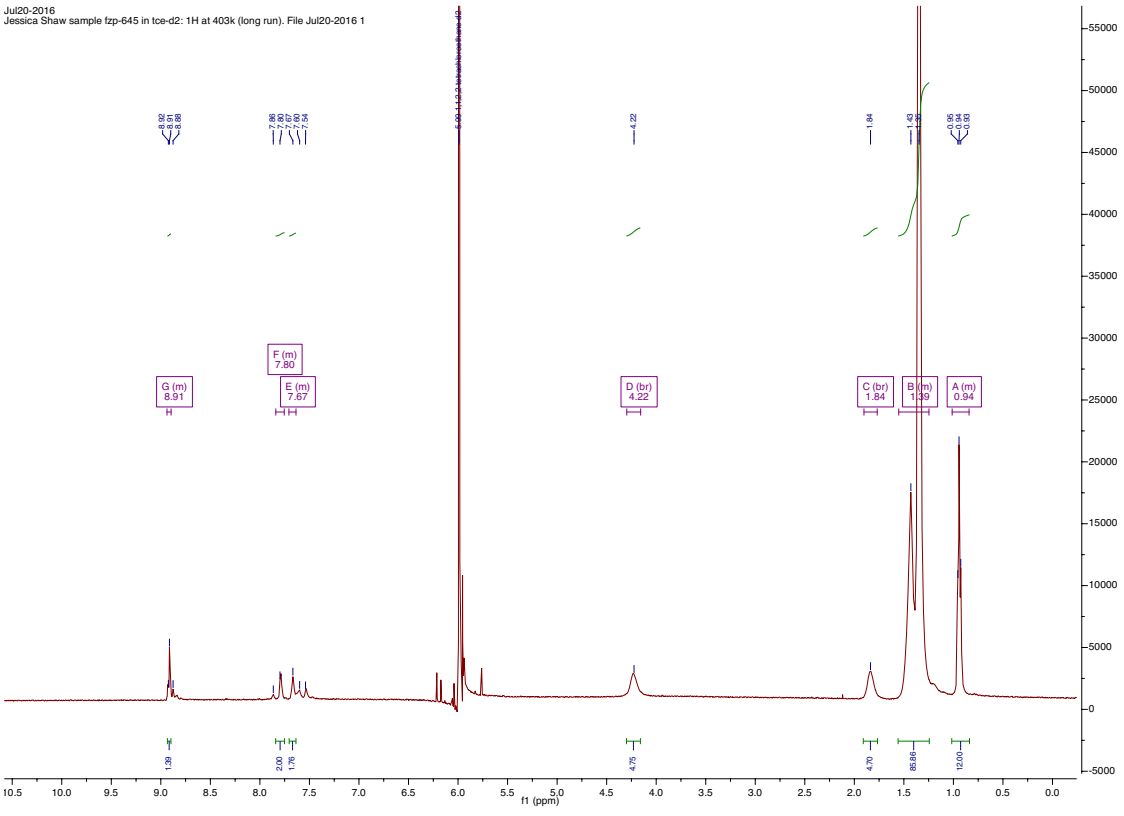

Figure A5.10. ^{1}H NMR of P16 at 130 °C in 1,1,2,2-tetrachloroethane-d_2.

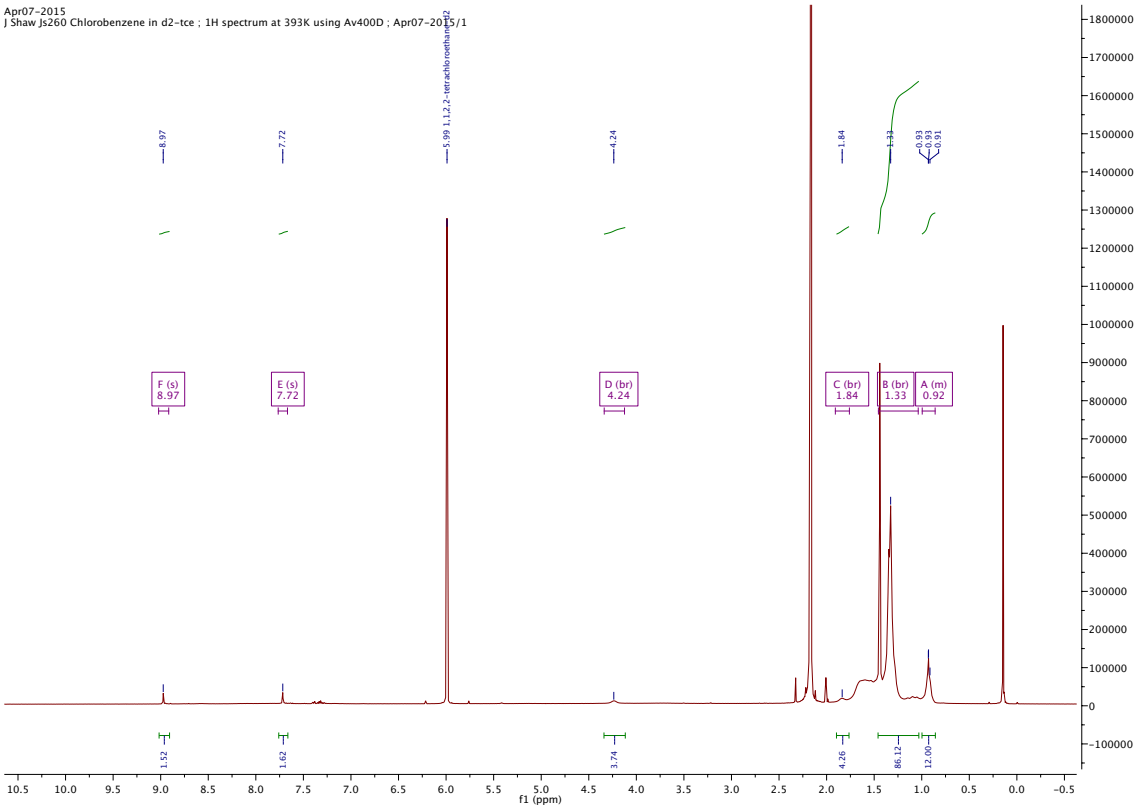

Figure A5.11. ^{1}H NMR of P17 at 130 °C in 1,1,2,2-tetrachloroethane-d_2.

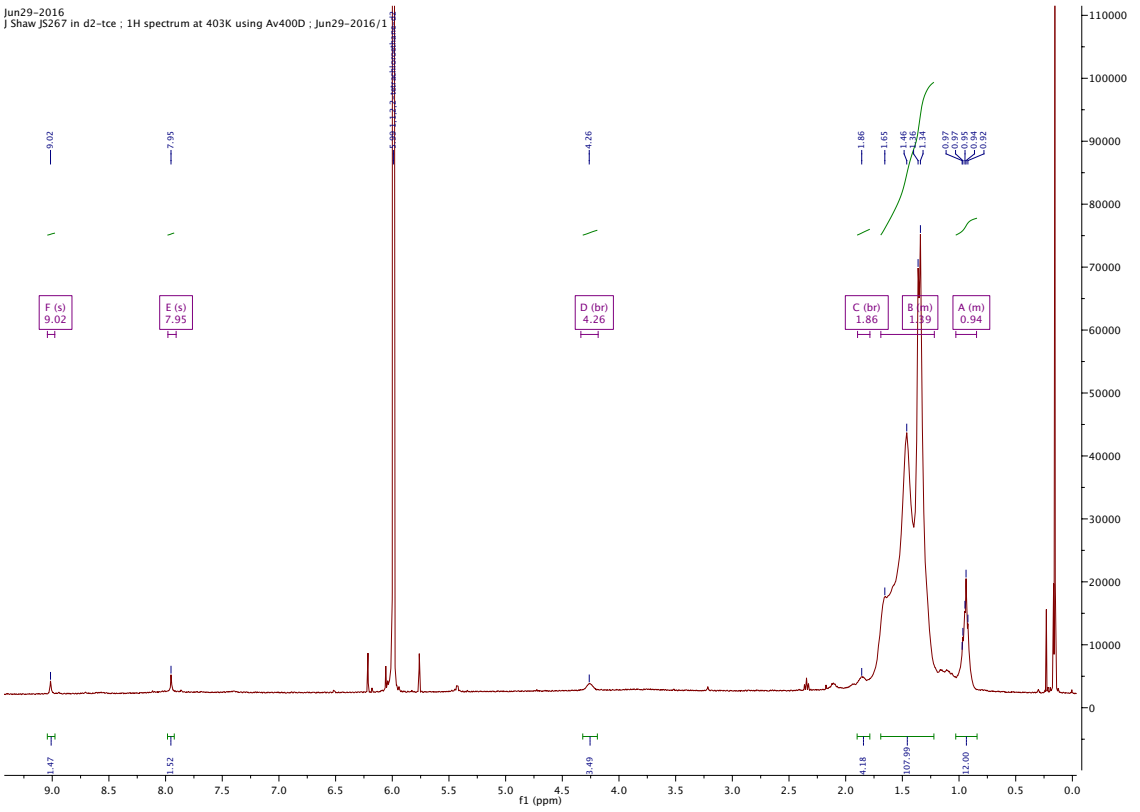

Figure A5.12. ^{1}H NMR of P18 at 130 °C in 1,1,2,2-tetrachloroethane-d_2.

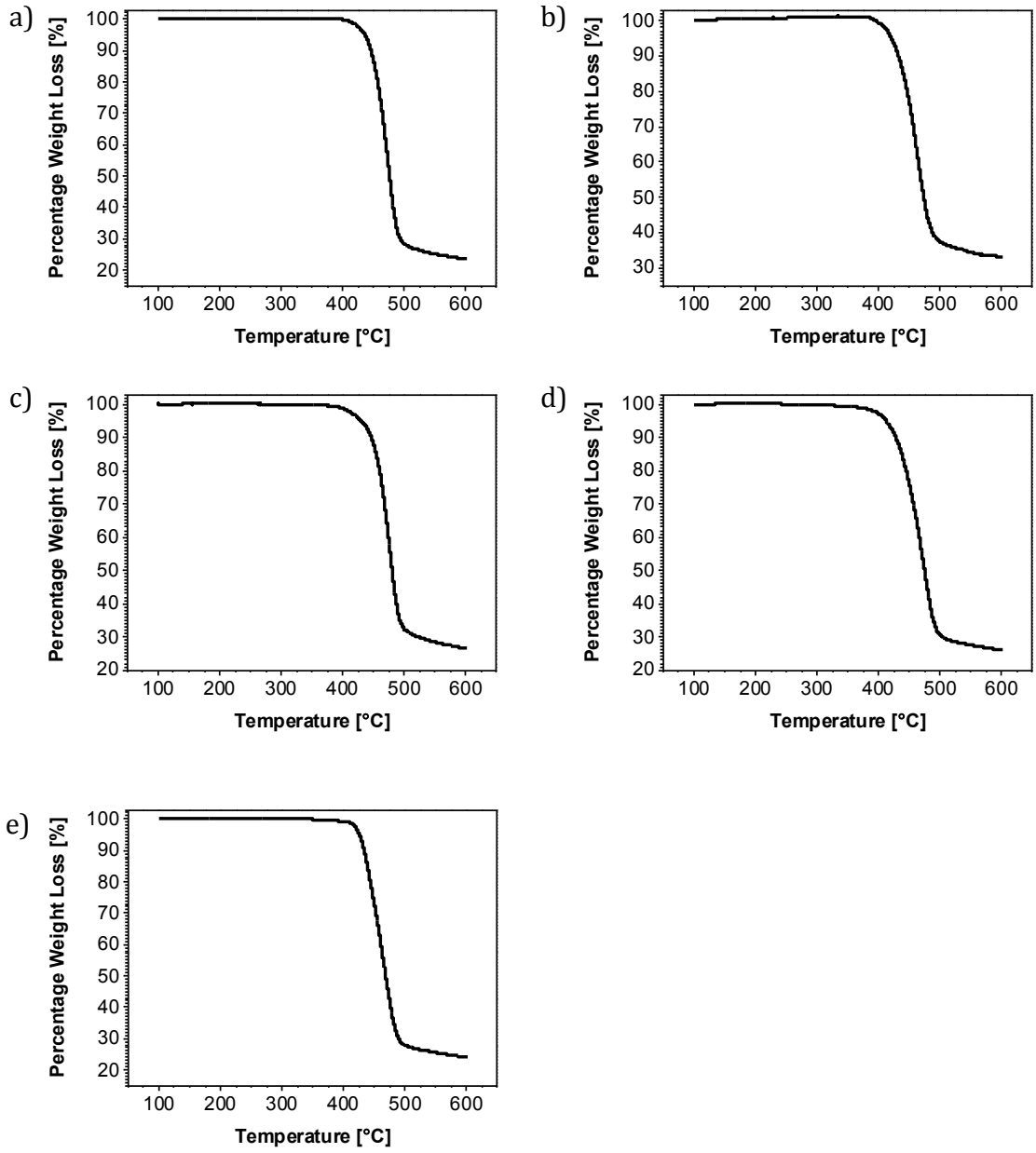

Figure A5.13. TGA thermograms of a) P13, b) P14, c) P15, d) P16, and e) P17, heating at a scan rate of 10 °C/min under a N_2 atmosphere.

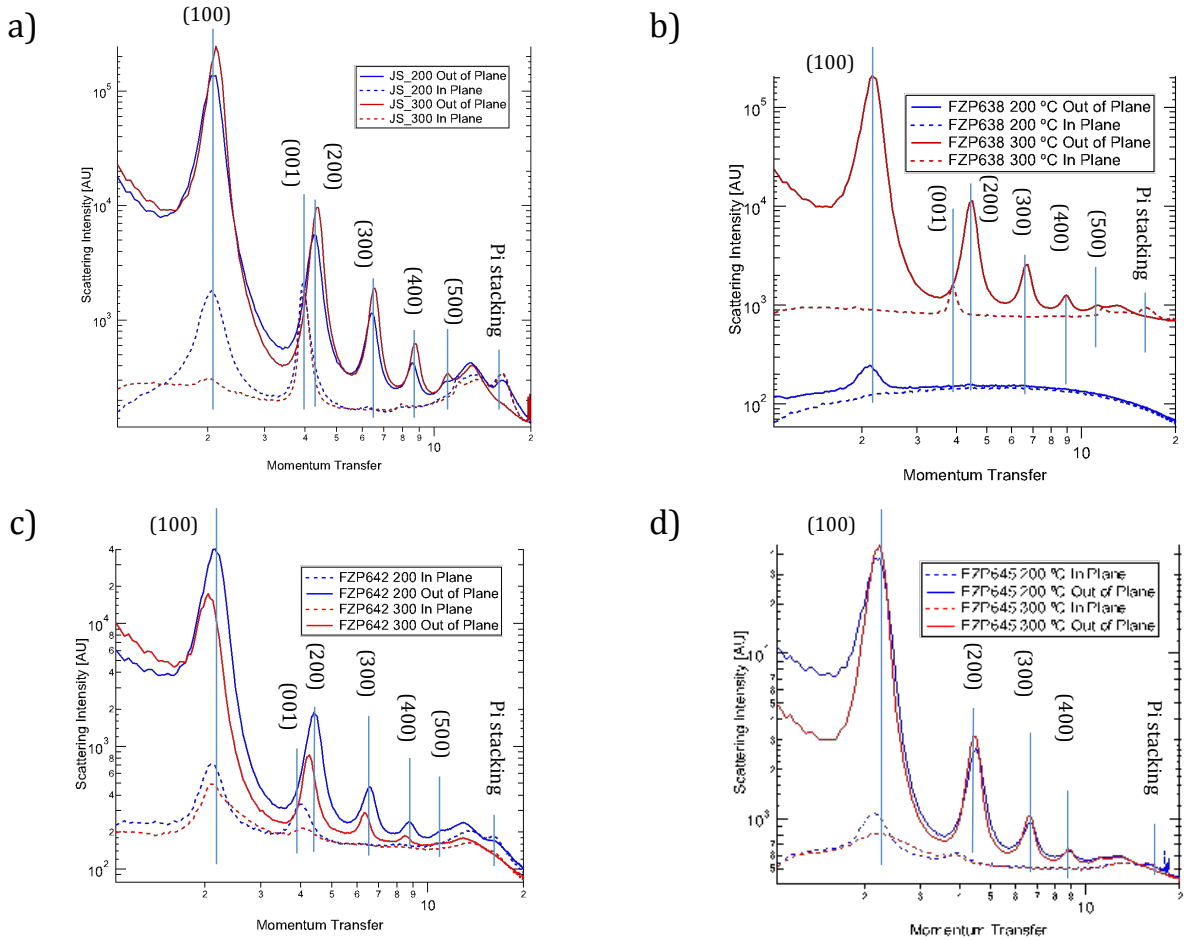

Figure A5.14. 1D-GIWAXS scattering profiles in-plane (dashed line) and out-of-plane (solid line) of films of a) P13, b) P14, c) P15, and d) P16, spin-coated on Si substrates (100) from *o*-dichlorobenzene (5 mg/mL), and annealed at 200 °C (blue), and 300 °C (red) for 30 min. N.B. The diffraction pattern of P14 annealed at 200 °C (Figure A5.14b) is misaligned.

Table A5.1. OFET Device Characteristics[a]

	Average	Peak		
	μ_{sat} [cm²/Vs]	μ_{sat} [cm²/Vs]	V_T [V]	I_{on}/I_{off}
P13	0.39 ± 0.036	0.42	12.1 ± 0.3	1 x 10^2 ~ 1 x 10^3
P14	0.25 ± 0.045	0.28	21.2 ± 1.4	1 x 10^2 ~ 1 x 10^3
P15	0.011 ± 0.0025	0.013	12.5 ± 0.6	1 x 10^3 ~ 1 x 10^4
P16	0.015	0.021	16.2	1 x 10^2

[a] TG-BC devices fabricated on glass substrates using Au (60 nm) source drain electrodes and a PMMA dielectric (80 mg/mL in n-butyl acetate, 120 kg/mol). Polymer active layers were spin-coated from *o*-DCB (5 mg/mL) and annealed at 300 °C for 15 min. N.B. for P16 almost all devices annealed at 300 °C failed.

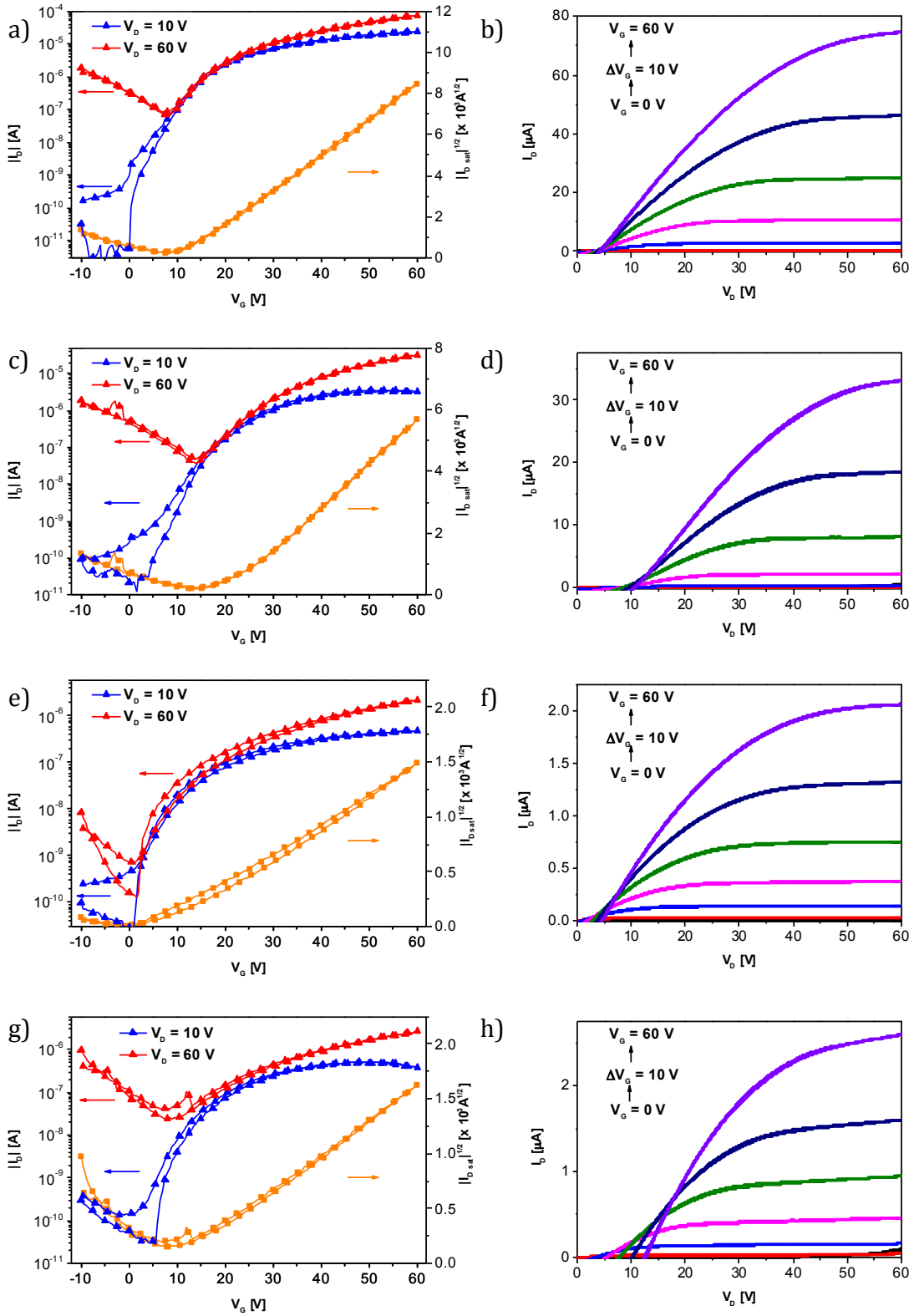

Figure A5.15. Transfer (left) and output (right) characteristics of the best performing TG-BC devices of P13: a) and b), P14: c) and d), P15: e) and f), and P16: g) and h), fabricated on glass substrates using Au (60 nm) source-drain electrodes, and PMMA (80 mg/ml in n-butyl acetate, 120 kg/mol) dielectric. Polymer active layers were spin-coated from *o*-dichlorobenzene solution (5 mg/mL) and annealed at 300 °C for 15 min. The channel width and length were 1000 μm and 40 μm, respectively.